Figure 9 Optical micrographs showing the LDPE coextrudates at various shear rate of skin or core layers (a) Increasing shear rate of core layer and (b) Increasing shear rate of skin layer.

increased, this effect would expect to be very small as the shear rate of the melt at the centre was relatively low.

When considering the swelling ratio in Figure 7, it was found that the swelling ratio of the LDPE coextrudate progressively increased with increasing $\dot{\gamma}_{skin}$, whereas the increase of $\dot{\gamma}_{core}$ did not significantly affect the swelling behavior of coextrudate. The physical swellings of the coextrudates by varying shear rate of core or skin layers are given in Figure 9. The increase of swelling ratio with increasing the $\dot{\gamma}_{skin}$ was attributed to an increasing amount of the stored elastic energies that were put into the skin layer which had relatively higher shearing stresses generated during the flow in the die, as mentioned earlier. These stored elastic energies would then be released on exiting the die and thus increased swelling ratio of the coextrudate. On the other hand, the unchanged swelling behavior of coextrudate obtained by increasing $\dot{\gamma}_{core}$ was due to the relatively low shear stresses occurred in core layer.[21]

In this work, recycled LDPE was extruded as the core layer in LDPE coextrudate as usually employed
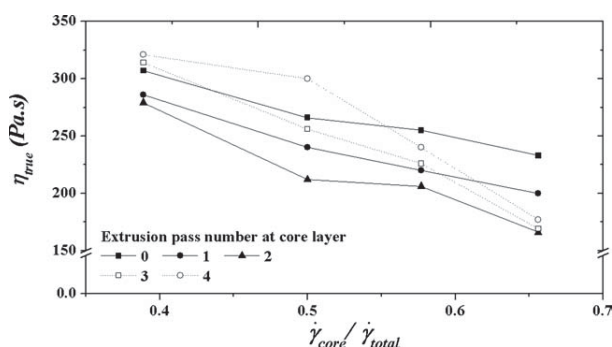
Figure 10 Influence of number of reprocessing at the core layer on viscosity for coextruded LDPE as a function of $\dot{\gamma}_{core}/\dot{\gamma}_{total}$.
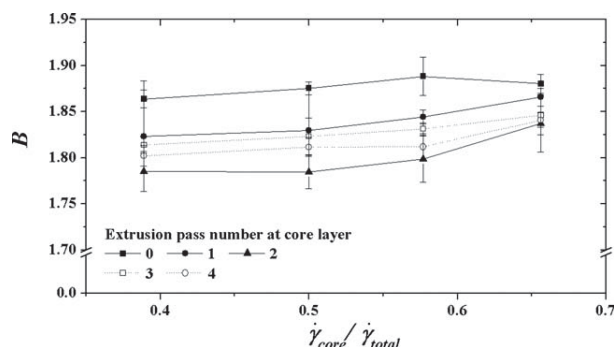
Figure 11 Influence of number of reprocessing at the core layer on swelling ratio for coextruded LDPE as a function of $\dot{\gamma}_{core}/\dot{\gamma}_{total}$.

in normal coextruded products for cost saving purposes. Figures 10 and 11 illustrate the influence of number of reprocessing at the core layer on the true viscosity and swelling behavior of coextruded LDPE. In comparison with the as-received virgin LDPE, it was clearly seen for the reprocessing numbers 1 and 2 that the true viscosity and die swell ratio of coextrudates decreased with increasing number of extrusion. The reductions in the viscosity and die swell ratio probably involved a shear modification of long chain branched LDPE at the core layer. That was, the molecular entanglement reduces as the melt experienced the shearing force. This shear modification theory was also stated by Han.[22] However, the increments of viscosity and die swell ratio were observed for the reprocessing numbers 3 and 4. This was thought to result mainly from a partial crosslinking effect of LDPE after prolonged thermal history. These explanations can be substantiated using gel content experiment which was carried out by immersion of the reprocessed LDPE in xylene solvent and the determination of gel content was calculated in accordance with the experimental method by ASTM D 2765-01 (2001). The gel content results for coextruded LDPE after extrusion are given in Table I. It can be seen that the gel contents extracted from the reprocessed LDPE samples gradually increased with increasing number of reprocessing, especially for numbers 3 and 4. The significant increases in the insoluble LDPE at the extrusion

TABLE I
Gel Contents for Recycled LDPE Coextrudates as a
Function of Number of Extrusion Pass

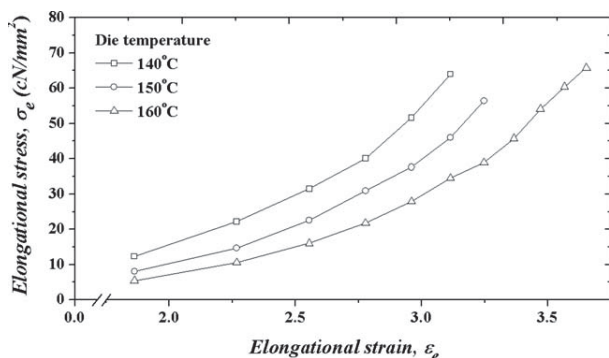| Number of extrusion pass	Gel Content (%)
1	1.37
2	2.3
3	7.25
4	12.48
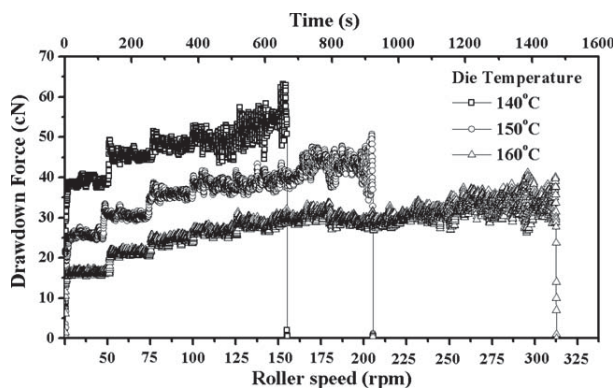
Figure 12 Relationship between measured drawdown forces against time with increasing roller speeds for coextruded virgin LDPE at various die temperatures.
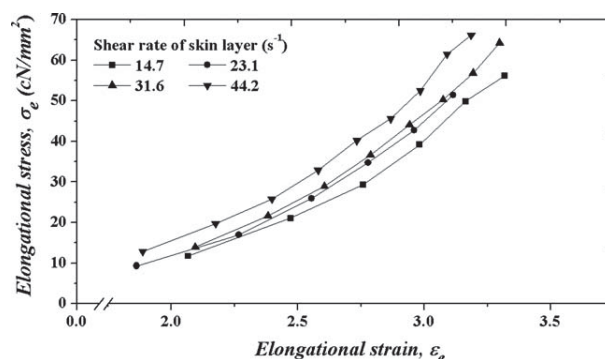
numbers 3 and 4 indicated the occurring some cross-linked molecules. This explains why the viscosity and the swelling ratio of the LDPE coextrudate increased at the reprocessing numbers 3 and 4. A similar observation was also reported in previous studies.[11,21,23]

Melt strength of coextruded LDPE

The effect of die temperature on the drawdown force of virgin LDPE coextrudate is given in Figure 12 at the $\dot{\gamma}_{core}/\dot{\gamma}_{total}$ ratio of 0.5. The experimental results were expressed in terms of drawdown force as a function roller speed and time. In general, at any given die temperature, it can be seen that the drawdown force sharply increased in the initial stage of increasing roller speed (0–50 rpm) and then slowly increased until to the final stage. The significant increase of drawdown force at the initial roller speed was associated with the branching characteristics of LDPE, resulting in the elastic resistances to the applied deformation. This behavior was also in line with previous investigations.[7,9–11] At higher

Figure 14 Effect of $\dot{\gamma}_{skin}/\dot{\gamma}_{total}$ total on elongational stress of coextruded virgin LDPE at die temperature of 150°C.

roller speeds (greater than 50 rpm), the increases in the drawdown force were marginal. This was because the molecular chains of LDPE in this stage became completely disentangled and could easily slip past each other, no further forces being required. Moreover, fluctuation of drawdown force was also observed during the final stage of increasing the roller speed. This was a result of draw resonance effect, which was reported and found by a number of publications.[7,10–13]

The plots between elongational stress (σ_e) and elongational strain (ε_e) for different die temperatures are shown in Figure 13 which could be explained in a similar fashion as given for Figure 12, in that the higher the die temperature, the lower elongational stress and the higher the elongational strain. Increasing the die temperature caused the increases in viscous deformation and chain mobility in the LDPE coextrudates which facilitated the deformation with a lower external stress. Figures 14 and 15 show the influence of shear rate of skin and core layers on the melt strength of virgin LDPE coextrudate. In all cases, especially for an increase of $\dot{\gamma}_{skin}/\dot{\gamma}_{total}$ as depicted in Figure 14, the higher the shear rate the
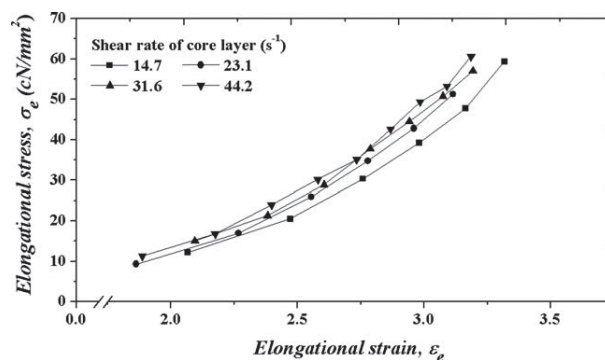

**Figure 13** Plots of elongational stress and elongational strain for coextruded virgin LDPE at various die temperatures.

Figure 15 Effect of $\dot{\gamma}_{core}/\dot{\gamma}_{total}$ on elongational stress of coextruded virgin LDPE at die temperature of 150°C.

greater the elongational stress and the higher the elongation at break. This was contributed to the fact that the greater amount of stored elastic energy given to the molten polymer at the higher shear rate. The recoverable energies could then release as kinetic energies within the extrudate and thus resulting in the increment of stress at break. This result was in agreement with the work carried out by previous researchers[7,8,10,11,24] in that the mechanical strength of molten polyolefin tended to increase with increasing extrusion rate. It was interesting to note that the changes in elongational stress appeared to be more sensitive and pronounced by altering the $\dot{\gamma}_{skin}/\dot{\gamma}_{total}$ as compared with by changing the $\dot{\gamma}_{core}/\dot{\gamma}_{total}$ as seen in Figure 14. Furthermore, Figure 16 shows a direct comparison of the elongational stress of coextruded LDPE using the $\dot{\gamma}_{skin}/\dot{\gamma}_{total}$ and $\dot{\gamma}_{core}/\dot{\gamma}_{total}$ of 0.66. It was found that the elongational stress obtained by using the $\dot{\gamma}_{skin}/\dot{\gamma}_{total}$ was also higher than that of $\dot{\gamma}_{core}/\dot{\gamma}_{total}$ for any given strain rates. The reason for this discrepancy was probably the same as that given to explain the rheological properties in Figures 6 and 7. The results in Figures 6, 7,14, and 15 confirmed that the skin layer had greater effect on the rheological properties and mechanical strength of the LDPE coextrudates than the core layer.

As mentioned earlier that recycled LDPE was usually used as the core layer in coextruded products. The elongational stress obtained from different numbers of reprocessing LDPE at the core layer is given in Figure 17. It can be seen that the elongation stress for the reprocessing numbers 3 and 4 were higher than that of virgin LDPE, while no significant differences were found for the reprocessing numbers 1 and 2. These results can be explained by the gel content results (in Table I) which indicated the crosslinked structure of LDPE at the reprocessing numbers 3 and 4, this resulting in higher melt strength of coextruded LDPE.
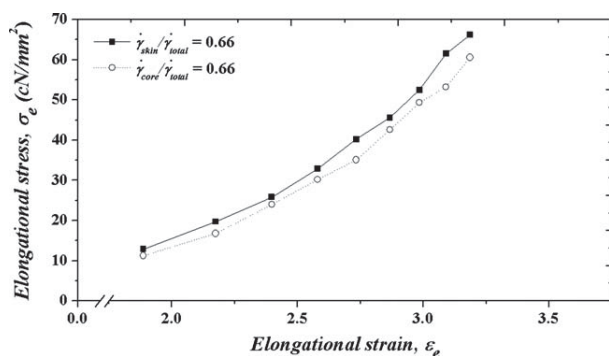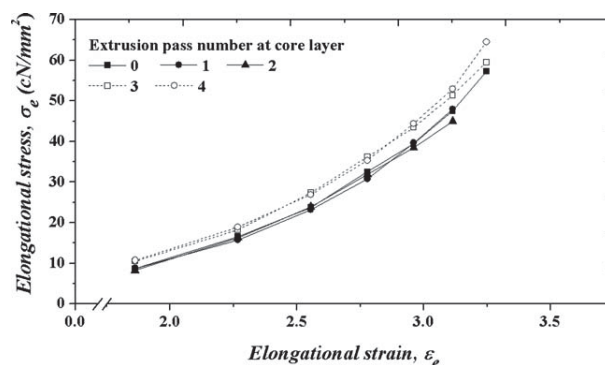
Figure 17 Effect of reprocessing number at core layer on elongational stress for coextruded LDPE at $\dot{\gamma}_{core}/\dot{\gamma}_{total}$ of 0.5.

CONCLUSION

In this study, the coextruded feed-block unit coupled with a mechanical strength measuring rig was specially constructed to determine the rheological properties and melt strength of coextruded LDPE. The effects of die temperature, shear rate, the number of extrusion passes at the core layer, and roller take-up speed were studied. As for the rheological properties of coextruded LDPE, it was found that the true viscosity and swelling ratio of the LDPE coextrudate decreased with increasing die temperature. The rheological properties and mechanical strength of LDPE coextrudates were more dependent on the shear rate of skin layer as compared to those of core layer. The reductions in viscosity and die swell ratio of coextrudate for reprocessing numbers 1 and 2 were probably caused by the disentanglement of long chain branching LDPE at the core layer. On the other hand, the increments of viscosity and die swell ratio for reprocessing numbers 3 and 4 resulted from crosslinking effect. The elongational stress of coextrudates was found to increase with increasing elongational strain, while tended to decrease with increasing die temperature. The changes in mechanical strength by the effects of shear rate and number of reprocessing corresponded well with the rheological measurements.

References

1. Michaeli, W. Extrusion Dies for Plastics and Rubbers: Design and Engineering Computations; Hanser Publishers: New York, 1992.
2. White, J. L.; Ufford, R. C.; Dharod, K. R. J Appl Polym Sci 1972, 16, 1313.
3. Han, C. D. J Appl Polym Sci 1973, 17, 1289.
4. Dooley, J.; Hyun, K. S.; Hughes, K. Polym Eng Sci 1998, 38, 1060.
5. Martin, O.; Averous, L. J Appl Polym Sci 2002, 86, 2586.
6. Yao, F.; Wu, Q. J Appl Polym Sci 2010, 118, 3594.
7. Wagner, M. H.; Bastian, H.; Bernnat, A.; Kurzbeck, S.; Chai, C. K. Rheol Acta 2002, 41, 316.

Figure 16 Comparison of elongational stress obtained using $\dot{\gamma}_{skin}/\dot{\gamma}_{total}$ total and $\dot{\gamma}_{core}/\dot{\gamma}_{total}$ of 0.66 at various elongational strain.

8. Muke, S.; Ivanov, I.; Kao, N.; Bhattacharya, S. N. J Non-Newt Fluid Mech 2001, 101, 77.

9. De Jesus, T.; Guadarrama-Medina J.; Perez-Gonzalez, J.; De Vargas, L. Rheol Acta 2005, 44, 278.

10. Sitticharoen W.; Intawong, N-T.; Sombatsompop, N. Polym Polym Compos 2010, 18, 359.

11. Harnnarongchai, W.; Intawong, N.-T.; Sombatsompop, N. J Macromol Sci B: Phys 2011, 50, 1074.

12. Harnnarongchai, W.; Sithicharoen, W.; Intawong, N.-T.; Sombatsompop, N. J Vinyl Addit Technol 2011, 17, 164.

13. Ghjisels, A.; Ente, J. J. S. M.; Raadsen, J. Int Polym Proc 1990, 5, 284.

14. Micic, P.; Bhattaqcharya, S. N.; Field, G. Int Polym Proc 1996, 11, 14.

15. Li, T. Q.; Wolcott, M. P. Compos A 2004, 35, 303.

16. Cogswell, F. N. Polymer Melt Rheology: A Guide for Industrial Practice; Godwin: London, 1981.

17. Sombatsompop, N.; Intawong, N.-T. Polym Test 2001, 20, 97.

18. Sombatsompop, N.; Panapoy, M. J Mater Sci 2000, 35, 6131.

19. Sombatsompop, N.; Patcharaphun, S. Polym J 2001, 33, 491.

20. Intawong, N.-T.; Sombatsompop, N. Polym Eng Sci 2004, 44, 1960.

21. Hinskena, H.; Mossb, S.; Pauqueta, J.-R.; Zweifela, H. Polym Degrad Stab 1991, 34(1-3),279.

22. Han, C. D. Rheology in Polymer Processing; Academic Press: New York, 1976.

23. Abad, M. J.; Ares, A.; Barral, L.; Cano, J.; Diez, F. J.; Garabal, S. G.; Lopez, J.; Ramirez, C. J Appl Polym Sci 2004, 9, 3910.

24. Baldi, F.; Francesschni, A.; Ricco, T. Rheol Acta 2007, 46, 965.

Melt Strength, Local Velocity, and Elongational Viscosity Profiles of Low-Density Polyethylene Filaments Affected by the Die Design and Process Conditions

Watcharin Sitticharoen,[1] Wanlop Harnnarongchai,[1] Naret Intawong,[2] Narongrit Sombatsompop[1]

[1]*Polymer Processing and Flow Group, Division of Materials Technology, School of Energy, Environment and Materials, King Mongkut's University of Technology Thonburi, Thongkru, Bangmod, Bangkok 10140, Thailand*
[2]*Department of Industrial Engineering, Faculty of Engineering, Rajamangala University of Technology Lanna, 128 Huay Kaew Road, Chiang Mai, 50300, Thailand*

ABSTRACT: An experimental arrangement to simultaneously measure the melt strength, velocity profiles, and elongational viscosity profiles across the cross section of a molten filament that emerged from either a circular or slit die for low-density polyethylene (LDPE) under nonisothermal and isothermal conditions is proposed. The proposed experimental rig was based on a parallel coextrusion technique of colored LDPE melt layers into an uncolored melt flowing from the barrel into and out of a die to form a continuous filament before they were pulled down by mechanical rollers until the filament failed. The experimental rig was also equipped with a high-speed data-logging system and a personal computer for real-time measurements. The results suggest that the draw-down forces changed continuously with changing roller speed, and the velocity profiles of the melt were not uniform across the LDPE filament during the stretching of the melt. Greater draw-down forces and local melt velocities were obtained in the slit die or under the nonisothermal condition. The draw-down forces and velocity profiles in both dies were affected by the volumetric flow rates from the extruder and the roller speeds used, with the effect being more pronounced for the circular die. The elongational viscosity profiles of the LDPE filament were not uniform across the filament cross section and corresponded well to the obtained velocity profiles. The elongational viscosities of the LDPE filament were relatively higher when the filament was extruded and stretched in the circular die and under the nonisothermal condition. The changes in the elongational viscosity profiles were more sensitive to changes in the volumetric flow rate and roller speed in the circular die. © 2011 Wiley Periodicals, Inc. J Appl Polym Sci 000: 000–000, 2011

Key words: mechanical properties; polymer extrusion; polyolefins; viscosity

INTRODUCTION

Melt spinning is a common process for generating molten polymer filaments and for measurements of melt properties under elongational deformation. The melt properties in this process are termed *melt strength, elongational stress*, and *strain* and *elongational viscosity*. Information on the elongational flow properties, extension force, and/or melt strength and melt viscosity is essential for understanding how the rheological behavior of polymer melts is greatly affected by the material properties (i.e., weight-average molecular weight, branching structure, and additives) and other process-related parameters, such as the volumetric flow rate, test temperature, roller speed and take-up style, draw ratio, ambient temperature, and die geometries.[1–11] Most polymers for elongational flow studies have been low-density polyethylene (LDPE),[4,8–10,11] linear low-density polyethylene (LLDPE),[4,7] high-density polyethylene,[1,3,4] polypropylene (PP),[2,4,5] and polystyrene.[4] Some polymer blends and composites have also been studied, including LLDPE/LDPE blends,[10,12–14] linear PP blends with long-chain-branched PP,[15] composite materials such as wood/thermoplastic composites,[16] wood/high-density polyethylene composites,[17] organoclay/polyamide 6 nanocomposites,[6] and carbon nanotube/polymers.[18] The die design and die temperature used for extruding the polymer melt also has a significant effect on the melt strength. Studies to improve the mechanical strength of polymer melts by materials modification[3,10–18] and die design.[2,5]

have also been proposed. Gupta and Bhattacharya[2] clearly suggested that the melt strength of PP increased with increasing die diameter, whereas the opposite effect was observed when the die length was increased. The extensional viscosity for PP under the nonisothermal condition was also found to be higher than that under the isothermal condition.[5]

One of the parameters that has been reported to affect the mechanical strength of polymer melts is the velocity gradient, which is usually determined under shear flow deformation.[19] The most widely used technique has been laser–Doppler velocimetry (LDV).[4,20,21] This technique is relatively accurate but very expensive, complicated to use, and not robust.[4,20–23] To measure the melt strength and velocity profiles of the melt under elongation deformation, a combination of at least two techniques is required. Wagner et al.[4] studied the local velocity and elongational viscosity of several polymer melts using LDV and Göttfert Rheotens and indicated that the local velocity distribution along the spin line increased to a concave form with increasing drawdown force. The reduction of the apparent elongational viscosity during the flow was due to a preshearing effect. Schneider et al.[20] investigated the velocity distribution along the axis of an LDPE melt strand extruded through an axisymmetric capillary die using the LDV technique. The results suggest that the strand velocity pull-down by a Rheotens did not increase linearly with increasing distance from the die exit. It was found that the acceleration of the strand increased monotonically, and the velocity near to the die exit decreased with the drawdown force used. A strain-hardening effect was observed for LDPE but not for LLDPE, and the velocity profiles generated in the channel of the slit die were parabolic in form, with the melt velocity being high in the middle of the slit channel and low near the die wall.[21] Kim et al.[24] studied the velocity profiles of poly(ethylene terephthalate) filaments within the spinneret orifice and along the spin line using the finite element method and found that the melt velocity at the exit of the die channel was increased to a plug flow in form. Intawong and Sombatsompop[19,25] investigated the radial velocity profile of the polystyrene melt in shear flow using a parallel coextrusion technique (PCT). The results indicate that the velocity profile generated in the capillary die was parabolic in shape. The radial velocity profiles of the melt changed continuously with extrusion time.

On the basis of the work by Intawong and Sombatsompop,[19,25] the velocities of the melt across the flow channel were different, although they would equalize as they exited the die. However, during free flow, the melt at the filament skin may encounter a cooling effect. This would probably cause a velocity gradient across the melt. If this was the case, the elongational strain would be an uneven elongational strain and elongational viscosity across the extruded filament. However, these kinds of information have not yet been fully discussed and understood, and this has become our interest.

To measure the local elongation viscosity profiles of the LDPE melt under elongational deformation, the draw-down forces and local velocity profiles across the cross section of the LDPE extruded filament during the spinning process had to be measured accurately. This study was carried out with an experimental rig that was specially designed and originally developed on the basis of PCT[19] to simultaneously measure the local velocity profiles and the melt strength of the LDPE. Two different die designs were used, circular and slit dies, for comparison purposes. In this work, the draw-down force was used as an indicator of the mechanical strength for the LDPE filament, and a relationship between the local velocity profiles and the local elongational viscosity profiles across the cross sections of the LDPE filaments extruded from either the circular or slit die were established and compared under nonisothermal and isothermal conditions through the effects of the volumetric flow rate and roller speed.
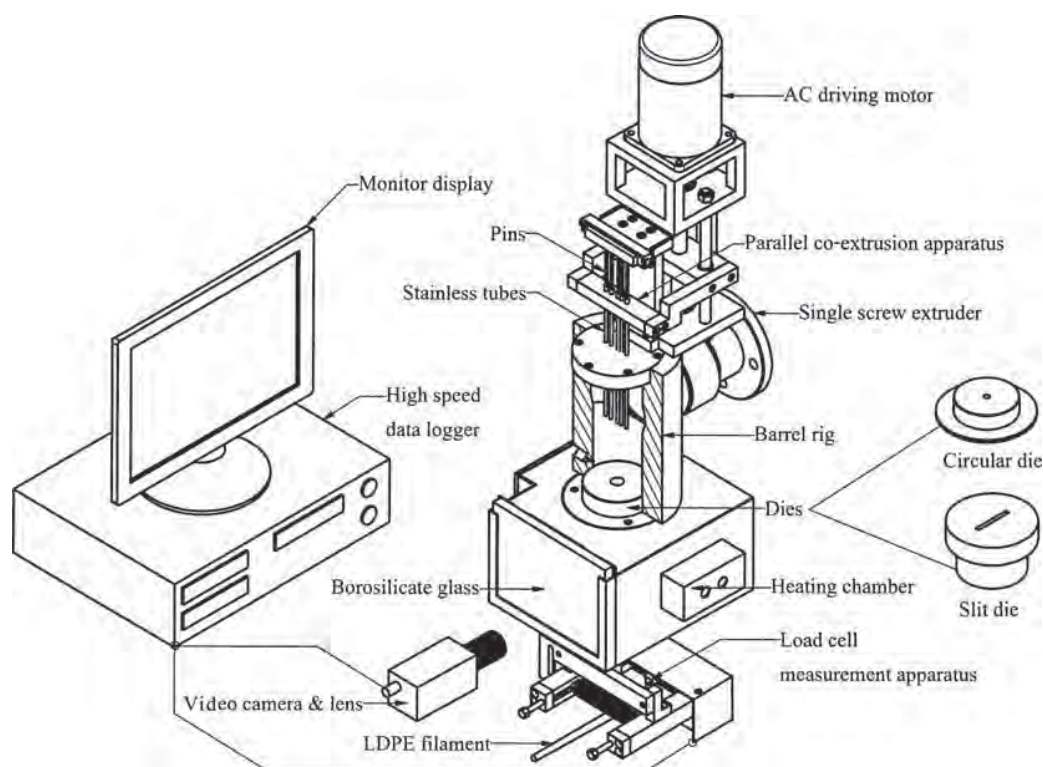
EXPERIMENTAL

Proposed experimental design and concept

In this work, PCT[19] was used for simultaneous measurements of the local velocity profiles and melt strength of an LDPE filament during a free-flow process (a melt-spinning process). The local melt velocity profile measurement via PCT was based on the parallel coextrusion of colored LDPE molten rods (layers) into an uncolored LDPE melt stream from the barrel into and out of the capillary die. The melt velocity profiles at local positions across the die diameter were then measured by the introduction of relatively light and small particles into the melt layers, and the times taken for the particles to travel for a given distance were measured. The melt strength in this study was referred to as the drawdown force measured during the stretching of the extruded LDPE. The draw-down force and the measured velocities measured across the cross section of the LDPE filament extruded from either the circular or slit die were then used to measure the elongational melt velocities across the filament cross section.

AQ7

Raw materials

LDPE (LD1905FA), with a melt flow rate of 5 g/10 min, was used a skin layer and was supplied by Thai Polyethylene Co., Ltd. (Bangkok, Thailand). On the basis of our previous work,[25] a red master batch (3.0%, Clariant Co., Ltd., Bangkok, Thailand) was used effectively

Figure 1 Experimental arrangement for the PCT for the measurement of the velocity profiles and melt strength of the LDPE filament.

for the colored LDPE core layers in the coextrusion process in the PCT. Corn particles (0.1 wt %) were used to follow the melt velocities in the colored LDPE core layer. The corn particles were relatively small, having an average particle size of 210 μm, and the maximum moisture content allowed was less than 5%.

Preparation of the LDPE colored layer rods

Neat LDPE and 3% red master batch were melt-blended in a single-screw extruder (En Mach Co., Ltd., Thailand) with a blending temperature profile on the extruder of 130, 140, 150, and 160°C from the hopper to die zones and a screw rotating speed of 10 rpm. A three-strand die, having a diameter of 3 mm for each strand and coupled with a palletizing unit, was used to produce the red LDPE pellets. The corn particles were dried to a constant weight to avoid any moisture during processing. Both the LDPE master-batched pellets and corn particles were held in an oven for 24 h at 80°C to avoid moisture before further processing. The experimental procedures to produce the red master-batch LDPE pellets with 0.1% corn particles can be found in our previous works.[19,25]

Experimental apparatus and procedures

PCT[19] coupled with roller take-up equipment, as given in Figure 1, was used for the measurements of the melt strength (as draw-down force) and the velocity profiles across the cross section of the LDPE filament. These two data sets could be used for the determination of the elongational viscosity profiles across the cross section of the LDPE filament. The experimental apparatus consisted of four parts: a single-screw extruder, an apparatus for measuring the melt strength, the PCT apparatus, and visualization equipment. The single-screw extruder (Thermo-haake model PolyDrive, Germany) was used to produce the molten LDPE rods. The length-to-diameter ratio of the barrel was 450/19 mm/mm, and the temperature profile on the extruder from the hopper to the die zones was 130, 140, 150, and 160°C. The circular die used in this work was 20 mm in length and 6 mm in diameter, and the slit die was 30 mm in width, 3 mm in height, and 30 mm in length. The melt strength measuring apparatus consisted of two principal parts: a load cell and a roller take-up device. The force, measured with a load cell, was measured in the range 0–444 cN. The roller or take-up speeds from 0 to 120 m/min were used to wind the molten filament. The parallel coextrusion apparatus involved coextrusion of the colored layer of the LDPE melt in the stainless tubes into the uncolored melt flowing into the barrel when all of the stainless tubes moved upward by a moving arm. The details of this technique were discussed elsewhere.[19] The visualization equipment was used to
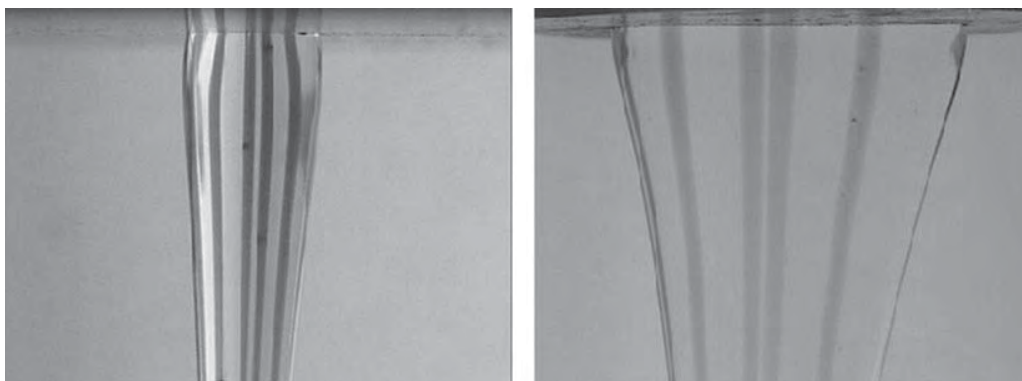
Figure 2 Flow visualization results for colored LDPE layers flowing in the LDPE filament at the die exit under stretching conditions: (a) circular die and (b) slit die. [Color figure can be viewed in the online issue, which is available at wileyonlinelibrary.com.]

assist in monitoring the colored layers of the LDPE melt and the corn particles within the colored layers for the velocity profile measurements across the cross section of the LDPE filament. Figure 2 shows the flow visualization of the colored LDPE layers flowing within the LDPE filament with circular and slit dies during the stretching of the melt at the die exit region. Because this work used corn particles as foreign objects to follow the velocity of the LDPE melt and LDPE master batch for coextrusion, it was essential to determine whether the corn particles and the LDPE master batch affected the flow properties of the LDPE melt. Figure 3 shows the results of the apparent wall shear stress and apparent wall shear rate for the LDPE melts with and without additions of corn particles and the LDPE master batch at 160°C. It was found that the flow curves for both LDPE systems were very similar, with the differences being within an experimental error of ±4.9%. It was, therefore, confirmed that the corn particles and the master batch did not affect the flow properties of the molten LDPE.

In this work, the measurements of melt strength (as draw-down force), velocity profiles, and elongational viscosity profiles across the cross section of the LDPE filament were carried out under nonisothermal and isothermal conditions. The nonisothermal condition refers to the condition where the filament was cooled down by ambient air, and the isothermal condition refers to the condition in which the temperature of the filament was controlled by a heating chamber, which was made of stainless steel (grade SUS304) and the front of the chamber was made with borosilicate glass. The heating chamber used two infrared heaters (500 W, 220 V) and a DD6 temperature controller system. The temperature of the heating chamber was constant along the chamber length, with the differences being within an error of ±2.5°C.

Calculations of the local velocity profiles and local elongational viscosities

We carried out and monitored the velocity profile measurements by recording the times taken for the corn particles in the LDPE core layers to travel a given distance (25–50 mm from the die exit) in the LDPE filament. All of the experimental data were recorded and displayed with a high speed data-logging and recording system and a personal computer. The average melt velocity (v_n) of each colored layer across the cross section of the LDPE filament at the reduced radius (r/R) position for the circular die and reduced width (w/W) for a slit die could be calculated with eq. (1)

$$v_n = \frac{L_0}{t_c} \qquad (1)$$
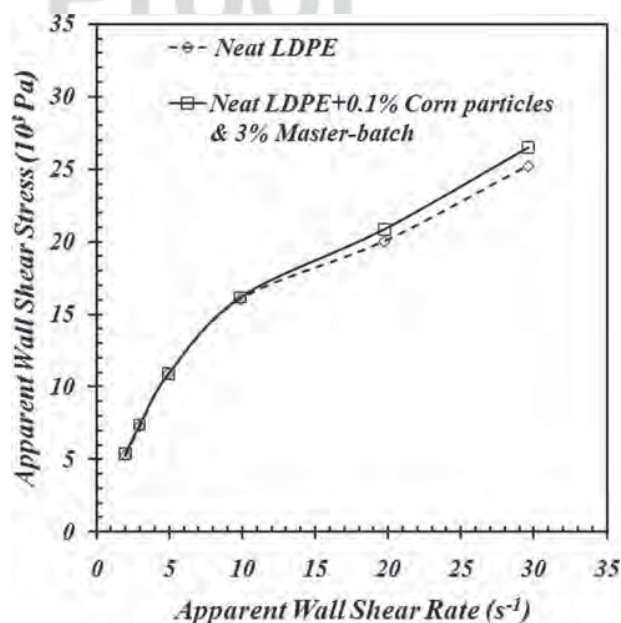
Figure 3 Flow curves for the molten LDPE with and without the corn particles and the LDPE master batch at a die temperature of 160°C.

TABLE I
Temperature Profiles under the Nonisothermal and Isothermal Conditions for the Circular Die at a Die Temperature of 160°C

Distance from the die exit (mm)	Temperature profile (°C)	
	Nonisothermal	Isothermal
5	120	160
25	107	162
50	84	161
60	76	156
75	67	137

where L_0 is the observed length of the measurement of 25×10^{-3} m for the circular die and 30×10^{-3} m for the slit die and t_c is the time that corn particle travels through L_0. Thus, the elongational viscosity (λ) is expressed by eq. (2):[1,6]

$$\lambda = \frac{FL}{Q\varepsilon_E} \qquad (2)$$

where F is the average draw-down force with increasing step-ladder roller speeds, L is the length of the spin line, and ε_E is the elongational strain, which is defined as $\ln(v_n/v_0)$, and v_0 is the melt velocity at the die exit. The viscosities for the LDPE melt were calculated with the melt velocities at any point across the filament diameters. The local elongational viscosities (λ_n) were calculated with the melt velocities, and the volumetric flow rate (Q) at any radial point across the LDPE filament diameter for the circular die is expressed by eq. (3), where r is the radius of each colored layer at the r/R position across the filament diameter and dr is the differentiate radius of each colored layer at the r/R position across the LDPE filament diameter:

$$\lambda_n = \frac{FL}{(2\pi r dr v_n) \times \ln\left(\frac{v_n}{v_0}\right)} \qquad (3)$$

The local elongational viscosities across the filament cross section for the slit die is given by eq. (4):

$$\lambda_n = \frac{FL}{(WHv_n) \times \ln\left(\frac{v_n}{v_0}\right)} \qquad (4)$$

where W is the thickness of the colored melt layer at each w/W position and H is the thickness of the LDPE filament.

Test variables

In this work, the test variables of interest included the volumetric flow rate and roller speed. The volu-

metric flow rate was varied from 4.5×10^{-8} to 9.0×10^{-8} m³/s for the circular die and from 2.0×10^{-7} to 2.7×10^{-7} m³/s for the slit die. It should be noted that there were two main reasons we did not use the same volumetric flow rates for the two dies. First, the geometries and dimensions of these two dies were different and on the basis of the volumetric flow rate calculations in eqs. (3) and (4), the volumetric flow rates obtained were expected to be different, even though one used the same screw-rotating speed. Second, the volumetric flow rate used for each die was deliberately selected and used so that the coextrusion process for the velocity profile measurement in each die was clearly visualized and accurate. The lengths of the spin line were fixed at 310 mm for the circular die and 295 mm for the slit die. The test temperature for the circular and slit dies was fixed at 160°C. The temperature profiles of the LDPE melt along the spin line under nonisothermal and isothermal conditions for the circular and slit dies are given in Tables I and II, respectively. It should be noted that the interesting filament temperature profiles were the same as those used for the velocity profile measurements, which were 25–50 mm away from the die exit. All of the reported experimental data are averages of at least five independent determinations.

T1 T2

RESULTS AND DISCUSSION

The main aim of this work was to study the effect of die geometry design and spinning process parameters (volumetric flow rate, take-up or roller speed, and isothermal condition) on the local elongational viscosity profiles across the cross section of the LDPE filament in a single-screw extruder with two different die geometries. On the basis of eqs. (3) and (4), to measure such local elongational viscosity profiles of the melt in the screw extruder with circular and slit dies, respectively, the draw-down forces and local velocity profiles across the cross section of the LDPE filament during the melt-spinning process were experimentally required.

TABLE II
Temperature Profiles under the Nonisothermal and Isothermal Conditions for the Slit Die at a Die Temperature of 160°C

Distance from the die exit (mm)	Temperature profile (°C)	
	Nonisothermal	Isothermal
5	120	164
25	104	165
50	86	160
60	76	156
75	68	136
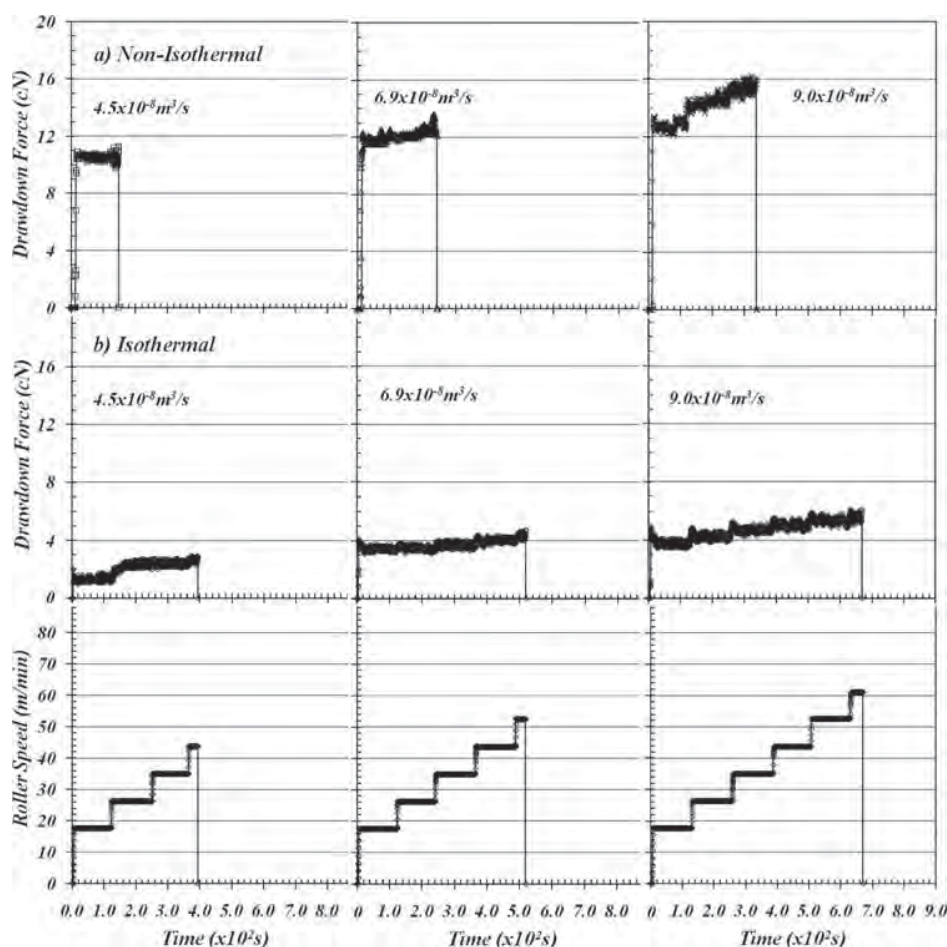
Figure 4 Draw-down force versus time as a function of the roller speed for the LDPE extrudate filament emerging from a circular die for three different volumetric flow rates: (a) nonisothermal filament stretching and (b) isothermal filament stretching.

Effects of the die geometry design and process parameters on the draw-down forces

F5 F4 Figures 4 and 5 show the draw-down force against extrusion time with increasing step-ladder roller speeds for the LDPE molten filament emerging from the circular and slit dies under nonisothermal and isothermal conditions for three different volumetric flow rates. The results indicate that the draw-down forces of the LDPE melt from the circular and slit dies sharply increased at the very beginning of the roller speed take-up and then gradually increased at further increasing roller speeds until the LDPE molten filament eventually failed. The changes in the draw-down forces with roller speed effect could be explained by the molecular entanglements and long-chain branching of LDPE, as detailed in our previous works.[8–10] For the effect of the volumetric flow rate from the extruder, it was found that the higher the volumetric flow rate was, the greater was the draw-down force that was required. The molten filament with a higher volumetric flow rate tended to generate

greater stored energies in the molten polymer, and this enhanced the draw-down force. This claim was supported by the works of Baldi et al.[1] and Gupta and Bhattacharya[2] and our previous works.[8–10]

For the effect of die design, we found that the draw-down force of the LDPE molten filament from the circular die at any given volumetric flow rate under nonisothermal and isothermal conditions were lower than that in the slit die. This was because the output rates in the slit die were greater than those in the circular die at the same screw rotating speed from the extruder. However, the roller speed to failure of the molten filament from the circular and slit dies at any volumetric flow rate were the same. Comparing the results between Figures 4(a,b) and 5(a,b), we noticed that for any given roller speed, the draw-down forces for the molten filament from the circular and slit dies under the nonisothermal condition were greater than those for the isothermal condition. This was caused by the fact that the molten filament under the nonisothermal condition tended to solidify during filament
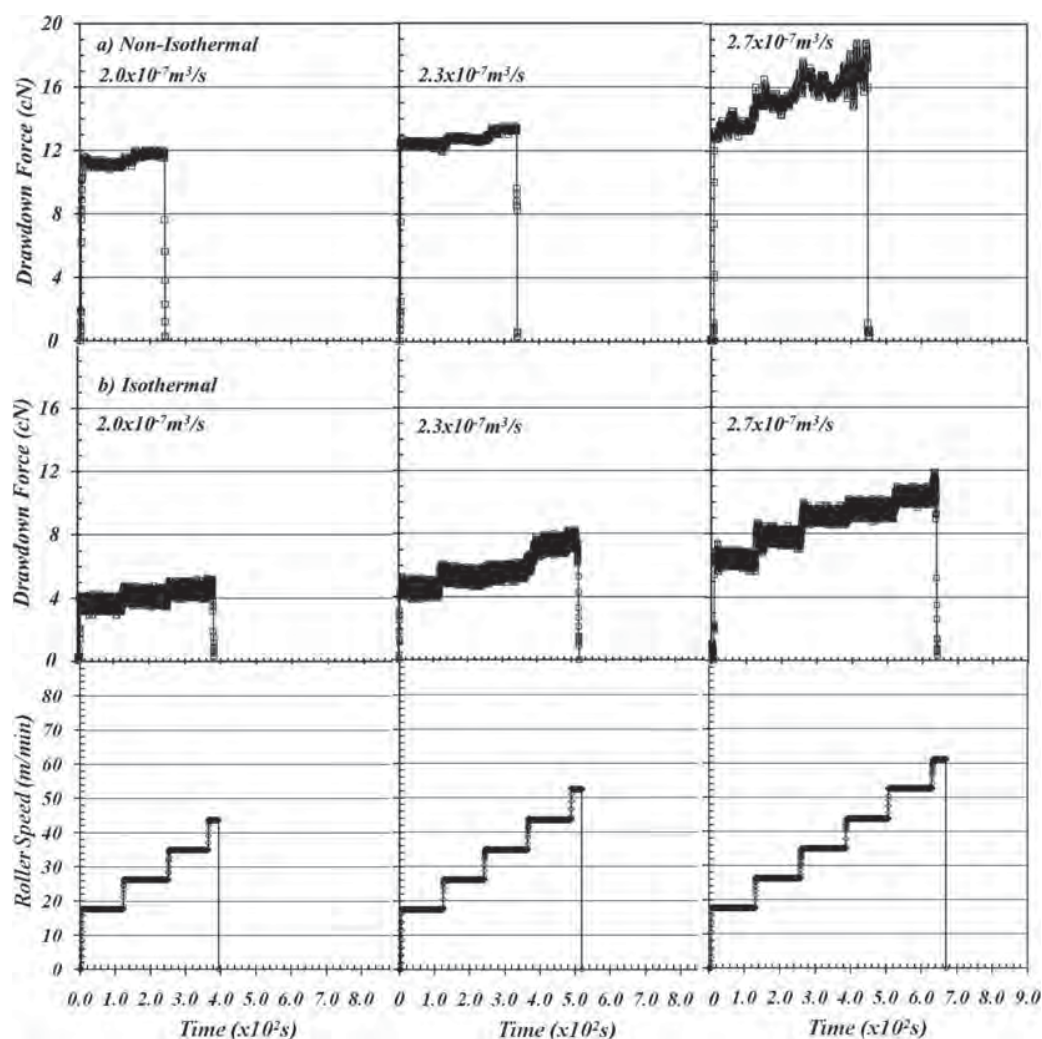
Figure 5 Draw-down force versus time as a function of the roller speed for the LDPE extrudate filament emerging from a slit die for three different volumetric flow rates: (a) nonisothermal filament stretching and (b) isothermal filament stretching.

stretching, especially on the surface of the molten filament, and this then led to a significant increase in the filament viscosity and, thus, increased draw-down forces. The elongational strains (or roller speed to failure) for the molten filaments from the circular and slit dies under the isothermal condition was greater than those under the nonisothermal condition. This may have been expected because the melt viscosity of the molten filament under the isothermal condition was lower and was not restricted by the cooling effect;[8,10,25] this allowed the molecular chains to slide past one another.

### Effects of the die geometry design and process parameters on the local velocity profiles

Unstretched molten filament

F6 Figure 6 shows the melt velocity profiles as a function of r/R position across the diameter for the

LDPE molten filament under the nonisothermal and isothermal conditions without stretching by the rollers, and Figure 7 shows the velocity profiles as a   F7
function of w/W across the cross section for the LDPE molten filament under the nonisothermal and isothermal conditions without stretching by the rollers for three different volumetric flow rates. It was found that the velocity profiles of the molten filament from the circular die were pluglike, with the melt velocities across the filament diameters being very similar. This was expected, as the melt flowed in the die and exited the die lip; the explanations were given elsewhere.[24,25] The velocity profiles of the LDPE melt that emerged from the slit die were pluglike for the unstretched melt condition under the isothermal condition, but the velocities of the melt under the nonisothermal condition were relatively low near the edge of the filament strand. This was due to the cooling effect under the
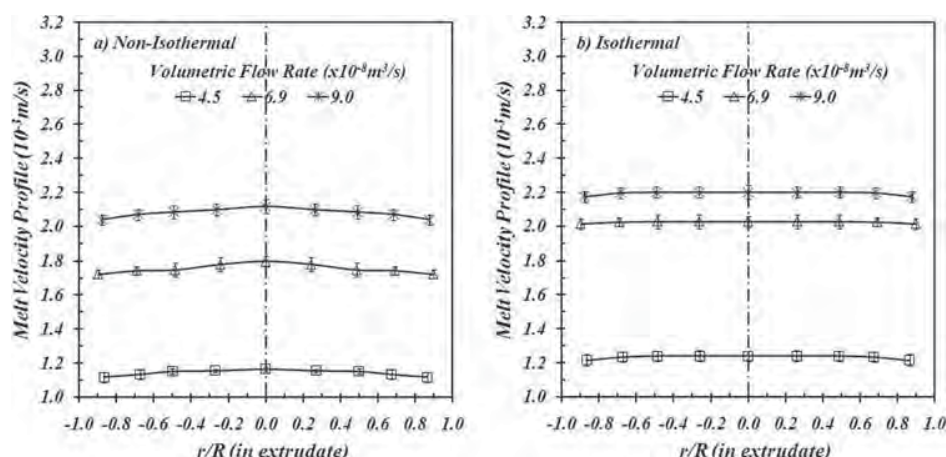
Figure 6 Melt velocity profiles for the LDPE filament emerging from a circular die without filament stretching for three different volumetric flow rates: (a) nonisothermal condition and (b) isothermal condition.

nonisothermal condition, as mentioned earlier. During free flow, the melt skin may have encountered cooler surroundings, and this would have probably caused the velocity gradient across the molten filament. However, the velocity gradients due to the cooling effect in the nonisothermal condition for the slit die was more pronounced than those for the circular die because of the relatively smaller width (3 mm) of the slit die as compared with the diameter (6 mm) of the circular die. The greater the volumetric flow rate from the extruder was, the higher the melt velocities were across the cross section of the molten filament for both die systems. For a given volumetric flow rate, the melt velocities for the molten filament under the isothermal and nonisothermal conditions for both die systems were slightly different, with the differences being within an experimental error of ±2.5%. However, the melt velocity profiles from the slit die under nonisothermal and isothermal conditions were greater than those of the

circular die, again due to the fact that higher volumetric flow rates were obtained for any given screw speed from the extruder. In addition, during the experiment, the melt extruded from the circular die had greater swelling than that from the slit die; this indicated some transverse flow direction of the melt and/or a lower melt velocity in the axial flow direction. Greater swelling of the LDPE melt by the circular die relative to the slit die was also found in our previous work.[26]

Stretched molten filament

Figure 8 shows the melt velocity profiles as a function of r/R position across the diameter for the LDPE molten filament under nonisothermal filament stretching with increasing step-ladder roller speeds, and Figure 9 shows the melt velocity profiles as a function of w/W position across the cross section for the LDPE molten filament from the slit die under
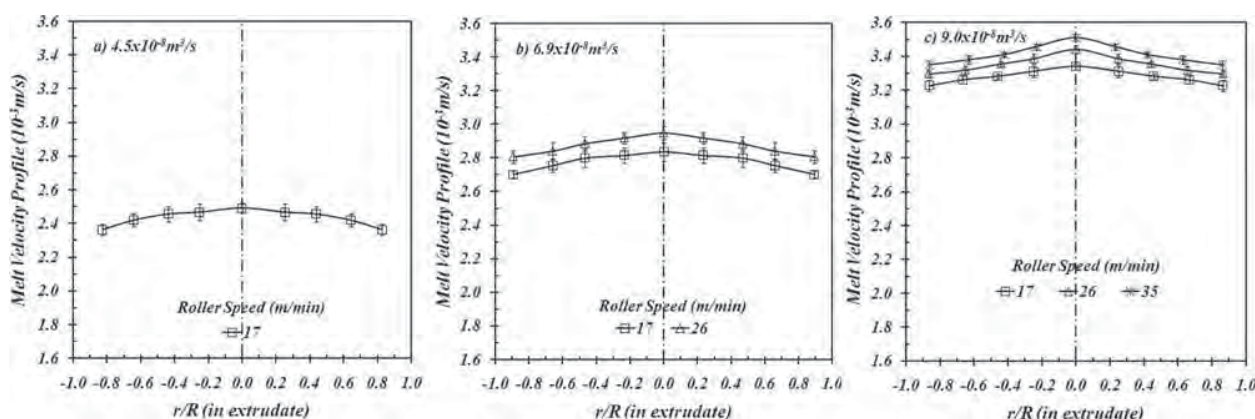
F8

F9
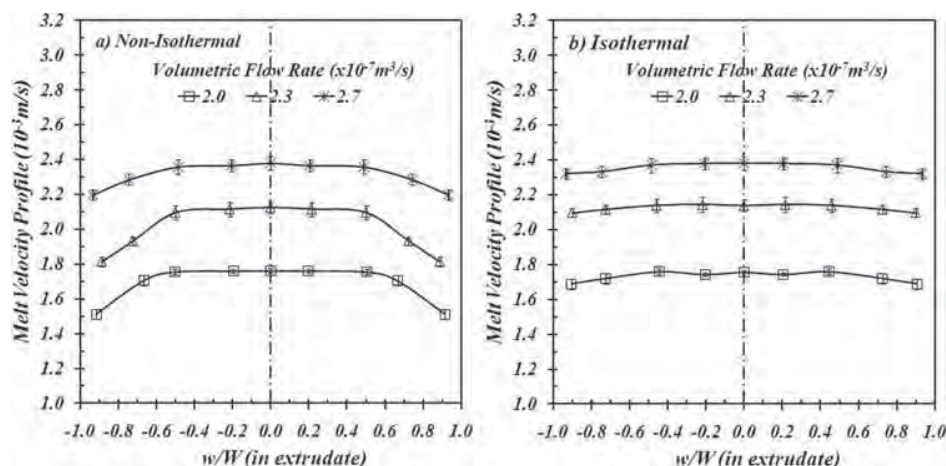
Figure 7 Melt velocity profiles for the LDPE filament emerging from a slit die without filament stretching for three different volumetric flow rates: (a) nonisothermal condition and (b) isothermal condition.
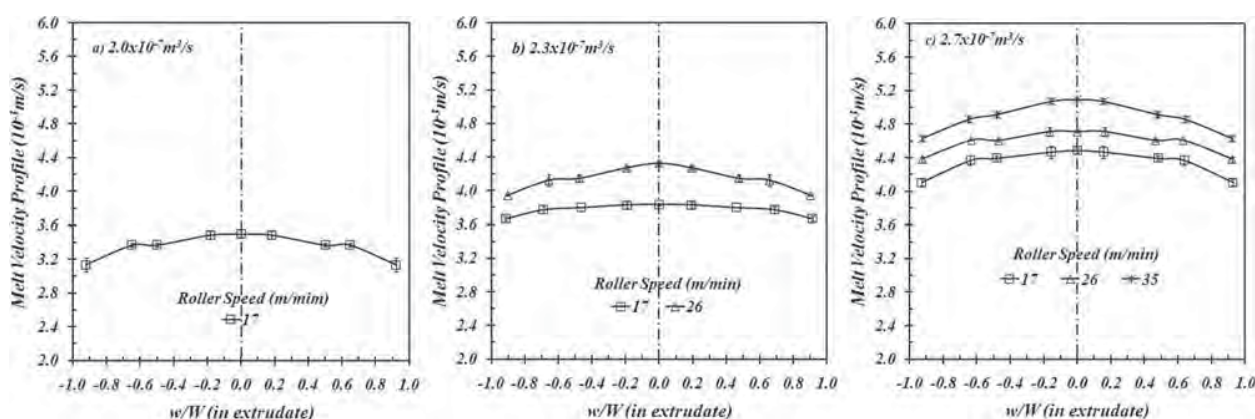
Figure 8 Melt velocity profiles for the LDPE filament from a circular die under nonisothermal filament stretching with increasing step-ladder roller speeds for three different volumetric flow rates: (a) 4.5×10^{-8}, (b) 6.9×10^{-8}, and (c) 9.0×10^{-8} m^3/s.
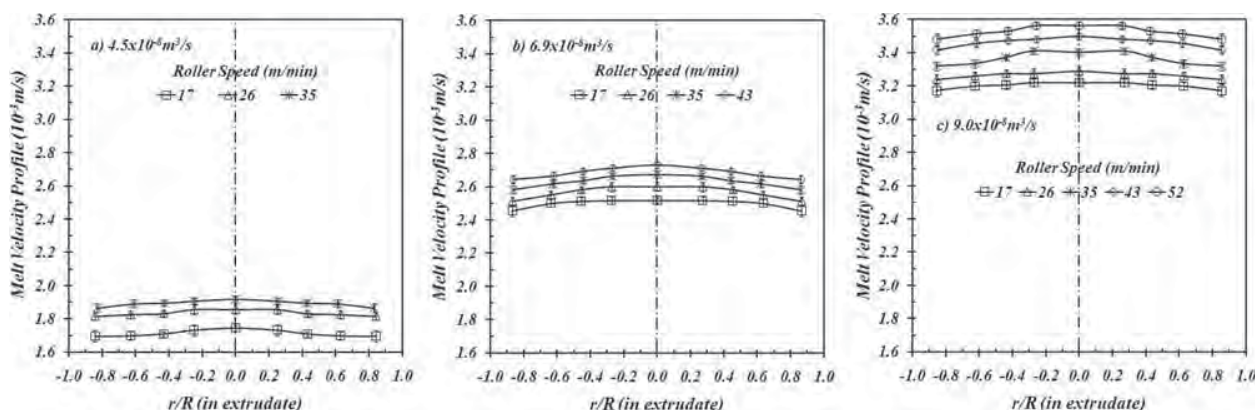
nonisothermal filament stretching with increasing step-ladder roller speeds for three different volumetric flow rates. It was observed that for a given volumetric flow rate, the velocity profiles of the molten polymer for both die systems decreased with increasing r/R position for the circular die and w/W position for the slit die, with a high melt velocity at the center position of the molten filament and a low melt velocity near the edge of the filament strand. The number of roller speeds used for each volumetric flow rates in the velocity profile measurements corresponded to those in the draw-down force measurements, as given in Figures 4 and 5. As the roller speed increased, the melt velocities at any radius/width point across the cross section of the molten filament increased. This view was supported by the work of Meerveld et al.,[27] who stated that the velocity profiles along spin line increased with increasing roller-speed take-up velocity. The melt velocities for both die systems also increased with increasing volumetric flow rate. It was interesting to note that the

roller speed to failure for both die systems increased with increasing volumetric flow rate; that is, the filament at volumetric flow rates of 4.5×10^{-8} m^3/s for a circular die and 2.0×10^{-7} m^3/s for a slit die failed at a take-up speed of 26 m/min, whereas that at the volumetric flow rates of 9.0×10^{-8} m^3/s for a circular die and 2.7×10^{-7} m^3/s for a slit die failed at a take-up speed of 43 m/min. This was associated with the increased stored energies within the filaments during the extrusions with higher volumetric flow rates.

The results of local velocity profiles under the isothermal stretching condition for the circular and slit dies as a function of the volumetric flow rate and roller speed are given in Figures 10 and 11, respectively. The general patterns of the melt velocity profiles as a function of r/R/w/W position, volumetric flow rate, and roller speed for both die systems were very similar to those in the nonisothermal stretching condition, as given in Figures 8 and 9. However, two differences were noted for both die

AQ7

F10 F11

Figure 9 Melt velocity profiles for the LDPE filament from a slit die under nonisothermal filament stretching with increasing step-ladder roller speeds for three different volumetric flow rates: (a) 2.0×10^{-7}, (b) 2.3×10^{-7}, and (c) 2.7×10^{-7} m^3/s.
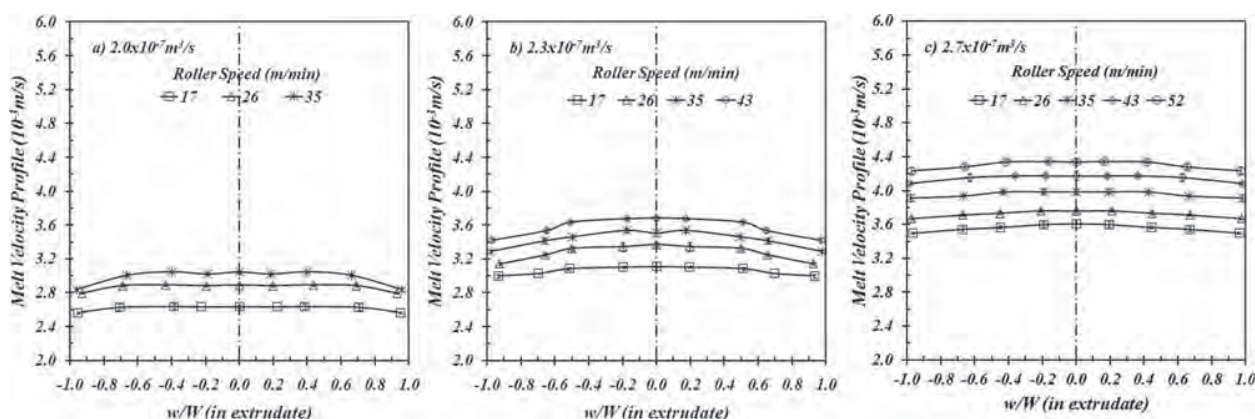
Figure 10   Melt velocity profiles for the LDPE filament from a circular die under isothermal filament stretching with increasing step-ladder roller speeds for three different volumetric flow rates: (a) 4.5×10^{-8}, (b) 6.9×10^{-8}, and (c) 9.0×10^{-8} m^3/s.

systems. First, the roller speeds to failure for any given volumetric flow rate between the nonisothermal and isothermal stretching conditions were different. The roller speed to failure for the isothermal stretching condition was higher than that for the nonisothermal one; this was probably related to the lower melt viscosity of the isothermal filament, which facilitated the molecular disentanglement during the flow. This could be supported by lower draw-down forces during the isothermal stretching condition, as noted by Figures 4 and 5. Second, for any given roller speed (e.g., 17–35 m/min for the volumetric flow rate of 9.0×10^{-8} m^3/s for the circular die and 2.7×10^{-7} m^3/s for the slit die), the velocity profiles for the nonisothermal filament were sharper, with the differences in the melt velocities at different $r/R/w/W$ positions being more obvious. This difference was caused by the cooling effect under the nonisothermal condition, as already discussed.

Having taken all the conditions into account, we observed that the melt velocity profiles from the slit die were greater than those from the circular die because of the higher volumetric flow rate from the extruder. It should be noted that direct comparisons of the velocity profiles obtained by these two dies for any given flow rate were not intended to be made because the volumetric flow rates obtained from these two dies were different. The reasons for using different volumetric flow rates were already mentioned in the Experimental section. One interesting point to mention was that during the experiment, we observed that for any given die geometry, volumetric flow rate, or roller speed, the melt extruded in the isothermal condition had greater swelling than that in the nonisothermal condition. The greater swelling ratio of the melt in the isothermal condition indicated some transverse flow direction of the melt, and this would have caused a lower velocity of the melt in the axial flow direction (comparing Fig. 8 with Fig. 10 and Fig. 9 with Fig. 11). This may have been one of the main reasons why the melt velocities for both die geometries under the

Figure 11   Melt velocity profiles for the LDPE filament from a slit die under isothermal filament stretching with increasing step-ladder roller speeds for three different volumetric flow rates: (a) 2.0×10^{-7}, (b) 2.3×10^{-7}, and (c) 2.7×10^{-7} m^3/s.
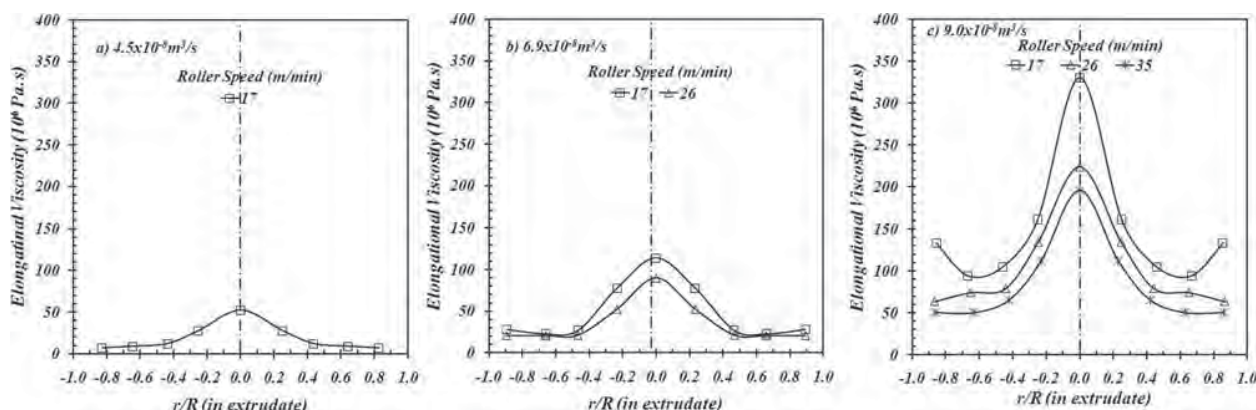
Figure 12 Elongational viscosity profiles for the LDPE filament flowing from a circular die under nonisothermal stretching for three different volumetric flow rates: (a) 4.5×10^{-8}, (b) 6.9×10^{-8}, and (c) 9.0×10^{-8} m^3/s.

isothermal condition were lower than those in the nonisothermal condition. At this point, we concluded that the melt velocity profiles across the cross section of the molten filament extruded through the circular and slit dies were affected by the temperature profiles of the filament, which were referred to as the nonisothermal and isothermal conditions during filament stretching. More obvious differences in the melt velocity profiles across the molten filament were observed for the nonisothermal filament stretching condition. If this was the case, one would expect, on the basis of eqs. (3) and (4), to have different elongational viscosities across the cross section of the molten filament.

Local elongational viscosity profiles

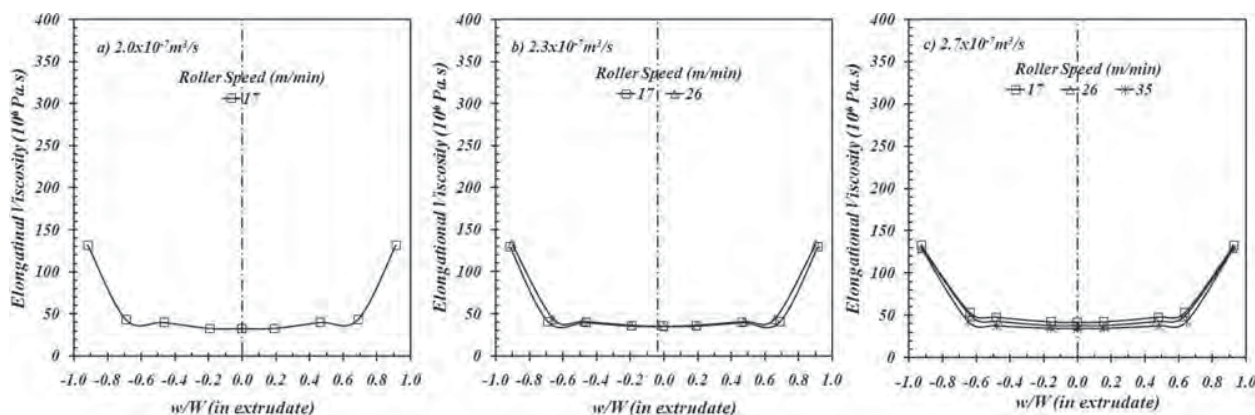### Nonisothermal stretching condition

In this section, we discuss the local elongational viscosity profiles across the LDPE filament diameter, which were derived and calculated, on the basis of eqs. (3) and (4), from the draw-down forces and velocity profiles with filament stretching conditions; this are given and discussed in Figures 4 and 5 and 8–11. The elongational viscosity profiles as a function of the r/R position of the LDPE filament for the circular die under the nonisothermal filament stretching condition with three different volumetric flow rates are given in Figure 12. It was found that the elongational viscosities of the molten LDPE were not uniform across the cross section of the filament diameter. The elongational viscosity appeared to decrease with increasing r/R position; it was high at the center position of the filament diameter and low near the edge of the LDPE filament. These uneven viscosities across the LDPE filament cross section seemed to be more pronounced for low roller speeds and high volumetric flow rates [see Fig. 12(c)]; this occurred because of the increased melt velocities at

the filament center with increasing volumetric flow rate and roller speed, as noted in Figure 8. Another reason for the decreases in the melt viscosities of the melt as the roller speed increased was the shear heating effect,[28,29] although the melt experienced and was dominated by elongational deformation.[8,9]

An opposite result of the elongational viscosity profiles was given when the slit die was used to extrude the LDPE melt. Figure 13 shows the elongational viscosity profiles as a function of the w/W position across the cross section of the LDPE melt stretched from the slit die under the nonisothermal condition with three different volumetric flow rates. It was again observed that the elongational viscosities of the molten LDPE were not uniform across w/W of the filament; that is, the elongational viscosity profiles around the center of the melt were flat and sharply increased near the edge of the melt. The exceptionally high elongational viscosity at the filament edge was probably caused by an obvious drop in the melt velocities at this region, as shown in Figure 9. Other differences in the viscosity profiles of the LDPE filament between the circular and slit dies were the sensitivities to the volumetric flow rate and roller speed effects. It was observed that the elongational viscosity profiles of the LDPE filament from the slit die, as shown in Figure 13, were unaffected by the volumetric flow rate and roller speed effects. On the basis of the results in Figures 5 and 9, this could be reasoned by balanced or equal increases in the draw-down forces and local melt velocities with changing volumetric flow rates and roller speeds.

It would be interesting to discuss and compare the differences in the elongational viscosity profiles from the circular and slit dies in terms of the effect of temperature gradients across the molten filaments. It was clearly noted by the experimental setup that the half-width (1.5 mm) in the slit die, in which the heat transfer across the filament occurred, was relatively smaller than the radius (3 mm) of the
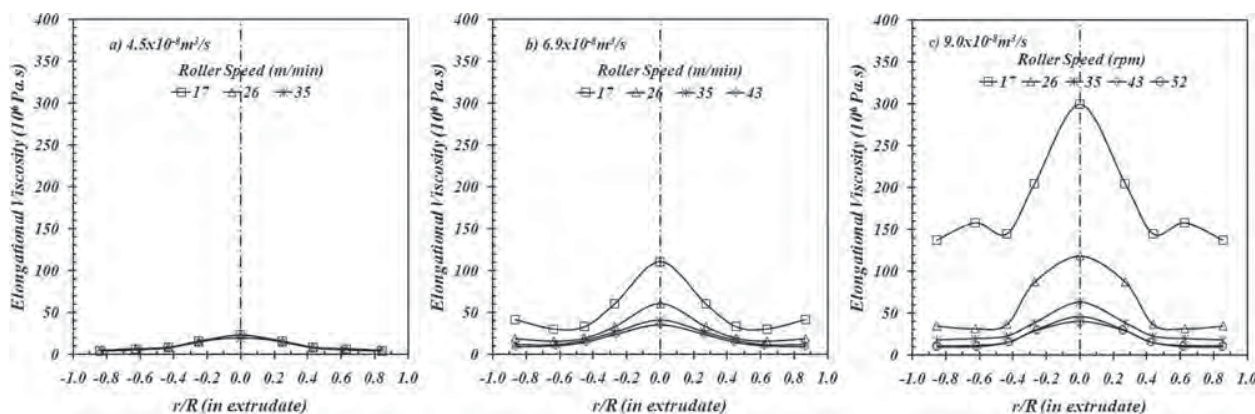
F12

F13

Figure 13   Elongational viscosity profiles for the LDPE filament flowing from a slit die under nonisothermal stretching for three different volumetric flow rates: (a) 2.0×10^{-7},(b) 2.3×10^{-7}, and (c) 2.7×10^{-7} m^3/s.

circular die. Therefore, the heat-transfer effect, which caused the filament to cool down (warmer), in the slit die would expected to be higher. This why the increases in the elongational viscosity around the die edge (wall) in the slit die were obvious. In the case of the circular die, the cooling effect was suppressed by the effect of the annular cross-sectional area that was used in the elongational viscosity calculations in eq. (3). That was, for a given dr, the area of the cross section ($2\pi r dr$) around the center was much lower than that near the die wall. When this was the case, on the basis of eq. (3), the elongational viscosity at the die center would increase, as observed in Figure 12.
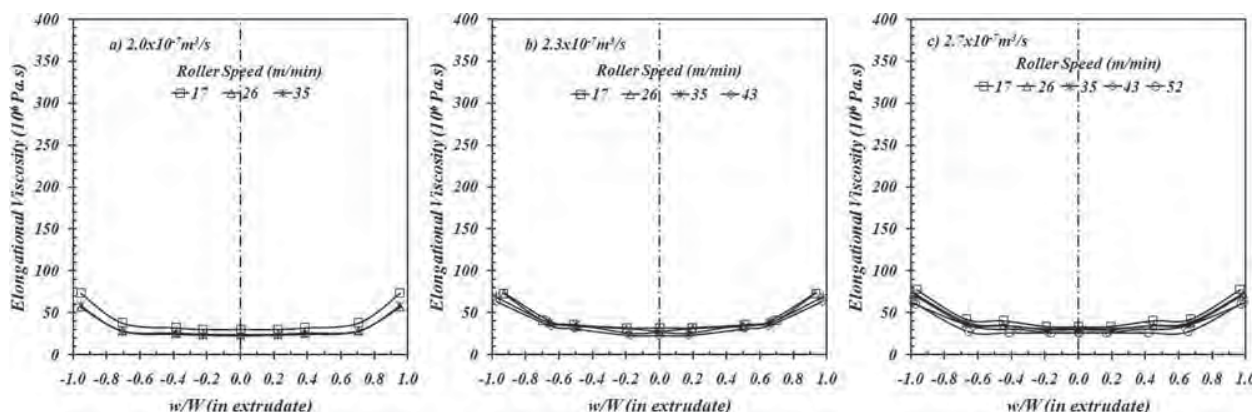
Isothermal stretching condition

The elongational viscosity profiles as functions of the r/R position in the circular die and the w/W position in the slit die for the LDPE filament are F15 F14 given in Figures 14 and 15, respectively, under the isothermal stretching condition for three different volumetric flow rates. Having compared the noniso-

thermal condition results in Figures 12 and 13, we found that the general viscosity profiles were similar, but for any specific volumetric flow rate or roller speed, the elongational viscosities of the LDPE melt under the nonisothermal stretching condition were greater than those under the isothermal condition. This statement was found to be true and more pronounced in the circular die. For example, the elongational viscosity of the LDPE melt under the nonisothermal stretching condition (Fig. 12) at a volumetric flow rate of 9.0×10^{-8} m^3/s with a take-up speed of 26 m/min was 220×10^6 Pa s, whereas that under the isothermal stretching condition (Fig. 14) under the same volumetric flow rate and roller speed was 115×10^6 Pa s. However, it was observed that the differences in the elongational melt viscosities in the case of the slit die between the isothermal and nonisothermal stretching conditions were only obvious at the edge region of the LDPE filament, with the viscosity values being about 130×10^6 Pa s for the nonisothermal condition and around $60–80 \times 10^6$ Pa s for the isothermal condition. The greater elongational viscosity for the nonisothermal condition

Figure 14   Elongational viscosity profiles for the LDPE filament flowing from a circular die under isothermal stretching for three different volumetric flow rates: (a) 4.5×10^{-8},(b) 6.9×10^{-8}, and (c) 9.0×10^{-8} m^3/s.

Figure 15 Elongational viscosity profiles for the LDPE filament flowing from a slit die under isothermal stretching for three different volumetric flow rates: (a) 2.0×10^{-7}, (b) 2.3×10^{-7}, and (c) 2.7×10^{-7} m^3/s.

corresponded very well to the findings by Muke et al.[5] One interesting aspect to note was that the elongational viscosity of the LDPE melt extruded and stretched from the circular die for any given roller speed was greater than those from the slit die. This may have been related to the higher draw-down forces and local melt velocities of the LDPE filament in the slit die, which tended to generate more shear heating effects to the melt stream and, thus, resulted in lower elongational melt viscosities in the slit die system. If this was the case, the LDPE melt in this work did not experience the strain-hardening effect during the stretching process during the experiment. This may have been because the strain rates used in this work ranged between 0.1–1.0 s^{-1}, which significantly exceeded the tension-thickening range, which has been reported to be around 10^{-3} to 10^{-1} s^{-1}.[30] Work by Padmanabhan and Macosko[31] investigated the elongational viscosity for the LDPE melt with Cogswell's analysis and suggested that the LDPE could exhibit a tension-thickening behavior only at low strain rates (ca. 10^{-1} s^{-1}).

It was also expected that for any given volumetric flow rate, the roller speed to failure for the isothermal stretching condition would be greater than that for the nonisothermal stretching condition because of the facilitating effect to the sliding molecular chains of LDPE, as mentioned earlier. This was also the case for both die design systems. The effects of the volumetric flow rate and the roller speed on the elongational viscosity profiles were found to be large with the circular die and very small for the slit die, with the latter case being related to the balanced increasing effects of the draw-down forces and melt velocities, as already discussed.

CONCLUSIONS

PCT was used successfully for simultaneous measurements of the draw-down forces (melt strength),

local velocity profiles, and elongational viscosity profiles across of molten LDPE filament from either a circular or slit die under nonisothermal and isothermal conditions. The following experimental results were noted:

- The draw-down forces from both dies sharply increased at the beginning of the roller speed and then leveled off for further increasing roller speeds until the LDPE molten filament failed. The higher the volumetric flow rate was, the greater was the draw-down force that was required. For any given volumetric flow rate or roller speed, the draw-down forces in the circular die were lower than that in the slit die, and the draw-down forces under the nonisothermal condition were greater than those for the isothermal condition.

- The velocity profiles of the melt were equalized at the die exit under the no-stretching condition but were not uniform when the melt was stretched. The melt velocities at any local point across the filament cross section appeared to increase with increasing volumetric flow rate and roller speed. The overall melt velocities in the slit die and under the nonisothermal condition were greater than those in the circular die and under the isothermal condition.

- The elongational viscosity profiles of the LDPE were not uniform across the cross section of the filament; this was pronounced when the circular die, low roller speeds, and high volumetric flow rates were used. The elongational viscosities of the LDPE melt extruded and stretched from the circular die ad under the nonisothermal condition were greater than those from the slit die and under isothermal stretching condition. The effects of the volumetric flow rate and the roller speed on the elongational viscosity profiles

were large with the circular die and rather small with the slit die.

References

1. Baldi, F.; Franceschini, A.; Riccò, T. Rheol Acta 2007, 46, 965.
2. Gupta, R. K.; Bhattacharya, S. N. J Polym Eng 2007, 27, 89.
3. Yamaguchi, M.; Suzaki, K.-I. J Appl Polym Sci 2002, 86, 79.
4. Wagner, M. H.; Bastian, H.; Bernnat, A.; Kurzbeck, S.; Chai, C. K. Rheol Acta 2002, 41, 316.
5. Muke, S.; Ivanov, I.; Kao, N.; Bhattacharya, S. N. J Non-Newt Fluid Mech 2001, 101, 77.
6. Baldi, F.; Franceschini, A.; Bignotti, F.; Tieghi, G.; Riccò, T. Rheol Acta 2009, 48, 73.
7. de Jeśus, T.; Guadarrama-Medina, T. J.; Pérez-González, J.; de Vargas, L. Rheol Acta 2005, 44, 278.
8. Sitticharoen, W.; Intawong, N.-T.; Sombatsompop, N. Polym Polym Compos 2010, 18, 359.
9. Harnnarongchai, W.; Intawong, N.-T.; Sombatsompop, N. J Macromol Sci Phys 2011, 50, 1074.
10. Harnnarongchai, W.; Sitticharoen, W.; Intawong, N.-T.; Sombatsompop, N. J Vinyl Addit Technol, to appear.
11. Wei, X.; Collier, J. R.; Petrovan, S. J Appl Polym Sci 2007, 104, 1184.
12. Wagner, M. H.; Kheirandish, S.; Yamaguchi, M. Rheol Acta 2004, 44, 198.
13. Pérez, R.; Rojo, E.; Fernández, M.; Leal, V.; Lafuente, P.; Santa-maría, A. Polymer 2005, 46, 8045.
14. Robledo, N.; Vega, J. F.; Nieto, J.; Martínez-Salazar, J. J Appl Polym Sci 2011, 119, 3217.
15. Wagner, M. H.; Kheirandish, S.; Stange, J.; Münstedt, H. Rheol Acta 2006, 46, 211.
16. Kozlowski, M.; Szczurek, S.; Szczurek, T.; Frackowiak, S. Int J Mater Forum 2008, 1, 751.
17. Li, T. Q.; Wolcott, M. P. Compos A 2004, 35, 303.
18. Dintcheva, N. T.; Arrigo, R.; Morreale, M.; Mantia, F. P. L.; Matassa, R.; Caponetti, E. Polym Adv Technol 2010.
19. Intawong, N.-T.; Sombatsompop, N. Polym Eng Sci 2004, 44, 1960.
20. Schneider, C.; Schwetz, M.; Münstedt, H.; Kaschta, J. Mech Time-Dependent Mat 2004, 8, 215.
21. Hertel, D.; Valette, R.; Münstedt, H. J Non-Newt Fluid Mech 2008, 153, 82.
22. Goutille, Y.; Guillet, J. J Non-Newt Fluid Mech 2002, 102, 19.
23. Schuberth, S.; Münstedt, H. Rheol Acta 2008, 47, 111.
24. Kim, H.; Chung, K.; Youn, J. R. Fiber Polym 2000, 1, 37.
25. Intawong, N.-T.; Sombatsompop, N. Polym Eng Sci 2004, 44, 2298.
26. Sombatsompop, N.; O-Charoen, N. Polym Adv Technol 2003, 14, 699.
27. Meerveld, J. V.; Hütter, M.; Peters, G. W. M. J Non-Newt Fluid Mech 2008, 150, 177.
28. Tan, L. P.; Joshi, S. C.; Yue, C. Y.; Lam, Y. C.; Hu, X.; Tam, K. C. Acta Mater 2003, 51, 6269.
29. Wapperom, P.; Hassager, O. Polym Eng Sci 1999, 39, 2007.
30. Feigl, K.; Tanner, F. X.; Edwards, B. J.; Collier, J. R. J Non--Newt Fluid Mech 2003, 115, 191.
31. Padmanabhan, M.; Macosko, C. W. Rheol Acta 1997, 36, 144.

AQ4

AQ5

AQ1: Please spell out "AC."

AQ2: Please spell out "OHEC."

AQ3: Please confirm "Thailand Research Fund."

AQ4: If the publication status has changed, please update the reference.

AQ5: Please provide the volume number and initial page number.

AQ6: Please note that it is the policy of this journal to charge authors for the additional cost of reproducing color figures in the printed version of the journal. Authors wishing to have figures printed in color in the journal should contact the journal's production office (APPjournal@wiley.com) for a price quote. Unless the publisher of this journal receives other instructions from the author, this figure will be printed in black and white and will appear in color in the online version of the article only.

AQ7: Please confirm the sentence as edited.

AQ8: Please provide the location of the manufacturer (city and state in the United States and city and country elsewhere).

Nitrile rubber · Cure behavior · Viscoelastic behavior · Rubber-filler interaction · Bound rubber

The present work aims to improve interaction between nitrile rubber (NBR) and carbon black (CB) using 2 functionalized liquid polybutadienes (Krasol LBH2000 and Ricon 130MA8) which differ mainly in functional groups and level of 1,2 vinyl content. Change in magnitude of NBR-CB interaction, and its effect on cure and viscoelastic behaviors of NBR compounds were investigated. The bound rubber (BR) content is increased by the use of Ricon 130MA8 while Krasol LBH2000 gives no significant change in the BR content. Curing retardation is resulted with increasing liquid PBs.

Rubber-Filler Interaction, Cure and Viscoelastic Properties in Black Filled Nitrile Rubber (NBR) Compounds Modified by Functionalized Liquid Polybutadiene

Einwirkung von funktionalisierten flüssigen BR auf die Kautschuk-Füllstoff Wechselwirkung, Vernetzungsverhalten und viskoelastische Eigenschaften von rußgefüllten NBR Mischungen.

Nitrilkautschuk · Vernetzungsverhalten · Viskoelastische Eigenschaften · Kautschuk-Füllstoff Wechselwirkung · Bound-Rubber

Die vorliegende Arbeit zielt auf die Verbesserung der Wechselwirkung zwischen NBR und Ruß durch zwei funktionalisierte flüssige Polybutadiene (Krasol LBH 2000 und Ricon 130 MA8), die sich in den funktionellen Gruppen und dem Gehalt an 1,2 –Einheiten unterscheiden. Die Änderung der NBR-Ruß Wechselwirkung wird über das Vernetzungsverhalten und das viskoelastische Verhalten der Compounds beschrieben. Der Gehalt an Bound-Rubber steigt mit dem Einsatz von Ricon 130 MA8. Mit Krasol LBH 2000 wurde bei BR keine merkliche Änderung registriert. Eine Verzögerung bei der Vernetzung wird durch saure Anteile des flüssigen BR hervorgerufen.

Figures and Tables:
By a kind approval of the authors

NBR is a copolymer of acrylonitrile and butadiene having a very good resistance to hydrocarbon oil. Depending on acrylonitrile content, the polarity of NBR can be adjusted to suit the applications of final rubber products; the greater the acrylonitrile content the higher the oil resistance. However, unlike natural rubber (NR), NBR possesses no strain-induced crystallization under deformation leading to its relatively low strength, and therefore the reinforcing fillers are required for raising NBR mechanical properties. Generally, there are two main reinforcing fillers used in rubber industry, namely, precipitated silica and carbon black (CB). The silica is one of the most important reinforcing fillers used mainly in the production of light colored products. With similar specific surface area, silica offers lower magnitude in reinforcement than CB which is attributed mainly to a large number of silanol groups (Si–OH) on the surface making silica highly polar. Such high polarity of silica results in a poor compatible with many nonpolar rubbers such as NR or styrene-butadiene rubber (SBR) [1]. In order to alleviate this problem of silica, silane coupling agents are used. Typically, the silane coupling agent composes of two functionally active end groups, i.e., the readily hydrolysable alkoxy group for reacting chemically with the silanol groups on silica surface and the organofunctional group for being compatible with rubbers. In other words, the silane coupling agent could act as a bridge between silica and rubber to enhance rubber–filler interaction, and thus significant improvements in properties of silica-filled compounds. In the case of CB as reinforcing filler, due to the absence of silanol group, the degree of agglomeration is much smaller than the silica making CB easier to be dispersed through-

out the rubber matrix. The surface reactivity of CB comes mainly from physically acive adsorption sites and surface roughness than from the oxygen-contained functional groups such as ketone, aldehyde and hydroxyl [2-5]. Compared with silane treated PSi, the CB offers weaker interaction to rubber matrix via the Van der Waals force which could cause molecular slippage of rubber molecules at CB surfaces at high strain of deformation. The energy dissipation process occurring from such slippage leads to the development of heat under cyclic deformation which is usually known as heat build-up (HBU). As a result, there have been attempts to enhance CB-rubber interaction via numerous approaches. Typically, the functional groups mainly amines are introduced to either polymer backbones or CB surfaces via the uses of amino-contained azide including p-aminobenzenesulfonyl azide and dinitrosodiamine [6-9]. Apart from the use of amine-based chemicals for CB surface treatment, the oxidation of CB surface by oxidizing agent such as sodium hypochlorite to promote reactivity of CB surface has been performed [10]. However, most treatment methods have to deal with

Authors

K. Hatthapanit, M. Nillawong,
C. Sirisinha, N. Sombatsompop,
Bangkok, P. Saeoui, Pathumthani

Corresponding author:
Chakrit Sirisinha
Mahidol University
Rama 6 Rd.
Bangkok 10400
Thailand
FAX: +662-441-0511
E-mail: sccsr@mahidol.ac.th

toxic chemicals. Thus, the present work aims to investigate the possibility of using functionalized liquid polybudatiene (PB) (i.e., liquid PBs with hydroxyl-terminated and maleated groups) for improving CB-rubber interaction in black filled NBR compounds. It is anticipated that the polar functional groups would react chemically with oxygen-contained groups on CB surfaces and/or acrylonitrile segments of NBR while the 1,2 vinyl groups of liquid PBs would be compatible with butadiene segments of NBR matrix which would thereafter participate in the vulcanization process, i.e., co-vulcanization with rubber matrix. In other words, the interaction between NBR matrix and CB might be improved by the functionalized liquid PBs added. Additionally, these functionalized liquid PBs might act as polymeric plasticizers which could facilitate processability of CB filled NBR compounds. Since NBR vulcanizates could practically prepared using sulfur and peroxide curing systems, it is of interest to investigate whether the difference in curing ingredients in NBR compounds would affect the cure and viscoelastic properties as well as the NBR-CB interaction development as one of objectives in this work.

Experimental

Materials

All mixing ingredients were used as received. Nitrile rubber (NBR, JSR N230) was supplied by JSR Co., Ltd. (Japan). Carbon black (N330) was manufactured by Thai Carbon Products Co. Ltd. (Thailand). Two types of functionalized liquid polybutadienes used, namely, Krasol LBH2000 and Ricon 130MA8 were supplied by Chemical Innovation Co., Ltd. (Thailand). The former is the hydroxyl-terminated PB with 65 % 1,2 vinyl content and number-average molecular weight of 2,100 g/mole while the latter is based on PB with 8 % maleic anhydride adducted, 20-35 % 1,2 vinyl content and number-average molecular weight of 3,100 g/mole. N-tert-butyl-2-benzothiazole Sulfenamide (Santocure-TBBS) was purchased from Reliance Technochem (Flexsys) Co., Ltd. (Thailand). Stearic acid, zinc oxide (ZnO), sulfur (S) and dicumyl peroxide (DCP) with 98 % active were supplied by Chemmin Co., Ltd. (Thailand).

### Preparation and testing of rubber compounds

A laboratory-size internal mixer (Haake Rheomix90, Germany), having mixing chamber volume of 79 cm3 equipped with cam-
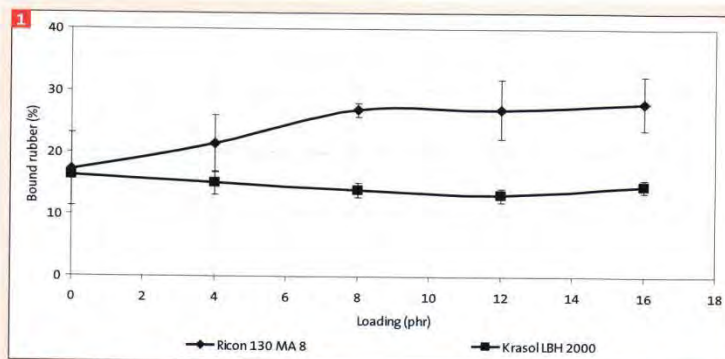
1 Bound rubber content of NBR compounds with different type and loading of functionalized liquid PBs (containing sulfur curing ingredients)
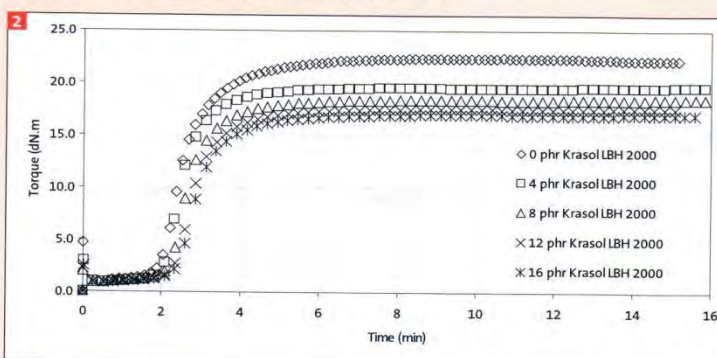
2 Cure curves of NBR compounds with various loadings of Krasol LBH2000 (containing sulfur curing ingredients)
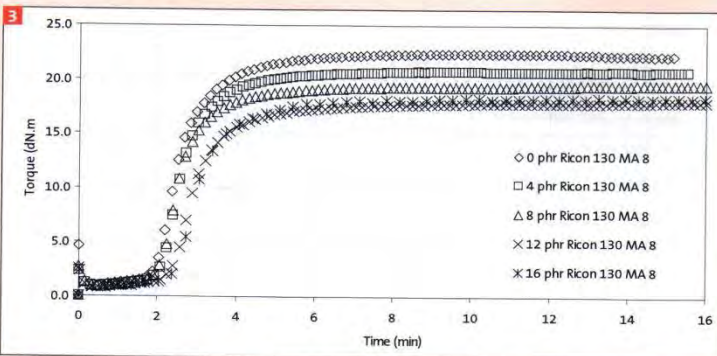
3 Cure curves of NBR compounds with various loading of Ricon 130MA8 (containing sulfur curing ingredients)

type rotors was employed to prepare rubber compounds. The fill factor and rotor speed were kept constant at 0.8 and 40 rpm, respectively. The two-stage mixing technique was conducted in order to avoid the premature vulcanization (scorch) of rubber compounds, i.e., the first stage was used for preparing black masterbatch and the sec-

ond stage was performed for incorporating the curatives. Mixing time was varied from 5 to 20 minutes giving the discharge temperatures of 140 and 80°C for the first and second stages, respectively. The compound formulation is given in Table 1. After mixing, the compounds were sheeted out using a two-roll mill (Collin W100T, USA).
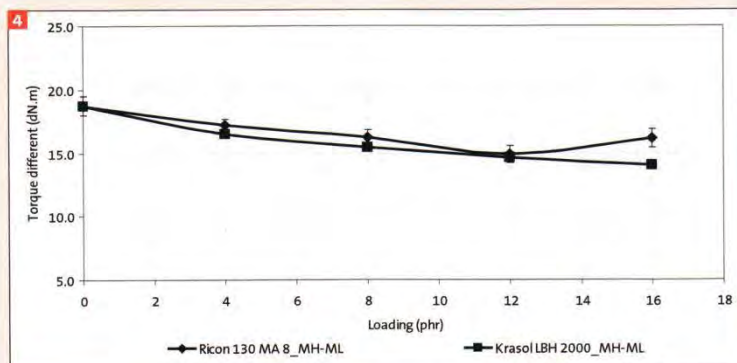
4 Torque difference as calculated from cure curves of CB filled NBR compounds with various loadings of Krasol LBH2000 and Ricon 130MA8 (containing sulfur curing ingredients)
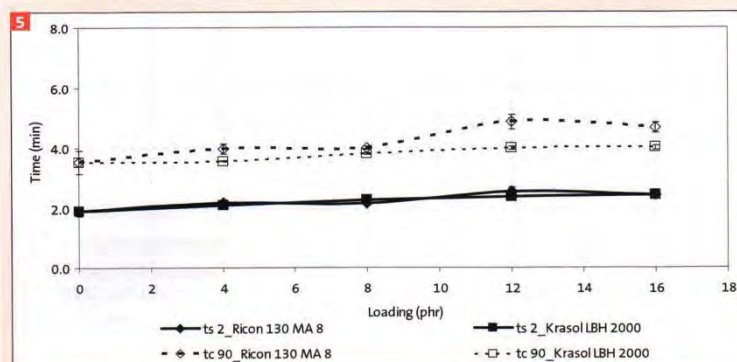
5 Scorch time (ts2) and optimum cure time (tc90) as calculated from cure curves of CB filled NBR compounds with various loadings of Krasol LBH2000 and Ricon 130MA8 (for sulfur curing system)

6 Storage modulus of CB filled NBR compounds with various loadings of Krasol LBH2000 (containing sulfur curing ingredients)
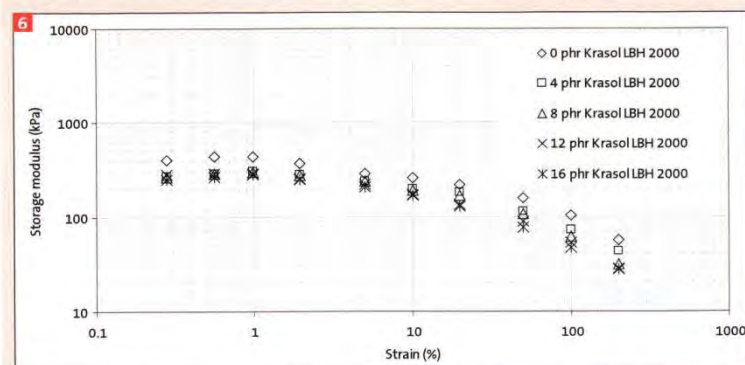
The determination of bound rubber (BR) content was based on the dissolution technique by immersing the black filled compound for 7 days in acetone as a good solvent for NBR in order to dissolve the unbound rubber. Then, the insoluble part was filtered, and then dried at 70°C overnight. Lastly, the dried portion was weighed, and the BR content was calculated using Equation (1) [11-13].

$$BR(\%) = \frac{m_0 - (m_2 - m_3)}{m_0} \times 100 \qquad \text{Equation (1)}$$

$$m_0 = \frac{((m_2 - m_1) \times 100)}{w_{compounds}} \qquad \text{Equation (2)}$$

Where m_0 is the rubber content in the sample, given in Equation (2), m_1 is the mass of the empty basket, $w_{compound}$ is the total formulation in part per hundred rubber (phr), m_2 is the mass of the basket plus the un-extracted sample, m_3 is the basket plus the extracted, dried sample.

Cure characteristics, including scorch time (ts2), optimum curing time (tc90), minimum torque (ML) and maximum torque (MH) were determined using a moving die rheometer (TechPro RheoTech MD+, USA). Viscoelastic behavior of compounds was monitored by the use of a Rubber Process Analyzer (RPA2000, Alpha Technology, USA). Strain and frequency sweep tests were conducted by varying strain from 0.5 to 1000% at test frequency of 10 rad/s, and by varying frequency from 0.5 to 100 rad/s at a given strain of 1% (within the linear viscoelastic region), respectively. The dynamic storage modulus (G') as functions of strain and angular frequency at 100°C was then recorded. The difference in storage moduli at low and high strains (ΔG'), widely known as the "Payne effect", is used to represent the degree of filler–filler interaction [14-15].

Results and discussion

It is known that NBR compounds could be cured with either sulfur or peroxide, depending on properties of NBR vulcanizates required. The former yields good mechanical properties with poor thermal resistance while the latter gives properties in the other way round. Since each curing system needs different curing ingredients, such difference might react with functionalized liquid PBs added in dissimilar manners. Thus, the results and discussion of NBR compounds containing sulfur and peroxide curing ingredients are separated from each other.

NBR compounds with sulfur vulcanizing ingredients

Bound rubber content

Typically, the degree of interaction between filler and rubber could be quantified by a measure of bound rubber (BR) content [11-13]. The greater the BR content, the higher the magnitude of rubber-filler interaction. Figure 1 shows a development of rubber-filler interaction in NBR compounds with functionalized liquid PBs having different functional groups. By increasing the amount of Ricon 130MA8, the BR content appears to increase and then level off. The rise in BR content implies the enhancement in NBR-

CB interaction via the presence of Ricon 130MA8. The maleic anhydride group of Ricon 130MA8 could react with active sites on CB surfaces, such as quinone, hydroxyl, aldehyde and/or at acrylonitrile (ACN) segments on NBR molecules, while the nonpolar PB backbone of Ricon 130MA8 associated with 1,2 vinyl structure could interact with butadiene segments of NBR matrix. By this means, the bridge between NBR matrix and CB is possible, leading to an increase in BR content, as illustrated in Figure 1. However, the excessive loading of Ricon 130MA8 does not yield any further improvement in NBR-CB interaction. On the contrary to the Ricon 130MA8, the Krasol LBH2000 added to NBR compounds shows no significant change in BR content, even with high loading of Krasol LBH2000. This could be explained by the fact that since the Krasol LBH2000 is the PB with hydroxyl terminated structure and high 1,2 vinyl content, the number of polar groups of such Krasol are limited to 2 groups per molecule as controlled solely by the hydroxyl terminal. This leads to the relatively low magnitude of NBR-CB interaction, and thus the BR content.

Cure behavior

Figures 2 and 3 reveal influences of Krasol LBH2000 and Ricon 130MA8 on cure behavior of NBR compounds containing sulfur curing chemicals. It is apparent that both Krasol LBH2000 and Ricon 130MA8 affect cure behavior in similar manner, i.e., both give slight reduction in minimum torque (M_L) and significant decrease in maximum torque (M_H). Basically, the M_L is used for predicting compound viscosity in the uncured state while the M_H is an indication of modulus of vulcanizate (i.e., the cured state). The results imply that both Krasol LBH2000 and Ricon 130MA8 play role on NBR properties in the cured state more obviously than the uncured state. One might know that there are two main reasons probably used for explaining such softening phenomenon: (i) plasticizing effect and (ii) reduced crosslink density effect. However, because the magnitude of reduction in M_L (i.e., compound viscosity) is relatively small, compared to that of M_H (i.e., vulcanizate modulus), the plasticizing effect on softening of modulus could be disregarded. By contrast, the crosslink density as determined from the torque difference (M_H-M_L) appears to progressively decrease with increasing functionalized liquid PBs, as illustrated in Figure 4. The magnitude of decrease in crosslink density is slightly greater in the case of Krasol LBH2000.
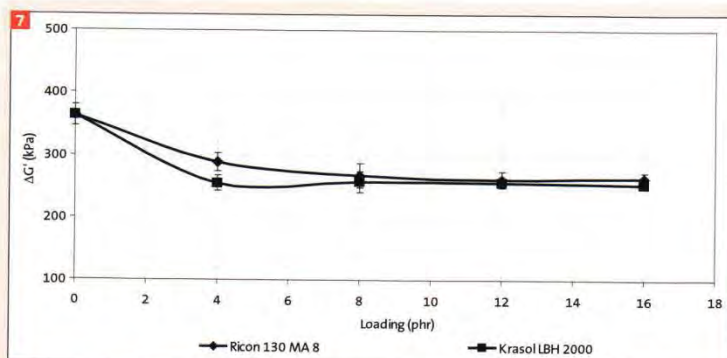
7 Magnitude of Payne effect in CB filled NBR compounds with different type and loadings of liquid PBs (containing sulfur curing ingredients)
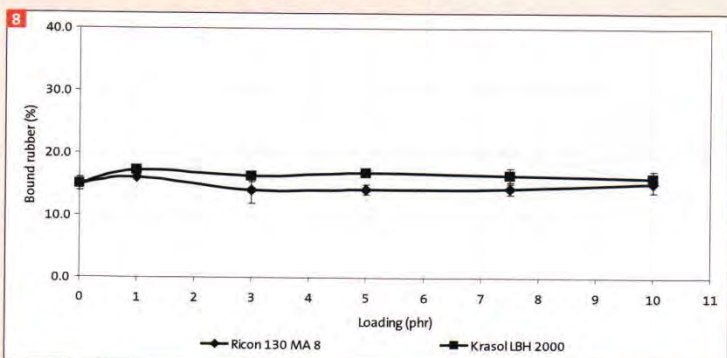
8 Bound rubber content of NBR compounds with different type and loading of liquid PBs (containing peroxide)
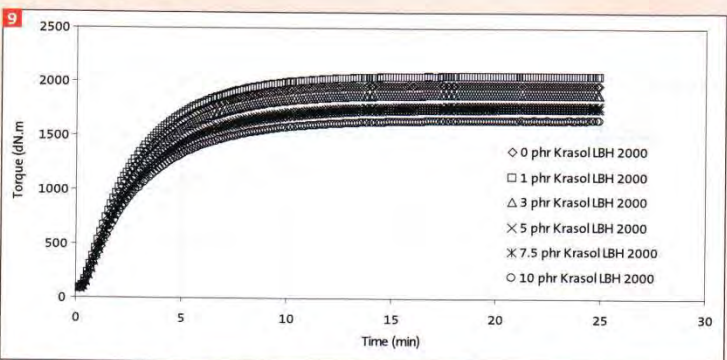
9 Cure curves of CB filled NBR compounds with various loadings of Krasol (containing peroxide)

Figure 5 exhibits scorch time (t_{s2}) and optimum cure time (t_{c90}) of NBR compounds with Krasol LBH2000 and Ricon 130MA8. By increasing the amounts of functionalized liquid PBs, both t_{s2} and t_{c90} increase progressively. At any given loading of liquid PBs, the NBR compounds with Ricon 130MA8 reveal slightly longer t_{c90}. A cure retardation phenomenon observed is attributed to the presence of hydroxyl and maleic anhydride functional groups in Krasol LBH2000 and Ricon 130MA8, respectively. Such functional groups might cause the absorption of curing ingredients including soluble zinc as cure activator and TBBS as cure accelerator in a similar fashion to the silanol groups on
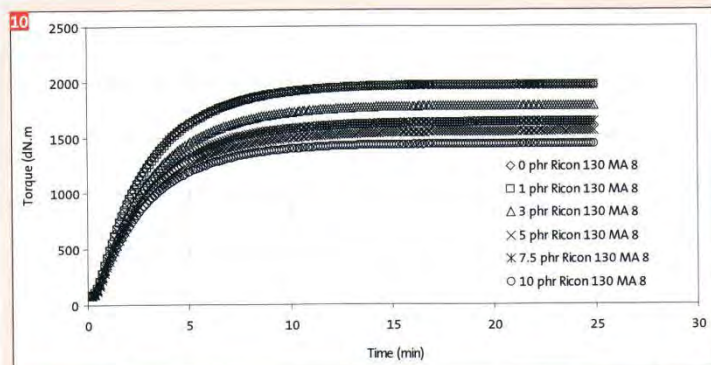
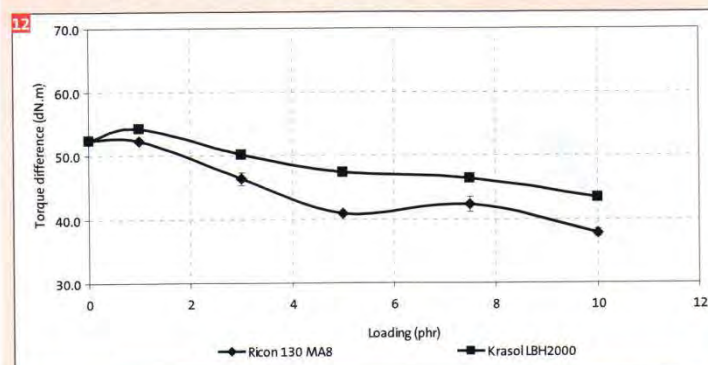**10** Cure curves of CB filled NBR compounds with various loadings of Ricon 130MA8 (containing peroxide)
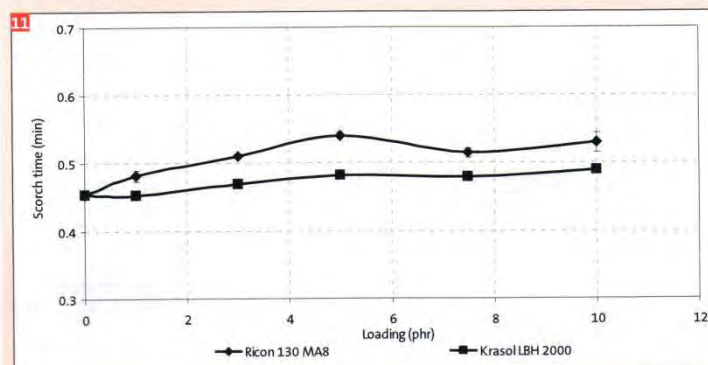
11 Scorch time (ts2) as calculated from cure curves of CB filled NBR compounds with various loadings of Krasol LBH2000 and Ricon 130MA8

12 Torque difference as calculated from cure curves of CB filled NBR compounds with various loadings of Krasol LBH2000 and Ricon 130MA8 (containing peroxide curing ingredient)

silica surfaces. This causes a depletion of active chemicals required for accelerating the curing process, and therefore the reduction in cure efficiency. Furthermore, there is a relatively high level of acidity in Ricon 130MA8 via the presence of maleic anhydride groups, giving the additional magnitude of cure retardation as demonstrated by the longer t_{c90}, compared to Krasol LBH2000 at a given liquid PB loading.

Viscoelastic properties

Figure 6 shows the dependence of storage modulus (G') on deformation strain (i.e., Payne effect) of NBR compounds incorporated with different type and loading of functionalized liquid PBs. The incorporation of functionalized liquid PB yields the reduction in G' significantly, and further increase in Krasol LBH2000 shows no further change in G'. The initial decrease in G' with increasing liquid PBs could be due to: (i) plasticizing effect and (ii) the enhancement in state-of-mix (i.e., reductions in filler agglomerations and filler transient network) [11,16-18]. Thus, to separate the state-of-mix effect from the plasticizing effect, the difference in G' at low strain and high strain (ΔG') or the magnitude of Payne effect is calculated, and the results are shown in Figure 7. Evidently, values of ΔG' decreases initially, and then becomes stable. The reduction in ΔG' implies an improvement in CB dispersion of NBR compounds. Beyond this loading, there is no change in the state-of-mix. It is noticeable that the results of Payne effect are independent of liquid PB type. Alternatively, the enhancement in CB dispersion degree in NBR compounds containing sulfur curing ingredients is possible by the addition of either Krasol LBH2000 or Ricon 130MA8. It is noticeable that the high polarity given by maleic anhydride in Ricon 130MA8 does not give any additional benefit, compared to Krasol LBH2000 with hydroxyl terminated groups.

NBR compounds with peroxide vulcanizing ingredients

As mentioned previously, it is anticipated that the difference in curing ingredients added to NBR compounds might interact with the functionalized liquid PBs in dissimilar fashion. Basically, the major ingredients used for sulfur curing include zinc oxide, stearic acid, amine-based accelerator, sulfur which are known to form the zinc complexes capable of releasing sulfur to rubber molecules for sulfidic linkage formation. These complexes are rather polar, compared to dicumyl peroxide (DCP) usually used solely as a curing agent in peroxide vulcanization. Consequently, any discrepancies in results found in this section from those previously reported would be attributed mainly to the difference in curing ingredients incorporated to the NBR compounds.

Bound rubber content

Figure 8 reveals effects of functionalized liquid PBs on BR content in NBR compounds having peroxide curing ingredient. Evidently, the addition of neither Krasol LBH2000 nor Ricon 130MA8 could increase the magnitude of NBR-CB interaction. The results are on the contrary to the system with sulfur curing ingredients. This is clear evidence that the DCP presented in compounds could

inhibit or even disrupt the CB-NBR interaction. In other words, the use of functionalized liquid PBs for improving CB-NBR interaction in NBR compounds containing DCP should be carried out with caution.

Cure properties

Figures 9 and 10 show that all NBR compounds reveal stable final torque with no marching phenomenon (i.e., a phenomenon having progressive increase in vulcanizate modulus as a function of curing time with no plateau), implying good curing efficiency at high cure temperature of 170 °C, regardless of type and loading of functionalized liquid PBs added. Also, cure characteristics including minimum torque (M_L), maximum torque (M_H) and torque difference (M_H-M_L) are dependent significantly on loading of functionalized liquid PBs which could be seen more clearly in Figures 11 and 12.

Figure 11 demonstrates scorch time (t_{s2}) as calculated from cure curves (Figures 9 and 10). It is evident that t_{s2} is not significantly affected by loading of either Krasol LBH2000 or Ricon 130MA8. In other words, the addition of these functionalized liquid PBs yields no profound effect on process safety. Regarding the crosslink density as determined from torque difference of cure curves (M_H-M_L), Figure 12 reveals that, with increasing the amount of liquid PBs, the values of M_H-M_L decrease which are more pronounced in the case of Ricon 130MA8. Such decreases imply the reduction in crosslink density in the NBR compounds as functionalized liquid PB is incorporated, which are partly caused by the increase in actual degree of unsaturation in the compounds. Since both liquid PBs contain a large amount of 1,2 vinyl configuration known to be readily reactive to peroxide vulcanization, the total amount of radicals available for crosslinking become insufficient, and thus the reduction in crosslink efficiency is resulted. Furthermore, in the case of Ricon 130MA8, the presence of maleic anhydride makes Ricon 130MA8 acidic, and therefore decreases the curing efficiency even more.

Viscoelastic properties

Figures 13 and 14 illustrate storage modulus (G') of NBR compounds as a function of deformation strain. It is clear that all compounds exhibit a linear viscoelastic (LVE) region at the strain up to 10 %. Further increase in strain would lead to a sharp drop in G'. Because the G' at low strain (in the LVE region) is governed mainly by molecular entanglement and a formation of transient filler network [11,16-18], the insignificant change in low-strain G' with increasing liq-
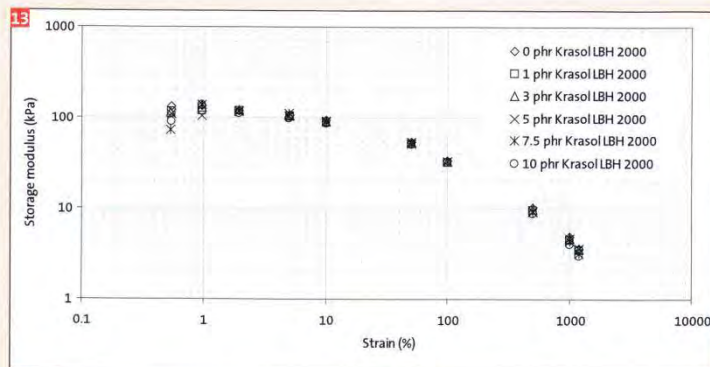
13 Storage modulus of CB filled NBR compounds with various amounts of Krasol LBH2000 (containing peroxide)
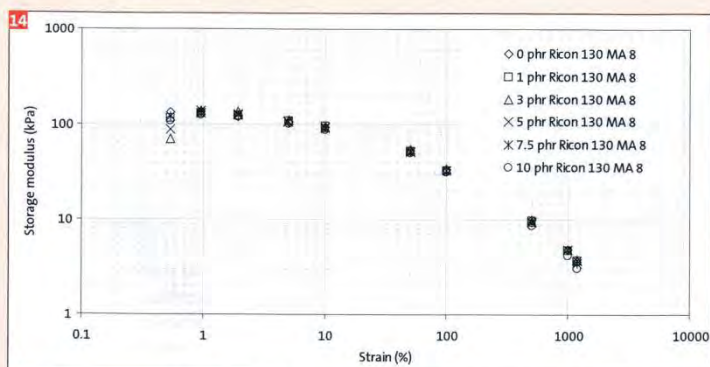
14 Storage modulus of CB filled NBR compounds with various amounts of Ricon 130MA8 (containing peroxide)
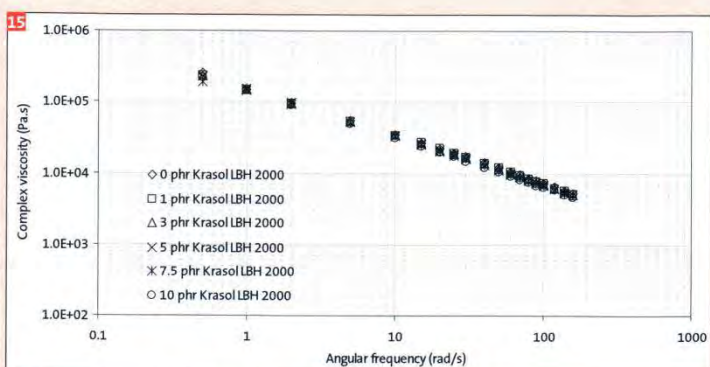
15 Complex viscosity of CB filled NBR compounds with various amounts of Krasol LBH2000 (containing peroxide)

uid PB loading exhibited in Figures 13 and 14 implies that the functionalized liquid PBs added affect neither viscous contribution via molecular flow nor the degree of dispersion (i.e., state-of-mix) via filler network disruption. Such insignificant changes might be due to the relatively high molecular weight of both PBs which could not fa-

cilitate molecular flow as effectively as the small-molecule plasticizers, such as, dibutylphthalate (DOP), which is conventionally incorporated to polar polymers including polyvinyl chloride (PVC) and NBR in order to increase viscous contribution of bulk systems by expanding molecular free volume.
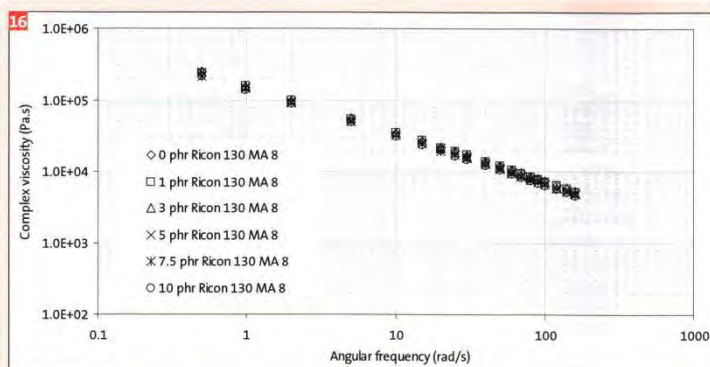
16 Complex viscosity of CB filled NBR compounds with various amounts of Ricon 130MA8 (containing peroxide)

Figures 15 and 16 demonstrate complex viscosity as a function of angular frequency of CB filled NBR compounds incorporated with Krasol LBH2000 and Ricon 130MA8, respectively. Regardless of type and loading of PBs, the decrease in complex viscosity at high frequency could be observed. This phenomenon is widely known as a pseudoplastic or shear-thinning behavior which is considered to be useful for processing aspect. The low viscosity at high shear rate would ease the flow ability of polymer melts causing a decrease in energy consumption during the shaping process. The molecular disentanglement associated with the disruption of filler transient network is believed to be responsible for such decrease in viscosity at high shear rate. Evidently, the addition of both liquid PBs gives similar result trend in a way that both cause no significant impact on complex viscosity throughout the range of test frequency. The results imply that both PBs could be justified as inefficient processing aids despite at high PB loading up to 10 phr. This is probably due to the relatively high molecular weight of functionalized liquid PBs leading to the ineffectiveness of plasticizing effect, compared to conventional plasticizers, such as, dibutylphthalate (DOP). The results of complex viscosity are in good accordance with those of G' as discussed previously.

Conclusions

Two types of functionalized liquid polybutadienes (Krasol LBH2000 and Ricon 130MA8) having major differences in functional group and level of 1,2 vinyl content were incorporated to nitrile rubber (NBR) compounds. Influences of types and loadings of liquid PBs on bound rubber content (as an indication of rubber-filler interaction), cure and viscoelastic behavior are investigated. In addition, the properties of NBR compounds containing different curing ingredients are compared. From overall results, the following conclusions could be drawn:

1. The interaction between NBR and carbon black (CB), as determined from the bound rubber (BR) content, could be enhanced by a certain amount of Ricon 130MA8 in NBR compounds containing curatives for sulfur vulcanization. However, none of functionalized liquid PBs yields improvement in NBR-CB interaction in the NBR compounds with the presence of DCP as a curative.

2. Cure properties are affected strongly by the addition of functionalized liquid PBs. The Ricon 130MA8 exhibits greater magnitude of cure suppression phenomenon.

3. Both functionalized liquid PBs affect NBR properties in the cured state more significantly than the uncured state.

4. Curing ingredients added to NBR compounds could influence significantly the results of functionalized liquid PB effect on NBR properties in different manners.

References
[1] J. T. Byers, Rubber World **218**(6) (1998) 38.
[2] M. L. Studebaker, Rubber Chem Technol **30** (1957) 1400.
[3] R. C. Bansal, J. B. Donnet and F. Stoeckli, "Active Carbon", Marcel Dekker, New York, (1988).
[4] J. B. Donnet and A. Adv. Vidal, Polym. Sci. **76** (1986) 103.
[5] M. J. Wang, S. Wolff and J. B. Donnet, Rubber Chem Technol **64** (1991) 714.
[6] U. S. Patent 5,026,494, (1991) W. Denzinger, H. Mach, J. Mohr, K. Oppenlaender, R. Schwen and H. Vogel.
[7] U. S. Patent 6,652,641 B2, (2003) T. Kawazura.
[8] U. S. Patent US 2009/0093594 A1, (2009) N. Kushida.
[9] L. Gonzalez, A. Rodriguez and J. L. Benito, Rubber Chem Technol **69** (1996) 266.
[10] U. S. Patent US 6,402,825 B1 J. Sun.
[11] J. L. Leblanc and B. Stragliati, J Appl Polym Sci **63** (1997) 959.
[12] S. S. Choi, J Appl Polym Sci **93** (2004) 1001.
[13] S. S. Choi, Polym. Test **21** (2002) 201.
[14] L. A. E. M. Reuvekamp, J. W. Ten Brinke, P. J. Van Swaaij and J. W. M. Noordermeer, Rubber Chem Technol **75** (2002) 187.
[15] A. R. Payne, R. E. Whittaker and J. F. Smith, J Appl Polym Sci **16** (1972) 1191.
[16] N. Phewthongin, P. Sae-oui and C. Sirisinha, Polym. Test **24** (2005) 227.
[17] N. Phewthongin, P. Sae-oui and C. Sirisinha, J Appl Polym Sci **100** (2006) 2565.
[18] P. Phewphong, P. Sae-oui and C. Sirisinha, J Appl Polym Sci **107** (2007) 2638.

1 Compound formulation

Ingredients		Amount (phr)										
		Sulfur vulcanization					Peroxide vulcanization					
		1	2	3	4	5	6	7	8	9	10	11
NBR		100	100	100	100	100	100	100	100	100	100	100
ZnO		5	5	5	5	5	0	0	0	0	0	0
Stearic acid		2	2	2	2	2	0	0	0	0	0	0
N330 CB		45	45	45	45	45	40	40	40	40	40	40
Krasol® LBH 2000 or Ricon® 130MA8		0	4	8	12	16	0	1	3	5	7.5	10
TBBS		2	2	2	2	2	0	0	0	0	0	0
Sulfur		2	2	2	2	2	0	0	0	0	0	0
DCP		0	0	0	0	0	2	2	2	2	2	2

Mechanical Strengths of Molten and Solidified LLDPE/LDPE Blends and Wood/LDPE Composites Under Tensile Deformation

Wanlop Harnnarongchai,[1] Watcharin Sitticharoen,[1] Naret Intawong,[2] Narongrit Sombatsompop[1]

[1]Polymer Processing and Flow (P-PROF) Group, Division of Materials Technology, School of Energy, Environment and Materials, King Mongkut's University of Technology Thonburi (KMUTT), Thongkru, Bangmod, Bangkok 10140, Thailand

[2]Department of Industrial Engineering, Faculty of Engineering, Rajamangala University of Technology Lanna, (RMUTL), Chiang Mai 50300, Thailand

The mechanical strengths of neat low-density polyethylene (LDPE), a blend of LDPE with linear low-density polyethylene (LLDPE), and a composite of LDPE with wood flour (wood/LDPE) were investigated in molten and solidified states under tensile deformation. The results are discussed in terms of the effects of LLDPE and wood contents, roller speed, and volumetric flow rate. In LLDPE/LDPE blends, incorporating LLDPE from 0 to 30 wt% into LDPE caused a slight increase in drawdown force, a larger fluctuation in drawdown force, and a reduction of maximum roller speed to failure. The mechanical properties of the solidified LLDPE/LDPE corresponded to those of the molten LLDPE/LDPE with regard to the effect of LLDPE content. For wood/LDPE composites, increasing the wood flour content in molten LDPE caused considerable reductions in drawdown time and maximum roller speed to failure. The drawdown force increased with increasing wood flour up to 10 wt% before it decreased at the wood loading of 20 wt%. A number of voids and pores on the extrudate surfaces became obvious for the composites with 20 wt% of wood content. Increasing wood content enhanced the tensile modulus for the solidified LDPE but decreased its tensile strength. Unlike those of LLDPE/LDPE blends, the changes in tensile modulus and strength of solidified wood/LDPE composites with wood content did not correspond to those of the molten composites. In all cases, the drawdown force increased with increasing roller speed. The effect of volumetric flow rate from the extruder on the mechanical strengths of the solidified blends was more pronounced than on those of the molten ones. J. VINYL ADDIT. TECHNOL., 17:164–176, 2011. © 2011 Society of Plastics Engineers

INTRODUCTION

Flows of polymer melts involve deformation and slippage of fluid particles and are strongly dependent on the geometries of the equipment into/along which the melts are flowing. Elongational flow of polymer melts plays an important role in many polymer processes, such as thermoforming, fiber spinning, blown film extrusion, convergent flows in dies and nozzles, extrusion coating, and extrusion blow molding. The elongational flow properties of polymers are usually varied by weight-average molecular weight and level of branching structure of the polymers used, additives, and processing variables (i.e., test temperature, draw ratio, roller speed) [1–3]. There have been a number of studies on the measurements of the elongational flow properties [1–11], mostly involving homopolymers, such as low-density polyethylene (LDPE) [3, 5–7], linear low-density polyethylene (LLDPE) [4–7], high-density polyethylene (HDPE) [1, 3, 8], polypropylene (PP) [9], and polycarbonate [11]. Attempts to improve the melt strength of homopolymer melts have also been made especially for tension-thinning melts, mainly by blending with a secondary polymer whose molecular structure is similar to that of the primary polymer but which contains a branching structure. Perez et al. [6] found that the drawdown force and elongational viscosity of m-LLDPE slightly enhanced with increasing LDPE content. Wagner et al. [7] suggested that LDPE and LLDPE/LDPE blends showed strong strain hardening, and the maximum drawdown force was observed with an LLDPE/LDPE blend having an LDPE content of 40–60 wt%. Yamaguchi and Suzaki [8] found that the addition of crosslinked HDPE to HDPE enhanced the melt strength without the sagging effect of the blend for thermoforming sheet applications. Park et al. [11] used a Meissner extensional rheometer and found that the extensional and complex viscosities for blends of linear polycarbonate (L-PC)

increased with increasing amounts of branched polycarbonate (Br-PC).

Polymer composites have recently received attention in the polymer industries, especially those composites between thermoplastics and natural fibers, because of good mechanical strength, cost savings, and favorable environmental profiles [12]. Unfortunately, information on the elongational flow properties of such composites has been very rare, and they need more scientific evidence for the improvement of their processabilities. Kozlowski et al. [10] suggested that the melt strength of PVC composites increased with the presence of wood flour. Li and Wolcott [13] studied the extensional viscosities of wood/HDPE composites using different wood species and found that the extensional viscosity was more dependent on the wood content.

Most researchers have found that adding natural fibers, wood flour, wood pulp, sisal, flax, bamboo, sunhemp, pineapple, and jute into thermoplastics usually results in lower ultimate mechanical strength of the composites [14–23], although work has been done to improve the mechanical and engineering properties of such composites, including chemical surface treatments, reinforcements with glass fibers [24] and long natural fibers [25], reinforcement with nanofillers [26–28], and processing and die designs [12]. MeÇndez et al. [14] found that the mechanical strength of PP decreased with increasing wood pulp content because of PP and wood incompatibilities. Similar behaviors were also observed for (cellulose fibers)/poly(methyl methacrylate) composites [16]. Rozman et al. [17] studied the tensile and flexural strengths of PP reinforced by oil palm empty fruit bunch (EFB). They suggested that although flexural and tensile moduli improved, the strengths decreased progressively with increasing EFB content. Sombatsompop et al. [15, 18, 19] studied the effects of wood content and chemical surface treatment on the mechanical properties of PVC, ABS, and PP and found that the stiffness of the composites was dependent on the type of thermoplastic used but that the effects on ultimate strength were the same for all thermoplastics studied. Sailaja [20] suggested that a small amount of poly(ethylene-*co*-glycidyl methacrylate) (PMMA) could improve the compatibility between LDPE and PMMA-grafted wood pulp. Joseph et al. [21] observed the effect of chemical treatments (sodium hydroxide, isocyanate, permanganate, and peroxide) on the tensile properties in short-sisal-fiber-reinforced LDPE and found that the peroxide most enhanced the tensile properties. The mechanical properties of the wood/thermoplastic composites were also dependent on the cross-sectional design of the test pieces used [22, 23].

When considering the tensile properties of thermoplastic composites with wood fibers in molten and solid states from the existing literature [10–13, 15, 18–23], it was understood that the tensile properties of the molten and solid wood/thermoplastic composites do not always have the same tendency. This statement suggests that one could

not expect that composites with high melt strength would definitely produce solidified composite products with high tensile properties, and *no* comparative studies on the tensile properties of wood/polymer composites tested in the molten and solidified states under the same experimental conditions have been available. In this work, a low-density polyethylene was used as the thermoplastic matrix; a linear low-density polyethylene was used as the minor phase for making polymer blends; and wood flour was used as the filler for wood/LDPE composites. The effects of LLDPE and wood contents, volumetric flow rate, and roller speed on the mechanical properties of the LLDPE/LDPE and wood/LDPE systems in both molten and solidified states were investigated under tension deformation. A single-screw extruder was used for the production of molten polymer blends and composites using a circular die. An in-house-constructed experimental rig was used to measure drawdown force. The extruded melts were then solidified and collected for tensile testing in solidified form. By following this procedure, one could ensure that the thermal and processing histories of the molten and solidified blend and the composite samples for mechanical property testing were identical.

EXPERIMENTAL

Raw Materials

1. Low-density polyethylene (LD1905FA) with a melt flow index of 5 g/10 min was used as received and was supplied in granule form by Thai Polyethylene, (Bangkok, Thailand).
2. Linear low-density polyethylene (L2009F) with a melt flow index of 1 g/10 min was used as received and was supplied in granule form by Thai Polyethylene, (Bangkok, Thailand).
3. Wood flour from carpentry and wood-working processes was supplied by V.P. Wood, (Bangkok, Thailand). The average size of the wood flour particles was in the range of 100–300 μm. The wood had to be dried to a constant weight in order to avoid any bubbles and voids during processing, the maximum moisture content allowed being less than 5%. This level was achieved by using an oven at 80°C for 24 h.

Preparation of LLDPE/LDPE Blends and Wood/LDPE Composites

LLDPE/LDPE Blends. The LDPE and LLDPE were dry blended with a high-speed mixer (LabTech Engineering, LMXS) before melt blending in a twin-screw extruder (Haake PolyLab-Rheomex CTW100P, Germany). The blending temperature profile on the extruder was 130, 140, 150, and 160°C from hopper to die zones, and the screw rotation speed was 50 rpm. A three-strand die having a diameter of 3 mm for each strand and coupled with

a pelletizing unit was used to produce the LLDPE/LDPE blend pellets, which were held in an oven for 24 h at 80°C before further processing. The LLDPE content was varied from 0 to 30 wt% of LDPE.

Wood/LDPE Composites. The dried wood particles were dry blended with the LDPE granules by using a high-speed mixer before melt blending in a twin-screw extruder. The blending temperature profile on the extruder was 130, 140, 150, and 160°C from hopper to die zones, and the screw rotation speed was 50 rpm. A three-strand die having a diameter of 3 mm for each strand and coupled with a pelletizing unit was used to produce the wood/LDPE composite pellets, which were held in an oven for 24 h at 80°C to avoid moisture regain before further processing. The wood content was varied from 0 to 20 wt%.

Measurement of Mechanical Strength for LLDPE/LDPE and Wood/LDPE

Mechanical Strength of Molten Blends and Composites. The mechanical strength of LLDPE/LDPE blends and wood/LDPE composites in the molten state is referred to as melt strength, which was measured in terms of drawdown force under tension deformation. Figure 1 shows an experimental arrangement for mechanical strength measurement of the molten LLDPE/LDPE blends or wood/LDPE composites in a filament winding process. This setup was connected to the end of a single-screw extruder. The experimental apparatus consisted of the single-screw extruder, an adaptor (barrel rig), a capillary die, a drawdown force measuring unit (load cell), a moving roller take-up, and control equipment. The detailed information for this experi-
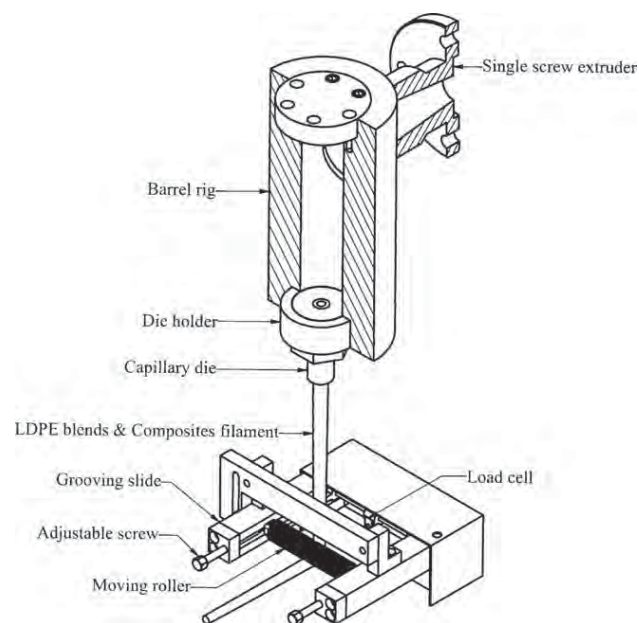

FIG. 1. Experimental arrangement for mechanical strength measurement of LLDPE/LDPE blends and wood/LDPE composites in a filament winding process.

mental rig, including component design, can be obtained from our previous work [5, 29]. Our in-house experimental rig allowed the adjustment of roller speed increasing in step-ladder fashion for drawdown force measurement with constant acceleration. The drawdown force data from increasing step-ladder roller speed were very useful, especially for clarifying the drawdown force at low roller speeds (less than 50 rpm) where the drawdown force was very sensitive to speed changes. The experimental procedures were commenced by extruding the molten polymers (LDPE, LLDPE, LLDPE/LDPE, or wood/LDPE) through a circular die before they were pulled down and solidified by ambient air to form a continuous filament. The die temperature used was 170°C throughout this work, and the length of the spin line for the filament was fixed at 280 mm. Only draw down forces measured during the filament stretching as a function of roller speed and time are given and discussed, because higher mechanical strength of the molten polymer filament will give higher draw down force. This procedure was followed for neat LDPE, neat LLDPE, LLDPE/LDPE blends, and wood/LDPE composites. It should be noted that all the measurements made on the molten state of all LDPE systems were restricted to non-isothermal conditions. All the experimental data were recorded and displayed by using a high-speed data-logging and recording system and a personal computer. The reported experimental data were averaged from at least five independent test runs.

Mechanical Strength of Solidified Blends and Composites. The solidified filaments of neat LDPE, neat LLDPE, LLDPE/LDPE blends, and wood/LDPE composites were collected for use in studying the tensile properties in the solid state. The tensile properties considered in this work were only tensile modulus and tensile strength through use of a crosshead speed of 50 mm/min and a gauge length of 30 mm. All the tests were run on a SHIMADZU universal tensile tester (Tokyo, Japan), and the reported data were averaged from at least five independent determinations.

Test Variables

The test variables included the LLDPE and wood flour contents and the volumetric flow rate from the screw extruder. The content of LLDPE was varied at 0, 10, 20, and 30 wt%. Neat LLDPE was also studied for comparison purposes. In the wood/LDPE composite system, the wood content used ranged from 0 to 20 wt%. The variations in volumetric flow rate were achieved by varying the screw rotation speed from 10 to 30 rpm, there by giving volumetric flow rates ranging from 1.4×10^{-7} to 4.1×10^{-7} m^3/s, respectively.

Determination of Crystallinity Level

Crystallinity levels of the solidified filaments of LLDPE/LDPE blends and wood/LDPE composites were measured by using a differential scanning calorimeter
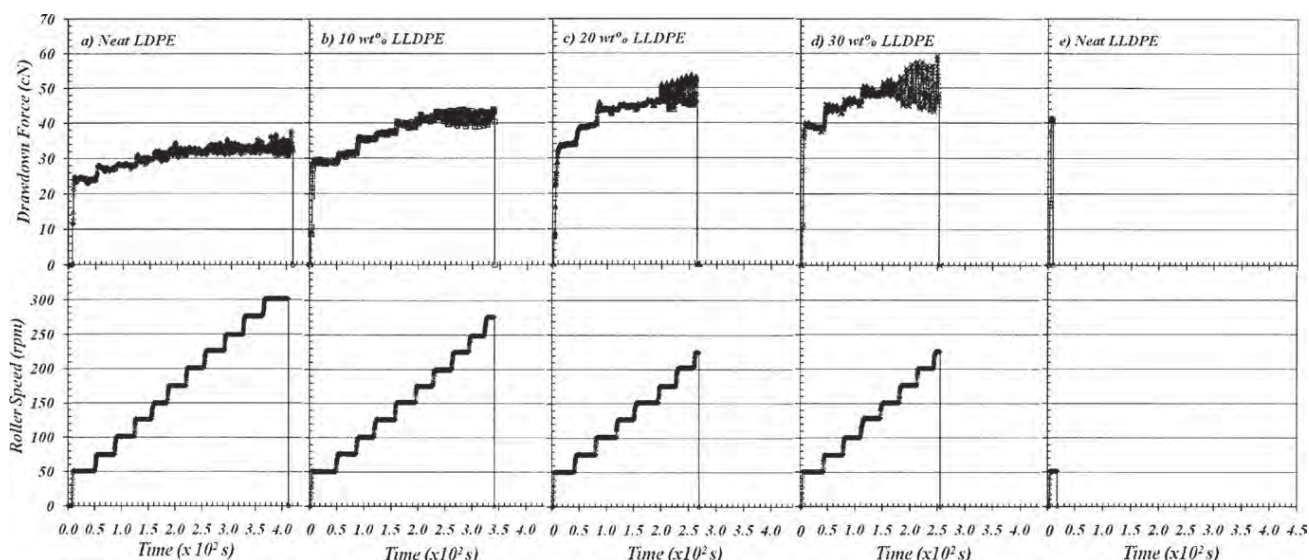
FIG. 2. Drawdown force against time with increasing LLDPE content under increasing step-ladder roller speed for LLDPE/LDPE blends at 170°C with a volumetric flow rate of 4.1×10^{-7} m³/s.

(DSC-200 F3 Maia®, NETZSCH, Germany). The solidified filament samples were heated from 50 to 200°C at a heating rate of 10°C/min. All the samples were cut into pieces weighing 6.3 ± 0.5 mg, then sealed securely in aluminum pans and examined in an atmosphere of nitrogen. The enthalpies of fusion at endothermic melting temperatures (T_m) were determined for all samples at the first heating scan. The level of crystallinity (X_c) was calculated as expressed in *Eq. 1* [30],

$$X_c = \frac{\Delta H_m}{\Delta H_0} \times 100\%$$ (1)

where ΔH_m is the enthalpy of fusion obtained from the integral area of a DSC heating curve, and ΔH_0 is the enthalpy of fusion for polyethylene with 100% crystallinity (290 J/g).

Scanning Electron Microscopy (SEM) Investigations

Failure analysis is usually required for the mechanical testing of wood/LDPE composites. In this work, the failure mechanism was investigated with a JEOL (JSM-6301F) SEM apparatus, (Tokyo, Japan) at 25 kV of accelerating voltage. The fractured surfaces of wood/LDPE composites were obtained after 2-min immersions in liquid nitrogen. The details of the experimental procedure and sample preparation for the SEM investigations can be obtained elsewhere [15].

RESULTS AND DISCUSSION

LLDPE/LDPE Blend System

Mechanical Properties of Molten LLDPE/LDPE Blends. Low-density polyethylene is often used for film appli-

cations because of its good processability and flexibility as a result of long-chain branching. However, LLDPE has better mechanical properties, thermal stability, and chemical resistance, but poorer processability as a result of short-chain branching. Therefore, blending LDPE with LLDPE would give promising processability and mechanical properties of the resultant films.

Figure 2 shows the effect of LLDPE content on drawdown force plotted against drawdown time with increasing step-ladder roller speed at a die temperature of 170°C and a volumetric flow rate of 4.1×10^{-7} m³/s. The results suggest that for a given LLDPE content, the drawdown force tended to increase with increasing roller speed. The drawdown force sharply increased in the initial stage of increasing roller speed of less than 50 sec drawdown and then increased to a lesser extent in the final stages of increasing roller speed. The sharp increase in the drawdown force at the initial (low) roller speeds was caused by the effects of molecular branching and entanglement, thus resulting in the mechanical interlocking of polymer molecule of molten LDPE in neat LDPE and in LLDPE/LDPE blends. This result was found to occur when observing the low melt strength of neat LLDPE. At higher roller speeds, the drawdown force required to deform the molten LDPE and LLDPE/LDPE blends appeared to be smaller because the molten polymer chains became disentangled in this stage and slipped past one another. Force fluctuations at the higher roller speeds were observed before failure points and were caused by the draw resonance effect [3].

Incorporating from 0 to 30 wt% of LLDPE into LDPE could result in three interesting changes in drawdown force and roller speed to failure, namely a slight increase in drawdown force, a larger fluctuation of drawdown force, and a reduction of maximum roller speed to failure.
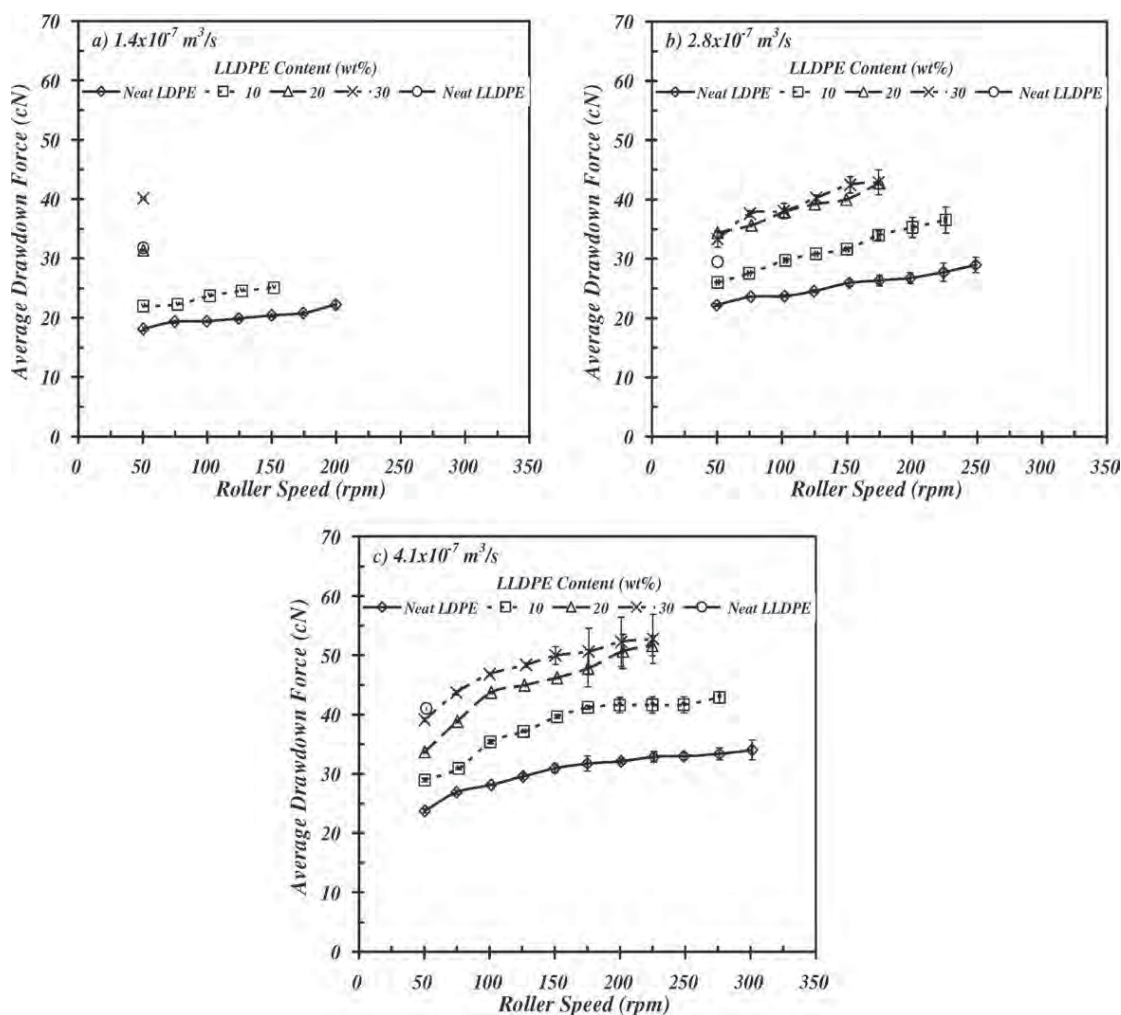
FIG. 3. Effects of volumetric flow rate on average drawdown force of LLDPE/LDPE blends at 170°C for the volumetric flow rates (a) 1.4×10^{-7} m^3/s, (b) 2.8×10^{-7} m^3/s, and (c) 4.1×10^{-7} m^3/s.

The increase in the drawdown force with increasing LLDPE content was obviously caused by the initially higher mechanical strength of neat LLDPE in comparison with that of neat LDPE (see Fig. 2e). This view could be supported by the work of Perez et al. [6] and Wagner et al. [7], who stated that the melt strength (drawdown force) of LLDPE/LDPE blends increased with increasing LLDPE content. The larger fluctuation in drawdown force with increasing LLDPE suggested molecular heterogeneity of the LDPE and LLDPE during the flow. Finally, the decrease in maximum roller speed to failure with increasing LLDPE content suggested a reduction of molecular interlocking level as the molten blend was being stretched. This result occurred because the added LLDPE had short-chain branches and shared tension-thinning behavior [6, 31, 32].

Figure 3 shows the average drawdown force for neat LDPE, LLDPE/LDPE blends, and neat LLDPE at a test temperature of 170°C for three different volumetric flow rates. It should be noted that the drawdown force data reported in Figure 3 were averaged from the drawdown force results given in Figure 2. Therefore, the changes in drawdown force could be explained in a similar fashion as for Figure 2, except for the effect of volumetric flow rate.

For any given roller speed, the drawdown force increased with increasing volumetric flow rate in the extruder from 1.4×10^{-7} to 4.1×10^{-7} m^3/s. This observation was in line with the work of Gupta and Bhattacharya [9] and our previous work [5, 29]. Higher volumetric flow rate was referred to as greater energy input or storage in the deformable polymer melts. The recoverable elastic energies in the molten LLDPE/LDPE blends would then release as kinetic energies within the filament, and this effect caused the increase in drawdown force which were detected by the load cell apparatus. This claim was also supported by Baldi et al. [1], who observed increased melt strength of polyolefin melts with increasing extrusion flow rate.

Mechanical Properties of Solidified LLDPE/LDPE Blends. Since this work aimed to establish a relation-
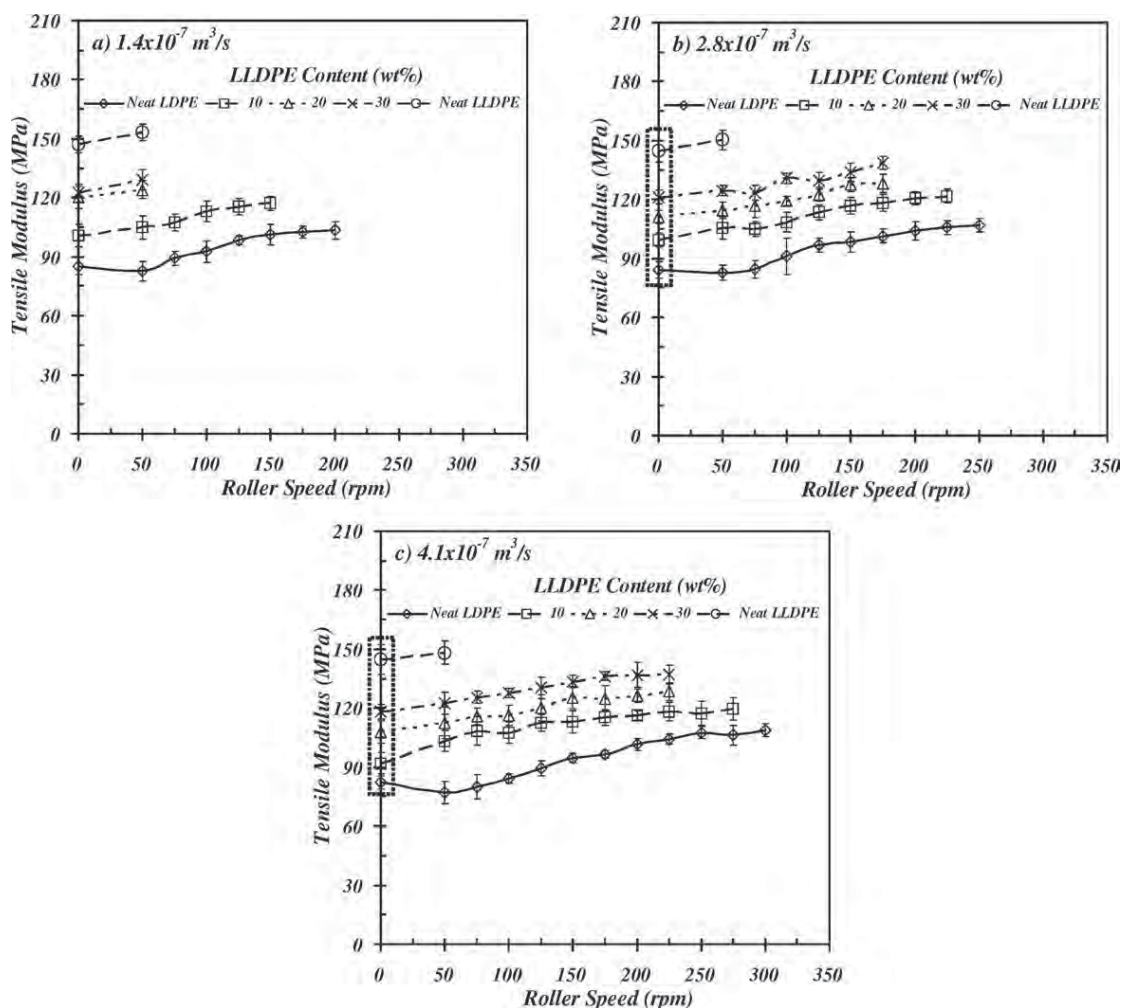
FIG. 4. Effects of roller speed and LLDPE content on tensile modulus of solidified LLDPE/LDPE blends for the volumetric flow rates (a) 1.4 × 10^{-7} m³/s, (b) 2.8 × 10^{-7} m³/s, and (c) 4.1 × 10^{-7} m³/s.

ship between the mechanical properties of LLDPE/LDPE blends in the molten and solidified states, the miscibility of LLDPE and LDPE on a molecular scale was not our main interest. The solidified filaments of neat LDPE, LLDPE/LDPE blends, and neat LLDPE that had been extruded and stretched by the melt-strength apparatus at different roller speeds and volumetric flow rates were collected and used for tensile testing at 25°C. Therefore, the number of data points for the solidified filaments corresponded to those for the molten filaments. The tensile results are expressed in terms of tensile modulus and tensile strength and are given in Figures 4 and 5, respectively.

The tensile modulus and tensile strength of the neat polymers and polymer blends slightly increased with increasing roller speed. This result occurred because higher roller speed could produce higher molecular orientations and stress-induced crystallization in neat LDPE, LLDPE/LDPE blends, and neat LLDPE solidified filaments. This claim was supported by Zhang et al. [31], who stated that LDPE could produce long and twisted la-

mellar orientation morphology, whereas LLDPE showed spherulite-like and random lamellar morphology at high draw ratios at the rollers of the extrusion blown film process. Figures 4 and 5 also show that the magnitude changes in the tensile properties of the molten and solidified filaments caused by the effects of roller speed and volumetric flow rate were not the same, but that those caused by the effect of LLDPE addition were very similar.

Figures 4 and 5 also show that the tensile modulus and strength of solidified LDPE improved with increasing LLDPE content. This finding could also be explained in terms of changes in crystallinity level, as given in Table 1, which clearly suggest that although the melting temperature of LDPE did not change with addition of LLDPE, the crystallinity level increased from 22.0% (neat LDPE) to 30.7% for LLDPE content increasing from 0 to 30 wt%. Similar findings were made in the work of Faheem [33] and Liu et al. [34]. Liu et al. [35] studied the thermal properties of LLDPE/LDPE blends and found that the increase in crystallinity level of the blends due to pres-
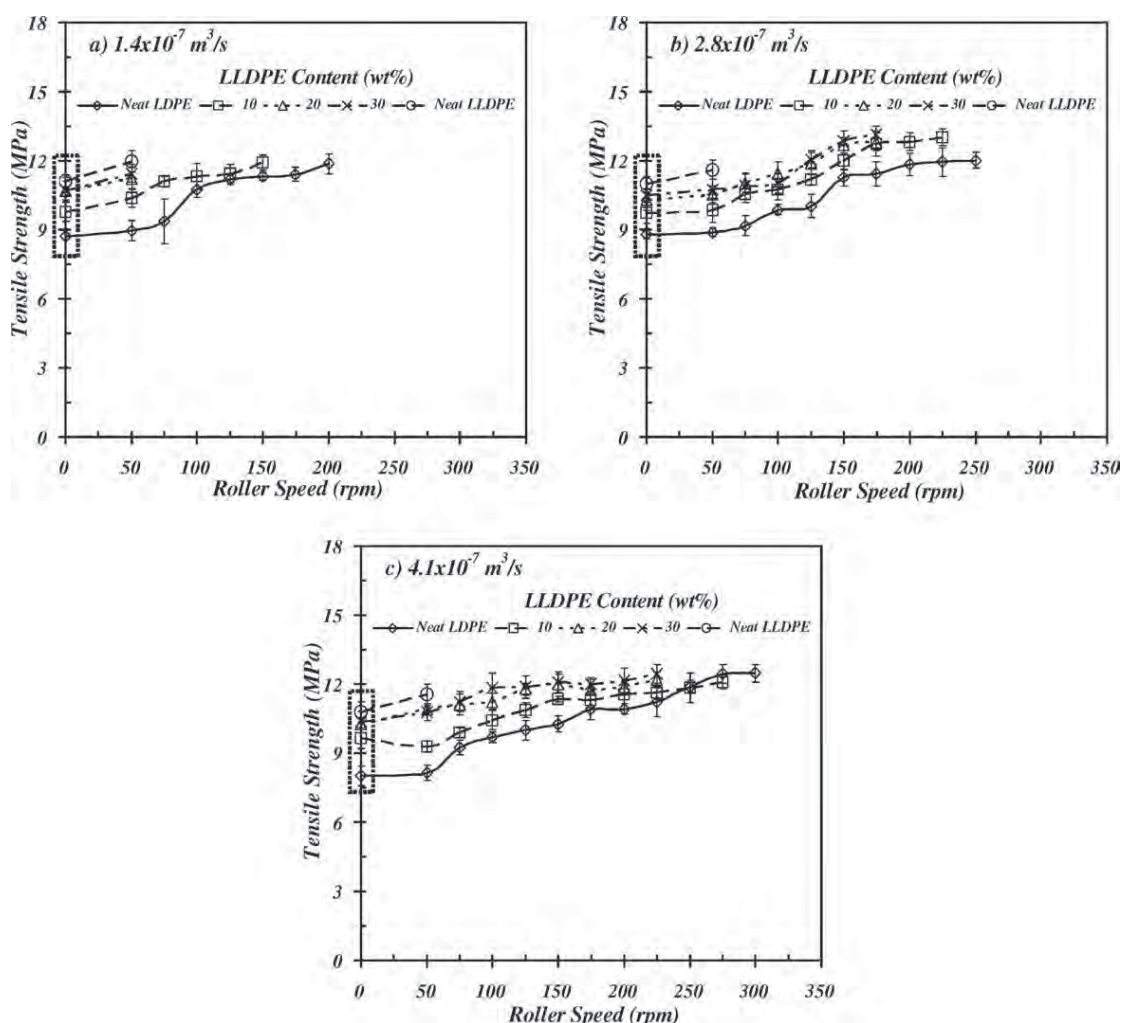
FIG. 5. Effects of roller speed and LLDPE content on ultimate tensile strength of solidified LLDPE/LDPE blends for the volumetric flow rates (a) 1.4 × 10^{-7} m^3/s, (b) 2.8 × 10^{-7} m^3/s, and (c) 4.1 × 10^{-7} m^3/s.

ence of LLDPE resulted from a higher cooling rate (easier crystallization) of LLDPE in the blends and that no cocrystallization occurred because of the high degree of branching of the LDPE phase. It was interesting to note that the tensile results in Figures 4 and 5 (solidified state) appeared to be in line with those in Figure 3 (molten state). This observation suggests that the mechanical properties of LLDPE/LDPE in the solidified state tended to correspond to those in the molten state with regard to the effect of LLDPE content despite different response mechanisms of the material in the molten (highly viscous response) and solid (highly elastic response) states during tensile deformation and different molecular orientations.

Wood/LDPE Composite System

Mechanical Properties of Molten wood/LDPE Composites. Figure 6 shows the drawdown force as a function of drawdown time with increasing step-ladder roller speed for three different wood flour contents at a die temperature of 170°C when using a 4.1 × 10^{-7} m^3/s volumetric flow rate from the extruder. The results suggests that the drawdown force of neat LDPE increased with increasing roller speed, the effect being most pronounced at 50 rpm roller speed. The explanation for this finding was already mentioned in the LLDPE/LDPE blends section. For wood/LDPE composites, it was obvious that increasing the wood flour content in LDPE caused significant decreases in drawdown time and maximum roller speed to failure. However, the drawdown force increased with

TABLE 1. DSC analysis for solidified LLDPE/LDPE blends

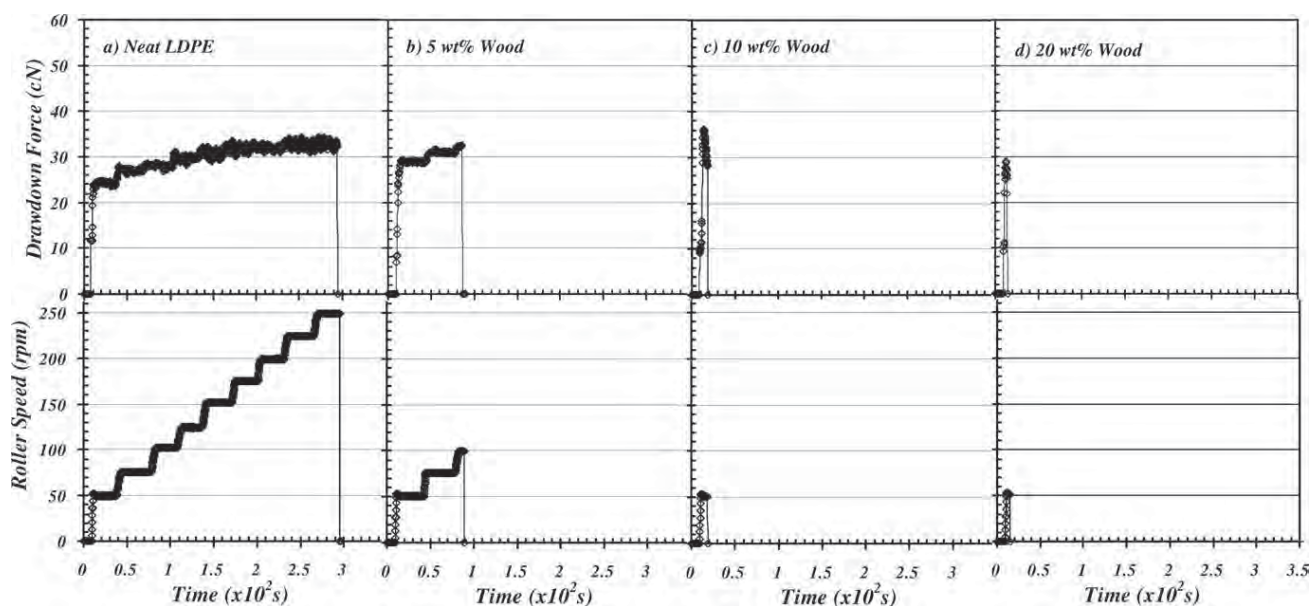| LLDPE content (wt%)	Thermal properties		
	T_m^* (°C)	ΔH_m (J/g)	X_c (%)
Neat LDPE	112.3	63.8	22.0
10	112.7	73.4	25.3
20	112.3	84.4	29.1
30	111.2	88.9	30.7
Neat LLDPE	125.4	95.1	32.8

FIG. 6. Drawdown force against time with increasing wood flour content under increasing step-ladder roller speed for wood/LDPE composites at 170°C with a the volumetric flow rate of 4.1×10^{-7} m^3/s.

increasing wood flour content up to 10 wt% before it decreased at the wood flour loading of 20 wt%. The increase in melt strength caused by wood flour was also observed by Kozlowski et al. [10] and by Li and Wolcott [13].

The increased drawdown force was associated with the rigidity of the wood that filled in the polymer, thus causing a reduction in mobility of the polymer chains. It was, however, surprising that the drawdown force of wood/LDPE composites at 20 wt% of wood flour was lower than that

FIG. 7. Photographs of extrudates of neat LDPE and wood/LDPE composites at various wood flour contents taken during extrusion. [Color figure can be viewed in the online issue, which is available at wileyonlinelibrary.com.]
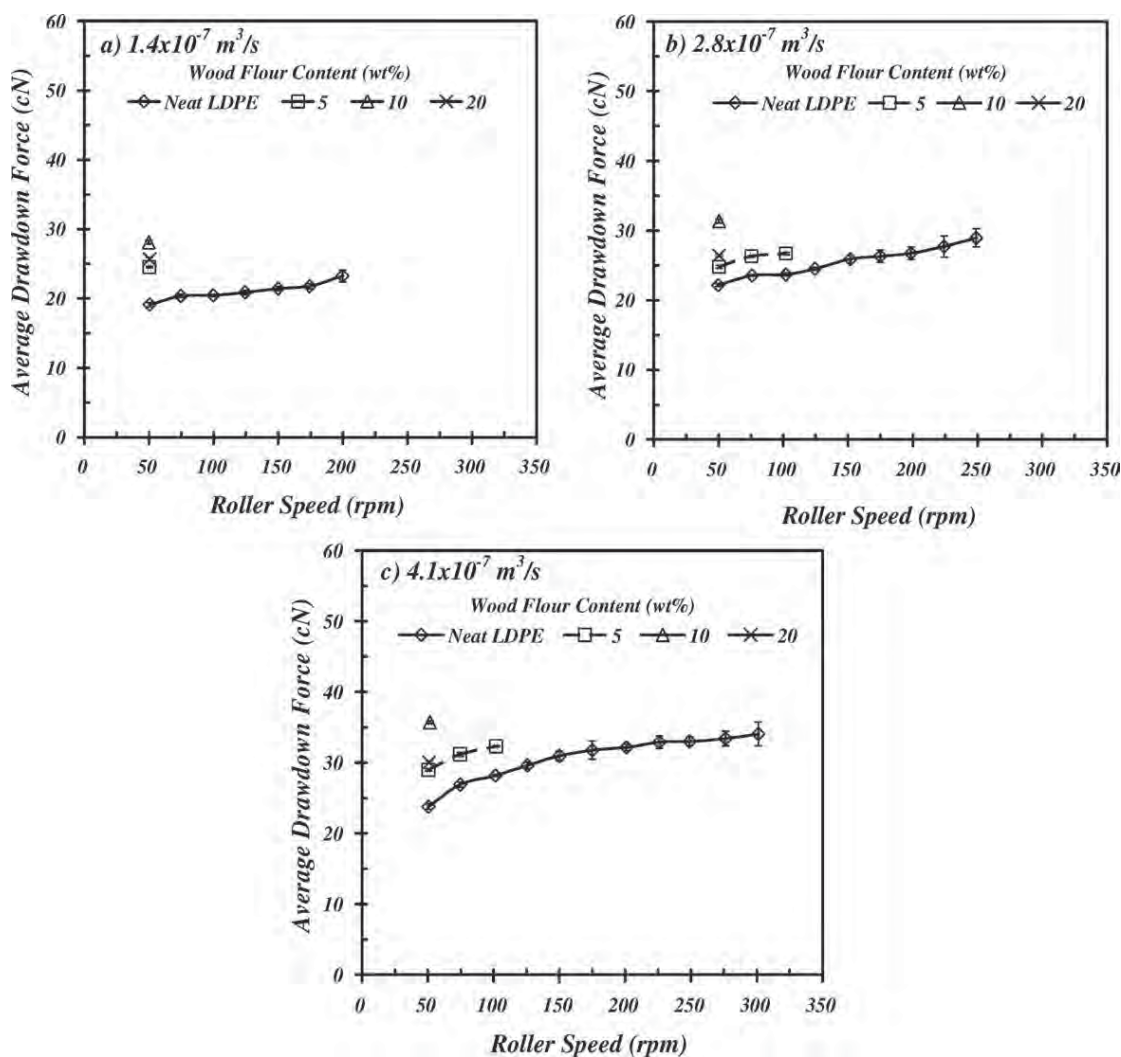
FIG. 8. Effects of volumetric flow rate on average drawdown force of wood/LDPE composites at 170°C for the volumetric flow rates (a) 1.4×10^{-7} m³/s, (b) 2.8×10^{-7} m³/s, and (c) 4.1×10^{-7} m³/s.

at 10 wt%. This result was probably caused by the occurrence of voids and pores and by agglomerations of wood particles in the wood/LDPE composites with 20 wt% wood content. Figure 7 shows photographs of extrudates of neat LDPE and wood/LDPE composites at various wood flour contents which were taken during extrusion. A number of large voids and pores on the rough extrudate surfaces are very obvious for the composites with 20 wt% of wood flour. They are probably due to excess moisture regain of the high wood content added into the polymer [36]. Besides, the rough extrudate surfaces also indicate that there were some stresses dissipated within the composite extrudates on exiting the die. These stresses eventually caused the lower strength of the composite extrudate while it was being pulled down by the rollers.

Figure 8 shows the average drawdown force for neat LDPE and wood/LDPE composites as a function of wood flour content when using a test temperature of 170°C for three different volumetric flow rates. The drawdown force

data reported in Figure 8 were averaged from the drawdown force results given in Figure 6. Therefore, the changes in drawdown force as a function of wood content could be explained in a similar fashion as for Figure 6 and will not be repeated here. As for the effect of volumetric flow rate from the extruder, it was found that the roller speed to failure for neat LDPE and wood/LDPE composites changed with changing volumetric flow rate. Higher volumetric flow rate contributed to greater average drawdown force and drawdown time because of the greater energy inputs given from the extruder [5, 29]. This behavior and its explanation are similar to those given for the LLDPE/LDPE blend system.

Mechanical Properties of Solidified Wood/LDPE Composites. Since this work was aimed toward establishing a relationship between the mechanical strengths of wood/LDPE composites in the molten and solidified states, the compatibility of LDPE and wood on the molecular scale
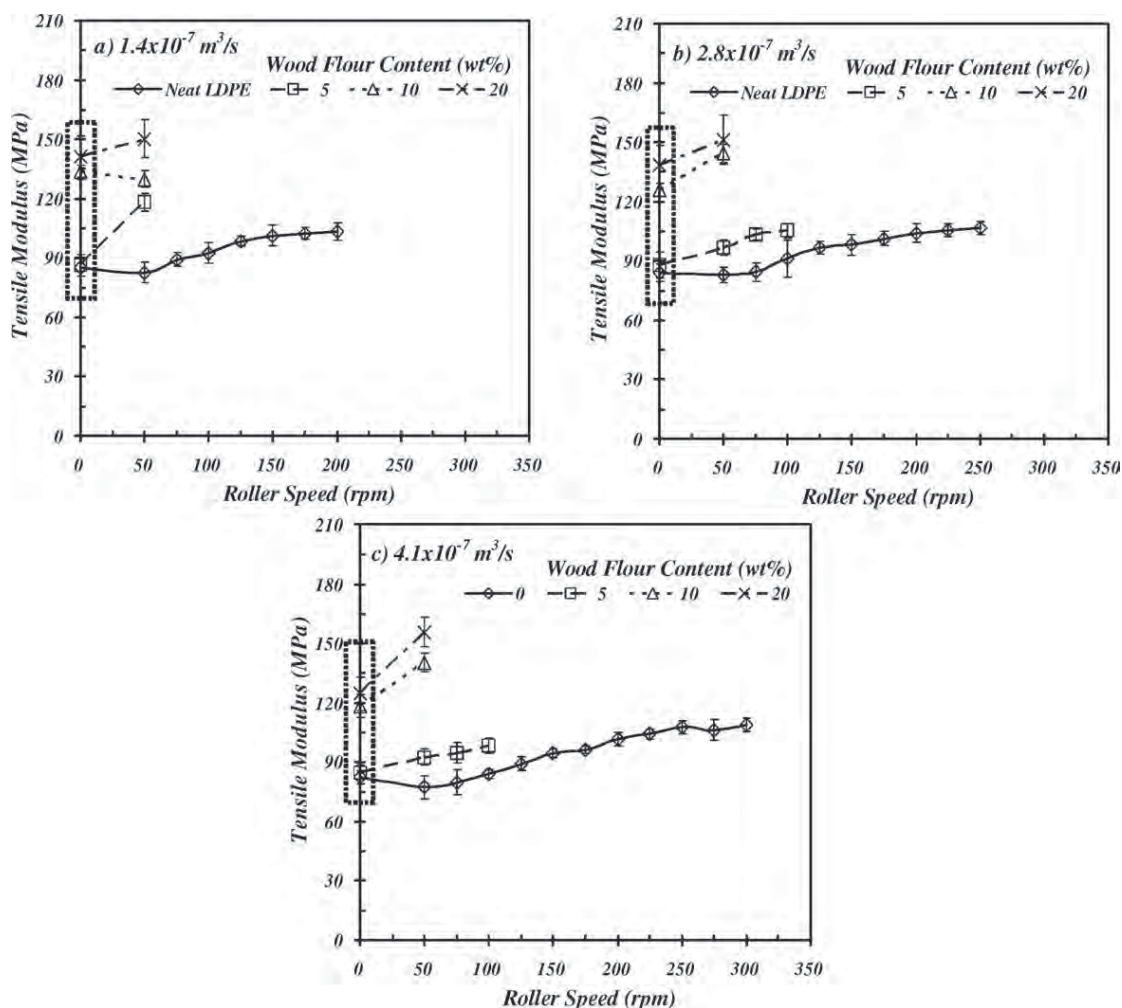
FIG. 9. Effects of roller speed and wood flour content on tensile modulus of solidified wood/LDPE composites for the volumetric flow rates (a) 1.4 × 10⁻⁷ m³/s, (b) 2.8 × 10⁻⁷ m³/s, and (c) 4.1 × 10⁻⁷ m³/s.

and the effect of chemical surface treatment on the wood particles were not the main interest. The solidified wood/LDPE filaments that were collected from the filament process (see the results from Figures 6–8) were used for tensile testing at 25°C. The tensile modulus and tensile strength results for the solidified composites are given in Figures 9a–9c and 10a–10c, respectively, as a function of roller speed, wood content, and volumetric flow rate. Unlike in the case of the molten wood/LDPE composites, for solidified wood/LDPE composites volumetric flow rate from the extruder had a minimal effect on the tensile modulus as a function of wood/LDPE content. For tensile modulus, it was generally observed that at 50 rpm roller speed, the tensile modulus for LDPE increased with increasing wood content when increasing the wood content from 5 to 10 wt%. At 20 wt% wood content, the tensile modulus decreased, but the value was still higher than that of the neat LDPE. The increases in tensile modulus may be explained by the presence of higher-rigidity material (wood particles) in the LDPE matrix [17–19] and a change in the crystallinity level of the LDPE. The latter

reason could be supported by the crystallinity (X_c) results as given in Table 2. It can be seen that as the wood content was increased, the X_c value increased from 22.0 to 28.4%, with a more obvious increase being observed when increasing the wood content from 5 to 10 wt%. These results that the wood particles acted as a nucleating agent in the LDPE matrix, although the melting temperature of LDPE did not obviously change. The increase in the crystallinity level could be supported by the work of Amash and Zugenmaier [37], Kositchaiyong and Sombatsompop [38], and Quan et al. [39], who suggested that cellulose fibers may act as a heterogeneous nucleating agent and nucleate crystallization along the interface. These nuclei would hinder the lateral extension and force growth in one direction, namely perpendicularly to the fiber surfaces, and result in a columnar crystalline layer, known as trans-crystallinity, leading to a higher crystallinity level. The decrease in tensile modulus of wood/LDPE composites at 20 wt% wood content was caused by the occurrence of voids and pores and by agglomerations of wood particles in the wood/LDPE composites, as
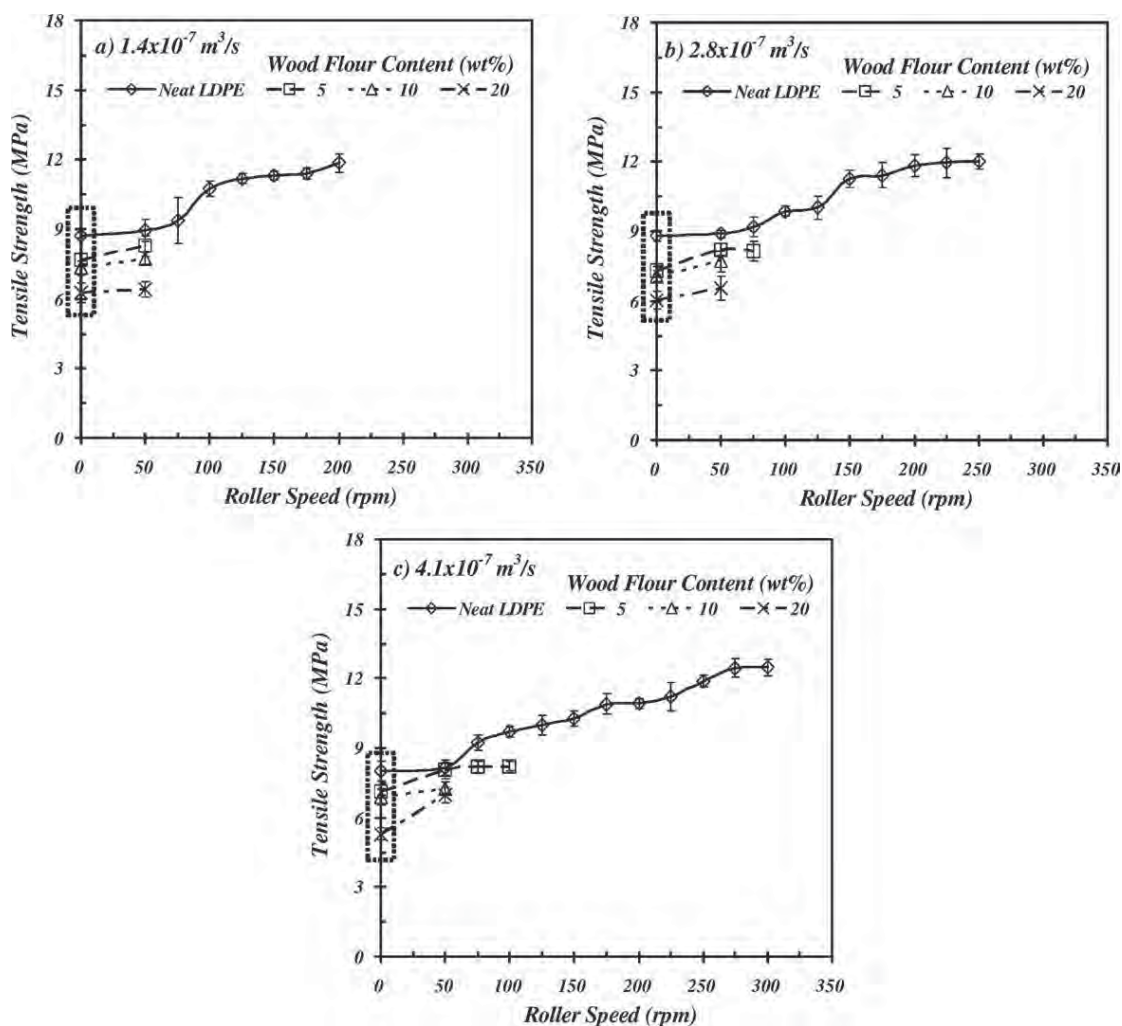
FIG. 10.   Effects of roller speed and wood flour content on ultimate tensile strength of solidified wood/LDPE composites for the volumetric flow rates (a) 1.4×10^{-7} m³/s, (b) 2.8×10^{-7} m³/s, and (c) 4.1×10^{-7} m³/s.

mentioned for Figure 7. The roller speed to failure decreased with increasing wood content, and this finding suggested the incompatibility between the wood and LDPE.

The changes in tensile strength for the solidified wood/LDPE composites shown as a function of wood flour content in Figure 10 were opposite to the variations in drawdown force for the molten wood/LDPE composites that are given in Figure 8. This difference could be explained by the role of wood particles in the LDPE matrix probably being different in the molten and solidified states of

TABLE 2.   DSC analysis for solidified wood/LDPE composites

| Wood flour content (wt%) | Thermal properties | | |
	T_m^* (°C)	ΔH_m (J/g)	X_c (%)
0	113.8	63.8	22.0
5	115.2	67.1	24.1
10	114.1	73.5	28.2
20	114.1	65.9	28.4

LDPE. In the molten state, the wood particles had the ability to restrict the molecular slippage of the LDPE chains during the stretching process of the LDPE filament, and this property would enhance the molecular entanglement and/or interlocking of the LDPE chains (i.e., cause an increase in the tension-thickening behavior). If this were the case, it would require higher force to break the composite filament. In the solidified state, the wood particles were likely to act as interfacial defects within the LDPE matrix because of their incompatibilities [14, 16, 17]. Since the LDPE and wood particles had different thermal conductivities, the pores and voids after solidification were then to be expected. These would cause the lower mechanical properties found when tensile testing.

The SEM micrographs of the fractured surfaces of wood/LDPE composites with various wood contents are given in Figure 11 in order to substantiate the wood-LDPE incompatibilities and the presence of voids and pores within the LDPE matrix. In terms of the effect of volumetric flow rate from the extruder, the change in
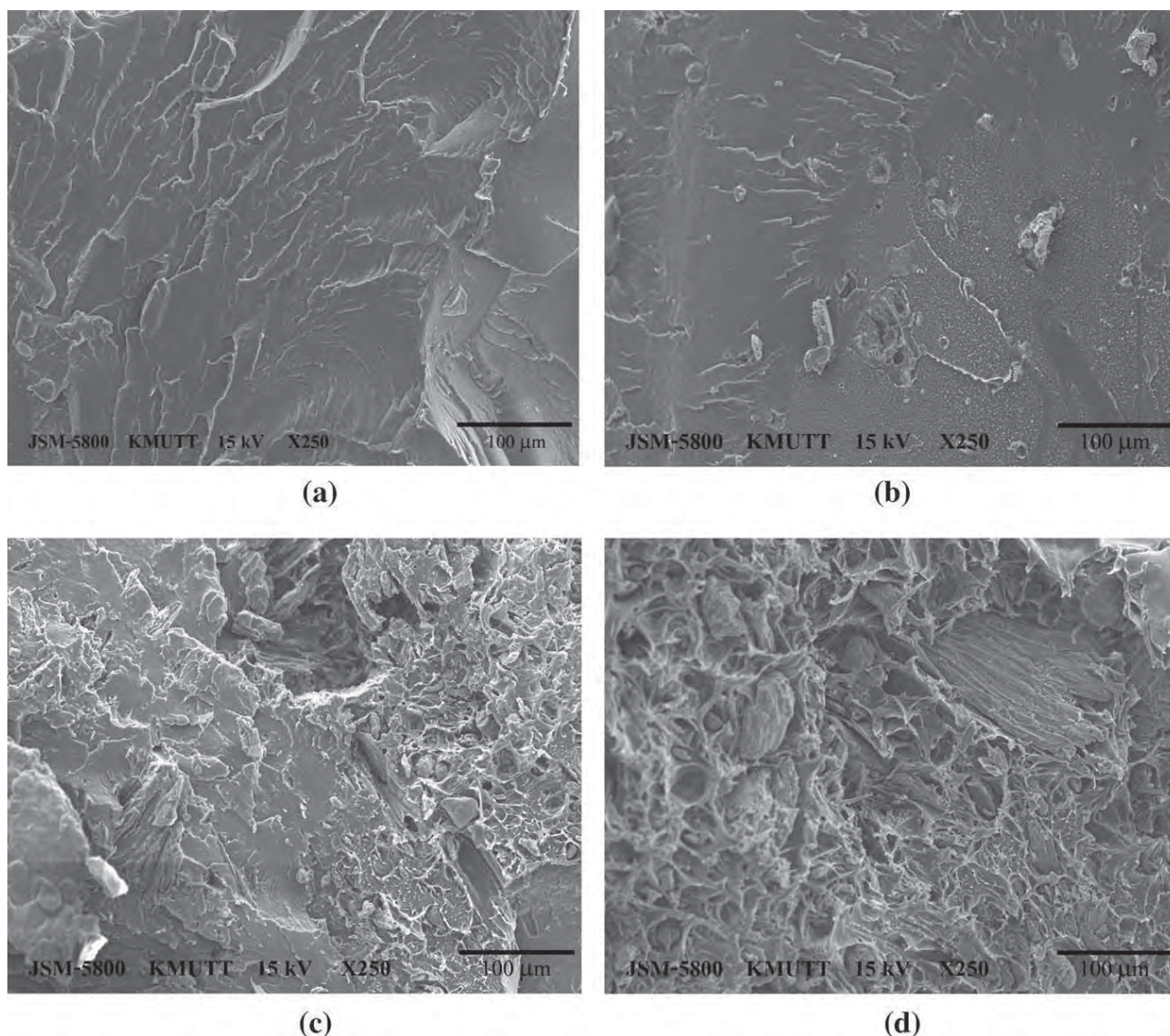
FIG. 11. SEM micrographs of wood/LDPE composites at a volumetric flow rate of 2.8×10^{-7} m^3/s and a roller speed of 50 rpm for different wood flour contents: (a) neat LDPE, (b) 5 wt%, (c) 10 wt%, and (d) 20 wt%.

tensile strength of the solidified wood/LDPE composites was very small as compared to that of the molten wood/LDPE composites.

CONCLUSION

In this work, LLDPE and wood particles were incorporated into LDPE, and the tensile properties were assessed in the molten and solidified states. For LLDPE/LDPE blends, the drawdown force for the molten LDPE increased with roller speed, volumetric flow rate, and LLDPE content. The results suggested that by knowing the mechanical properties of neat LDPE and LLDPE, the mechanical properties of LLDPE/LDPE in the solidified state could be predetermined from those in the molten state, especially with respect to the effect of LLDPE content. In wood/LDPE composites, as the wood content was increased in molten LDPE, the drawdown time and maximum roller speed to failure considerably decreased. The drawdown force of molten wood/LDPE composites increased with increasing wood flour content up to 10 wt% and then decreased at the wood content of 20 wt% because of the presence of voids and pores. Increasing wood content increased the tensile modulus of the solidified LDPE but decreased the tensile strength. The mechanical strength of wood/LDPE composites in the solidified state did not correspond to that in the molten state with regard to the effect of wood content. The effects of roller speed and volumetric flow rate in the wood/LDPE composite system were very similar to those in the LLDPE/LDPE blend system. The effect of volumetric flow rate from the extruder on the mechanical properties of the solidified blends and composites was very small as compared to that on the properties of the molten ones.

REFERENCES

1. F. Baldi, A. Franceschini, and T. Riccò, *Rheol. Acta*, **46**, 965 (2007).

2. M.H. Wagner, H. Bastian, A. Bernnat, S. Kurzbeck, and C.K. Chai, *Rheol. Acta*, **41**, 316 (2002).

3. A. Bernnat, Polymer Melt Rheology and the Rheotens Test, Ph.D Thesis, Universität Stuttgart, 2001.

4. T.D. Jesus, G. Medina, J.P. Gonzalez, and L.D. Vargas, *Rheol. Acta*, **44**, 278 (2005).

5. W. Harnnarongchai, N.T. Intawong, and N. Sombatsompop, *J. Macromol. Sci. B: Phys.*, **50**, 1074 (2011).

6. R. Pérez, E. Rojo, M. Fernández, V. Leal, P. Lafuente, and A. Santamaría, *Polymer*, **46**, 8045 (2005).

7. M.H. Wagner, S. Kheirandish, and M. Yamaguchi, *Rheol. Acta*, **44**, 198 (2004).

8. M. Yamaguchi and K.-I. Suzaki, *J. Appl. Polym. Sci.*, **86**, 79 (2002).

9. R.K. Gupta and S.N. Bhattacharya, *J. Polym. Eng.*, **27**, 89 (2007).

10. M. Kozlowski, S. Szczurek, T. Szczurek, and S. Frackowiak, *Int. J. Mater. Form.*, **1**, 751 (2008).

11. J.H. Park, J.C. Hyun, W.N. Kim, S.R. Kim, and S.C. Ryu, *Macromol. Res.*, **10**, 135 (2002).

12. H. Djidjelli, J.J. Martinez-Vega, J. Farenc, and D. Benachour, *Macromol. Mater. Eng.*, **287**, 611 (2002).

13. T.Q. Li and M.P. Wolcott, *Composites*, **A35**, 303 (2004).

14. A. Méndez, F. Vilaseca, A. Pèlach, P. Lépez, L. Barberà, X. Turon, J. Gironès, and P. Mutjé, *J. Appl. Polym. Sci.*, **105**, 3588 (2007).

15. N. Sombatsompop, K. Chaochanchaikul, C. Phromchirasuk, and S. Thongsang, *Polym. Int.*, **52**, 1847 (2003).

16. G. Canché, J. Laviada, I. Cupul, E. Mendizábal, E. Puig, and J. Franco, *Composites*, **A33**, 539 (2002).

17. H.D. Rozman, G.S. Tay, R.N. Kumar, A. Abusamah, H. Ismail, and Z.A. Ishak, *Eur. Polym. J.*, **37**, 1283 (2001).

18. L. Chotirat, K. Chaochanchaikul, and N. Sombatsompop, *Int. J. Adhes. Adhes.*, **27**, 669 (2007).

19. N. Sombatsompop, C. Yotinwattanakumtorn, and C. Thongpin, *J. Appl. Polym. Sci.*, **97**, 475 (2005).

20. R.R.N. Sailaja, *Compos. Sci. Technol.*, **66**, 2039 (2006).

21. K. Joseph, S. Thomas, and C. Pavithran, *Polymer*, **37**, 5139 (1999).

22. N. Sombatsompop, W. Prapruit, K. Chaochanchaikul, T. Pulngern, and V. Rosarpitak, *J. Vinyl Addit. Technol.*, **16**, 33 (2010).

23. T. Pulngern, S. Choocheepsakul, C. Padyenchean, V. Rosarpitak, W. Prapruit, K. Chaochanchaikul, and N. Sombatsompop, *J. Vinyl Addit. Technol.*, **16**, 42 (2010).

24. S. Tungjitpornkull, K. Chaochanchaikul, and N. Sombatsompop, *J. Thermo. Compos. Mater.*, **20**, 535 (2007).

25. I. Ghasemi, H. Azizi, and N. Naeimian, *J. Vinyl Addit. Technol.*, **15**, 113 (2009).

26. G.M. Rizvi and H. Semeralul, *J. Vinyl Addit. Technol.*, **14**, 39 (2008).

27. S. Jin and L.M. Matuana, *J. Vinyl Addit. Technol.*, **14**, 197 (2008).

28. O. Faruk and L.M. Matuana, *Compos. Sci. Technol.*, **68**, 2073 (2008).

29. W. Sitticharoen, N.T. Intawong, and N. Sombatsompop, *Polym. Polym. Compos.*, **18**, 359 (2010).

30. H. Zhu, Y. Wang, X. Zhang, Y. Su, X. Dong, Q. Chen, Y. Zhao, C. Geng, S. Zhu, C.C. Han, and D. Wang, *Polymer*, **48**, 5098 (2007).

31. X.M. Zhang, S. Elkoun, A. Ajji, and M.A. Huneault, *Polymer*, **45**, 217 (2004).

32. R.A. Bubeck, *Mater. Sci. Eng.*, **R39**, 1 (2002).

33. M. Faheem, M.S. Thesis, A study of tensile and microhardness properties of m-LLDPE/LDPE blends, King Fahd University of Petroleum and Minerals, Dhahran, Saudi Arabia, 2003.

34. G. Liu, Y.-F. Li, F.-Y. Yan, Z.-X. Zhao, L.-C. Zhou, and Q.-J. Xue, *J. Polym. Environ.*, **13**, 339 (2005).

35. C. Liu, J. Wang, and J. He, *Polymer*, **43**, 3811 (2002).

36. N. Sombatsompop and K. Chaochanchaikul, *Polym. Int.* **53**, 1210 (2004).

37. A. Amash and P. Zugenmaier, *Polymer*, **41**, 1589 (2000).

38. N. Sombatsompop, A. Kositchaiyong, and E. Wimolmala, *J. Appl. Polym. Sci.*, **102**, 1896 (2006).

39. H. Quan, Z.-M. Li, M.-B. Yang, and R. Huang, *Compos. Sci. Technol.*, **65**, 999 (2005).

Stabilizations of Molecular Structures and Mechanical Properties of PVC and Wood/PVC Composites by Tinuvin and TiO$_2$ Stabilizers

Kantima Chaochanchaikul, Narongrit Sombatsompop
Polymer PROcessing and Flow (P-PROF) Group, School of Energy, Environment and Materials,
King Mongkut's University of Technology Thonburi (KMUTT), Thongkru, Bangmod, Bangkok 10140, Thailand

Three different UV stabilizers, 2-(2H-benzotriazol-2-yl)-4,6-ditertpentylphenol (Tinuvin XT833), 2-(2H-benzotriazol-2-yl)-*p*-cresol (Tinuvin P), or rutile–titanium dioxide (TiO$_2$) were incorporated into poly(vinyl chloride) (PVC) and wood/PVC (WPVC) composite, and mechanical and physical properties and photostabilities were monitored. The polyene and carbonyl sequences of PVC increased with UV weathering time and with presence of wood flour. The yellowness index increased because of polyene and carbonyl productions, whereas the brightness increased because of the photobleaching of lignin in wood. The photostabilities of PVC and WPVC could be improved through the use of UV stabilizers. Tinuvin P was recommended in this work as the most effective stabilizer for PVC and WPVC composites. The stabilization effect was interfered by presence of wood particles. The mechanical property changes corresponded well to the structural changes under UV for neat PVC. For WPVC composites, the presence of wood particles played more significant effect on the mechanical properties during UV aging than the UV stabilizer. POLYM. ENG. SCI., 51:1354–1365, 2011. © 2011 Society of Plastics Engineers

INTRODUCTION

Wood/polyvinyl chloride (WPVC) composite is one of the commonest wood/polymer composites (WPC) and is most suitable for outdoor decorations, buildings and construction applications because of high mechanical properties and strong chemical resistances. In addition, WPVC composites have relatively good flame retarding properties as a result of having chlorine atoms in the PVC molecules. However, WPVC composites may be thermally and photochemically unstable due to dehydrochlorination and photo-oxidation reactions. If this

is the case, the WPVC composites are quickly deteriorated, especially discolored appearances, and worsening of physical and mechanical properties [1, 2].

Photodegradations in PVC and wood have been discussed separately by a number of published articles [3–10]. The photodegradation reaction in PVC has been widely considered to initiate at labile structures in the PVC chains which include allylic and tertiary chlorine atoms as well as hydroperoxide, carbonyl and polyene groups. These labile structures or chromophores may arise during the polymerization and processing. The UV radiation could produce photochemical degradations in PVC under a wavelength close to 310 nm and this photodegradation of PVC molecules can be complex process due to the coexistence of oxidation and hydrogen chloride (HCl) elimination reactions. There have been a number of literatures studying the effects on photodegradation in PVC [3–5]. Real et al. [3] investigated the effect of weathering conditions on the photodegradation of PVC, and found that resistance of PVC surface on photodegradation increased when exposed in a long preliminary period of UV irradiation. The degradation thickness profiles of PVC under the accelerated weathering were studied by Anton-Prinet et al. [4] who revealed that the carbonyl and chain scissions were predominant at the superficial zone of thickness lower than 100 μm whereas the HCl elimination reaction and crosslinking occurred predominantly at 100 and 400 μm deep from the surface of PVC. Torikai et al. [5] indicated that photodegradation of PVC was accelerated under the longer wavelength radiation (simulating terrestrial sunlight) by preirradiation with shorter wavelength radiation ($\lambda = 253.7$ nm). To prevent the photodegradation of PVC, UV absorbers and stabilizers are strongly recommended in the PVC compound formulations [6–8]. Xiang et al. [6] found that UV absorber (Chimassorb 81) and the mixture of Chimassorb 81 with organic calcium complex had good ability to inhibit the photodegradation reaction of PVC. Xu et al. [7] synthesized, 5′-disulfide-bis[2-(2-hydroxy-3,5-di-tert-butylphenyl)-2Hbenzotriazole] (DSBHTBB) UV absorber and studied its effectiveness with some common commercial benzotriazole UV absorbers in terms of discolorations of PVC. They showed that

DSBHTBB could greatly inhibit discolorations of PVC during UV exposure. Bruan and Rabie [8] revealed that the natural calcium carbonate ($CaCO_3$) could act as filler and also costabilizer under UV light in PVC which were compounded with Calcium-Zinc (Ca-Zn) stearate and dibutyltin-S,S' -di(isooctyl thioglycolate) stabilizing systems. In woods, lignin is the key structure and responsible for photodegradation reaction as the lignin has ability to absorb in the UV/visible region because of its chromophoric groups [9]. Colom et al. [9] examined the structural changes in the cellulose and lignin components of both woods using Fourier transform infrared (FTIR) spectroscopy, and found that all characteristic bands of lignin (1595, 1510, and 1465 cm^{-1}) decreased with increasing UV ageing times. Moisture was the significant factor that accelerated the photodegradation reaction in the wood [10].

Regarding studies on photodegradations in WPC, most available literatures have focused on the photodegradations for wood/polyolefin composites [11–17], whereas a few have given attentions for wood/PVC [1, 2, 18–20]. Stark et al. [11] studied the durability of wood/high-density polyethylene (wood/HDPE) composite after ultraviolet exposure, and found that surface oxidation occurred immediately after UV exposure, and the surface oxidation for the wood/HDPE composites was greater than that for the neat HDPE. The photodegradation of the lignin in wood components has been reported to be the main reason for the color fading with a smaller extent of color-fading contribution from polymer matrices [12, 13]. Muasher and Sain [12] proposed that the wood/HDPE composites underwent two competing redox reactions upon UV exposure. The first was the oxidation of lignin which led to formation of paraquinone chromophoric structures within the first 250 hr of UV exposure, and the second was the reduction of the paraquinone structures to hydroquinones which led to photobleaching after 250 hr of UV exposure. The structural changes in wood/polymer composites also have significant effects on mechanical, physical and structural properties. Matuana et al. [2] and Raghi et al. [18] found that the tensile properties of WPVC composites changed after weathering and the light stability of WPVC samples decreased with increasing wood flour content as a result of chromophoric groups in the wood flour that could accelerate the degradation of the PVC [1, 19]. Fabiyi and McDonald [20], they studied effect of weathering under different weathering regimes on the WPVC composites and found that natural and accelerated xenon-arc and UVA weathering regimes increased total color change, carbonyl concentration and wood loss on the surface of the weathered WPVC composites. However, the light stability of the WPVC could be improved through use of rutile titanium dioxide photoactive pigment [1]. Apart from UV light, WPVC composites are also sensitive to heat during processing. Work by Sombatsompop et al. [21] suggested that the additions of zinc and lead stearates into WPVC composite could

TABLE 1. Materials formulations for PVC compound and WPVC composites.

Ingredients	Concentration (phr)
Suspension PVC (SIAMVIC® 258RB)	100.0
External lubricant (Finalux® G-741)	0.6
Internal lubricant (Ca-St)	0.6
Processing aids (PA-20)	6.0
Thermal stabilizer (PF608)	3.6
Natural filler (wood flour)	Varied (0, 50, 100)
UV stabilizers (type and dosage)	
Rutile titanium dioxide	Varied (0, 2.5, 5.0)
Tinuvin P	Varied (0, 1.0, 2.0)
Tinuvin XT833	Varied (0, 1.0, 2.0)

improve the thermal stability of the PVC in WPVC by retarding the upzipped reaction and by reducing the conjugated double bonds in PVC molecules.
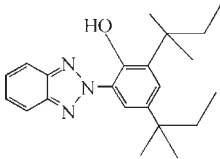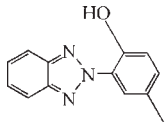
One of the most conventional methods to stabilize PVC and/or wood/PVC composites during UV exposure is addition of UV stabilizers, and according to recent literatures [11–20], studies on the effects of UV stabilizers on structural changes and stabilities of the WPVC composites are rare and still open for discussion among scientists and technologists. This is because wood flour in PVC compound is likely to affect the stabilizing performance of the UV stabilizers used. This was supported by the work of Matuana et al. [2] that the tensile properties and light stability of WPVC samples decreased with increasing wood flour content as a result of chromophoric groups in the wood flour that could accelerate the degradation of the PVC. Therefore, it would be interesting to investigate the stabilization mechanism of UV stabilizers in PVC compound by the presence of wood flour. In this work, three different UV stabilizers were introduced into both neat PVC compound and wood/PVC composite, and the mechanical and physical properties, and photostabilities of the PVC and WPVC were monitored. The effects of type and content of UV stabilizers, UV weathering time and the presence of wood flour on the molecular structure and mechanical properties were our main interest in this work. The stabilizing mechanisms of all UV stabilizers used in the PVC and WPVC composites were proposed and discussed.

EXPERIMENTAL

Raw Materials

Suspension PVC. Suspension poly(vinyl chloride) (PVC) was supplied by V.P. Wood Co. (Bangkok Thailand) in the form of powder and used trade name as SIAMVIC 258RB having a K value of 58. The PVC powder was dry blended with various necessary additives as listed in Table 1, this being referred to as PVC compound.

TABLE 2. Chemical descriptions and structures for UV stabilizers used in this work.

Trade name	Chemical description	M_w	Chemical structure
Tinuvin XT833	2-(2H-benzotriazol-2-yl)-4,6-ditertpentylphenol	351.49	
Tinuvin P	2-(2H-benzotriazol-2-yl)-p-cresol	225	
Tiona 696 (TiO$_2$)	Rutile titanium dioxide	79.87	TiO$_2$

Wood Flour Particles. Wood flour particles were obtained from carpentry and wood-working processes and supplied by V.P. Wood Co. (Bangkok Thailand). The average size of wood particles used in this work was in the range of 100–300 μm. In this work, the content of wood sawdust particles in the PVC compounds was varied from 0, 50, and 100 parts per hundred resin (phr) of PVC powder, and the wood particles were chemically treated with 1.0 wt% N-2(aminoethyl)3-aminopropyl trimethoxysilane having a weight average molecular weight of 222.4.

UV Stabilizers. Three UV stabilizers were used in this work, these being 2-(2H-benzotriazol-2-yl)-4,6-ditertpentylphenol (trade name as Tinuvin XT833), 2-(2H-benzotriazol-2-yl)-p-cresol (trade name as Tinuvin P), supplied by Ciba Specialty Chemicals Co. (Bangkok, Thailand), and rutile titanium dioxide (trade name as Tiona 696, TiO$_2$), supplied by Millennium Chemicals (Shanghai, China) Inc. Work by Markarian [22] suggested that Tinuvin P and XT833 could act as effective and high performance UV stabilizers for PVC, and TiO$_2$ was suggested by Kamisli, and Turan [23] to be UV screener which is highly reflective at visible wavelength and absorptive at UV wavelength. Their chemical structures and descriptions are listed in Table 2. It should be noted that the concentrations used for Tinuvin XT833, Tinuvin P and TiO$_2$ were based on recommendation by the supplier (Ciba Specialty Chemicals Co. (Bangkok, Thailand), and Kamisli and Turan [23]). This work was to compare the effectiveness of these three UV stabilizers for any given concentrations by evaluating the changes in structural and mechanical properties of PVC and WPVC samples during UV weathering as a result of increasing the contents of each stabilizer.

Sample Preparation

In this work, WPVC composites produced by an industrial-scale twin screw extruder and the wood flour content added into the PVC compound was varied from 0 to 100 phr of PVC. Before blending of wood particles and PVC compound, the wood particles were subjected to heat treat-

ment in an oven at 80°C for 24 hr until the weight of the wood was constant. After that, the PVC compound was dry blended with the wood particles by a high speed mixer for 2 min before they were melt blended in an industrial-scale twin screw extruder (D-521, Reifenhäuser GmbH & Co. Maschinenfabrik, Germany) with counter-rotating screws. The processing temperature profiles on the extruder from hopper to die zones were 170, 160, 150, 140, 135, and 170°C. The decreases of the processing temperatures from 170 to 135°C were used for compensation for the shear heating effect of the molten PVC and WPVC composites during the flow along the barrel length whereas the increases of the processing temperatures from 135 to 170°C were used for minimization of the sharkskin effect of the melts exiting the die. The screw rotating speed was 16 rpm A slit die, whose dimensions (width x height x length) were 40 × 4 × 180 mm^3, was used to produce slit extrudates. The extrudates were then solidified by passing through a cooling system and a size-control device before collection for preparing specimens.

Weathering Testing

The PVC and WPVC specimens were cut from extrudates whose dimensions were dependent on the standard testing methods used. The prepared PVC and WPVC specimens were weathered in a QUV weatherometer (Q-panel, OH) operated according to ASTM G154 (2006). The PVC and WPVC specimens were UV-weathered in the cyclic UV/condensation exposures using 8 hr of UV light exposure at 60°C with the 313 nm fluorescent UV (UVB) lamps followed by 4 hr of condensation temperatures of 50°C. The mechanical properties, and structural and color changes of the weathered neat PVC and WPVC specimens were evaluated as a function of UV weathering time ranging from 0 to 720 hr.

Characterizations

Mechanical Properties. The mechanical properties of un-weathered and weathered neat PVC and WPVC speci-

mens were investigated through tensile and flexural deformation modes. The tensile testing was performed on a SHIMADZU tensile tester (Tokyo, Japan) at crosshead speed of 5 mm/min. The tensile test procedure followed the ASTM D638 (1990) Specimen Type I. The flexural properties were determined using ASTM D790 (1990). The specimen dimensions were 15.0×80.0 mm^2 with a support span of 64 mm, and a crosshead speed of 1.71 mm/min.

Structural Change Analysis. Polyene and carbonyl indices were determined using attenuated total reflectance Fourier transform infrared (ATR-FTIR) analysis to assess the extent of degradation of the PVC and WPVC. This was performed by measuring the reflectance difference percentage at the surface of the un-weathered and weathered specimens. The dimensions of specimens used (width x length x thickness) were $15 \times 80 \times 4$ mm^3. The tests were performed using ATR-FTIR Spectrometer (Nicolet 6700 FT-IR spectrometer, USA) to produce spectra of reflectance against wave number. In this work, polyene index was calculated by subtracting the value of % reflectance of the peak of interest ($\%R_{1630}$) from the baseline ($\%R_{baseline}$) and dividing it by the reference value ($\%R_{2920}$) subtracted from the baseline ($\%R_{baseline}$) as shown in Eq. *1* [21]. The different wave numbers followed were 2920 and 1650 cm^{-1} for C—H stretching and polyene sequences, respectively. For carbonyl index, it was calculated according to Eq. *2*. The wave number of 1730 cm^{-1} represents carbonyl group.

$$\text{Polyene index} = \frac{\%R_{1650} - \%R_{baseline}}{\%R_{2920} - \%R_{baseline}} \quad (1)$$

$$\text{Carbonyl index} = \frac{\%R_{1730} - \%R_{baseline}}{\%R_{2920} - \%R_{baseline}} \quad (2)$$

Discoloration Testing. The color changes of un-weathered and weathered PVC and WPVC specimens were determined by yellowness index (*YI*) and *L*a*b** coordinates. The *YI* were estimated by using a UV-Vis Spectrophotometer (Shimatsu UV-Vis 3100 Spectrophotometer, Japan) under the standard source C. The *YI* of un-weathered and weathered specimens before was calculated by measured *X, Y* and *Z* tristimulus values as shown in Eq. *3* [21]. The values of *YI* were estimated under the standard source C due to Eq. *3* defined by source C only.

$$YI = \frac{100(1.28X_{CIE} - 1.06Z_{CIE})}{Y_{CIE}} \quad (3)$$

In addition, a UV–Vis spectrophotometer was used to measure color changes of PVC and WPVC samples before and after UV weathering using the CIELAB color system. *L*a*b** coordinates of un-weathered and weathered PVC and WPVC specimens were calculated based

on a D65 light source. *L** represents the lightness whereas *a** and *b** are the chromaticity coordinates. The higher the *L** value the lighter the sample. The *a** coordinate represents red-green coordinate, whereas the *b** coordinate represents yellow-blue coordinate. The total color changes or discolorations of the UV-weathered specimens was calculated from differences of lightness and chromatic coordinates (ΔE) of un-weathered and weathered PVC and WPVC specimens as expressed in Eq. *4* [2, 6].

$$\Delta E^* = \sqrt{(L_2^* - L_1^*)^2 + (a_2^* - a_1^*)^2 + (b_2^* - b_1^*)^2} \quad (4)$$

where subscript 1 denotes the values of un-weathered PVC and WPVC specimen and subscript 2 denotes the values of weathered PVC and WPVC specimen.

RESULTS AND DISCUSSION

Structural Changes

In this work, polyene and carbonyl sequences were assessed for structural change evaluations using ATR-FTIR analysis and used for estimations of photodegradation in neat PVC and WPVC composites. Considering PVC and WPVC without UV stabilizers, it was found that the polyene contents for neat PVC and WPVC composites in Fig. 1 increased with UV weathering time. This was probably due to a photodegradation of PVC in the neat PVC and WPVC samples. The increases in polyene sequences in the WPVC samples were more pronounced than those in the neat PVC. This was because of chromophore in lignin which was more able to absorb UV light onto the surface of the WPVC sample [15, 19] compared with the neat PVC sample. This would eventually result in the production of more polyene sequences in the PVC structure.

Figure 2 shows FTIR spectrum for neat PVC compound with and without UV stabilizer. This was seen from Figs. 1 and 2 that a progressive decrease in polyene content was observed when adding the UV stabilizers, although the polyene content still increased with increasing UV weathering time. The stabilization mechanism of Tinuvin P and Tinuvin XT833 involved strong intramolecular hydrogen bonds between hydroxyl groups and nitrogen atoms in Tinuvin, and this resulted in methyl and intercyclic torsional movements at low frequencies and thus the radiationless deactivation [24]. In the case of TiO$_2$, the photostability concerned a high screen effect of the UV light, the photostability for TiO$_2$ being found elsewhere [4]. From the experimental results in Fig. 1, it was observed that among three UV stabilizers used, it was found that Tinuvin P and TiO$_2$ were more effective than Tinuvin XT833, indicated by the magnitude decreases in the polyene contents with increasing the content of each UV stabilizer. The differences in the stabilization levels between Tinuvin P and Tinuvin XT833 involved the differences in their molecular structures (Table 2) which
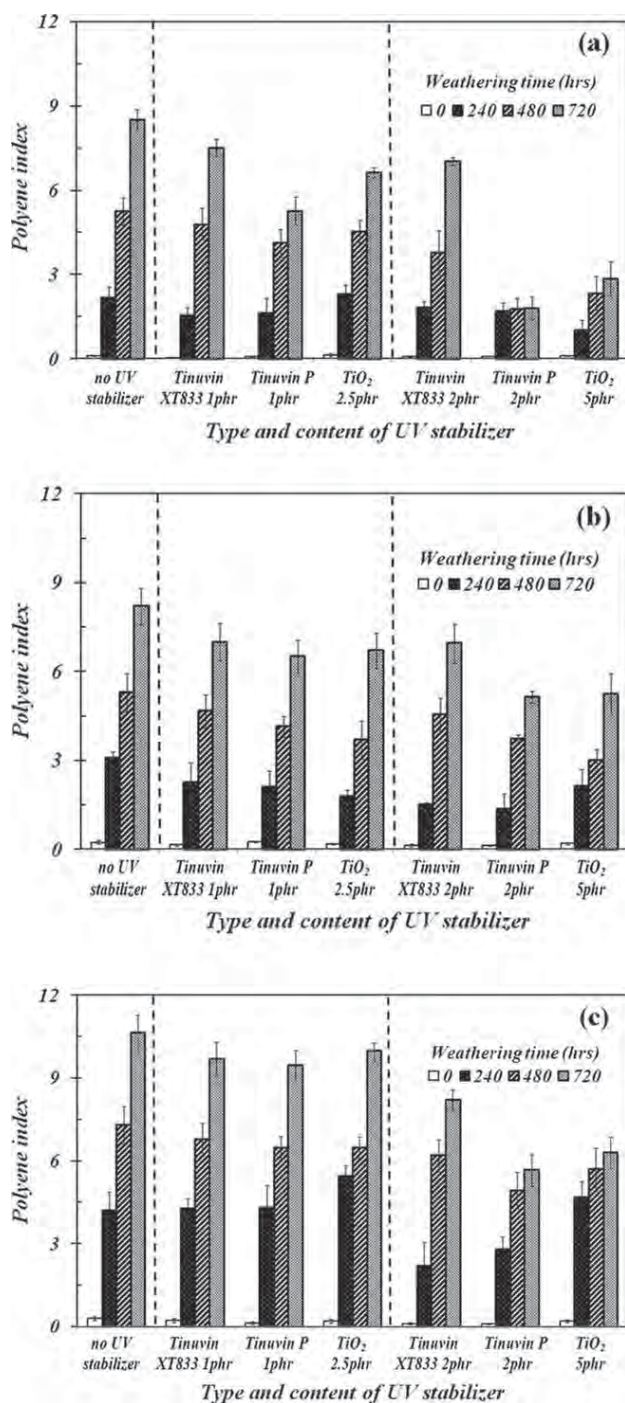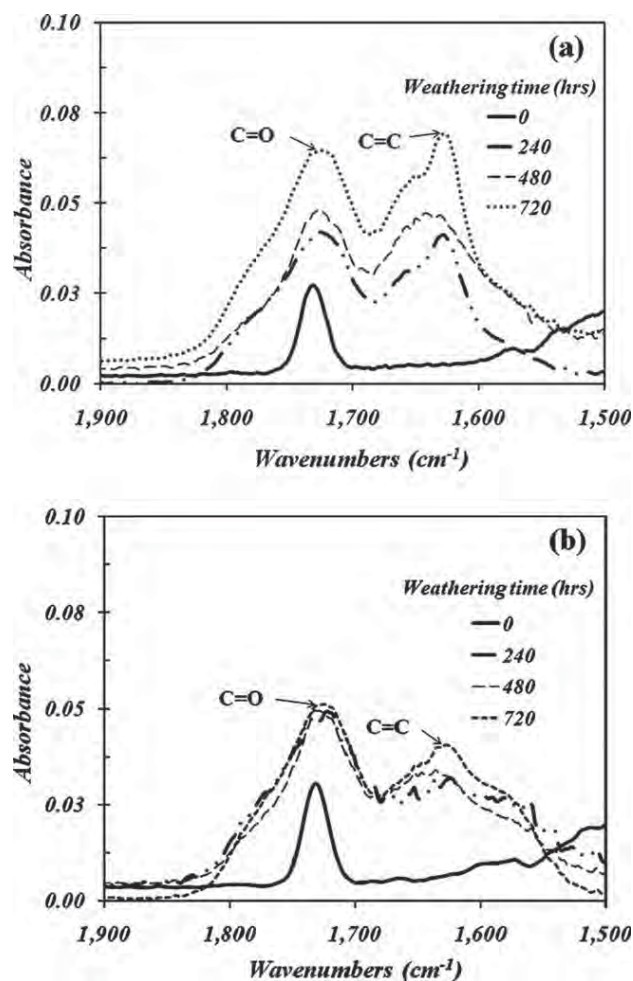
FIG. 2. FTIR spectrum for neat PVC compound with and without Tinuvin P neat PVC without UV stabilizer (b) neat PVC with Tinuvin P 2 phr.

words, for given UV stabilizers the polyene content in the WPVC composites was much higher than that in the neat PVC. This could be explained by hydrogen bondings between the wood surfaces and UV stabilizers (Tinuvin P and Tinuvin XT833). This statement could be explained schematically using Scheme 1. If the hydrogen bondings

FIG. 1. Polyene index of neat PVC and WPVC composites containing Tinuvin P, Tinuvin XT833, or TiO$_2$ neat PVC, (b) PVC with wood flour at 50 phr, and (c) PVC with wood flour at 100 phr.

affected the torsional movements of intercyclic and methyl groups. That was, it was expected for Tinuvin XT833 to have a steric effect around the phenol groups. This would make the intercyclic torsional movements more difficult to occur, and thus less effective for photo-stabilizing the PVC molecules. In all cases, increasing UV stabilizer concentration decreased the polyene content, more obvious being for the neat PVC. In other
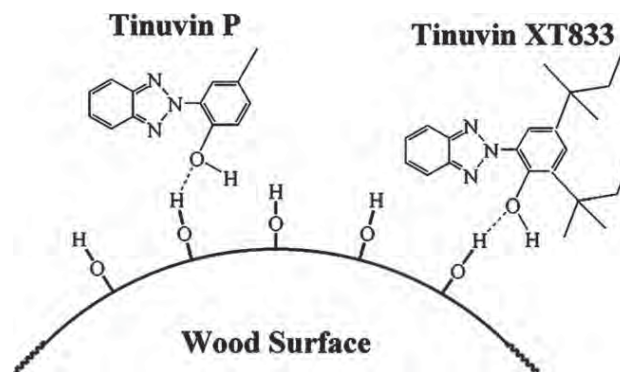

SCHEME 1. A proposed mechanism of hydrogen bonds between wood surface and Tinuvin P or Tinuvin XT833 stabilizer.
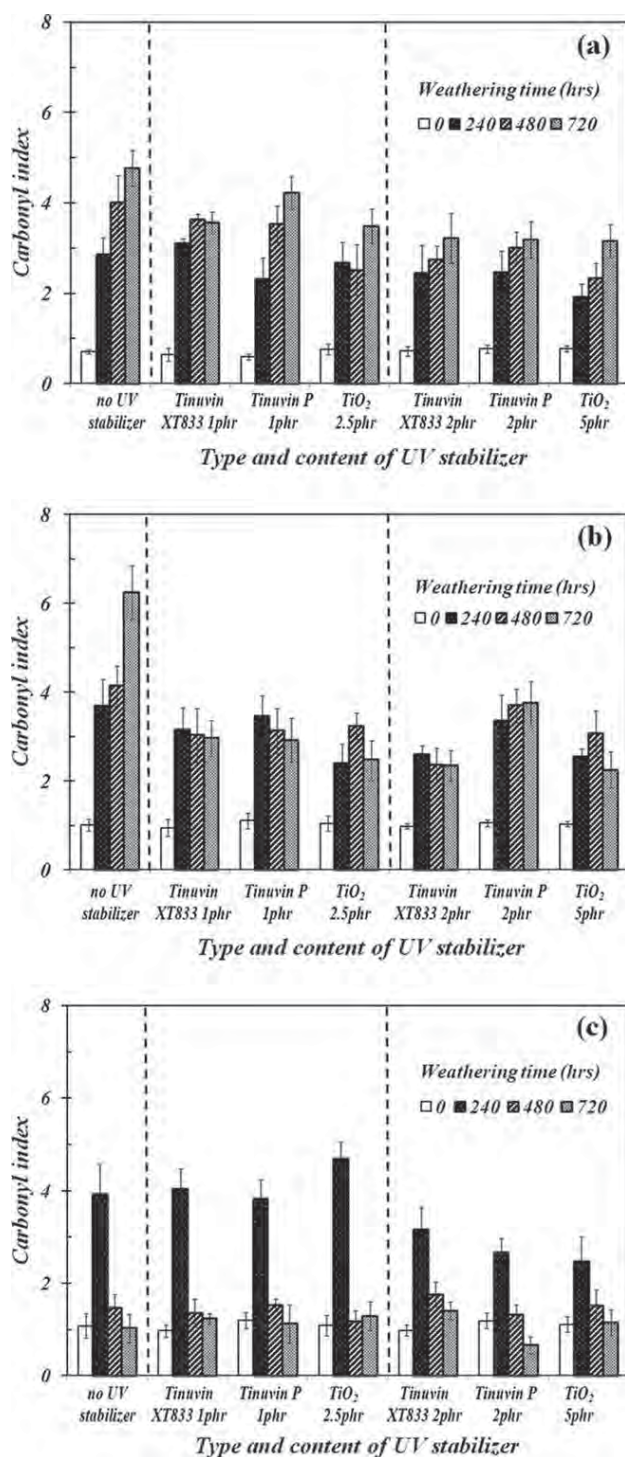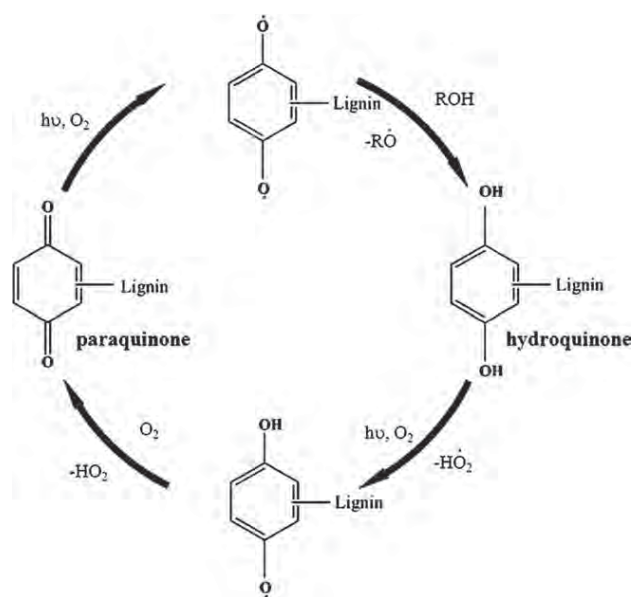
FIG. 3. Effect of type and content of UV stabilizers on carbonyl groups in neat PVC and WPVC composites neat PVC (b), PVC with wood flour at 50 phr, and (c) PVC with wood flour at 100 phr.

between the wood surfaces and Tinuvin UV stabilizers were formed, the abilities of the Tinuvin P and Tinuvin XT833 stabilizers to absorb the UV light would automatically reduce. Therefore, PVC in the WPVC composites would no longer be fully stabilized by Tinuvin P and Tinuvin XT833.

Figure 3 shows carbonyl index as a function of UV weathering time for neat PVC and WPVC composites with and without UV stabilizers. Without UV stabilizers, the changes in carbonyl index increased with UV weathering time for both neat PVC and WPVC composites, except for WPVC with the wood content of 100 phr. The increases in carbonyl group were attributed to the oxidation reaction of PVC structures in neat PVC and WPVC composites. When adding the UV stabilizers, the changes in carbonyl contents were minimized as compared with the samples without UV stabilizers. The changes in carbonyl contents in WPVC composites were not the same as those in neat PVC. In WPVC composites, for any given UV stabilizers, the carbonyl content increased and then decreased at high UV weathering times, more pronounced effect being observed for the wood content of 100 phr. In the case of PVC with wood content of 100 phr, the carbonyl content increased at the first 240 hr weathering time and then decreased after 240 h. This behavior was also observed by Fabiyi and McDonald [20]. The carbonyl groups at first 240 hr resulted from an oxidation reaction of lignin which led to the formation of paraquinone chromophoric structures under UV and oxygen environment whereas those after 240 hr weathering time resulted from transformation of the paraquinone to hydroquinone structures. This paraquinone-to-hydroquinone transformation process caused the reduction of the carbonyl groups in the PVC. This explanation could be shown schematically by Scheme 2. The paraquinone-to-hydroquinone transformation was detailed by the work of Muasher et al. [12]. The results in Fig. 3 also indicated that the addition of UV stabilizers reduced the oxidation reaction in the WPVC composites by retarding the trans-

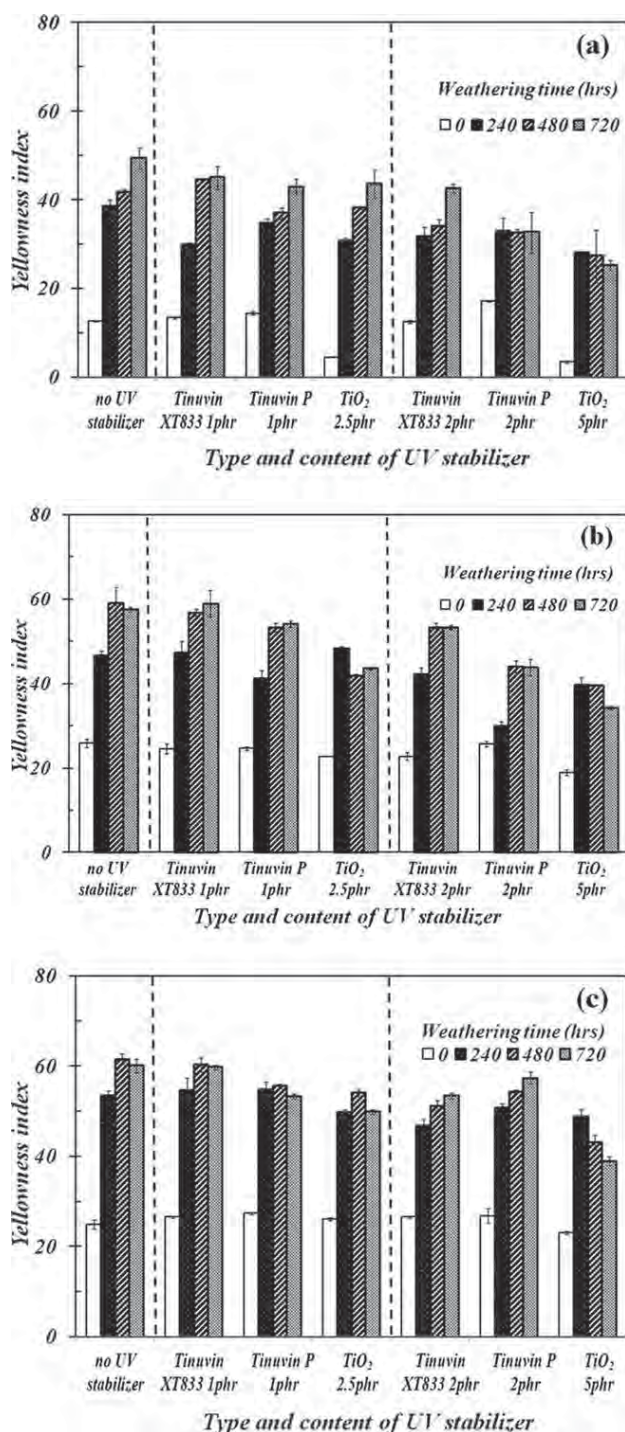SCHEME 2. Redox reactions of hydroquinone and paraquinone in lignin.

FIG. 4. Yellowness index for neat PVC and WPVC composites containing Tinuvin P, Tinuvin XT833, or TiO$_2$ stabilizer neat PVC, (b) PVC with wood flour at 50 phr, and (c) PVC with wood flour at 100 phr.

formation reactions of hydroquinone to paraquinone structures. The higher the UV stabilizer content the lower the carbonyl content. Similar to polyene content in Fig. 1, the carbonyl results also suggested that Tinuvin P and TiO$_2$ stabilizers exhibited more effective photostabilities than Tinuvin XT833 stabilizer.

Discolorations

Physical appearances of PVC and WPVC with and without UV stabilizers after a prolonged UV weathering time were assessed in this work by measuring yellowness index, lightness and total color change. Figure 4 shows the results of yellowness index for neat PVC and WPVC composites. The yellowness index for neat PVC and WPVC composites sharply increased at 240 hr weathering time and then slightly changed at 480 and 720 hr weathering times. The increases in yellowness index were caused by the generation of conjugated double bonds (polyene) as a result of photodegradation reactions of PVC molecules. The yellowness index for the WPVC composites before and after UV weathering were higher than that for the neat PVC due to that the initial color of wood particles themselves. The effects of all UV stabilizers on yellowness index were not as apparent as those on polyene and carbonyl indices. Figure 5 shows the lightness (L^*) as a function of UV weathering time for neat PVC and WPVC composites with and without UV stabilizers. It was noticeable that the lightness for the neat PVC decreased with increasing weathering time whereas that for the WPVC composites exhibited the opposite. The differences in the initial colors of PVC and WPVC were dependent on intrinsic colors of each material (PVC or wood). It is widely known that photodegradation in PVC leads to color change of PVC from white to yellow or brown whereas wood under UV light will exhibit photobleaching reaction in the lignin [12, 13]. In relation to this work, the WPVC composites were expected to color fading after a prolonged UV weathering time, suggesting that the photobleaching effect of lignin was more predominant than the photodegradation effect in PVC for the WPVC composites. For the effect of UV stabilizers, it was observed that the addition of UV stabilizers improved the photostability of neat PVC, but no positive effects were observed for WPVC composites. The increases in the lightness of the WPVC composites as a function of UV weathering time were predominantly caused by the photobleaching of the lignin. An exceptional high lightness for the neat PVC and WPVC composites stabilized by TiO$_2$ was caused by the high initial lightness of the TiO$_2$ itself.

The total color change or discoloration results are given in Fig. 6. The lower the ΔE value the lesser the discoloration level for the PVC and WPVC samples. Considering neat PVC sample, Tinuvin P at 2 phr gave the lowest ΔE value suggesting the smallest discoloration level of the PVC sample. As the UV weathering time was increased the discoloration become more apparent (increasing ΔE). The PVC samples with UV stabilizers exhibited slower discolorations as compared with those without UV stabilizers, this being considered from the slope of the ΔE changes as a function of UV weathering time. In the case of WPVC composites, TiO$_2$ gave the lowest ΔE value with no change in ΔE when the UV
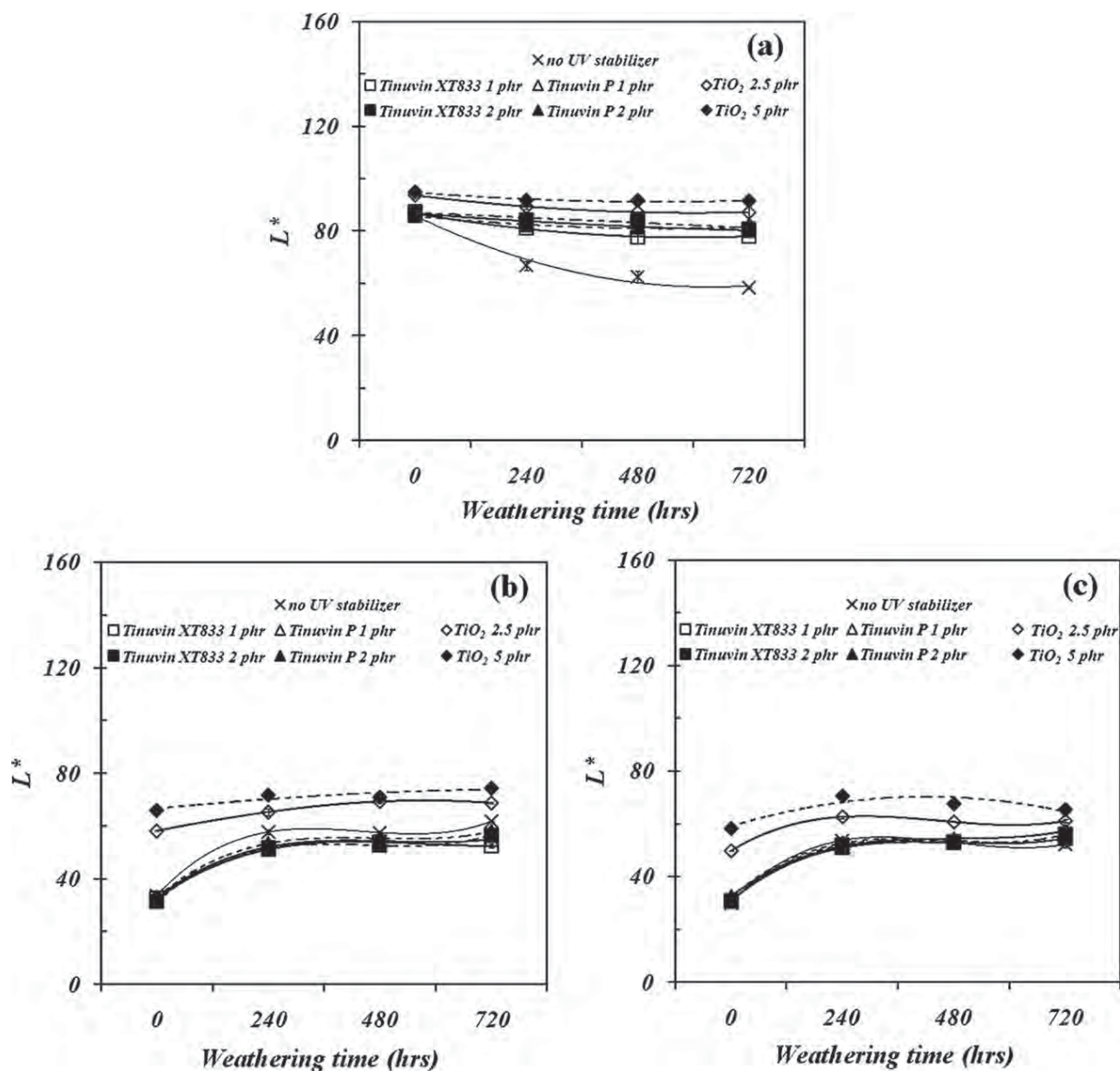
FIG. 5. Lightness for neat PVC and WPVC composites containing Tinuvin P, Tinuvin XT833, or TiO$_2$ stabilizer neat PVC, (b) PVC with wood flour at 50 phr, and (c) PVC with wood flour at 100 phr.

weathering time was increased. The lowest ΔE for the TiO$_2$ added WPVC composite was the result of initial color of TiO$_2$ particles as mentioned earlier. However, when considering the visual photographs of the WPVC composites with the three UV stabilizer (Fig. 7), it was found that the initial color of the TiO$_2$ added WPVC deviated from natural wood-like products, and this made the TiO$_2$ added WPVC composites more difficult to be used in practice.

Mechanical Properties

Tables 3–5 show tensile and flexural properties of neat PVC and WPVC composites before and after UV weath-

ering at various times for different types and concentrations of the UV stabilizers. Tensile and flexural properties of neat PVC with Tinuvin XT833, Tinuvin P and TiO$_2$ before and after UV weathering are given in Table 3. In neat PVC without UV stabilizers, the average tensile and flexural moduli remained unchanged during a weather time period of 0–720 hr, the values being of 1.0 and 2.9 GPa, respectively. The tensile and flexural strength for PVC increased from 37.7 to 40.8 MPa, and from 60.6 to 70.9 MPa, respectively. However, a significant decrease in the tensile elongation at break was observed when increasing UV weathering time. The significant drop in elongation at break indicated that the PVC became more brittle after UV weathering. This was possibly due to
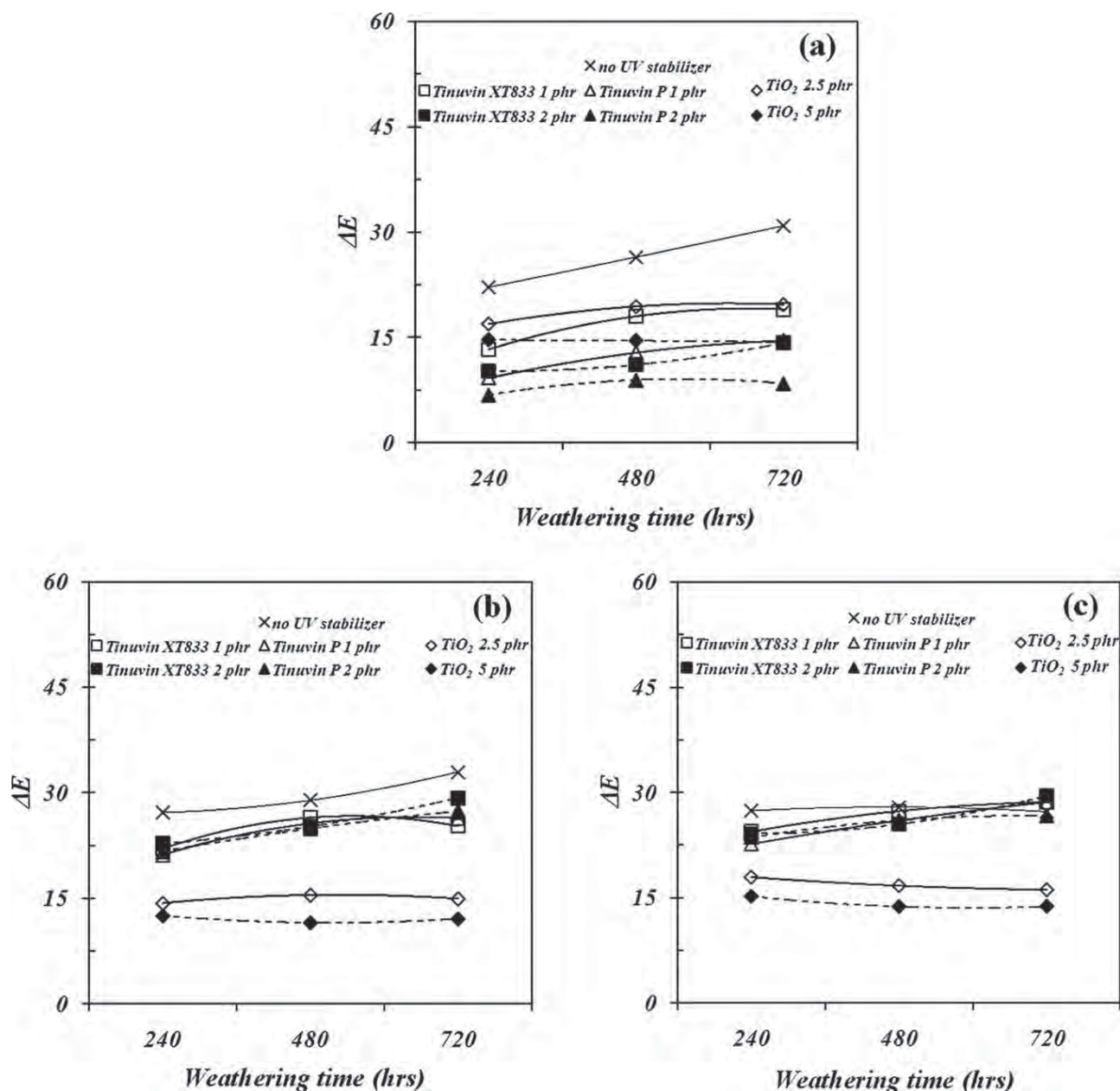
FIG. 6. Discoloration level of neat PVC and WPVC composites containing Tinuvin P, Tinuvin XT833, or TiO$_2$ stabilizer neat PVC, (b) PVC with wood flour at 50 phr, and (c) PVC with wood flour at 100 phr.

losses of volatile materials in the PVC compound [25] as well as the photodegradation reaction of the PVC. The latter could be proven by the addition of UV stabilizers into the neat PVC. It was found that after adding the UV stabilizers, the initial tensile and flexural moduli, strengths and elongation did not change, expect for Tinuvin XT833 stabilizer. The addition of Tinuvin XT833 into the neat PVC decreased the mechanical properties of the unweathered neat PVC, especially the elongation at break. This behavior was supported by the experimental results by Kamisli and Turan [23]. More importantly, the reduction of the elongation al break as a function of weathering

FIG. 7. Digital photographs of PVC containing 50 phr wood particles with and without UV stabilizer.

TABLE 3. Tensile and flexural properties for neat PVC added by UV stabilizers.

Pvc Formula	Type and content of UV stabilizer	UV Weathering time (hr)	Tensile properties N. Sombatsompop, K. Chaochanchaikul			Flexural properties	
			Tensile modulus (GPa)	UTS (MPa)	Elongation at break (%)	Flexural modulus (GPa)	Flexural strength (MPa)
Neat PVC	No UV stabilizer	0	1.0 ± 0.07	37.7 ± 0.27	41.1 ± 3.45	2.9 ± 0.05	60.6 ± 0.65
		240	1.0 ± 0.04	39.6 ± 0.57	24.5 ± 3.23	2.9 ± 0.09	70.6 ± 1.92
		480	1.0 ± 0.03	40.0 ± 0.85	24.5 ± 3.29	2.9 ± 0.02	71.5 ± 1.04
		720	1.0 ± 0.03	40.8 ± 0.73	18.3 ± 2.65	2.9 ± 0.11	70.9 ± 1.29
	Tinuvin XT833 (1 phr)	0	1.0 ± 0.07	35.3 ± 0.65	28.3 ± 2.60	2.8 ± 0.07	59.5 ± 0.74
		240	1.0 ± 0.05	39.7 ± 0.64	27.3 ± 2.44	2.7 ± 0.05	67.8 ± 0.47
		480	1.1 ± 0.07	40.0 ± 0.89	23.1 ± 2.40	2.7 ± 0.05	68.2 ± 1.03
		720	1.1 ± 0.02	39.9 ± 0.99	23.2 ± 2.32	2.7 ± 0.06	67.4 ± 0.84
	Tinuvin P (1 phr)	0	1.0 ± 0.10	37.4 ± 0.58	40.8 ± 3.90	2.8 ± 0.31	61.2 ± 0.76
		240	1.0 ± 0.02	41.0 ± 0.60	28.7 ± 3.32	2.9 ± 0.06	70.4 ± 1.45
		480	1.1 ± 0.06	41.5 ± 0.56	25.9 ± 3.59	2.8 ± 0.06	70.7 ± 0.75
		720	1.1 ± 0.10	41.4 ± 1.06	25.1 ± 3.08	2.9 ± 0.07	70.6 ± 1.65
	TiO$_2$ (2.5 phr)	0	0.9 ± 0.04	35.2 ± 0.36	39.1 ± 2.52	2.9 ± 0.06	58.8 ± 0.57
		240	0.9 ± 0.05	38.0 ± 0.21	19.8 ± 3.47	2.8 ± 0.01	67.3 ± 0.73
		480	1.0 ± 0.04	38.0 ± 0.62	17.5 ± 2.25	2.9 ± 0.05	66.6 ± 0.41
		720	1.0 ± 0.07	38.9 ± 0.57	19.0 ± 2.31	2.8 ± 0.06	67.5 ± 0.69
	Tinuvin XT833 (2 phr)	0	1.0 ± 0.04	31.5 ± 1.00	16.4 ± 1.96	2.6 ± 0.02	54.7 ± 0.77
		240	1.0 ± 0.06	34.3 ± 0.46	11.9 ± 1.95	2.6 ± 0.05	61.5 ± 0.93
		480	1.0 ± 0.08	34.8 ± 0.67	14.7 ± 2.13	2.8 ± 0.05	66.1 ± 1.59
		720	1.1 ± 0.05	34.4 ± 1.07	15.1 ± 1.81	2.7 ± 0.08	66.9 ± 1.54
	Tinuvin P (2 phr)	0	1.0 ± 0.03	38.7 ± 0.29	39.5 ± 4.41	3.0 ± 0.03	64.7 ± 0.94
		240	1.1 ± 0.03	42.9 ± 0.59	28.5 ± 3.64	3.0 ± 0.09	72.6 ± 1.35
		480	1.1 ± 0.04	43.6 ± 2.54	27.2 ± 3.73	3.0 ± 0.12	76.7 ± 1.34
		720	1.1 ± 0.06	43.2 ± 0.85	31.2 ± 2.09	3.0 ± 0.10	77.6 ± 0.93
	TiO$_2$ (5 phr)	0	1.0 ± 0.11	35.3 ± 0.46	40.8 ± 2.58	2.8 ± 0.07	59.5 ± 0.99
		240	1.1 ± 0.07	40.3 ± 0.42	24.3 ± 2.13	2.8 ± 0.04	67.7 ± 1.09
		480	1.0 ± 0.04	40.4 ± 0.55	22.1 ± 2.37	2.8 ± 0.08	68.7 ± 1.30
		720	1.1 ± 0.09	39.8 ± 0.30	24.6 ± 2.86	2.8 ± 0.11	72.3 ± 1.54

time became diminished by the additions of UV stabilizers, suggesting minimization of the photodegradation reaction. Among three stabilizers used, Tinuvin P at 2 phr gave the neat PVC compound with optimum tensile and flexural properties. This statement was in good agreement with the polyene and carbonyl indices already shown and discussed in Figs. 1 and 2.

In WPVC composites (Tables 4 and 5), the tensile properties for WPVC composites for both wood contents of 50 and 100 phr did not change with increasing UV weathering time, and with the additions of UV stabilizers. The tensile modulus for WPVC was greater than those for neat PVC whereas the opposite trend was found for tensile strength and elongation at break. The differences in the tensile properties resulted from the presence of wood particles which led to a number of property worsening factors, such as interfacial defects, molecular incompatibility and moisture regain [26]. It was interesting to note that the flexural properties of WPVC composites were affected by the UV weathering time. The flexural modulus and strength decreased with increasing UV weathering time. This was due to that the wood particles may absorb moisture during the condensation stage in the QUV weatherometer and this led to softening of the WPVC composites. The effect of UV stabilizer could not be observed in this case because the moisture absorption in wood particles exhibited more predominant effect than the UV stabilization effect. This statement was drawn because the UV photodegradation may occur and affect the WPVC composites mainly on the sample surface, whereas the moisture may have regained into the composite bulk, thus resulting in the reductions of flexural properties for the WPVC composites.

It should be noted that, unlike the neat PVC tested under UV weathering, the properties of WPVC under UV light were affected not only by the photodegradation and oxidation reactions mainly on the composite surface, but also by the photobleaching reaction in lignin and wood related defects (interfacial defects, molecular incompatibility and moisture regain) within the whole WPVC composite samples. The mechanical properties of WPVC were more affected by the presence of wood particles rather than the structural changes in PVC molecules. If this was the case, the changes in molecular structures and physical appearances for WPVC composite samples may not be necessary to correspond to their mechanical properties. The results in this work clearly indicated that the wood flour play an important effect on the photostabilization of WPVC by interfering the photostabilization mechanism of PVC by the added UV stabilizer. Therefore, it would be

TABLE 4. Tensile and flexural properties for PVC containing 50 phr wood particles with and without UV stabilizers.

WPVC (PVC:wood)	Type and content of UV stabilizer	UV Weathering Time (hr)	Tensile properties			Flexural properties	
			Tensile modulus (GPa)	UTS (MPa)	Elongation at break (%)	Flexural modulus (GPa)	Flexural strength (MPa)
100:50	No UV stabilizer	0	1.4 ± 0.05	28.9 ± 1.29	5.3 ± 0.81	4.5 ± 0.20	51.9 ± 0.33
		240	1.4 ± 0.06	29.4 ± 0.72	4.8 ± 0.49	3.9 ± 0.13	51.0 ± 0.82
		480	1.4 ± 0.03	30.6 ± 0.62	5.2 ± 0.24	3.6 ± 0.13	46.6 ± 0.71
		720	1.4 ± 0.05	29.8 ± 0.42	5.5 ± 0.39	3.5 ± 0.11	46.6 ± 0.29
	Tinuvin XT833 (1 phr)	0	1.4 ± 0.08	29.6 ± 1.85	5.0 ± 0.55	4.4 ± 0.20	51.6 ± 1.36
		240	1.4 ± 0.10	30.9 ± 0.99	5.4 ± 0.51	3.5 ± 0.18	49.1 ± 1.12
		480	1.5 ± 0.03	30.7 ± 0.84	5.4 ± 0.70	3.6 ± 0.06	49.1 ± 0.83
		720	1.5 ± 0.03	30.3 ± 0.92	4.8 ± 0.51	3.5 ± 0.17	47.3 ± 0.86
	Tinuvin P (1 phr)	0	1.4 ± 0.04	29.8 ± 1.77	5.7 ± 0.74	4.6 ± 0.09	55.6 ± 0.30
		240	1.4 ± 0.05	31.6 ± 0.69	5.7 ± 0.48	3.8 ± 0.09	52.2 ± 0.89
		480	1.5 ± 0.04	31.9 ± 0.71	5.8 ± 0.38	4.0 ± 0.04	51.8 ± 0.30
		720	1.5 ± 0.04	30.3 ± 0.91	4.8 ± 0.29	3.8 ± 0.15	50.7 ± 1.08
	TiO$_2$ (2.5 phr)	0	1.5 ± 0.10	30.3 ± 1.76	5.3 ± 0.54	4.5 ± 0.14	52.4 ± 0.74
		240	1.4 ± 0.04	30.9 ± 0.64	5.5 ± 0.32	4.0 ± 0.12	50.7 ± 1.29
		480	1.4 ± 0.05	29.1 ± 1.33	5.4 ± 0.68	3.7 ± 0.09	49.0 ± 0.71
		720	1.4 ± 0.06	29.3 ± 0.71	5.5 ± 0.46	3.6 ± 0.14	47.8 ± 1.21
	Tinuvin XT833 (2 phr)	0	1.4 ± 0.09	29.8 ± 0.72	5.3 ± 0.73	4.3 ± 0.15	53.4 ± 0.99
		240	1.4 ± 0.06	29.3 ± 0.79	4.8 ± 0.51	3.6 ± 0.09	48.3 ± 0.89
		480	1.5 ± 0.05	30.8 ± 0.83	5.8 ± 0.86	3.6 ± 0.08	47.5 ± 1.17
		720	1.5 ± 0.03	31.0 ± 1.83	5.9 ± 0.69	3.6 ± 0.18	49.4 ± 0.90
	Tinuvin P (2 phr)	0	1.4 ± 0.02	28.5 ± 1.71	5.8 ± 0.54	4.7 ± 0.13	55.8 ± 1.42
		240	1.4 ± 0.03	30.6 ± 1.20	5.3 ± 0.44	3.9 ± 0.18	51.2 ± 0.98
		480	1.5 ± 0.05	31.1 ± 1.19	5.2 ± 0.42	3.8 ± 0.11	50.0 ± 0.97
		720	1.5 ± 0.05	31.0 ± 0.55	5.5 ± 0.33	3.8 ± 0.07	49.7 ± 0.62
	TiO$_2$ (5 phr)	0	1.5 ± 0.10	28.2 ± 1.56	5.7 ± 0.74	4.3 + 0.11	51.4 ± 0.67
		240	1.3 ± 0.05	30.2 ± 0.81	5.1 ± 0.48	3.8 ± 0.06	50.1 ± 1.23
		480	1.4 ± 0.03	28.9 ± 1.07	5.6 ± 0.94	3.6 ± 0.12	48.3 ± 0.84
		720	1.3 ± 0.13	30.0 ± 1.10	5.9 ± 0.46	3.7 ± 0.08	47.8 ± 0.70

TABLE 5. Tensile and flexural properties for PVC containing 100 phr wood particles with and without UV stabilizers.

WPVC (PVC:wood)	Type and content of UV stabilizer	UV weathering time (hr)	Tensile properties			Flexural properties	
			Tensile modulus (GPa)	UTS (MPa)	Elongation at break (%)	Flexural modulus (GPa)	Flexural strength (MPa)
100:100	No UV stabilizer	0	1.4 ± 0.11	20.9 ± 1.06	4.2 ± 0.43	5.5 ± 0.16	46.2 ± 1.09
		240	1.4 ± 0.05	23.7 ± 1.23	4.2 ± 0.64	4.2 ± 0.11	41.2 ± 1.42
		480	1.4 ± 0.05	21.8 ± 1.51	3.8 ± 0.45	3.9 ± 0.14	39.8 ± 0.95
		720	1.4 ± 0.05	23.7 ± 0.85	3.8 ± 0.42	3.8 ± 0.07	40.2 ± 0.59
	Tinuvin XT833 (1 phr)	0	1.4 ± 0.08	20.9 ± 1.46	4.9 ± 0.67	4.8 ± 0.13	42.9 ± 0.86
		240	1.3 ± 0.09	21.2 ± 1.56	4.8 ± 1.18	3.5 ± 0.11	36.8 ± 1.46
		480	1.3 ± 0.08	23.5 ± 0.82	3.4 ± 0.73	3.1 ± 0.19	36.0 ± 1.54
		720	1.4 ± 0.08	24.7 ± 0.09	3.3 ± 0.26	3.0 ± 0.09	34.9 ± 1.20
	Tinuvin P (1 phr)	0	1.5 ± 0.02	19.8 ± 1.29	5.1 ± 1.85	5.1 ± 0.26	42.7 ± 1.58
		240	1.4 ± 0.07	22.2 ± 1.59	4.0 ± 0.59	3.7 ± 0.14	38.1 ± 0.64
		480	1.4 ± 0.14	21.5 ± 1.48	3.4 ± 1.49	3.5 ± 0.13	36.9 ± 1.00
		720	1.4 ± 0.06	23.7 ± 1.23	3.2 ± 0.07	3.4 ± 0.19	36.6 ± 1.42
	TiO$_2$ (2.5 phr)	0	1.4 ± 0.07	22.0 ± 0.91	4.6 ± 0.44	5.4 ± 0.23	46.8 ± 1.25
		240	1.3 ± 0.12	23.6 ± 1.61	4.4 ± 0.57	3.8 ± 0.17	40.6 ± 1.61
		480	1.4 ± 0.15	23.9 ± 1.09	4.2 ± 0.52	3.7 ± 0.24	39.5 ± 1.35
		720	1.3 ± 0.07	23.4 ± 1.65	4.4 ± 0.42	3.4 ± 0.28	37.5 ± 1.42
	Tinuvin XT833 (2 phr)	0	1.3 ± 0.09	18.2 ± 1.43	4.7 ± 1.24	4.6 ± 0.35	40.2 ± 1.32
		240	1.2 ± 0.11	18.7 ± 0.93	3.7 ± 0.68	3.1 ± 0.10	33.9 ± 0.89
		480	1.3 ± 0.05	21.2 ± 0.54	3.1 ± 0.45	2.9 ± 0.07	33.8 ± 0.46
		720	1.3 ± 0.08	21.3 ± 1.38	3.0 ± 0.24	2.8 ± 0.23	32.8 ± 1.38
	Tinuvin P (2 phr)	0	1.6 ± 0.02	25.0 ± 0.73	4.2 ± 0.96	5.1 ± 0.26	46.0 ± 1.26
		240	1.6 ± 0.06	27.3 ± 0.58	3.3 ± 0.29	3.7 ± 0.18	39.8 ± 0.99
		480	1.3 ± 0.15	24.1 ± 1.17	4.0 ± 0.55	3.7 ± 0.16	39.7 ± 0.65
		720	1.3 ± 0.05	26.4 ± 1.01	3.9 ± 0.36	3.6 ± 0.14	39.8 ± 1.18
	TiO$_2$ (5 phr)	0	1.5 ± 0.08	24.5 ± 1.26	4.2 ± 0.56	5.1 ± 0.07	44.4 ± 0.33
		240	1.5 ± 0.09	25.8 ± 0.35	3.3 ± 0.17	3.7 ± 0.07	38.4 ± 1.04
		480	1.4 ± 0.04	24.5 ± 0.92	3.6 ± 0.23	3.5 ± 0.11	38.2 ± 0.56
		720	1.4 ± 0.06	23.9 ± 1.48	3.4 ± 0.28	3.5 ± 0.07	37.5 ± 0.55

interesting for a future work to investigate effect of chemical compositions or wood species on the structural stabilization of WPVC composites.

CONCLUSION

In this work, structural and mechanical properties of PVC and WPVC after a prolonged UV light were assessed through the use of three different UV stabilizers. The experimental results suggested that the polyene and carbonyl sequences, and discolorations appeared to increase with increasing UV weathering time from 0 to 720 hr. The yellowness index increased as a result of polyene and carbonyl productions whereas the brightness increased because of photobleaching of lignin in wood particles. The UV stabilizers could enhance the photo-stabilities of PVC and WPVC. The most effective UV stabilizer suggested in this work was Tinuvin P. The photo-stabilities in UV-stabilized WPVC composites were interfered by the presence of wood particles as a result of hydrogen bonds of hydroxyl groups on the wood surface and Tinuvin stabilizer. The mechanical properties of WPVC were more affected by wood particles, but independent of addition of UV stabilizers.

ACKNOWLEDGMENTS

REFERENCES

1. L.M. Matuana, D.P. Kamdem, and J. Zhang, *J. Appl. Polym. Sci.*, **80**, 1943 (2001).

2. L.M. Matuana and D.P. Kamdem, *Polym. Eng. Sci.*, **42**, 1657 (2002).

3. L.P. Real, A.M. Ferraria, and A.M. Botelho do Rego, *Polym. Test.*, **26**, 77 (2007).

4. C. Anton-Prinet, J. Dubois, G. Mur, M. Gay, L. Audouin, and J. Verdu, *Polym. Degrad. Stabil.*, **60**, 275 (1998).

5. A. Torikai and H. Hasegaawa, *Polym. Degrad. Stabil.*, **63**, 441 (1999).

6. X. Xiang, S. Chen, J. Zhang, and R. Chai, *J. Vinyl Addit. Technol.*, **16**, 23 (2010).

7. S. Xu, D. Cao, and M. Chen, *J. Vinyl Addit. Technol.*, **13**, 195 (2007).

8. D. Bruan and S.T. Rabie, *J. Vinyl Addit. Technol.*, **15**, 224 (2009).

9. X. Colom, F. Carrillo, F. Nogués, and P. Garriga, *Polym. Degrad. Stabil.*, **80**, 543 (2003).

10. H. Turkulin, H. Derbyshire, and E.R. Miller, *Holz. Roh. Werkst.*, **62**, 307 (2004).

11. N.M. Stark and L.M. Matuana, *Polym. Degrad. Stabil.*, **91**, 3048 (2006).

12. M. Muasher and M. Sain, *Polym. Degrad. Stabil.*, **91**, 1156 (2006).

13. M. Bengtsson, N.M. Stark, and K. Oksman, *Compos. Sci. Technol.*, **67**, 2728 (2007).

14. J.S. Fabiyi, A.G. McDonald, and D. McIlroy, *J. Polym. Environ.*, **17**, 34 (2009).

15. D. Ndiaye, E. Fanton, S. Morlat-Therias, L. Vidal, A. Tidjani, and J.L. Gardette, *Compos. Sci. Technol.*, **68**, 2779 (2008).

16. J.L. Lopez, M. Sain, and P. Cooper, *J. Appl. Polym. Sci.*, **99**, 2570 (2006).

17. T. Ludin, S.M. Cramer, R.H. Falk, and C. Felton, *J. Mater. Civil. Eng.*, **16**, 547 (2004).

18. S. El Raghi, R.R. Zahran, and B.E. Gebril, *Mater. Lett.*, **46**, 332 (2000).

19. A. Abu Bakar, A. Hassan, and A.F. Mohd Yusof, *Iran. Polym. J.*, **14**, 627 (2005).

20. J.S. Fabiyi and A.G. McDonald, *J. Polym. Environ.*, **18**, 57 (2010).

21. N. Sombatsompop, K. Taptim, K. Chaochanchaikul, C. Thongpin, and V. Rosarpitak, *J. Macromol. Sci. Pure Appl. Chem.*, **A45**, 535 (2008).

22. J. Markarian, *Plast. Addit. Comp.*, **6**, 46 (2004).

23. F. Kamisli and C. Turan, *J. Mater. Process. Tech.*, **159**, 40 (2005).

24. J. Catalàn, J.L.G. De Paz, M.R. Torres, and J.D. Tornereo, *J. Chem. Soc. Faraday Trans.*, **93**, 1691 (1997).

25. N. Jakubowicz, N. Yarahmadi, and T. Gevert, *Polym. Degrad. Stabil.*, **66**, 415 (1999).

26. N. Sombatsompop and K. Chaochanchaikul, *Polym. Intl.*, **53**, 1210 (2004).

Effects of Roller Speed, Die Temperature, Volumetric Flow Rate, and Multiple Extrusions on Mechanical Strength of Molten and Solidified LDPE under Tensile Deformation

Wanlop Harnnarongchai[a]; Naret Intawong[b]; Narongrit Sombatsompop[a]

[a] Polymer PROcessing and Flow (P-PROF) Group, Division of Materials Technology, School of Energy, Environment and Materials, King Mongkut's University of Technology Thonburi (KMUTT), Thongkru, Bangmod, Bangkok, Thailand [b] Department of Industrial Engineering, Faculty of Engineering, Rajamangala University of Technology Lanna, (RMUTL), Chiang Mai, Thailand

PLEASE SCROLL DOWN FOR ARTICLE

Taylor & Francis
Taylor & Francis Group

Effects of Roller Speed, Die Temperature, Volumetric Flow Rate, and Multiple Extrusions on Mechanical Strength of Molten and Solidified LDPE under Tensile Deformation

WANLOP HARNNARONGCHAI,[1] NARET INTAWONG,[2]
AND NARONGRIT SOMBATSOMPOP[1]

[1]Polymer PROcessing and Flow (P-PROF) Group, Division of Materials
Technology, School of Energy, Environment and Materials, King Mongkut's
University of Technology Thonburi (KMUTT), Thongkru, Bangmod,
Bangkok, Thailand
[2]Department of Industrial Engineering, Faculty of Engineering, Rajamangala
University of Technology Lanna, (RMUTL), Chiang Mai, Thailand

An experimental rig coupled with a high speed data-logging and recording system and a personal computer was specially designed and constructed for the real-time measurement of mechanical strength (in terms of drawdown force) as a function of volumetric flow rate and roller speed for virgin low-density polyethylene (LDPE) and reprocessed LDPE during a filament stretching process. The effect of the number of extrusion passes for the reprocessed LDPE was our main interest. The experimental rig was connected to the end of a single-screw extruder, which was used to melt and extrude the polymers. The LDPE filaments were then solidified and collected for studying the mechanical properties. The mechanical strength of the virgin LDPE and reprocessed LDPE were investigated in both molten and solidified states. The mechanical strengths of the virgin and reprocessed LDPEs under these two states are discussed and compared in terms of change in magnitude under a wide range of processing conditions (volumetric flow rate, die temperature, and roller speed). The results suggested that in the molten state the drawdown force for LDPE melts was dependent on volumetric flow rate, die temperature, roller speed, and the number of reprocessing passes. The drawdown force being affected by the number of reprocessing passes could be explained by molecular degradation and gelation effects when using high volumetric flow rates. In the solidified state, the tensile properties of the solidified LDPE increased with roller speed. The effect of the number of extrusion passes for the solidified LDPE was similar to that for the molten LDPE. In the case of volumetric flow rates, the mechanical properties of the solidified LDPE decreased with increasing volumetric flow rate, whereas those of the molten LDPE exhibited the opposite effect. Thus, the mechanical strength of the molten LDPE could not always be used to assess the mechanical properties of the solidified LDPE.

Keywords LDPE, mechanical strength, recycling, rheological properties

Introduction

In polymer processes like extrusion blow molding, fiber spinning, film blowing, and thermoforming, shear flow is not only the type of flow that occurs. Another type of flow is elongational flow, which can be analyzed and determined by means of drawdown force, elongational stress, and strain rate, and elongational viscosity as a function of drawdown speed or time. The investigations of flow properties for polymer melts under tension deformation can be carried out by extruding and stretching a polymer filament in the molten state, and measuring the drawdown forces occurring. The measured elongational flow properties are affected by the molecular weight and structure of the polymers used, as well as the draw ratio, test temperature, roller speed, and die geometry.[1–3] Viscoelastic behavior of the polymer melt under extensional deformation is usually expected at low draw ratios, but it may reach the viscous behavior when the stretching level or draw ratio is sufficiently high[4] A number of studies on measurements of elongational flow properties using various techniques have been given in the literature.[1–10] Therefore, they are not detailed in this work.

In polymer processing, effects of temperature, pressure, and shear rate on the flow properties of polymer melts are considered as reversible effects, whereas those of thermal history and reprocessing are irreversible ones. The temperature has both reversible and irreversible effects on the flow properties of the polymer. The irreversible effects generally involve changes in molar masses (either chain scission or crosslinking), which result from oxidative, thermal, and mechanical degradation processes. These effects play more significant roles for polymer melts flowing with a long residence time, under high deformations, for processes such as blown film extrusion, blow molding, and melt spinning, as well as reprocessing/recycling. Low-density polyethylene (LDPE) and polypropylene (PP) can undergo thermo-mechanical and thermo-oxidative degradations even under short processing times. The starting reactions form free radicals that can react with oxygen or undergo disproportionation or combination reactions to form crosslinks and chain branching, depending on the polymer compositions.[11]

The effects of reprocessing on rheological properties have been extensively studied mostly under shear deformation mode in various screw extrusion geometries. Scaffaro et al.[12] investigated the rheological properties of postconsumer pipes produced from LLDPE/LDPE blend after reprocessing in a single-screw extruder. They found that the viscosities of the polymer in the reprocessed pipes dropped slightly as compared to that in the virgin pipes. This behavior was opposite with the result of Kartalis et al.[13] who found a decrease in the melt flow rate of recycled MDPE/LDPE packaging film after multiple extrusion cycles. Pedroso et al.[14] evaluated the rheological and thermal properties of a recycled LDPE/corn or starch blends, and found that Melt Flow Index (MFI) values for virgin and recycled LDPE were not significantly different, whereas the result from dynamic mechanical thermal analysis indicated higher storage modulus (E′) and lower loss modulus (E″) for the recycled LDPE. Costa et al.[15] investigated the rheological properties of PP during multiple extrusions with two different die temperatures. They found that the complex viscosity (η^*) decreased gradually with the number of extrusion cycles and faster at higher die temperatures. Camacho and Karlsson[16] investigated the effect of recycling of PP/HDPE blends on rheological properties, and found that up to the third extrusion, the shear force induced the chain scissions of the PP backbone with the molecular weight of the blend remaining almost unchanged for further reprocessing. This statement was similar to the work by Vargas et al.[17] Dostal et al.[18] studied the influence of the repeated extrusion on the molecular parameters for LDPE, and concluded that the molecular changes by chain scission was

dominant only in the first two extrusions, and a dramatic increase in molar mass (M_w and M_n) was observed after five processing cycles.

According to recent literatures,[12–18] there have been a large number of investigations on the effects of reprocessing on thermo-mechanical properties, and of flow properties under shear deformation for a wide range of polymers. Very rare have been studies on the effect of reprocessing on the elongational flow properties of polymer melts, and their mechanical properties of the polymer in the solidified form, under multiple extrusion processes where the molten polymers are under tension deformation.[19–21] Kim et al.[19] investigated the tensile properties of PP filled with nanoclay after being stretched at high draw ratio, and found that the tensile properties of the polymer hybrid decreased with increasing the drawdown ratio. Dintcheva et al.[20] suggested that the rheological properties of greenhouse film were not significantly affected by the number of extrusion passes, but the mechanical properties of the solidified film decreased. Dastjerdi et al.[21] found that the tensile modulus and tenacity of modified filament yarn with nanofiller produced by a single-screw extruder improved by extruding at high drawdown ratio, but an inverse effect was observed when using a twin screw extruder.

In this work, an experimental apparatus was designed and constructed for measurement of elongational flow properties of LDPE. The rig was connected to the end of a single-screw extruder used for production of molten polymers, which were then extruded through a circular die. The extruded melts (filaments) were then solidified and collected for studying the tensile properties. The mechanical strength of virgin LDPE and reprocessed LDPE were investigated in both the molten and solidified states and the results were then discussed and compared in terms of magnitude changes under a wide range of processing conditions (volumetric flow rate, die temperature, and roller speed). The effect of number of extrusion passes for the reprocessed LDPE was one of our main interests in this work.

Experimental

Raw Material

LDPE (LD1905FA) with a melt flow index of 5 g/10 min was used, supplied by Thai Polyethylene Co. Ltd. (Bangkok, Thailand).

Design and Manufacture of the Experimental Apparatus

The mechanical strength of LDPE melt was evaluated under tension deformation. Figure 1 shows an experimental arrangement for mechanical strength measurement of the LDPE using the filament-winding process, which was fed by a single-screw extruder. The experimental apparatus consisted of a single-screw extruder, an adaptor (a barrel rig), drawdown force measuring unit, roller take-up device, and visualization and control equipment. The assembly of the experimental apparatus and the functions of all the rig components are detailed below.

Single-screw extruder: A single-screw extruder (RMUTL-SE001 MUSHIKNG Poly-Lab) supplied by RMUTL (Chiang Mai, Thailand) was used for the production of molten LDPE. The length/diameter ratio of the barrel was 600/25 mm/mm, and the temperature profiles on the extruder were 130, 140, 150, and 160°C from hopper to die zones; the die temperature was varied from 160 to 180°C.
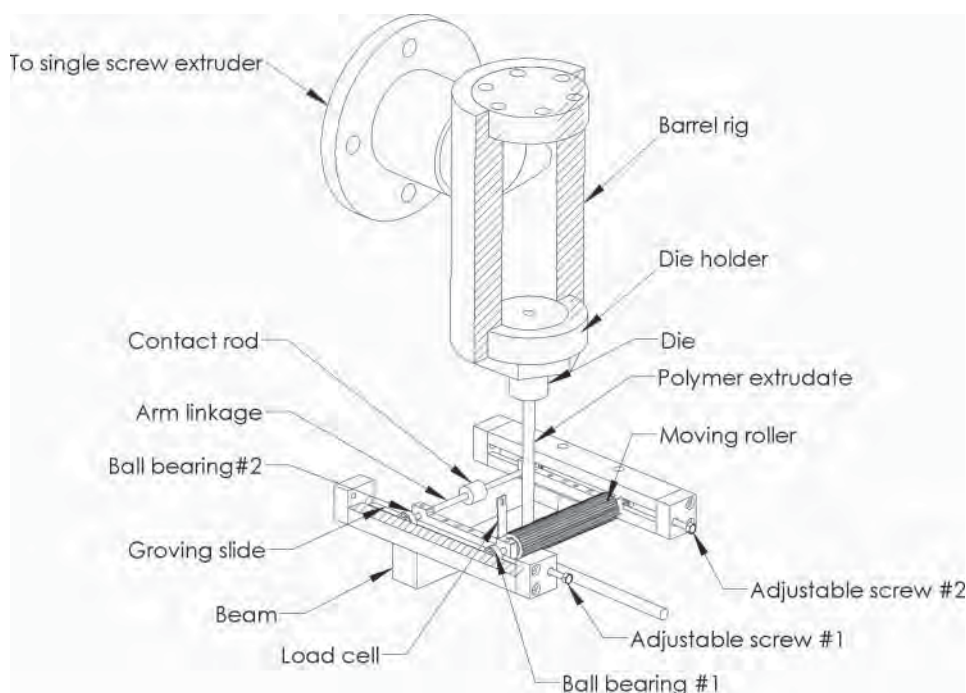
Figure 1. An experimental arrangement for mechanical strength measurement of the LDPE under filament winding process.

Adaptor: The so-called barrel rig was assembled at the end of the single-screw extruder. The adaptor was necessary for connecting the single-screw extruder to the melt strength measuring unit. It consisted of a cylinder barrel rig, die, and die holder. The barrel was made of S55C high-carbon steel that can be used at elevated temperatures. The barrel was 40 mm in diameter, 200 mm in length. The circular die used was 60 mm in length and 6 mm in diameter, and made of S55C high-carbon steel.

Drawdown force measuring unit: This unit consisted of two principal parts, the load cell and roller take-up devices. The load cell device (OMEGA, Model no. LCL-454G, USA) was utilized for the drawdown force measurement of the highly viscous LDPE melts as shown in Fig. 1. The load cell was mounting by clamping with a polyamide 6 screw to the support beam. The moving roller was connected to a pair of arm linkages and put on ball bearings #1 and #2 at the end of the moving roller and contact rod to keep the movement of the moving roller fluent, and to lessen the friction on the grooving slides. The arm linkages were connected to the contact rod transmitting tensional forces to the load cell where the measurements were recorded as an electrical voltage form which was then translated into force data with the use of a calibration curve given in Fig. 2. The workable range for the load cell was 0–343 cN. The roller take-up device was used to wind the filament. A shaft was connected to a sprocket gear with a mechanical chain for transmitting mechanical power from a sprocket gear at the bottom to another sprocket gear above and coupled to roller take-up device. The power was provided from an AC motor source (380 V, 60 Hz, 3000 rpm) to a gear box (1:10) connected to the shaft for rotating the rollers. The roller speed for the take-up device could be adjusted between 0 and 343 rpm.
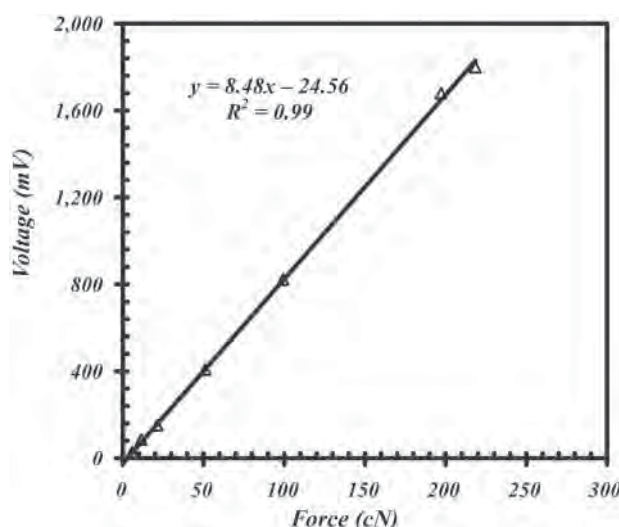
Figure 2. A calibration curve of electrical voltage VS force.

The visualization equipment: This was designed for visualizing the exact filament size (diameter) at the failure point for accurate measurement of the elongational stress as well as the elongational viscosity of the LDPE melt. A color video-camera (SSC- DC398P with 752Hx582V pixels and 480 TV lines) with high-speed and high-resolution macro-zoom lens (3.3 × magnifications) was used to record the exact filament size which was captured and displayed in real time using a personal computer. All the experimental data were collected using a high-speed data logging and recording system coupled with a personal computer with use of a visual basic program.

Control equipment: The temperature of the experimental apparatus was controlled using a DD6 temperature controller (Changchai Motor, Bangkok, Thailand). The pressure occurring in the screw extruder and in the barrel was measured using a pressure sensor (Dynisco, Model PT460E-2CB-6, Franklin, MA, USA).

Extrusion Process and Filament Winding Equipment

All the experimental data on the screw extruder for virgin LDPE and reprocessed LDPE during filament stretching process were recorded using a high-speed data-logging and recording system and a personal computer. The molten LDPE was extruded through a circular die before being pulled down to form a continuous filament, which was then solidified by ambient air, and collected for studying the tensile properties. To produce reprocessed LDPE, the extruded LDPE were pelletized using a pelletizing and cooling unit, collected and refed into the extruder for the desired number of extrusion passes.

Test Variables

In this work the test variables included the following:

Volumetric flow rate: This was achieved by varying the screw rotating speed ranging from 10 to 30 rpm, producing volumetric flow rates of LDPE melt of 2.9–8.3 $\times$ 10^{-7} m^3/s.

Die temperature: Die temperatures of 160, 170, and 180°C were used and controlled using a DD6 temperature controller (Changchai Motor, Bangkok, Thailand).

Reprocessing pass: In order to vary the thermal histories of the LDPE and study the effects on elongational flow properties of the molten LDPE, and on tensile properties of the solidified LDPE, the number of extrusion passes was varied from one to four times. Each extrusion pass used the same processing conditions.

Measurement of Mechanical Strength

The mechanical strength of the virgin LDPE and reprocessed LDPE were studied under both molten and solidified states. For molten LDPE filament, only drawdown forces as a function of time and roller speed are shown and discussed. It is commonly assumed that a higher mechanical strength of polymer filament will require a higher drawdown force. It should be noted that all the measurements during the molten state of the LDPE were restricted to nonisothermal condition. For solidified LDPE filament, the tensile properties (tensile modulus and tensile strength) were measured using a crosshead speed of 50 mm/min and a gauge length of 30 mm. All the tests were run on a SHIMADZU universal tensile tester (Tokyo, Japan), and the reported data were averaged from at least five independent determinations.

Results and Discussion

Mechanical Properties of Molten LDPE

Virgin LDPE Melt. The mechanical strength for virgin LDPE in this work was expressed in terms of drawdown force as a function of roller speed and time. Figure 3 shows curves of drawdown force against drawdown time for three different volumetric flow rates with increasing step-ladder roller speed using a die temperature of 160°C. The results suggested that the drawdown force tended to increase nonlinearly with increasing roller speeds. The drawdown force sharply increased in the initial stages of increasing roller speeds of less
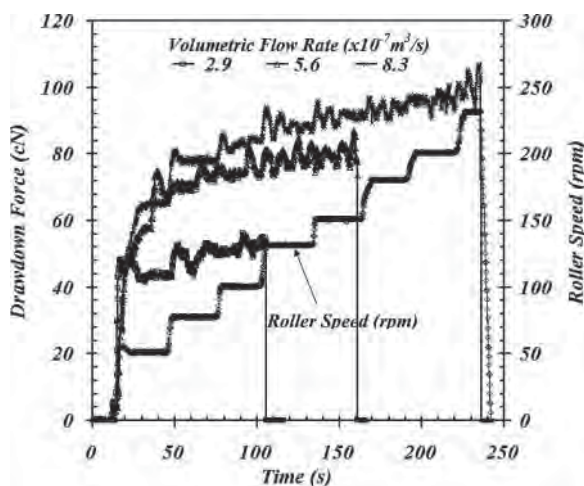
Figure 3. Plots of drawdown force against time with increasing roller speeds in the step-ladder form for LDPE melt at three different volumetric flow rates.

than 50 s drawdown, and then increased to a lesser extent during the final stage of increasing roller speeds. The significant increases in the drawdown force at the initial roller speeds were associated with relatively high molecular entanglement resulting in elastic resistances to the applied deformation. The force required to deform the melt at higher roller speeds increased to a smaller extent as compared to that at lower roller speeds. This was due to the fact that the LDPE melt at this stage had become disentangled and the molecules slipped past one another. Fluctuations of the drawdown forces were also observed during the tests, especially at higher roller speeds. The force fluctuations resulted from the draw resonance effect.[22]

It was observed that the higher the volumetric flow rate the greater the drawdown force with longer drawdown time and force to failure. This is attributed to higher energy inputs from the extruder with higher extrusion rate, with such energy being stored elastically within the LDPE melt during the flow in the die, and thus detected by the load cell apparatus. This claim was substantiated by the works of Muke et al.[5] and Baldi et al.[2] The drawdown forces upon fracture of the LDPE melts at volumetric flow rates of 2.9×10^{-7}, 5.6×10^{-7}, and 8.3×10^{-7} m³/s were 52.6, 81.7, and 100.8 cN, respectively. It was interesting to note that during the transitions of each roller speed there were overshoots of the drawdown forces. The overshoots for the drawdown forces became more frequent near the failure point, and were caused by the draw resonance effect. This behavior was also observed and claimed by a number of works.[22,23]

Effects of Reprocessing and Die Temperature

Figure 4 shows plots of drawdown force against time with step-ladder increasing roller speed at a die temperature of 160°C using three different volumetric flow rates (Figs. 4a–c). The changes in drawdown forces as a function of time (or roller speed) were similar to those discussed for Fig. 3. The effect of reprocessing on the drawdown force and time at the volumetric flow rate of 2.9×10^{-7} m³/s (Fig. 4a) was not significant as compared to that at the volumetric flow rates of 5.6×10^{-7} and 8.3×10^{-7} m³/s (Figs. 4b and c). This was due to the relatively low viscous heating effect for the LDPE melt with the volumetric flow rate of 2.9×10^{-7} m³/s. The viscous heating effect occurring at the higher volumetric flow rates probably caused molecular chain scission and/or crosslinking reactions. The latter could be assessed, comparatively among the LDPE samples being extruded for different extrusion passes, by a gel-content experiment which was carried out by immersion of the solidified LDPE extrudates experienced from different numbers of extrusion pass in xylene solvent. The gel content determination was then calculated according to ASTM D 2765–01 (2001). The gel content results for LDPE extrudates made at the three different volumetric flow rates and different numbers of extrusion pass are given in Table 1. The changes in gel content were not significant for the sample made at low volumetric flow rate of 2.9×10^{-7} m³/s, suggesting that there was no apparent crosslinking occurring in the LDPE. That was why there were no differences in the drawdown force stated in Fig. 4a. Table 1 also suggests that the crosslinking occurred most significantly during extrusion pass number #4 for LDPE with volumetric flow rate of 5.6×10^{-7} m³/s and for the extrusion pass numbers #3 and #4 for LDPE with volumetric flow rate of 8.3×10^{-7} m³/s. The gel content results in Table 1 corresponded well to the drawdown force results in Fig. 4, which suggested that the possible crosslinking structures resulted in increases in the drawdown force and drawdown time.

Figure 5 shows the relationship between drawdown force and roller speed for LDPE melt using different numbers of extrusion passes and die temperatures using the
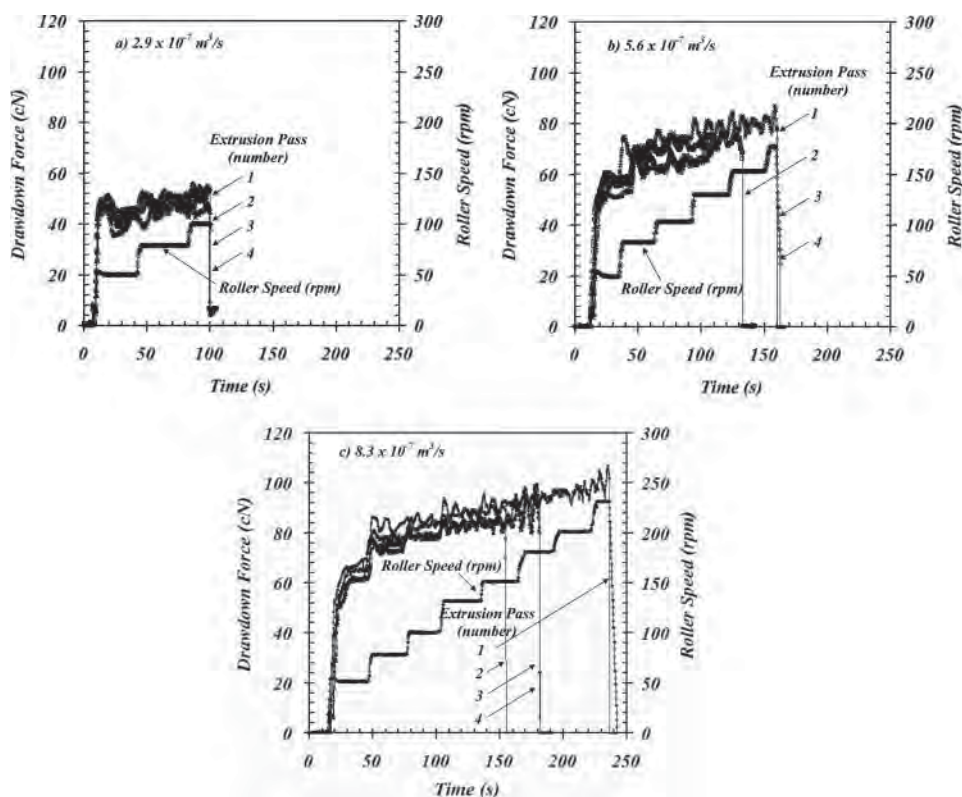
Figure 4. Plots of drawdown force against time with increasing number of extrusion passes under increasing roller speeds for LDPE melt at 160°C using three different volumetric flow rates: (a) 2.9×10^{-7} m³/s, (b) 5.6×10^{-7} m³/s, and (c) 8.3×10^{-7} m³/s.

volumetric flow rate of 8.3×10^{-7} m³/s. Again, increasing drawdown speed increased the drawdown force for any given numbers of extrusion passes and die temperatures. For a given roller speed, the drawdown force decreased with increasing die temperature due to an increase in viscous deformation and molecular mobility of the LDPE melt.[24] The effect of

Table 1
Gelation results for solidified LDPE in xylene solvent

Number of extrusion pass	Gel content (%) Volume metric flow rate (m³/s)		
	2.9×10^{-7}	5.6×10^{-7}	8.3×10^{-7}
1	0.51	0.95	0.57
2	0.67	1.04	1.86
3	1.11	1.24	9.64
4	0.85	4.87	18.23
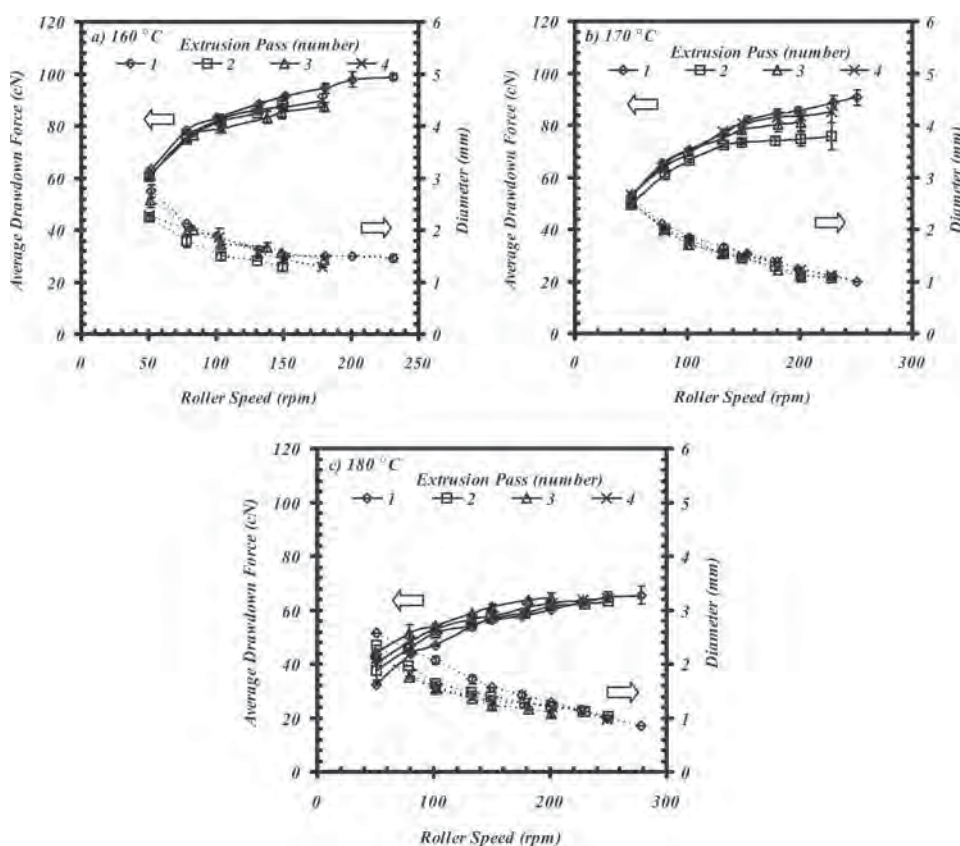
Figure 5. Effects of die temperature and number of extrusion pass on average drawdown force and filament diameter at failure point for LDPE melt. (a) 160°C, (b) 170°C, and (c) 180°C.

number of extrusion passes for all die temperatures was similar to that discussed relative to Fig. 4c.

Mechanical Properties of Solidified LDPE

Figures 6 and 7 show tensile modulus and tensile strength for virgin LDPE and reprocessed LDPE samples using a die temperature of 160°C collected from different roller speeds and three different volumetric flow rates. For all volumetric flow rates, as the roller speed was increased the tensile modulus and strength appeared to increase. This was because higher roller speed, which produced higher drawdown force as stated in Fig. 3, had led to higher molecular orientations and stress-induced crystallization of LDPE during solidification process. This view could also be supported by the work of Zhang et al.[25] who stated that LDPE could produce long and twisted lamellae (i.e., large lateral size, wavy lamellae interlocking from adjacent row nuclei) orientation morphology at high draw ratio from the melt spinning process.

The number of extrusion pass had a very interesting effect on the mechanical properties of the solidified LDPE. For the volumetric flow rate of 2.9×10^{-7} m^3/s (Fig. 6a) the tensile properties appeared to decrease with increasing number of extrusion passes. This was
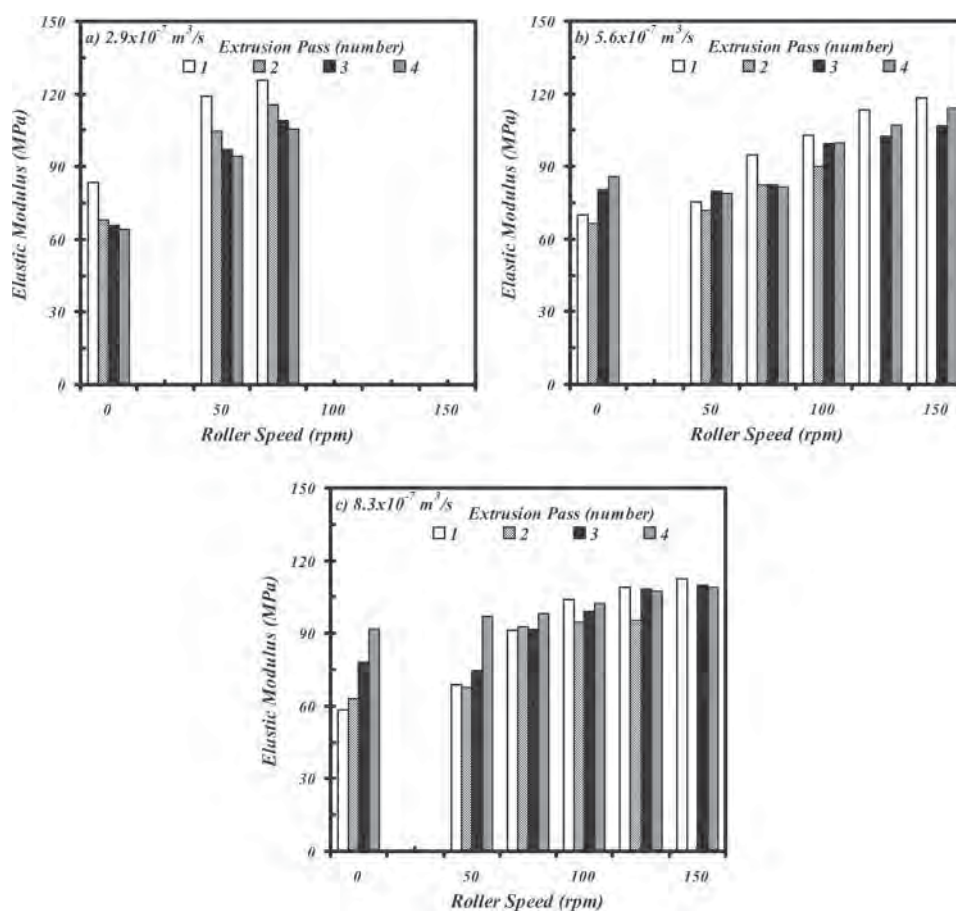
Figure 6. Effect of roller speed and number of extrusion pass on elastic modulus for solidified LDPE for different vo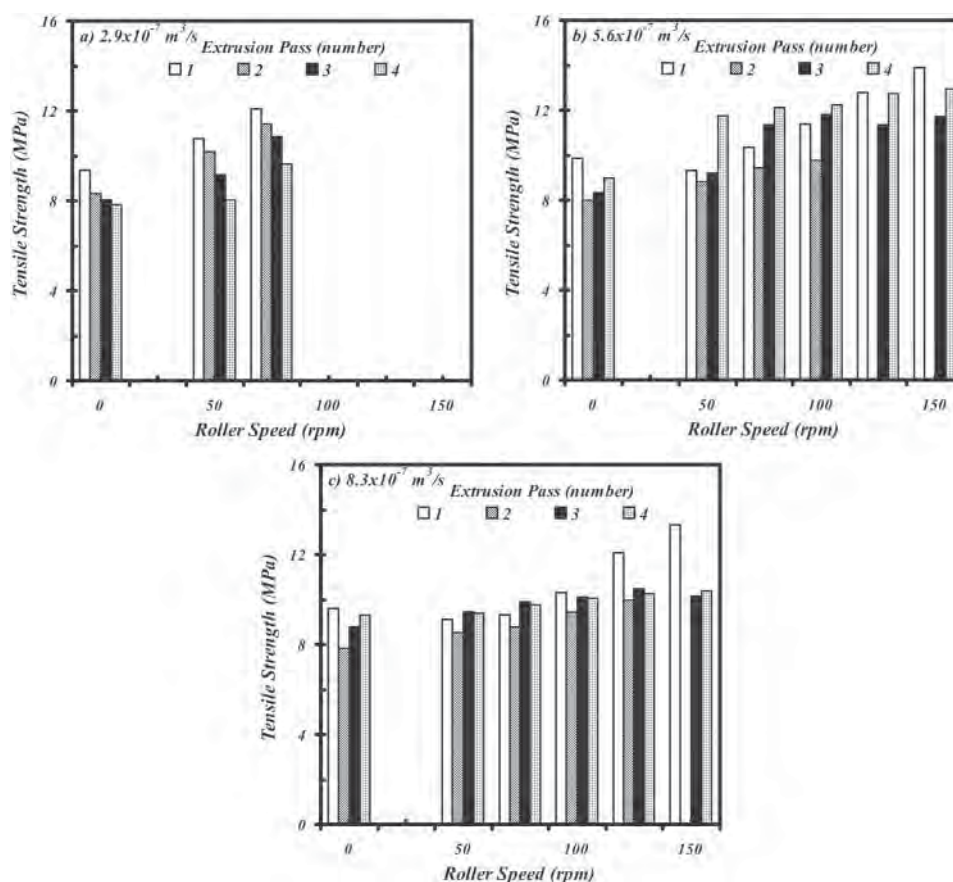lumetric flow rates: (a) 2.9×10^{-7} m^3/s, (b) 5.6×10^{-7} m^3/s, and (c) 8.3×10^{-7} m^3/s.

probably due to a decrease in molar mass of the LDPE. The gel content results in Table 1 suggested that there was no crosslinking in the LDPE sample. The LDPE samples collected from the volumetric flow rates of 5.6×10^{-7} and 8.3×10^{-7} m^3/s (Figs. 6b and c) show a decrease in tensile properties for the extrusion pass number #2, but started to regain or increase for the extrusion pass numbers #3 and #4 although only small percentage gel content (up to 18.23%) was observed. The increases in the tensile properties were associated with the small gel-content results given in Table 1. The increases in mechanical properties by the crosslinking of polyolefins were also noted by the work of Shen et al.[26]

The results in Fig. 6 interestingly suggest that, for any given roller speeds, increasing the volumetric flow rate resulted in decreases in tensile properties. This was due to the higher extrusion rate or volumetric flow rate producing higher shearing stresses to the melt during the flow and this would cause more molecular degradation of the LDPE melt and thus weakening the mechanical strength of the solidified LDPE. Besides, the crosslinked structure of molten LDPE may make it more difficult to crystallize during the solidification process.

Figure 7. Effect of roller speed and number of extrusion pass on ultimate tensile strength modulus for solidified LDPE for different volumetric flow rates: (a) 2.9×10^{-7} m³/s, (b) 5.6×10^{-7} m³/s, and (c) 8.3×10^{-7} m³/s.

Comparative Discussion of Mechanical Strengths of Molten and Solidified LDPE

This section gives a comparative discussion on the effects of volumetric flow rate, die temperature, number of extrusion passes, and roller speed on the mechanical properties of molten and solidified LDPE. It could be concluded that the mechanical properties of LDPE in both molten and solidified states were affected by die temperature, number of extrusion passes, roller speed, and volumetric flow rate. For the effects of die temperature, number of extrusion passes and roller speed, the mechanical properties of LDPE in both the molten and solidified stages were influenced in the same way, which were explained by viscous-elastic components, crosslinking, and molecular orientations, respectively. In the case of volumetric flow rate effect, the mechanical properties of the LDPE in the molten and solidified states were not the same, i.e., the mechanical properties of the solidified LDPE reduced with increasing volumetric flow rate (see Figs. 6a–c), but the opposite result was given for the molten state (see Fig. 3). The differences in the results for the volumetric flow rate effect were probably associated with viscous heating effects in the molten state and

crystallization effects in the solidified state. The experimental evidences for this claim are beyond the scope of this paper, but are to be further investigated in our future work.

Conclusion

An experimental apparatus was designed and constructed for this work that could be used for measurement of mechanical strength of molten LDPE and the results were then compared with those for solidified LDPE. The experimental results suggested that in the molten state, the drawdown force for LDPE melts were very dependent on volumetric flow rate, die temperature, roller speed, and the number of reprocessing times. The drawdown force for molten LDPE was not affected by number of extrusion passes at low volumetric flow rate, but was influenced at high volumetric flow rates. The tensile properties of the solidified LDPE appeared to increase with roller speed. The effect of number of extrusions on tensile properties for solidified LDPE was similar to that for molten LDPE. In the case of volumetric flow rates, the tensile properties for the solidified LDPE worsened when the volumetric flow rate was increased, but the opposite was observed for the molten LDPE. Thus the mechanical strength of the molten LDPE could not always be used to assess the mechanical properties of the solidified LDPE.

Acknowledgments

References

1. Wagner, M.H.; Collignon, B.; Verbeke, J. Rheotens-master curves and drawability of polymer melts. Rheol. Acta. **1996**, *35*, 117.
2. Baldi, F.; Franceschini, A.; Riccò, T. Determination of the elongational viscosity of polymer melts by melt spinning experiments. A comparison with different experimental techniques. Rheol. Acta. **2007**, *46*, 965.
3. Wagner, M.H.; Bastian, H.; Bernnat, A.; Kurzbeck, S.; Chai, C.K. Determination of elongational viscosity of polymer melts by RME and Rheotens experiments. Rheol. Acta. **2002**, *41*, 316.
4. Bernnat, A. Polymer Melt Rheology and the Rheotens Test, Ph.D. Thesis, Universität Stuttgart, **2001**.
5. Muke, S.; Ivanov, I.; Kao, N.; Bhattacharya, S.N. Extensional rheology of polypropylene melts from the Rheotens test. J. Non-Newt. Fluid. Mech. **2001**, *101*, 77.
6. Jesus, T.D.; Medina, G.; Gonzalez, J.P.; Vargas, L.D. Enhanced melt strength and stretching of linear low-density polyethylene extruded under strong slip conditions. Rheol. Acta. **2005**, *44*, 278.
7. Stadler, F.J.; Nishioka, A.; Koyama, K. Comparison of the elongational behavior of various polyolefins in uniaxial and equibiaxial flows. Rheol. Acta. **2007**, *46*, 1003.
8. Collier, J.; Petrovan, S.; Patil, P.; Collier, B. Elongational rheology of fiber forming polymers. J. Mater. Sci. **2005**, *40*, 5133.
9. Yamaguchi, M.; Wagner, M.H. Impact of processing history on rheological properties for branched polypropylene. Polymer **2006**, *47*, 3629.
10. Gupta, R.K.; Bhattacharya, N.S. The effect of die geometries and extrusion rates on melt strength of high melt strength polypropylene. J. Polym. Eng. **2007**, *27*, 89.
11. Dintcheva, N.T.; Mantia, F.P.L.; Scaffaro, R.; Paci, M. Reprocessing and restabilization of greenhouse films. Polym. Degrad. Stab. **2002**, *75*, 459.

12. Scaffaro, R.; Mantia, F.P.L.; Dintcheva, N.T. Effect of the additive level and of the processing temperature on the re-building of post-consumer pipes from polyethylene blends. Eur. Polym. J. **2007**, *43*, 2947.

13. Kartalis, C.N.; Papaspyrides, C.D.; Pfaendner, R. Recycling of post-used PE packaging film using the restabilization technique. Polym. Degrad. Stab. **2000**, *70*, 189.

14. Pedroso, A.G.; Rosa, D.S. Mechanical, thermal and morphological characterization of recycled LDPE/corn starch blends. Carbohyd. Polym. **2005**, *59*, 1.

15. Costa, H.M.; Ramos, V.D.; Rocha, M. C. G. Rheological properties of polypropylene during multiple extrusions. Polym. Test. **2005**, *24*, 86.

16. Camacho, W.; Karlsson, S. Assessment of thermal and thermo-oxidative stability of multi-extruded recycled PP, HDPE and a blend thereof. Polym. Degrad. Stab. **2002**, *78*, 385.

17. Vargas, E.R.; Rodriguez, D.N.; Menchaca, B.; Martinez, B.M.; Mezta, M.P. Degradation effects on the rheological and mechanical properties of multi-extruded blends of impact-modified polypropylene and poly(ethylene-co-vinyl acetate). Polym. Degrad. Stab. **2004**, *86*, 301.

18. Dostal, J.; Kasparkova, V.; Zatloukal, M.; Muras, J.; Simek, L. The influence of the repeated extrusion on the degradation of polyethylene. Structure changes in low density polyethylene. Eur. Polym. J. **2008**, *44*, 2652.

19. Santos, A.S.F.; Agnelli, J.A.M., Trevisan, D.W.; Manrich, S. Degradation and stabilization of polyolefins from municipal plastic waste during multiple extrusions under different reprocessing conditions. Polym. Degrad. Stab. **2002**, *77*, 441.

20. Kim, J.K.; Chang, J.H. Comparison of the properties of poly(butylene terephthalate nanocomposite fibers with different organoclays. Macromol. Res. **2007**, *15*, 449.

21. Dastjerdi, R.; Mojtahedi, M.R.M.; Shoshtari, A.M. Comparing the effect of three processing methods for modification of filament yarns with inorganic nanocomposite filler and their bioactive against *Staphylococcus aureus*. Macromol. Res. **2009**, *17*, 378.

22. Hyun, J.C. Draw resonance in polymer processing: A short chronology & a new approach. Korea-Australia Rheol. J. **1999**, *11*, 279.

23. De Jesus, T.; Guadarrama-Medina, T.J.; Pérez-González J.; de Vargas L (2005) Enhanced melt strength and stretching of linear low-density polyethylene extruded under strong slip conditions. Rheol. Acta. **2005**, *44*, 278.

24. Intawong, N-T.; Sombatsompop, N. Experimental studies on changes in radial extrudate swell and velocity profiles of flowing PS melt in an electro-magnetized die of an extrusion rheometer. Polym. Eng. Sci. **2004**, *44*, 2298.

25. Zhang, X.M.; Elkoun, S.; Ajji, A.; Huneault, M.A. Oriented structure and anisotropy properties of polymer blown films: HDPE, LLDPE and LDPE. Polymer **2004**, *45*, 217.

26. Shen, Y.; Xie, B.; Yang, W.; Li, Z.; Yang, M. J. Effect of EPDM content on melt flow, Microstructures and fracture behavior of dynamically vulcanized PP/EPDM blends. Macromol. Sci. Phys. **2007**, *46*, 1127.

Flexural and creep strengthening for wood/PVC composite members using flat bar strips

T. Pulngern [a,*], C. Padyenchean [a], V. Rosarpitak [b], W. Prapruit [c], N. Sombatsompop [c]

[a] Department of Civil Engineering, Faculty of Engineering, King Mongkut's University of Technology Thonburi (KMUTT), Thongkru, Bangmod, Bangkok 10140, Thailand
[b] V.P. Wood Co., Ltd., 25/5 Moo 4, Soi Suksawad 66, Bangmod, Thungkru, Bangkok 10140, Thailand
[c] Polymer PROcessing and Flow (P-PROF) Group, School of Energy, Environment and Materials, King Mongkut's University of Technology Thonburi (KMUTT), Thongkru, Bangmod, Bangkok 10140, Thailand

ARTICLE INFO

ABSTRACT

This paper presents the flexural and creep performances of the strengthened wood/poly(vinyl chloride) (WPVC) composite members by using various types of flat bar strips adhered to the tension side. The WPVC composite member used was produced by an industrial-scale twin-screw extruder using the weight ratio of the wood to PVC compound of 1:1. High carbon steel (HCS) flat bar was selected a suitable material for the strengthening of WPVC composite members because of its high tensile stress, thin and light weight. For tension failure control, the flexural properties of strengthened WPVC composite member were improved with thickness and number of HCS strip used. By using one strip of HCS with 0.5 mm thickness adhered in tension side of WPVC composite member, the ultimate loads increased significantly up to 64% and 101% under flat-wise and edge-wise loading directions, respectively. Moreover, the strengthening of WPVC by using the HCS flat bar could reduce significantly the creep behavior, especially in edge-wise direction. Due to the same sustained load, the creep displacements of the strengthening WPVC composite members reduced significantly for 48% under flat-wise direction, and 11% under edge-wise loading direction. The creep displacement per sustained load and fraction deflection was found to reduce significantly by the HCS strengthening method.

1. Introduction

Attention to wood plastic composites (WPC) material are increasing as new materials for many applications [1], such as pallets [2] and structural member as deck and small beams [3,4]. This is because of that WPC is a lightweight material with corrosion resistance, long-term durability, and low maintenance requirements. Basically, many types of polymer matrices are used for making WPC materials. However, wood/polyvinyl chloride (WPVC) [1,3–6] was frequently found in literatures. Our previous works [3,4] clearly suggested that WPVC composites were anisotropic, non-homogenous, and had lower mechanical properties than natural woods. Besides, their properties including time dependent properties like creep and fatigue behaviors were greatly affected by cross section design and loading direction [3,4]. Since their mechanical strength limits were still questionable, many researchers have focused on strength improvements for the WPC materials. Recent literatures stated that the strength improvements for WPC materials could be carried out by a number of methods, such as

reinforcement with glass–fibres [6], manufacturing techniques [7], and addition of nanoparticles in WPC matrix [8–10]. Faruk and Matuana [8] suggested that melt blending technique was the best approach for incorporating nanoclay into wood/high-density polyethylene (HDPE) to enhance the mechanical properties. The approach of melt blending technique was also well-applicable in the case of wood/PVC composites using carbon nanotube (CNT) [9]. Shi et al. [10] attempted to enhance the stiffness of wood/polypropylene (PP) composites using vapor-grown carbon nanofibres (CNFs). A wide range of agricultural fibres were also found to affect the mechanical properties, thermal stability, and water resistance of wood/WPVC composites [11]. Glass–fibre was also applied for the internal reinforcement of WPC composites materials and presented significant improvement in the properties [12,13]. The effects of glass–fibre type and fibre orientation were presented in work of Jiang et al. [13] and Mongkollapkit et al. [14]. Although, the mechanical properties of WPC composites can be improved by internal reinforcing with natural fibre, glass–fibre, and nanoparticles, but the improvement of these strengthening methods was found to be about 30–60%.

Fibre, glass–fibre, and carbon-fibre-reinforced polymers (FRP, GFPR, and CFRP) sheets were typically performed for strengthening concrete structural members because of their high tensile stresses

---

* Corresponding author. Tel.: +66 2 470 9145; fax: +66 2 427 9063.
E-mail address: Tawich.pul@kmutt.ac.th (T. Pulngern).

and very light weights [15–21]. The pre-stressing FRP sheet before bonding also suggested as efficient solution to strengthen the concrete beams [18–20]. FRP sheet could also be used for strengthening of WPC composite members. For example, Dura et al. [22] presented the improvement of flexural properties of wood/PP using FRP sheet and Naghipour et al. [23] introduced an analytical model based on nonlinear material theory to predict the ultimate bending moment capacities of WPC beam strengthening using FRP sheet. They stated that the FRP sheet was discovered to be efficient in strengthening the WPC since it could enhance the flexural behaviors of WPC in terms of strength and ductility. Although, the FRP, CFRP, and GFRP sheets were accepted widely for external strengthening of structural members [15–23] because of the advantage in term of the strength/density ratio, but the cost of these FRP materials was very high [24,25]. For example, for strengthening the concrete bridge deck, the material cost for the FRP reinforced deck bridge were 60% higher than that of the steel reinforced deck bridge [25].

Although the external strengthening WPC composite members using FRP sheet were reported previously [22,23] research works of the external strengthening of WPC composites were still rare and limited, in comparison with those of the internal strengthening as above-mentioned [6–14]. Besides, using more economic materials for external strengthening of WPVC composites is also very interesting. Therefore, the objective of this paper was to report the external strengthening for WPVC composite members using flat bar strips adhered at the tension side. The effects of flat bar material, flat bar thickness, and number of strip were assessed. The external strengthening of an industrial-scale WPVC composite member using lower cost materials would discriminate this work from other published works [22,23]. The loading direction effect was also included since WPVC composites were found to be anisotropic material [3,4]. Moreover, the creep characteristics of strengthened WPVC composite members were also studied to indicate the long-term performance of the composite member.

2. Experimental

2.1. WPVC composites materials

The polymer matrix used in this work was suspension poly(vinyl chloride) (PVC) powder, supplied by V.P. Wood Co., Ltd. (Bangkok Thailand) under a trade name of SIAMVIC-266RB having a K value of 66. The PVC powder was initially dry-blended with various necessary additives to give PVC compound before melt-blending with wood particles in making wood/PVC composites (WPVC). Based on our previous work [5], N-2(aminoethyl)3-aminopropyl trimethoxysilane (KBM603, M_w = 222.4) was most suitable for WPVC, and was thus used in this work. The other additives in parts per hundred (pph) of PVC; SIAMVIC 266RB)] included a PVC organic complex stabilizer (TS-DBL-Pb-Ba, 3.6 pph), an external lubricant (Finalux G-741, 0.6 pph), calcium carbonate (Omyacarb-2T, 9 pph), calcium stearate (0.3 pph), and acrylic-based processing aids (PA20, 8 pph). The wood particles, supplied by V.P. Wood Co., Ltd. (Bangkok Thailand), had an average size of 100–300 μm. In this work, the content of the wood particles in the PVC compounds was fixed at 100 (in part per hundred (pph) of PVC powder), or wood particles 100 parts in 100 parts of PVC powder by weight. The wood particles were chemically treated with 1.0 wt.% KBM 603 coupling agent [5–7].

2.2. Preparation of WPVC composite member

An industrial-scale twin-screw extruder with counter-rotating screws (KMD-90-36, KraussMaffei Technologies GmbH, Germany)

was used for preparation of WPVC composites. The melt blending and sample preparation processes were commenced by (i) drying the KBM603 treated wood particles in hot oven with temperature of 80 °C, (ii) dry-blending the PVC compound with the dried wood particles using a high speed mixer, (iii) melt-blending in the twin-screw extruder with the blending temperature of 180 °C, (iv) extruding the molten WPVC composites through the die, and (v) passing through a cooling-system for composites solidification. The solidified WPVC composite member had four hollow cores with body dimensions of 38×144 mm^2. The thicknesses of top and bottom flanges were 6 mm while the web thickness was 6 mm as shown in Fig. 1. This WPVC composite member has been industrial commercialized with a large quantity of fabrication. The consistency in dimensions and properties were accepted with the customer. These applications of the cross sections were used for decks (installation in flat-wise) and small beams (installation in edge-wise), which have been widely used, especially in the Southeast Asian region.

2.3. Flat bars

Flat bar type was varied in order to seek the suitable material of flat bar strips for strengthening the WPVC composites. Three flat bar types, which included high carbon steel (HCS), aluminum (Al), and plastic (Pl), were used in this investigation. The selection of flat bar material was considered based on their tensile strength based on the averaged values of three independent specimens. The dimensions and mechanical properties of all flat bar strips used in this study are given in Table 1.

2.4. Commercial epoxy

An epoxy adhesive (Sikadur-31 CF normal) was used for bonding the flat bar strip with WPVC composite member. The epoxy adhesive consisted of parts A and B, which the mixing ratio was 2:1 by volume. Part A was the oxirane, mono [(C12-14-alkyloxy) methyl], reaction product, and the epoxy resin. Part B consisted of 3-aminomethyl, trimethylcyclohexylamine, diazoctane, and diamine. The mechanical properties of the epoxy adhesive, at temperature of 23 °C and 3 days curing time, were 17–23 N/mm^2 for tensile strength, 11–15 N/mm^2 for bending strength, and 50–70 N/mm^2 for compressive strength.

2.5. Characterizations

2.5.1. Flexural testing

Four-point bending test for WPVC composite member before and after strengthening with flat bar were evaluated in accordance with ASTM-D198-09 [26]. The WPVC composite specimen was installed on two-end supports with span length of L. The load evener was applied at the third point location with a load span of $L/3$ from one-end support. The rate of loading (R) used in this section was
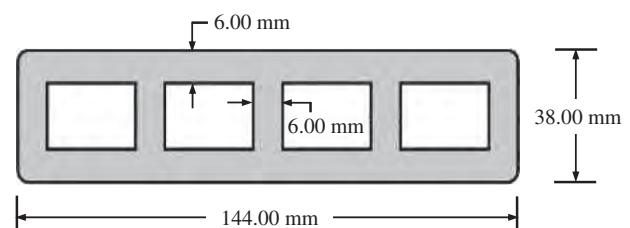
Fig. 1. Cross section and dimensions of WPVC composite member (flat-wise).

Table 1
Engineering properties of flat bars used.

Flat bar type	Size		Area (mm²)	Ultimate load (kN)	Tensile stress (MPa)	Elastic modulus (MPa)
	Width (mm)	Thickness (mm)				
High-carbon steel strip (HCS)	25.00	0.20	5.0	8.41 (0.030)	1.68×10^3 (6.000)	1.99×10^5 (0.001)
	25.00	0.50	12.5	20.84 (0.046)	1.67×10^3 (3.667)	1.99×10^5 (0.001)
Aluminum strip (Al)	25.00	0.50	12.5	1.55 (0.017)	124.00 (1.386)	6.90×10^3 (0.001)
Plastic band (Pl)	15.00	2.00	30.0	0.20 (0.010)	6.70 (0.333)	2.00×10^3 (0.002)

Remarks: The values in parenthesis are the standard deviation (S.D.) from three independent determinations.
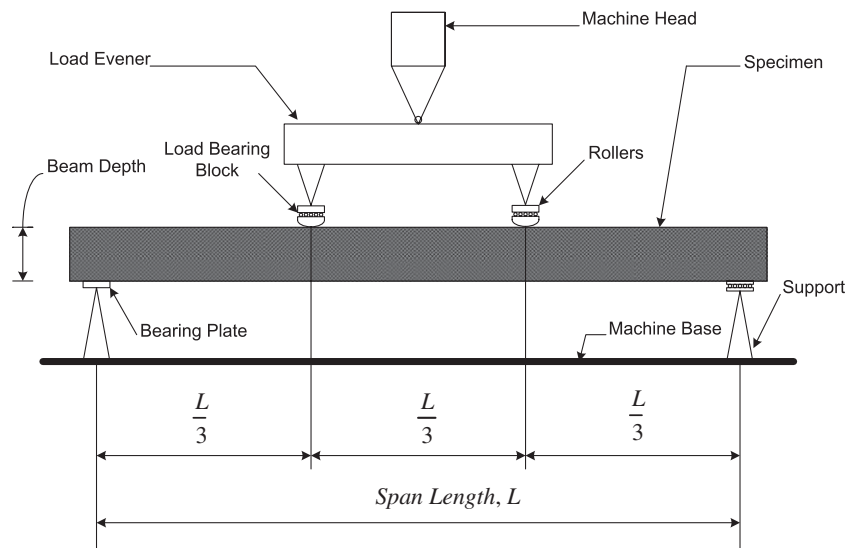
Fig. 2. Static four-point bending test setup.
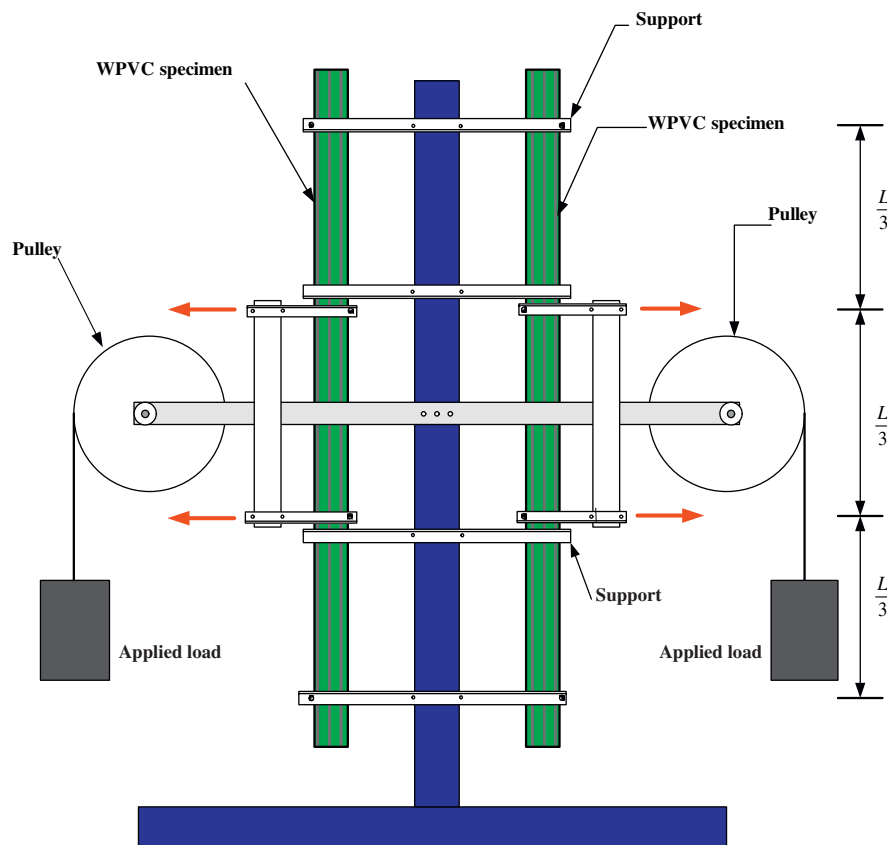
Fig. 3. An experimental setup for creep testing.

calculated in accordance with ASTM-D790-07 [27]. The flexural properties were averaged from five individual tested specimens, focusing on ultimate load, ultimate moment capacity, modulus of rupture, modulus of elasticity, and bending stiffness. For loading direction effect, WPVC composite member was used to perform the flexural testing under edge-wise and flat-wise loading directions. Fig. 2 shows experimental arrangement for static four-point bending tests as described.

2.5.2. Creep testing

The creep testing for WPVC beams was setup based on four-point bending method which followed ASTM-D198-09 [26]. The creep testing frame was designed to bend the WPVC composite member vertically using the solid-steel weights, which were hung from pulleys, as used for the initial applied load. The schematic diagram of the creep testing apparatus is given in Fig. 3. The initial deflections at the mid span of the WPVC member and additional deflections as a function of time under sustained loading were recorded in accordance with ASTM D2990-09 [28] which monitored the changes in the displacements in minute intervals (1, 6, 12, 30 min), and subsequently in hour intervals (1, 2, 5, 20, 50, 100, 200, 500, 700 and 1000 h). The applied loadings were varied from 20% to 40% of the ultimate loading obtained from the static flexural test. The load intervals used were based on the designing of wood plastic composite members, which the allowable stresses were limited in this region [29]. The initial displacement, final displacement, and creep displacement averaged from four individual test specimens were given. For loading direction effect, WPVC beam was used to perform the creep testing under edge-wise and flat-wise directions.

3. Results and discussion

3.1. Flexural properties

3.1.1. Effect of flat bar materials

Table 2 gives the average flexural properties from five individual flexural testing of WPVC composite member before and after strengthening with HCS, Al, and Pl flat bar under flat-wise loading direction. The results indicated that strengthening of WPVC composite member using HCS flat bar strip with 0.20 mm thickness improved the ultimate load and ultimate moment capacity from 6984 N to 9475 N (approximately 35%). Modulus of rapture and bending stiffness was also improved. The strengthening of WPVC by Al and Pl flat bars could not improve the flexural properties. The additional flexural properties of the strengthened WPVC was obtained by multiplying the tension force in flat bar strip (F_s) with the corresponding distance (d_2) between tension and compression forces (C) in the top flange as presented in Fig 4. This may be why the WPVC composite member adhered the high tensile stress HCS flat bar gave relatively high ultimate moment capacity. This also gives a practical implication that HCS flat bar was a suitable material for strengthening the WPVC composite member. Moreover, HCS flat bar had high tensile stress but it was thin and light weight. The strength per weight ratio of HCS flat bar was highest in comparison with other materials. Therefore, HCS flat bar was selected to strengthen the industrial-scale WPVC composite member for next sections of this work.

3.1.2. Effect of flat bar thickness and number of strip

From the previous section, the flexural properties of WPVC composite member were greatly improved by attaching the HCS

Table 2
Flexural properties of strengthened WPVC composites by varying flat bar types in flat-wise direction.

Specimen code	Moment of inertia (mm⁴)	Deflection at max. load × 10⁻² (m)	Ultimate load (N)	Ultimate. moment capacity (N m)	Modulus of rupture (MPa)	Modulus of elasticity (MPa)	Bending stiffness EI (kN m²)
WPVC	491,492	1.86 (0.53)	6984 (219.32)	719 (22.59)	27.81 (0.87)	3583 (111.36)	1.76
WPVC + HCS	591,594	1.82 (0.50)	9476 (211.87)	976 (21.03)	31.34 (1.63)	3346 (253.77)	1.98
WPVC + Al	500,306	1.81 (1.77)	7045 (232.34)	726 (23.93)	27.56 (0.91)	3370 (298.27)	1.69
WPVC + Pl	516,659	1.89 (0.58)	6975 (207.56)	718 (21.38)	26.42 (0.79)	3395 (62.82)	1.75

Remarks: The values in parenthesis are the standard deviation (S.D) from five independent determinations.
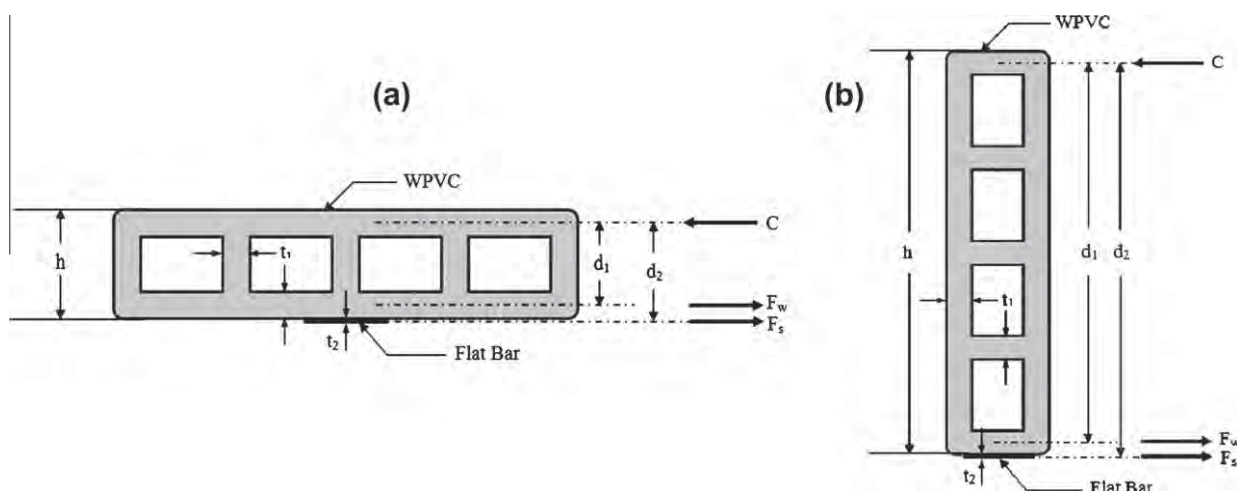
Fig. 4. Cross section of strengthened WPVC composites: (a) flat–wise direction and (b) edge-wise direction.

Table 3
Flexural properties of before and after strengthening the WPVC by varying thicknesses & numbers of strip in flat-wise direction.

| Specimen code	Thickness (mm)	No. of strips	Moment of inertia (mm⁴)	Deflection at max. load × 10⁻² (m)	Ultimate load (N)	Ultimate moment capacity (N m)	Modulus of rupture (MPa)	Modulus of elasticity (MPa)	Bending stiffness EI (kN m²)
WPVC	–	–	491,492	1.86 (0.53)	6984 (219.32)	719 (22.59)	27.81 (0.87)	3583 (111.36)	1.76
WPVC + HCS	0.2	1	591,594	1.82 (0.50)	9476 (211.87)	976 (21.03)	31.34 (1.63)	3346 (253.77)	1.98
		2	691,697	2.53 (0.74)	12,713 (313.40)	1309 (32.28)	35.97 (0.89)	3415 (117.50)	2.36
	0.5	1	745,694	2.27 (0.21)	11,485 (290.59)	1183 (20.03)	30.14 (2.60)	2771 (44.89)	2.07
		2	999,897	1.87 (0.33)	12,393 (118.92)	1276 (19.95)	24.25 (0.04)	2198 (113.90)	2.20

Remarks: The values in parenthesis are the standard deviation (S.D.) from five independent determinations.
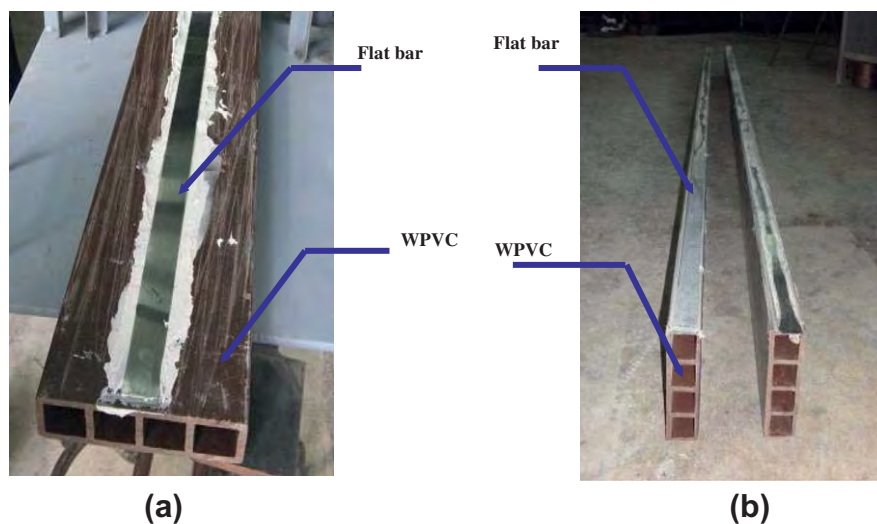
Fig. 5. Installation of flat bar on the tensile side of WPVC composite member: (a) flat-wise direction and (b) edge-wise direction.

flat bar to the tension side. It was reasonable to increase the flexural properties of the strengthened WPVC composite member by increasing the HCS thickness and number of HCS strip. This could be carried out by either varying number of strip (one and two strips) or by varying the flat bar thicknesses (0.20 and 0.50 mm). The tested results are given in Table 3. The results indicated that the flexural properties of the strengthened WPVC composite members increased with number of HCS strip and HCS thickness. This was because the increments of thickness and number of HCS strip were the increments in flat bar area to resist the exerted tensile forces. The higher flat bar area, the higher flexural properties. For installation of one and two HCS strips with 25 mm width and 0.20 mm thickness, the cross sectional area to resist the tension increased from 5 to 10 mm², and the ultimate moment capacity increased 29% (from 6984 to 8974 N) and 82% (from 6984 to 12,713 N), respectively. The performance of the strengthened WPVC composites in this case was directly related with the cross sectional area of HCS flat bar. In case of installation of one and two HCS strips with 25 mm width and 0.5 mm thickness, the cross sectional area to resist the tension were 12.5 and 25 mm², respectively. It could increase the ultimate moment capacities of 64% (from 6984 to 11,485 N) and 77% (from 6984 to 12,393 N), although the cross section area to resist the tension was double. The reason was based on the fact that the increment of the cross sectional area to resist the tension was the improvement of strengthened WPVC member only in the tension side. The failures

of the strengthened WPVC composite member had changed from the tension failure to the compression failure (top side). Therefore, the final ultimate moment capacities did not increase as expected.

3.1.3. Effect of loading direction

For the effect of loading direction, the strengthened WPVC composite member were prepared by installing one strip of HCS flat bar with 0.5 mm thickness at the tension side under flat-wise and edge-wise loading directions as given in Fig. 5. The load–displacement curves for WPVC composite member before and after strengthening under flat-wise and edge-wise loading directions are presented in Fig. 6. It can be seen that strengthening the WPVC significantly increased ultimate load in both flat-wise and edge-wise loading directions. The load–deflection slopes of the strengthened WPVC composite member in both loading directions were increased indicating the greater flexural properties of the strengthened WPVC composite member. For the specified applied load, the deflections of the strengthened WPVC composite member decreased. The improvement of flexural properties in the edge-wise direction was greater than that in the flat-wise direction. Table 4 compares the flexural properties of WPVC members before and after strengthening in flat-wise and edge-wise directions. It was very difficult to compare the results between these two loading directions because they used in different span-lengths. It was observed that the ultimate load and ultimate moment capacity increased about 64% (from 6984 to 11,485 N) in the flat-wise direction, and about
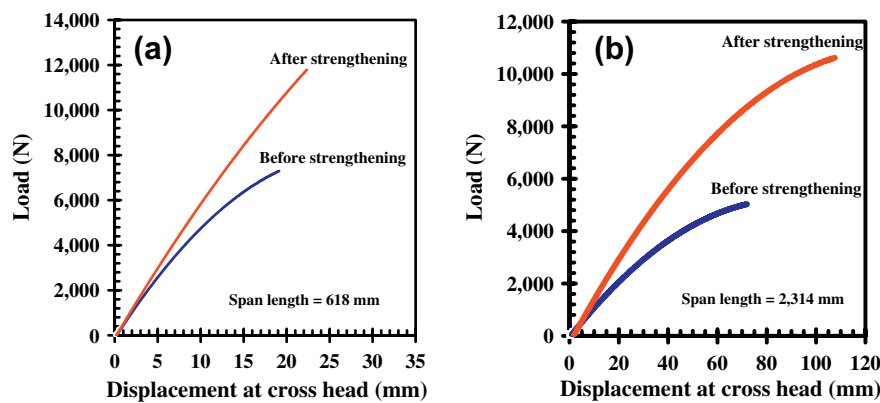
Fig. 6. Load–displacement curves before and after strengthening the WPVC composite members: (a) flat-wise direction and (b) edge-wise direction.

Table 4
Comparison of the flexural properties of WPVC composite members before and after strengthening in flat-wise and edge-wise directions.

Loading direction	Condition	Moment of inertia (mm^4)	Deflection at max. load $\times 10^{-2}$ (m)	Ultimate load (N)	Ultimate moment capacity (N m)	Modulus of rupture (MPa)	Modulus of elasticity (MPa)	Bending stiffness EI (kN m^2)
Flat-wise	Before	491,492	1.86 (0.53)	6984 (219.32)	719 (22.59)	27.81 (0.87)	3583 (111.36)	1.76
	After	745,694	2.27 (0.21)	11,485 (290.59)	1183 (20.03)	30.14 (2.60)	2771 (44.89)	2.07
Edge-wise	Before	4845,114	7.15 (0.47)	5029 (140.08)	1939 (15.36)	28.82 (0.32)	4012 (72.71)	19.44
	After	8426,033	9.82 (0.82)	10,109 (169.51)	3899 (64.98)	33.32 (0.56)	3186 (207.37)	26.84

Remarks: The values in parenthesis are the standard deviation (S.D.) from five independent determinations.

101% (from 5029 to 10,109 N) in the edge-wise direction. The strengthening of the WPVC composite member by adhering the HCS flat bar to the tension side could increase the bending stiffness (EI) of the member, especially in the edge-wise direction. The modulus of rupture of the strengthened WPVC composite members also increased, but in a lower magnitude. It was worthy discussing the results found in this work with other researchers whose works were related to the strengthening the WPC using fibre-reinforced polymer (e.g., CFRP and GFRP). Dura et al. [22] presented that the WPC strengthened using CFRP sheet bonding in top and bottom sides under edge-wise loading direction increased the first failure load, ultimate load, and load deflection slope about 103%, 141%, and 73%, respectively. By bonding with CFRP sheet with thickness of 0.12 mm under edge-wise loading direction [23], the ultimate load was improved with number of CFRP and GFRP layer which were 22% to 80%, respectively. The main reason of the improvement was the particularity strength of the reinforcing materials. Therefore, it was difficult to compare directly the results from this work with those of previous works [22,23] because the different materials, number of layer, and sheet thickness were used. However, this work indicated that more economic material of HCS flat bar could be alternative material for strengthening the WPVC composite member.

3.2. Creep properties

3.2.1. Effect of loading direction

Table 5 presents the ultimate load to failure obtained from four-point bending test and the sustained load for creep test in flat-wise and edge-wise directions for WPVC composite member before and after strengthening using HCS strip with 0.50 mm thickness. In case of flat-wise direction, the sustained loads of the WPVC composite member before strengthening were 1397, 2095, and

2794 N while there were 2297, 3447, and 4594 N for the strengthened WPVC composite member, respectively. In case of edge-wise direction, the sustained loads were 1006, 1509, and 2012 N for the un-strengthened WPVC composite member, and 2022 N, 3033 N, and 4044 N for strengthened WPVC composite member. Since the ultimate loads and the sustained loads of WPVC composite member before and after strengthening were not the same, it was very difficult to compare directly for the creep displacement as well as the creep rate. However, 40% of ultimate load for un-strengthened WPVC composite member was very close with those of 20% of the strengthened WPVC composite member. The comparison could, thus, be done with this condition. Fig. 7 presents the comparison of displacement–time curves (creep curve) between un-strengthening and strengthening members under flat-wise loading directions. It can be seen that significant lower in creep displacements, magnitude changes of creep displacement over time, and slope of creep curves for the strengthened WPVC composite member of all applied loads were reduced significantly, representing the greater creep resistance of strengthened composite members. Another important behavior was that the tertiary creep

Table 5
Ultimate load to failure from static flexural test and applied load for creep testing for WPVC composite member in edge-wise and flat-wise directions.

Loading direction	Specimen span length (mm)	Conditions	Ultimate load (N)	20% of ultimate load	30% of ultimate load	40% of ultimate load
				Sustained load (N)		
Flat-wise	618	Before	6984	1397	2095	2794
		After	11,485	2297	3446	4594
Edge-wise	2314	Before	5029	1006	1509	2012
		After	10,109	2022	3033	4044

Fig. 7. Displacement–time curves for WPVC composite member with various applied loads in flat-wise direction; (a) before strengthening and (b) after strengthening.

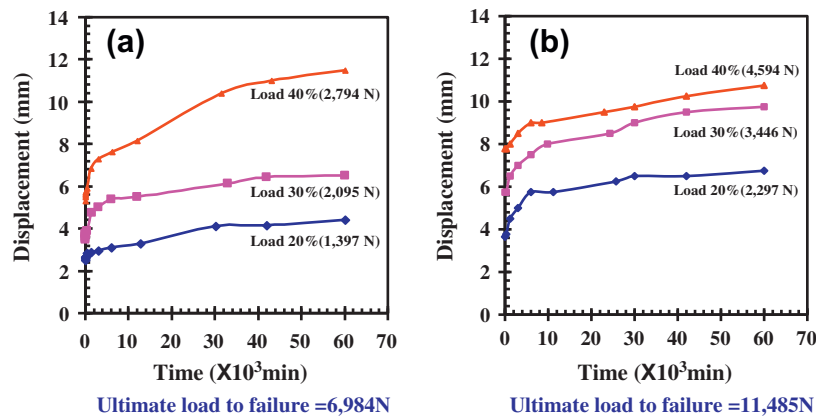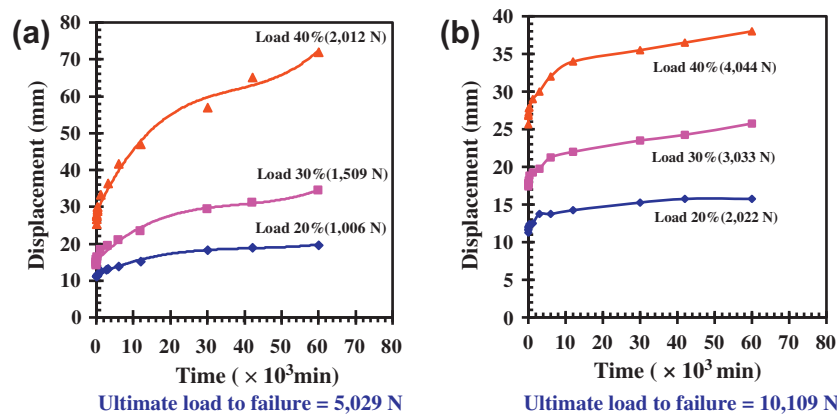**Fig. 8.** Displacement–time curves for WPVC composite member with various applied loads in edge-wise direction: (a) before strengthening and (b) after strengthening.

state did not appear at 40% of sustained load for the strengthened WPVC composite member while it appeared for the un-strengthened WPVC composite member. The reason was based on the fact that HCS flat bar adhered to the tension side could resist the tensile strain occurring in the WPVC composite member. In case of edge-wise direction as shown in Fig. 8, similar behaviors were found, the differences in creep behavior before and after strengthening being clearly seen representing the greater creep resistance. The tertiary creep which appeared for the un-strengthened WPVC composite member, at the stress levels of 30% and 40% of sustained load did not appear for the strengthened WPVC composite member.presents the results of initial displacement, final displacement at 1000 h, as well as the creep displacement before and after strengthening using HCS flat bar. For the flat-wise direction and comparing between the sustained load of 2794 N (40% stress level of member before strengthening) and load of 2297 N (20% stress level of member after strengthening), the creep displacement reduced from 6.18 to 2.98 mm (remaining 48%). Similarly, in case of edge-wise direction, between the sustained load of 2012 N (40% stress level of member before strengthening) and load of 2022 N (20% stress level of member after strengthening), the creep displacement reduced from 39.75 to 4.48 mm (remaining only 11%). These statements confirmed that the creep behavior of the strengthened WPVC composite member could be improved significantly by using the HCS flat bar, especially under the edge-wise loading direction. The differences in creep resistances between flat-wise and edge-wise direction of WPVC composite member

were based on the fact that the load application in the flat-wise direction encountered greater number of cores than that in edge-wise direction [4].

The results for creep displacement per sustained load of all applied stress levels are also given Table 6. It was found that the creep displacement per sustained load of the strengthened WPVC composite member was lower than those of the un-strengthened WPVC composite members, the effect being pronounced in the edge-wise direction. In edge-wise direction, the creep displacement per sustained load ranged from 7.63 to 19.76 for un-strengthened member, and ranged from 2.22 to 3.07 for strengthened members (remaining only 15.5–29.1%). The HCS strengthened WPVC composite member could reduce creep displacement or creep behavior, this indicating improved long-term performance of the WPC material in practical applications. The fraction deflection, which was the ratio of final displacement on the initial displacement, recorded from creep experiments were also determined, and it was found that the fraction deflection for the un-strengthened WPVC composite members were ranged from 1.60 to 2.56, and ranged from 1.47 to 1.56 for strengthened WPVC composite member. In the edge-wise direction and at the 40% applied stress ratio, the fraction deflection of strengthening WPVC composite members reduced by 42% (from 2.56 to be 1.48). It was worthy comparing the results obtained in this work with Dura et al. [22] related to the strengthening the WPC using fibre-reinforced polymer (hybrid WPC–FRP members) under the sustained load. The fractional deflections of hybrid WPC–FRP members ranged from 1.47 to 1.56 (for sustained load

Table 6
Comparison of creep behavior before and after strengthening the WPVC composite members in flat-wise and edge-wise directions.

Load Direction	Load level (%)	Initial displacement (mm)		Final displacemen (mm)		Creep displacement (mm)		Creep displacement/sustained load ($\times 10^{-3}$ mm/N)		Fraction deflection	
		Before	After	Before	After	Before	After	Before	After	Before	After
Flat-wise	20	2.51 (0.22)	3.77 (0.28)	4.40 (0.57)	6.75 (0.35)	1.89	2.98	1.67	1.30	1.75	1.79
	30	3.50 (0.21)	5.74 (0.24)	6.50 (0.30)	9.75 (0.36)	3.00	4.01	1.77	1.16	1.86	1.70
	40	5.32 (0.37)	7.78 (0.55)	11.50 (0.64)	10.75 (0.35)	6.18	2.97	2.74	0.65	2.16	1.38
Edge-wise	20	11.22 (1.62)	11.27 (0.31)	18.90 (0.84)	15.75 (0.65)	7.68	4.48	7.63	2.22	1.68	1.40
	30	14.25 (0.41)	17.42 (1.11)	31.25 (2.54)	24.25 (1.77)	17.00	6.83	11.27	2.25	2.19	1.39
	40	25.50 (0.71)	25.60 (0.93)	65.25 (2.83)	38.00 (1.41)	39.75	12.40	19.76	3.07	2.56	1.48

Remarks: The values in parenthesis are standard deviation (S.D.) from four independent determinations. Creep displacement = final displacement–initial displacement, Fraction deflection = final displacement/initial displacement.

of 90 days and stress level 15–45%), which was in the same magnitude of this study mentioned earlier. However, it was difficult to compare directly the results from this work with the previous works [22] because of the differences in the strengthening material, numbers of layer, and sheet thicknesses. Moreover, the fraction deflection, creep displacement, and creep rate were also related with the applied stress ratio. However, the results in this work have clearly confirmed the possibility of using HCS flat bar to strengthen for the WPVC composite member, not only enhancing the flexural performance, but also the creep resistance of the composites.

4. Conclusion

This work presents the effectiveness of strengthening the WPVC composite member using flat bar strip adhered to the tension side. The following conclusions were noted:

(1) Flat bar materials affected directly the performance of the strengthened WPVC composite member, and, it was found that HCS flat bar strip was the most suitable strengthening material.
(2) In case of tension failure controlled, the flexural properties of the strengthened WPVC composite members could be improved by increasing the thickness and number of HCS strip.
(3) Ultimate load and ultimate moment capacity of the strengthened WPC composite member increased significantly to about 64% under the flat-wise loading direction and increased to about 101% under the edge-wise loading direction representing the loading direction effect on the anisotropic materials.
(4) Creep displacements of the strengthening WPVC composite members reduced significantly for 48% under flat-wise direction, and 11% under edge-wise loading direction. The creep displacement per sustained load and fraction deflection also decreased, indicating an improved long-term efficiency of the strengthened WPC composite members.

Acknowledgments

References

[1] Jaing H, Kamdem DP. Development of poly(vinyl chloride)/wood composite: a literature review. J Vinyl Addit Technol 2004;10(2):59–69.

[2] Soury E, Behravesh AH, Rouhani Esfahani E, Zolfaghari A. Design optimization and manufacturing of wood plastic composite pallet. Mater Design 2009;30(10):4183–91.

[3] Sombatsompop N, Prapruit W, Chaochanchaikul K, Pulngern T, Rosapitak V. Effect of cross section design and testing conditions on the flexural properties of wood/PVC composite beams. J Vinyl Addit Technol 2010;16(1):33–41.

[4] Pulngern T, Chucheepsakul S, Padyenchean C, Sombatsompop N, Prapruit W, Chaochanchaikul K, et al. Effect of cross section design and testing conditions on the creep and fatigue properties of wood/PVC composite beams. J Vinyl Addit Technol 2010;16(1):42–9.

[5] Sombatsompop N, Chaochanchaikul K. Average mixing torque, tensile, and impact properties and thermal stability of PVC/sawdust composites with different silane coupling agents. J Appl Polym Sci 2005;96(1):213–21.

[6] Tungjitpornkull S, Chaochanchaikul K, Sombatsompop N. Mechanical characterization of e-chopped strand glass fiber reinforced wood/PVC composites. J Thermo Compos Mater 2007;20(6):535–50.

[7] Tungjitpornkull S, Sombatsompop N. Processing technique and fiber orientation angle affecting the mechanical properties of e-glass fiber reinforced wood/PVC composites. J Mater Process Technol 2009;209(6):3079–88.

[8] Farak O, Matuana LM. Nanoclay reinforced HDPE as a matrix for wood plastic composite. Compos Sci Technol 2008;68(9):2073–7.

[9] Farak O, Matuana LM. Reinforcement of rigid PVC/wood flour composite with multi walled carbon nanotubes. J Vinyl Addit Technol 2008;14(2):60–4.

[10] Shi J, Zhang J, Pittman CU, Toghiani H, Xue Y. Preliminary study of the stiffness enhancement of wood–plastic composites using carbon nanofibers. Holz Roh Werkst 2008;66(5):313–22.

[11] Xu Y, Wu Q, Lei Y, Yao F, Zhang Q. Natural fiber reinforced poly (vinyl chloride) composites: effects of fiber type and impact modifier. J Polym Environ 2008;16(4):250–7.

[12] Rizvi GM, Semeralul H. Glass fiber reinforced wood/plastic composites. J Vinyl Addit Technol 2008;14(1):39–42.

[13] Jiang H, Kamdem DP, Bezubic B, Ruede P. Mechanical properties of poly(vinyl chloride)/wood flour/glass fiber hybrid composite. J Vinyl Addit Technol 2003;9(3):138–45.

[14] Mongkollapkit N, Kositchaiyong A, Rosarpitak V, Sombatsompop N. Mechanical and morphological properties of sandwich composites of wood/PVC and glass fiber/PVC layers. J Appl Polym Sci 2010;116(6):3429–36.

[15] Ritchie PA, Thomas DA, Lu L, Connelly GM. External reinforcement of concrete beams using fiber reinforced plastics. ACI Struct J 1991;88(4):224–32.

[16] Spadea G, Bencardino F, Swamy RN. Structural behavior of composite RC beams with externally bonded CFRP. J Compos Constr 1998;2(3):132–7.

[17] Lamanna AJ, Bank LC, Scott DW. Flexural strengthening of reinforced concrete beam using fasteners and fiber-reinforced polymer strips. ACI Struct J 2001;98(3):368–76.

[18] Garden HN, Hallaway LC, Thore AM. The strengthening and deformation behaviour of reinforced concrete beams upgraded using prestressed composite plates. Mater Struct 1998;31(4):247–58.

[19] Park SY. Ultimate strength of precast high-strength concrete beams strengthening in bending with different steel and glued FRP reinforcement ratios. KSCE J Civil Eng 2001;5(4):339–45.

[20] Quantrill RJ, Hollaway LC. The flexural rehabilitation of reinforced concrete beams by the use of prestressed advanced composite plates. Compos Sci Technol 1998;58(8):1259–75.

[21] Akbarzadeh H, Maghsoudi AA. Experimental and analytical investigation of reinforced high strength concrete continuous beams strengthening with fiber reinforced polymer. Mater Design 2010;31(3):1130–47.

[22] Dura M, Lopez-Anido R, Dagher H, Gardner D, O'Neil S, Stephens K. Experimental behavior of hybrid wood plastic composite–FRP structure members for use in sustained loading applications. In: Proc of 8th inter conf on wood plastics composites. Madison, WI; May 23–25, 2005.

[23] Naghipour M, Nematzadeh M, Yahyazadeh Q. Analytical and experimental study on flexural performance of WPC–FRP beams. Constr Build Mater 2011;25(2):829–37.

[24] Erki MA, Rizkalla SH. FRP reinforcement for concrete structures. Concr Int 1993:48–53.

[25] Berg AC, Bank LC, Oliva MG, Russell JS. Construction and cost analysis of an FRP reinforced concrete bridge deck. Constr Build Mater 2006;20(1):515–26.

[26] American Society for Testing and Materials. Standard test methods of static tests of lumber in structural sizes. ASTM D198-09. Philadelphia; 2009.

[27] American Society for Testing and Materials. Standard test methods for flexural properties of unreinforced and reinforced plastics and electrical insulating materials. ASTM D790-07. Philadelphia; 2007.

[28] American Society for Testing and Materials. Standard test methods for tensile, compressive, and flexural creep and creep-rupture of plastics. ASTM D2990-09. Philadelphia; 2009.

[29] Haiar KJ. Performance and design of proto type wood–plastic composite sections. MS thesis. Dept. of Civil and Environmental Engineering Washington State University, Pullman, Wash; 2000.

Effect of Chemical Structure of Thermoplastics on Antibacterial Activity and Physical Diffusion of Triclosan Doped in Vinyl Thermoplastics and Their Composites with CaCO₃

Karn Silapasorn,[1] Kwannate Sombatsompop,[2] Apisit Kositchaiyong,[1] Ekachai Wimolmala,[1] Teerasak Markpin,[1] Narongrit Sombatsompop[1]

[1]*Polymer Processing and Flow (P-PROF) Group, School of Energy, Environment and Materials, King Mongkut's University of Technology Thonburi(KMUTT), Thongkru, Bangkok, 10140, Thailand*
[2]*Department of Civil and Environmental Engineering Technology, College of Industrial Technology, King Mongkut's University of Technology North Bangkok(KMUTNB), Bangkok, 10800, Thailand*

ABSTRACT: Triclosan was used as antibacterial agent in various vinyl thermoplastics and calcium carbonate (CaCO₃)/thermoplastic composites and the antibacterial performances were studied through Halo and Plate-Count-Agar (PCA) test methods. The thermoplastics used were polyethylene (LDPE, MDPE, HDPE), polypropylene (PP), polystyrene (PS) and poly(vinyl chloride) (PVC). *Escherichia coli (E.coli*, ATCC 25922) and *Stapphylococcus aureus (S.aureus*, ATCC 25923) were used as the testing bacteria. The color index results suggested that introducing triclosan did not change the color of all thermoplastics used. The antibacterial results showed that the inhibition zone increased with increasing triclosan for nonpolar thermoplastics like LDPE, MDPE, HDPE, PP, and PS films whereas the opposite effect was observed for polar PVC film. The antibacterial efficacies of the triclosan decreased in the order of LDPE > MDPE > HDPE > PP > PS > PVC and this was confirmed by the triclosan releasing and FT-IR results. The differences in the antibacterial performances of the studied thermoplastics with triclosan were associated with their rigidities, abilities to crystallize, and free volume or molecular density. The sensitivities of *E.coli* and *S.aureus* bacteria to the triclosan were found to be dependent on the testing methods used for the antibacterial performance evaluations. The addition of CaCO₃ worsened the antibacterial performances in the triclosan filled HDPE and PS blends, but had a benefit for improved bacterial reduction in the triclosan-filled PVC blend. © 2011 Wiley Periodicals, Inc. J Appl Polym Sci 121: 253–261, 2011

Key words: additives; thermoplastics; polymer composites; antimicrobials

INTRODUCTION

Because of the increasingly high demands for hygienic thermoplastic products, attention has been extensively placed on active thermoplasticic materials in food packaging applications, the medical professions, and household products. The thermoplastics used for such applications include polyolefin, poly(vinyl chloride), polyamide, and polyurethane and are usually incorporated with antimicrobial agents.[1,2] There are a number of antimicrobial agents available and used, including Carbendazim, 2-Hydroxypropyl-3-Piperazinyl-Quinoline carboxylic acid, Methacrylate, Silver and Silver substituted zeolite, Triclosan, Benzoic acid, Benzoic anhydride, Sorbic acid, Potassium sorbate, Nisin, Lysozyme, Glucose oxidase, Cinnamic Caffeic, nano-Titanium dioxide, *p*-Coumaic acid.[3–10] The efficacies of these antimicrobial agents are dependent on mixing method, contact time, carrier and thermoplastic types, standard testing methods.[5]

A number of scientific research evidences[8–14] have been made on antimicrobial efficacies of polymeric packaging products, mostly considering the effects of polymer matrix selection, type and loading of antibacterial agents, and processing conditions. Pei et al.[8] investigated the releasing of loaded-triclosan on the synthesized hollow TiO₂ nanocapsules using UV-vis absorption technique, and found that the releasing rate of triclosan was rapid in the initial stage then slow down. Zhang et al.[9] used plasma immersion ion implantation (PIII) to modify the surface of medical-grade PVC and then coated with triclosan and bronopol for the enhancing antibacterial properties via plate count agar technique. They

found that the plasma technique produced more hydrophilic functional groups and subsequently, resulted in more effective coating of the triclosan and bronopol on the modified PVC surface. The results showed that the plasma-modified PVC with triclean had more antibacterial efficiency against *E. coli* than that with bronopol. Similar results were found for polyethylene surface-modified by plasma immersion ion implantation.[11] Recent work by Asadinezhad et al.[12] developed a novel surface active antibacterial medical-grade PVC by coating Irgasan as antibacterial agent onto the PVC, which was surface-modified by a multistep physicochemical approach, to impart antimicrobial properties, that was assessed through the agar diffusion test method. They found an improved hydro-philicity on the sample surface and bacteriostatic characteristics of the Irgasan coated samples. Similar approach was used for other antimicrobial agents including bronopol, benzalkonium chloride, and chlorhexidine, which were also coated onto the functionalized PVC samples.[13] Park et al.[14] indicated that thermoplastics synthesized from vinyl monomer derivatives in different forms of phenol and benzoic acid exhibited different bacteria inhibition zones. The polymers with greater glass-transition temperatures tended to show lower antimicrobial performances. Chung et al.[15] suggested that the effect of triclosan in a styrene-acrylate cothermoplastic on diffusion performance using water, ethanol and *n*-hexane as diffusion media. It was found that the efficiency for killing bacteria was dependent on the diffusion ability in the media, and diffusion in the ethanol exhibited the highest antimicrobial efficiency. Camilloto et al.[16] developed antimicrobial extruded PE films containing triclosan at 2000 and 4000 mg kg^{-1} for sliced cooked ham. The PE films efficacies were studied against *Escherichia coli, Staphylococcus aureus, Listeria innocua, Salmonella choleraesuis,* and *Pseudomonas aeruginosa* growth using agar diffusion test. They found that the addition of triclosan did not affect the mechanical properties of the films. Films containing triclosan showed an antimicrobial effect for *E. coli* and *S. aureus* detected by formation of an inhibition halo, but this was not the case for *L. innocua, S. choleraesuis,* and *P. aeruginosa.*

The chemical structures of thermoplastics, which are usually used as packaging products, can be considered as one of the important factors to affect the antimicrobial performance of the thermoplastic products. This involves their polarities and hydrophilic properties,[9] molecular orientations,[7] abilities to crystallize, and the bulk density. Iconomopoulou et al.[7] studied the effect of molecular orientation of uniaxially drawn triclosan doped HDPE flims on controlled release of triclosan using UV-Vis absorption spectroscopy up to 15-month period. They

found that the relevant release rate of triclosan from the drawn specimens was lower than the non-stretched samples due to the molecular orientation developed during the drawing process. Kalyon et al.[17] assessed the antibacterial efficacy of triclosan-incorporated PS disks against *Escherichia coli* and *Bacillus thuringiensis*. The results suggested that triclosan-filled PS inhibited the bacteria growth for some periods, after which bacteria growth resumed and the bulk of the triclosan in the polymer was not available for interaction with bacteria.

Available literatures have shown that the antibacterial performances of triclosan-incorporated thermoplastics have been studied extensively, but most of them have been carried out separately for individual thermoplastics with unfilled thermoplastic systems.[7–17] None of these studies have addressed relationship between triclosan and chemical structure of thermoplastics on the antibacterial activities. Besides, In practical point of view, fillers (reinforcing and extending fillers) are usually required for promoting the physical and mechanical properties, for stabilizing the chemical structures, and for reducing the product costs. But the information on the effect of filler addition on the antibacterial performance of triclosan-doped thermoplastic blend has not been conducted thoroughly. These missing information have, therefore, led to this present work on the effects of chemical or molecular structures of six thermoplastics on the antibacterial performance and physical diffusion mechanism of triclosan/thermoplastic blends with and without calcium carbonate ($CaCO_3$) filler. *Escherichia coli (E.coli*, ATCC 25922) and *Staphylococcus aureus (S.aureus*, ATCC 25923) were used as the testing bacteria.

EXPERIMENTAL

Materials and chemicals

Six thermoplastics used were a low-density polyethylene (LDPE, 1902F, SCG Public, Thailand), a medium-density polyethylene (MDPE, M380RU/RUP, Thai Polyethylene, Thailand), a high-density polyethylene (HDPE, HD6000F, PTT Thermoplastic Marketing, Thailand), a polypropylene (PP-401S, SCG Public, Thailand), a polystyrene (PS, Styron-656D267, Siam Polystyrene, Thailand) and a poly(vinyl chloride) (PVC, SIAMVIC 258RB, V.P.Wood, Thailand). Calcium carbonate ($CaCO_3$, Hicoat-410, Sand and Soil Industry, Thailand) was used as filler to make thermoplastic composites. Triclosan (2,4,4′-trichloro-2′-hydroxlydiphenylether, 24USP, Koventure, Bangkok, Thailand) was used as the antibacterial agent. The specifications, including suppliers, grades, physical and thermal properties and chemical structures, for all thermoplastics and additives used are given

Specifications and Physical and Thermal Properties for Thermoplastics, $CaCO_3$, and Triclosan
(Bulk Density and Hardness Shore D at 25°C)

Materials	Grade	Supplier	Physical and thermal properties	Chemical structure
Low density polyethylene (LDPE)	1902F	SCG public Co., Ltd. (Thailand)	Density 0.919 g cm^3 Hardness = 48 $T_m = 110°C$ $T_g = -110°C$	$\left[CH_2-CH_2 \right]_n$
Medium density polyethylene (MDPE)	M380RU/RUP	Thai polyethylene Co., Ltd. (Thailand)	Density 0.940 g cm^3 Hardness = 52 $T_m = 126°C$ $T_g = -100°C$	$\left[CH_2-CH_2 \right]_n$
High density polyethylene (HDPE)	HD6000F	PTT polymer marketing Co., Ltd. (Thailand)	Density 0.956 g cm^3 Hardness = 55 $T_m = 131°C$ $T_g = -90°C$	$\left[CH_2-CH_2 \right]_n$
Polypropylene (PP)	401S	SCG public Co., Ltd. (Thailand)	Density 0.910 g·cm^3 Hardness = 62 $T_m = 163°C$ $T_g = -20°C$	$\left[CH_2-CH(CH_3) \right]_n$
Polystyrene (PS)	Styron 656D267	Siam polystyrene Co., Ltd. (Thailand)	Density 1.05 g cm^3 Hardness = 83 $T_g = 95°C$	$\left[CH_2-CH(C_6H_5) \right]_n$
Polyvinylchloride (PVC)	SIAMVIC 258RB	V.P. wood Co., Ltd. (Thailand)	Density 1.380 g cm^3 Hardness = 78 $T_g = 82°C$	$\left[CH_2-CH(Cl) \right]_n$
Calcium carbonate ($CaCO_3$)	Hicoat 410	Sand and Soil Industry Co., Ltd. (Thailand)	Average diameter of 1 micrometer	–
Triclosan (2,4,4'-trichloro-2'-hydroxlydiphenylether)	24 USP grade	Goventure Co., Ltd. (Thailand)	White powder from Average size of micrometer $T_m = 56–58°C$ $T_d > 280°C$	

in Table I, the experimental procedures for obtaining the physical and thermal properties being obtained elsewhere.[18] *Escherichia coli* (*E.coli*, ATCC 25922) and *Stapphylococcus aureus* (*S.aureus*, ATCC 25923), as gram negative and gram positive, respectively, were used as the testing bacteria.

Specimen preparation

All triclosan/thermoplastic blend and $CaCO_3$/thermoplastic composite specimens were molded in film test-piece form which was prepared by melt-blending triclosan with thermoplastics using an internal mixer (Haake Rheomix5000, Germany) to obtain a good dispersive blend, before made into the film form by using a compression molding technique. The processing temperatures for LDPE, MDPE, HDPE, PP, PS, and PVC in the compression mold were 160, 170, 180, 210, 150, and 170°C, respectively. The triclosan/thermoplastic blend was placed on a

square mold at the desired mold temperature and then preheated for 10min under a pressure of 100 kg/cm^2 before cooled down to an ambient temperature (30°C) to obtain the resultant film of 0.2 mm thick. The films were made in a circular disc of 6 mm in diameter for the halo test, and in a square piece of 5 × 5 cm^2 for the plate count agar (PCA) method as will be detailed later. The triclosan concentration used was between 0 and 1.5×10^4ppm.

Antibacterial efficacy evaluations

Halo test

Inhibition zone was examined to qualitatively assess the antibacterial efficiency through the growth of bacteria by diffusion of antibacterial agent onto the agar media. In this work, the soft agar technique was introduced to prepare the testing media. The soft agar was performed by mixing nutrient agar and nutrient broth in the bottle at the ratio 50 : 50. After that, the agar

was calibrated at an initial concentration of 10^6 cfu/mL using a UV spectrometer. The prepared soft agar of 5 mL was poured on the solidified nutrient agar as substrate. The triclosan/thermoplastic blend test-pieces were carefully placed over the soft agar at the determined position. Finally, the plates were incubated at 37°C ± 0.5°C for 24 h. The results were reported in terms of "inhibition zone" as given by Eq. (1)[5] where D_C and D_S were diameters of inhibition zone and testing specimen, respectively.

$$\text{Inhibition zone} = \frac{D_C - D_S}{2} \tag{1}$$

Plate count agar method

Plate Count Agar (PCA) is appropriate for quantitative evaluation of bacteria-colony reduction in triclosan incorporated thermoplastic specimens.[5,9] The PCA test followed the ASTM E-2149 (2001) test method. The bacteria were inoculated overnight in 5 mL of nutrient borth (NB) at 37°C. The growing medium for the tested bacteria was peptone solution (prepared by 1 g/L peptone at pH of 6.8–7.2). The initial concentration of bacteria cell in 50 mL of peptone was 10^6 cfu/mL. The required bacteria suspensions were then added by the film specimens and then shaked by a reciprocal shaker at a speed of 100–120 rpm at 37°C ± 0.5°C for a desired contact time. Contact time, defined as the time that the triclosan incorporated thermoplastic specimens were shaken in the peptone solution which contained either *E.coli* or *S.aureus*, used was 60 min throughout this work. Then, a 10-fold serial dilution was conducted for bacteria colony counting. This was done by putting 100 μL of the bacteria solution over the agar in sterilized Petri dishes. Finally, the inoculated plates were kept at 37°C ± 0.5°C overnight before evaluating the antibacterial efficacy. The results were reported in terms of percentage reduction of bacteria-colony via Eq. (2).[9,11]

$$R = \frac{A - B}{A} \times 100 \tag{2}$$

where, R is the percentage reduction of bacteria (%), A is the average number of bacteria colonies from unfilled thermoplastic blend (CFU/mL), and B is the average number of bacteria colonies from triclosan filled thermoplastic blend (CFU/mL).

Materials characterizations

Triclosan releasing study

The releasing rate of triclosan form testing specimens was performed by measuring the UV absorbance of triclosan solution.[7,8] The specimens were put in the flask containing 50 mL of ethanol solution (95% v/v) and then the flask was shaked under the same conditions with shake flask method (37°C, 100 rpm for shaking speed and 1.0 h contact time). After the determined contact time, the ethanol solution was pipetted for 20 mL into cuvet to measure UV absorbance value using UV-Vis spectrophotometer (HACH DR/4000U) at the wavelength of 287–290 nm. The absorbance value was translated in triclosan concentration using a calibration curve (not shown here).

Color change test

The color changes of triclosan-filled thermoplastic were observed using UV-Vis spectrophotometer. The CIE-LAB color system, $L^*a^*b^*$ coordinates, were collected and calculated based on a D65 light source L^* represents the lightness whereas a^* and b^* are the chromatic coordinates. The higher the L^* value the lighter the sample. The a^* coordinate represents red-green coordinate while the b^* coordinate represents yellow-blue coordinate. The total color changes or discolorations of the triclosan/thermoplastic blend test-pieces were calculated from differences in lightness and chromatic coordinates (ΔE) were calculated based on a D65 light source. Eq. 3 was used to express the lightness and chromatic alterations of the test-piece specimens.[19]

$$\Delta E^* = \sqrt{(L_2^* - L_1^*)^2 + (a_2^* - a_1^*)^2 + (b_2^* - b_1^*)^2} \tag{3}$$

RESULTS AND DISCUSSION

Physical appearance of thermoplastic films added with triclosan

This section studied the physical appearances of the vinyl thermoplastic films without triclosan addition, and with 1.5×10^4 ppm triclosan (i.e., maximum dosage). This was achieved by assessing the changes in color and %light transmission, whose results are given in Table II. It can be seen that all the color indices (L^*, a^*, b^*, ΔE) and %light transmission (%T) for the thermoplastic films with and without triclosan were very similar, the differences being within the experimental errors (±2.0%). This suggested that the addition of triclosan had no significant effect on the physical appearances of the thermoplastic films, which appeared to be beneficial in practical point of view. The reason may be because the amount of the triclosan incorporated into the thermoplastics was relatively small (even up to 15,000 ppm triclosan). The unaffected mechanical properties of thermoplastics added with triclosan were also noted by Camilloto et al.[16]

TABLE II
Changes in Color and Light Transmission for Triclosan Incorporated Thermoplastics

Color Index	Thermoplastics with Triclosan ($\times 10^4$ ppm)											
	LDPE		MDPE		HDPE		PP		PS		PVC	
	0	1.5	0	1.5	0	1.5	0	1.5	0	1.5	0	1.5
L^*	37.54	41.3	39.26	39.02	47.77	41.31	34.39	33.84	37.6	37.26	29.68	32.77
a^*	0.06	−0.12	0.14	−0.19	−0.3	−0.76	−0.07	−0.23	−0.09	−0.2	2.68	2.63
b^*	−2.85	−3.79	−2.99	−2.01	−7.01	−1.5	−1.63	−0.31	−1.13	−0.46	2.81	2.88
ΔE^*	–	3.88	–	1.06	–	8.50	–	1.44	–	0.76	–	3.09
%T	88	83.2	86.3	85	78.3	82	89.4	90.1	89.3	88.1	70.9	72.5

Effect of triclosan content on inhibition zone

The halo test was used to qualitatively assess the antibacterial performance of triclosan-filled thermoplastics and the results are given in terms of inhibition zone. Figure 1 shows the effects of triclosan content on inhibition zone for all vinyl thermoplastic films for *E.coli* and *S.aureus* bacteria. The greater inhibition zone only indicated the ability of the triclosan to diffuse from the thermoplastic to react with and kill the bacteria. The results suggested that different thermoplastics had different effects on the inhibition zone. That was, LDPE, MDPE and HDPE and PP films showed relatively higher inhibition zone compared with PS and PVC films. Among the thermoplastics used, it was observed that at the lowest triclosan concentration (5000 ppm), the inhibition zone for PS was the smallest. Work by Kalyon et al.[17] suggested that the triclosan-filled PS could inhibit the bacteria growth (*E.coli* and *B.thuringiensis*) *only* for a short period of time because triclosan could not effectively diffuse through the PS to kill the bacteria.

In this work, three possible explanations for the differences in inhibition zones for all thermoplastics

used were proposed, these including (i) rigidities of the thermoplastics, (ii) abilities to crystallize, (iii) free volume or molecular density. First, based on their glass transition temperatures and hardness results as given in Table I, the rigidities of the thermoplastics decreased in the order of PVC > PS > PP > HDPE > MDPE > LDPE. It was reasonable to state that it was more difficult for triclosan to diffuse through the thermoplastics with higher rigidities (like PS and PVC). Such claim could be substantiated by Park et al.[14] who suggested that, the polymers with greater glass-transition temperatures yielded lower antimicrobial activities. This was why relatively low inhibition zone was observed for more rigid thermoplastics like PS and PVC. Second, triclosan seemed to diffuse better in the crystalline thermoplastics (HDPE, MDPE, LDPE, and PP) compared to the amorphous thermoplastics (PS and PVC). It was thought that the triclosan could interact better with PS due to the benzene groups in PS and triclosan, and polarities of PVC and triclosan molecules. These interactions could probably cause difficulty for triclosan to diffuse away from the PS and PVC films to kill the bacteria, thus less inhibition zone being observed. Finally, the differences in inhibition zones among LDPE, MDPE,
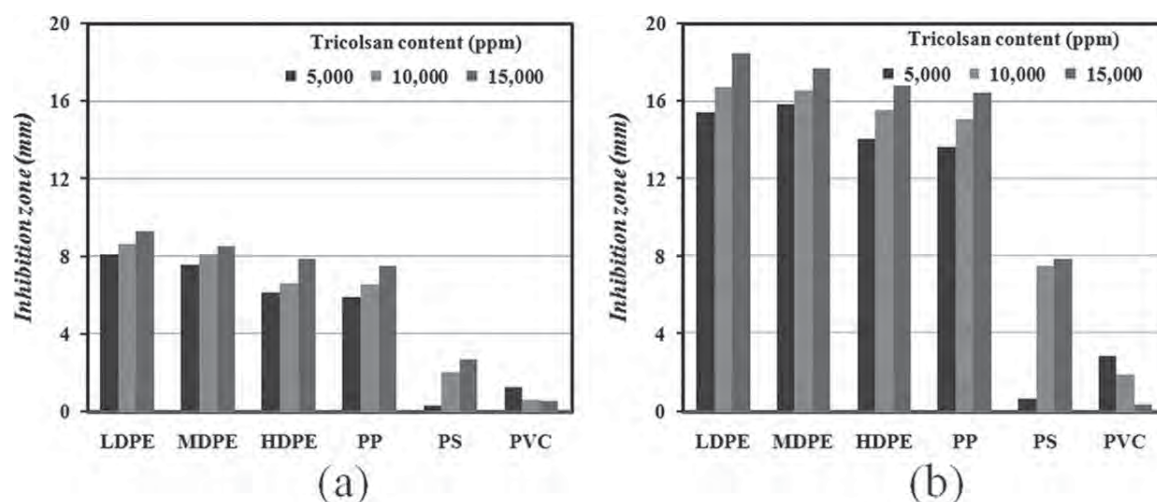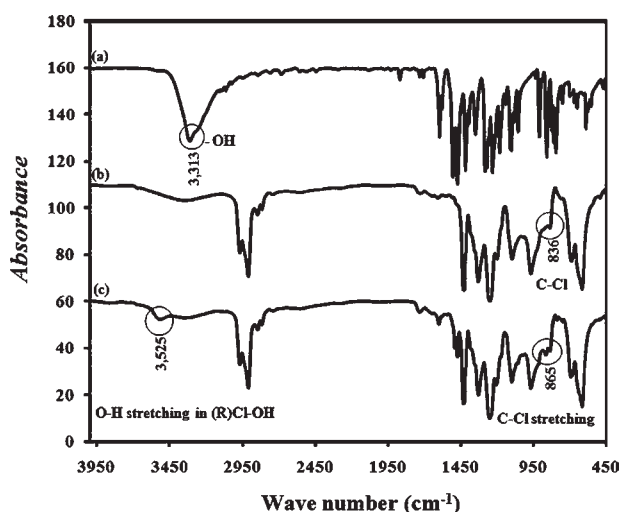

Figure 1 Inhibition zone results from Halo test for different thermoplastic film specimens for different loadings of triclosan (a) *E.coli* and (b) *S.aureus*.

Figure 2 FT-IR spectra (a) Triclosan (b) PVC and (c) PVC containing 15,000 ppm triclosan.

HDPE, and PP were explained by differences in free volume or molecular orientations. That was, the greater the free volume the higher the triclosan to diffuse or release. This suggested why the LDPE had the greatest inhibition zone. This explanation could be linked and supported with the work by Iconomopoulou et al.[7] who investigated the effect of molecular orientation of uniaxially drawn triclosan doped HDPE films on controlled diffusion rate of triclosan. They found that the triclosan diffusion rate for the drawn specimens was lower than the nonstretched samples.

Considering the effect of triclosan content on the inhibition zone, one may expect that increasing triclosan loading would result in an increase in inhibition zone. This was not always true according to the results obtained in this work. The inhibition zone increased with increasing triclosan content for the nonpolar thermoplastics (LDPE, MDPE and HDPE, PP and PS) whereas the opposite effect was observed for the polar PVC. The decreases in inhibition zone as a result of increasing triclosan content in PVC could be explained through chemical and physical interactions between triclosan and PVC molecules as described here;

- Chemical interaction: This involved a polar-polar interaction between the PVC and triclosan molecules. An evidence to support such interaction was given using Fourier Transform Infrared (FT-IR) analysis [FTIR Spectrometer Spectrum One, Perkin–Elmer, with resolution of 4 cm^{-1} and scanning between 400 and 4000 cm^{-1}]. The FT-IR analysis was performed for pure triclosan, neat PVC, and triclosan/PVC blend and the results are given in Figure 2. The polar–polar interaction between triclosan and PVC could be evidenced by two shifted peaks, O—H stretching at 3525 cm^{-1} of R(Cl)—OH in triclosan/PVC blend, and C—Cl stretching at 865 cm^{-1} of PVC in the triclosan/PVC blend. However, the shifting of the peaks was not pronounced as one would expect, due to the small amount of the triclosan added into the PVC. This observation was similar to the work by Zhang et al.[9] who worked on the antibacterial properties of bronopol- and triclosan-coated PVC.
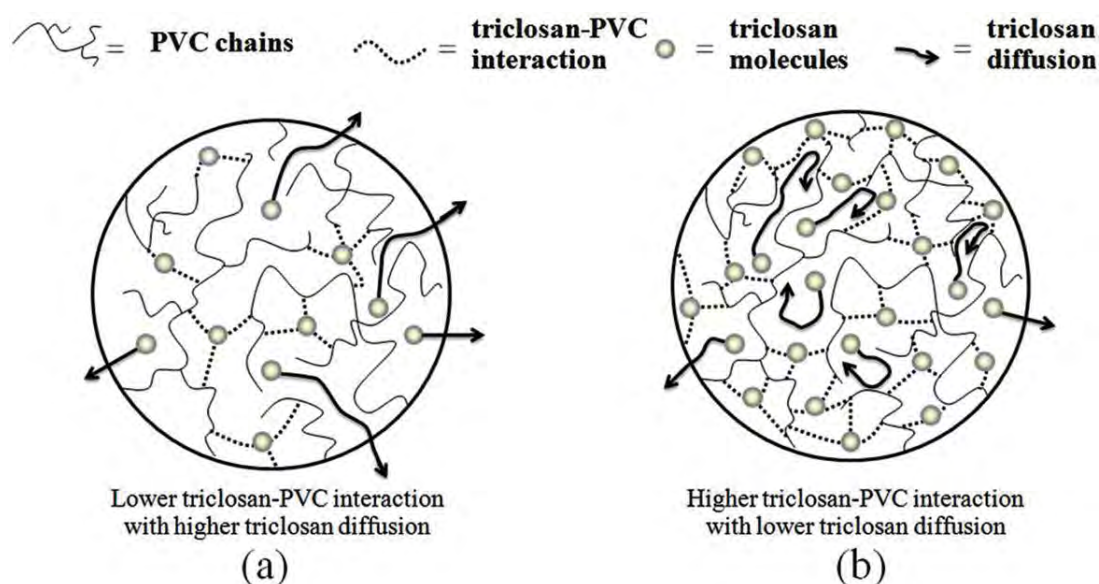
Figure 3 A proposed schematic model for diffusions mechanism of triclosan molecules in PVC (a) low triclosan concentration (b) high triclosan concentration. [Color figure can be viewed in the online issue, which is available at wileyonlinelibrary.com.]
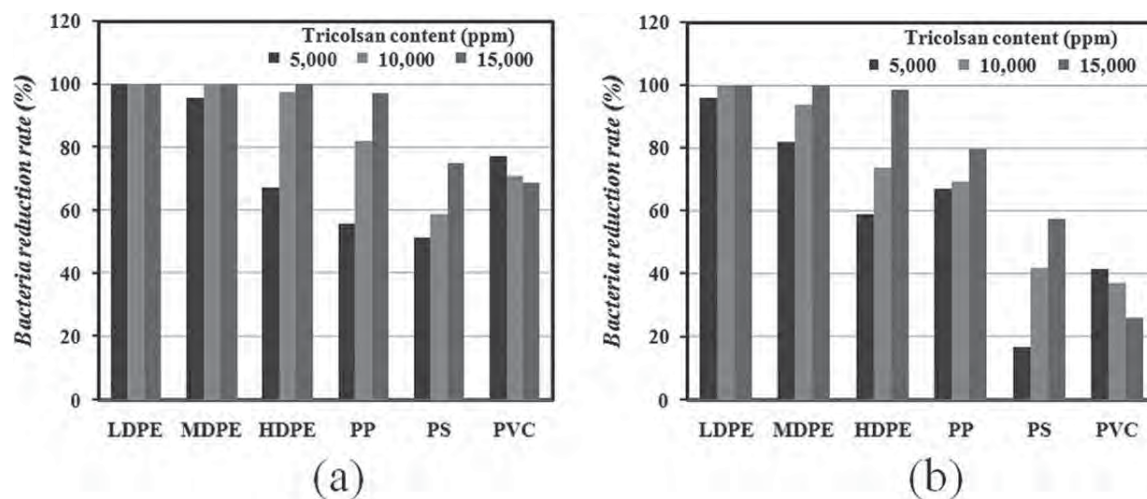
Figure 4 Percentage reduction rates for different thermoplastics at various triclosan contents by PCA method (a) *E.coli* and (b) *S.aureus*.

• Physical interaction: This can be referred to as diffusion of triclosan through the PVC matrix at different triclosan loadings. The results in Figure 1 suggested that the diffusion rate of triclosan was likely to differ with triclosan content. The explanation for this is schematically given in Figure 3, showing differences of triclosan diffusion-away within the triclosan/PVC blends with low and high triclosan contents. It was believed that the blend with high triclosan content was expected to have higher polar–polar interaction between PVC and triclosan molecules and this would probably retard further diffusions of triclosan to kill the bactetia at the sample surface. This was why the inhibition zone of PVC with higher triclosan content was lower than that with lower triclosan content.

The results in Figure 1 also indicate that the effects of triclosan loading and type of thermoplastics had a similar trend for both *E.coli* and *S.aureus* bacteria. But, for any given triclosan contents and types of thermoplastics, *S.aureus* appeared to be more sensitive to the triclosan loading than *E.coli*, considering the level of the inhibition zone.
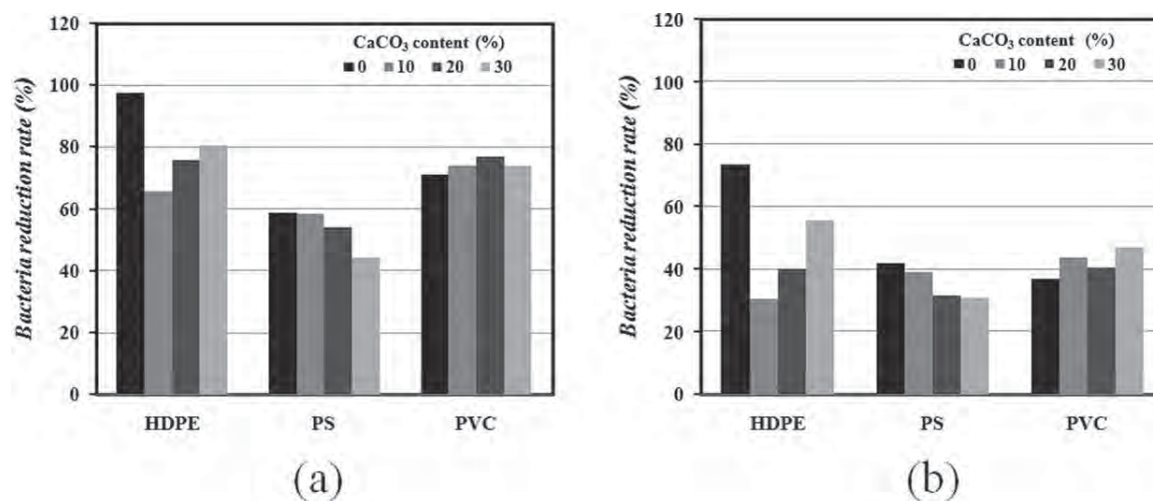
Effect of triclosan content on percentage reduction of bacteria

Figure 4 shows the percentage reductions of *E.coli* and *S.aureus* for different vinyl thermoplastics for different triclosan loadings. It can be seen that the changing trends of the PCA results in Figure 4 for all thermoplastics corresponded well with those of the inhibition zone results in Figure 1. That was, the triclosan exhibited a most effective antibacterial agent for nonpolar polymers with high free volume

structure (LDPE). The results and explanations for the triclosan diffusion in the different thermoplastics were substantiated by the triclosan releasing rate results as given in Table III. Higher triclosan releasing rate directly indicates higher triclosan diffusion and greater antibacterial efficacy. The results in Table III clearly suggest that relatively greater triclosan releasing rates were noted for nonpolar thermoplastics, the most pronounced effect being observed for the LDPE (32.6 to 100.2×10^{-5} g). However, a slight decrease of triclosan releasing rate with changing triclosan contents was observed for PVC matrix. It was worth mentioning that the magnitude changes in the results of inhibition zone in Figure 1, reduction rate of bacteria in Figure 4 and the triclosan releasing rate in Table III were different for all thermoplastics with various triclosan contents, although their changing trends of the results were similar. This may be expected since these three test-results were performed in different environments; i.e., the inhibition zone carried out in the soft agar, the %reduction rate performed in peptone solution, and the triclosan releasing result obtained via ethanol solution. Work by Chung et al.[15] found that the efficiency for killing bacteria was dependent on the diffusion ability in

TABLE III
Triclosan Releasing Rate Results for Thermoplastic Films with Different Triclosan Loadings after 1.0-h Contact Time in Ethanol Solution

Triclosan content (ppm)	Triclosan releasing rate ($\times 10^{-5}$ g)					
	LDPE	MDPE	HDPE	PP	PS	PVC
5,000	32.6	20.4	10.2	8.7	8.0	9.5
10,000	85.2	24.2	13.7	9.4	8.0	8.4
15,000	100.2	29.5	14.2	9.8	8.3	8.1

Figure 5 Effect of CaCO$_3$ content on percentage reduction rate for HDPE, PS, and PVC film specimens with 10,000 ppm triclosan content. (a) *E.coli* and (b) *S.aureus*.

the media. In the comparison of Figures 1 and 4 and Table III, it was found that even low triclosan releasing rates of MDPE, HDPE, and PP could result in high level of percentage reduction of the *E.coli* and *S.aureus* (up to 50–99% bacteria reduction).

Considering the triclosan sensitivities by *E.coli* and *S.aureus* bacteria in Halo test (Fig. 1) and PCA method (Fig. 4), it was surprising that the PCA method indicated higher triclosan sensitivity for the *E.coli* while the opposite effect was found for the Halo test. This difference was probably due to the fact that the *E.coli* in general have higher growth rate as compared to the *S.aureus*. Besides, in PCA method which was performed in peptone solution, the bacteria had made contacts very thoroughly with triclosan. The newly grown *E.coli* during the shaking in peptone was probably weak, and was easily killed by the triclosan as compared to the *S.aureus* which have lower growth rate. This was the reason of why the %reduction rate of the *E.coli* by triclosan was higher than that of the *S.aureus* in the PCA method. This finding was in good agreement with Zhang et al.[11]

Effect of CaCO$_3$ incorporation

In this section, three vinyl thermoplastics, namely HDPE, PS, and PVC, with 10,000 ppm triclosan content were selected based on their differences in abilities to crystalize and polarities, and the PCA method was used for antibacterial performance evaluations. Figure 5 shows the effect of CaCO$_3$ content on percentage reduction for *E.coli* and *S.aureus* for triclosan-HDPE, -PS, and -PVC blends. The %reduction rates of bacteria for triclosan-HDPE and -PS films appeared to reduce with CaCO$_3$ loading as compared with the films without CaCO$_3$. It was

probably because the presence of CaCO$_3$ resulted in increases in rigidity and hardness of the thermoplastics,[20] and then this led to difficulty in the diffusion of the triclosan through the triclosan-HDPE and -PS films. It should be noted that the differences in the bacteria reduction rates as a function of CaCO$_3$ loading for each thermoplastic with triclosan were dependent on dispersion level of CaCO$_3$ which may be associated with CaCO$_3$-thermoplastic[20] and triclosan-CaCO$_3$ interactions, which is beyond the scope of this work, but to be explored for our future works.

In the case of the PVC film, the addition of CaCO$_3$ was found to improve the %bacteria reduction. This could be associated with an interfering effect of the polar–polar interaction between the PVC and the triclosan by presence of CaCO$_3$ filler. In connection with the proposed schematic model in Figure 3, if the polar–polar interaction of PVC and triclosan was interfered and reduced, the diffusion rate of triclosan through the PVC should probably be facilitated. As a consequence, the %bacteria reduction for the triclosan/PVC blend would be improved. The results were in a similar trend for both *E.coli* and *S.aureus* bacteria.

CONCLUSIONS

Triclosan was proposed to be suitable for nonpolar thermoplastics with high free volume structure. The effectiveness of the triclosan added in the vinyl thermoplastics decreased in the order of LDPE > MDPE > HDPE > PP > PS > PVC. The rigidities, abilities to crystallize, and free volume and molecular density were proposed to be responsible for the differences in the antibacterial performances among the thermoplastics used. The addition of triclosan did not change

the physical appearances of all the thermoplastics. The results showed that the antibacterial performance was improved with increasing triclosan content for nonpolar LDPE, MDPE, HDPE, PP, and PS films, but worsened for polar PVC. The addition of CaCO$_3$ slowed down the %reduction rates of *E.coli* and *S.aureus* in the triclosan-filled HDPE and PS blends, but enhanced the bacteria reduction rate for the triclosan filled PVC blend. Triclosan had similar effect on the inhibitions of *E.coli* and *S.aureus* bacteria for any given thermoplastics and thermoplastic composites with CaCO$_3$, but their sensitivities to the added triclosan were dependent on the test methods used.

References

1. Niall, A. Plast Addit Compound 2001, 3, 12.
2. Holme, M. Addit Polym 2006, 6, 11.
3. Jiang, G.; Zeng, J. J Appl Polym Sci 2010, 116, 779.
4. Quintavalla, S.; Vacini, L. Meat Sci 2002, 62, 373.
5. Chammanee, P.; Sombatsompop, K.; Kositchaiyong, A.; Sombatsompop, N. J Macromol Sci Phys 2009, 48, 755.
6. Lee, H. J.; Jeong, S. H. Text Res J 2005, 75, 551.
7. Iconomopoulou, S. M.; Voyiatzis, G. A. J Control Release 2005, 103, 451.
8. Pei, A. H.; Shen, Z. W.; Yang, G. S. Mater Lett 2007, 61, 2757.
9. Zhang, W.; Chu, P. K.; Ji, J.; Zhang, Y.; Liu, X.; Fu, R. K. Y.; Ha, P. C. T.; Yan, Q. Biomaterials 2006, 27, 44.
10. Joerger, R. D. Pack Technol Sci 2007, 20, 231.
11. Zhang, W.; Chu, P. K.; Ji, J.; Zhang, Y.; Fu, R. K. Y.; Yan, Q. Polymer 2006, 47, 931.
12. Asadinezhad, A.; Novak, I.; Lehocký, M.; Sedlarik, V.; Vesel, A.; Junkar, I.; Saha, P.; Chodak, I. Plasma Process Polym 2010, 7, 504.
13. Asadinezhad, A.; Novak, I.; Lehocký, M.; Sedlarik, V.; Vesel, A.; Junkar, I.; Saha, P.; Chodak, I. Colloid Surface B 2010, 77, 246.
14. Park, E. S.; Moon, W. S.; Song, M. J.; Kim, M. N.; Chung, K. H.; Yoon, J. S. Intl J Biodeter Biodegrad 2001, 47, 209.
15. Chung, D.; Papadakis, S. E.; Yam, K. L. Intl J Food Sci Technol 2003, 38, 165.
16. Camilloto, G. P.; Soares, N. D. F. F.; Pires, A. C. D. S.; Paula, F. S. D. Pack Tech Sci 2009, 22, 471.
17. Kalyon, B. D.; Olgun, U. Am J Infect Control 2001, 29, 124.
18. Miichaeli, W.; Greif, H.; Wolters, L.; Vosseburger, F.-J. Training in Plastics Technology; Hanser Publishers: Munich, 1998.
19. Xiang, X.; Chen, S.; Zhang, J.; Chai, R. J Vinyl Addit Technol 2010, 16, 23.
20. Chaochanchaikul, K.; Kositchaiyong, A.; Sombatsompop, N. Polym Polym Compos 2009, 17, 281.

A Die Rotating System for Moderations of Extrusion Load and Pressure Drop Profiles for Molten PP and Wood/ Polypropylene Composites in Extrusion Processes

Naret Intawong,[1] Chatchawan Kantala,[2] Watit Lotaisong,[2] Narongrit Sombatsompop[2]

[1]*Department of Industrial Engineering, Faculty of Engineering, Rajamangala University of Technology Lanna, (RMUTL), Chiang Mai, 50300, Thailand*
[2]*Polymer Processing and Flow (P-PROF) Group, School of Energy, Environment and Materials, King Mongkut's University of Technology Thonburi (KMUTT), Thongkru, Bangmod, Bangkok 10140, Thailand*

ABSTRACT: A die-rotating system was proposed in this work for moderations of extrusion forces and entrance pressure drop for molten polypropylene (PP) and wood/ polypropylene (WPP) composites in a capillary rheometer and a single screw extruder. The effects of processing conditions and wood loading in PP were of our interests. The extrusion force and entrance pressure drop with and without the die rotating system were monitored in real-time. This was the first time that the die-rotating system was used for processing of highly viscous wood/polymer composite materials. It was found that the flow properties of the molten PP and WPP composites obeyed pseudoplastic non-Newtonian behavior. The behavior was more obvious at wood contents of above 6 wt % and in the capillary rheometer. The rotation of the die could moderate the extrusion load by 60% and entrance pressure drop by 20% in the capillary rheometer, and the entrance pressure drop by 30% in the single screw extruder, especially at the conditions where the viscosities of the WPP and the extrusion rate were high. Greater fluctuations in entrance pressure drop caused by die rotation were observed in the single screw extruder. © 2010 Wiley Periodicals, Inc. J Appl Polym Sci 120: 1006–1016, 2011

Key words: wood polymer composites; extrusion; polypropylene; processing

INTRODUCTION

Wood polymer composites (WPCs) have attracted scientists and engineers because of their cost savings, good mechanical properties, better dimension stability, environmentally friendly products and low density, as compared with synthetic fibers/plastic composites. The applications for WPC products are limited to decorative or nonstructural applications which include decking, exterior window and door profiles, automobile paneling, panel inserts, and flower pots, due to the limitations in their mechanical properties as compared with solid or natural woods. Recently, a number of methods have been proposed to make use of WPC materials for structural and engineering properties, these including chemical and physical surface treatments,[1–3] additions of synthetic fibers[4,5] and nano-particles,[6] selections of appropriate processing techniques[7–10] and design of product-shaping components.[11] De Albuquerque et al.[1] found greater mechanical properties of jute roving reinforced polyester composites could be obtained by an improved adhesion and mechanical locking between the treated-fiber and the polyester matrix using NaOH treatment. Sombatsompop et al.[2] suggested that the 2% MAH-*g*-PP agent with 11% impact modifier was sufficient for improving the overall mechanical properties of the composites while Me'ndez et al.[3] claimed that the MAPP coupling agent of 6% would be required for improving the wood and PP adhesion. Tungjitpornkull et al.[4] found that at low glass fiber contents (10–20%) the concentration of carbonyl groups to form chemical interaction with WPVC composites was important whereas the effect of final length of glass fiber after final processing became the dominant factor at high glass fiber loading (30%). A considerable improvement in tensile properties of wood/HDPE could be obtained by introducing 5 wt % glass fiber[5] or by incorporating nanoclay[6] into the wood/HDPE composites.

Processing techniques and their processing variables have significant effects on the properties of natural fiber/polymer composites. Liu et al.[7] measured

the impact strength of kenaf fiber reinforced soy-based bio-composites using different manufacturing processes, and found that the compression molding could produce the composites with higher impact strength. The results were in line with those of Tungjitpornkul et al.[4] Practical views for reducing the void volume using small wood particles, and high compaction pressure were presented by Wol-cott and Englund.[8] Xu et al.[9] studied life cycle assessment of PP and wood/PP using a compression molding technique, and also demonstrated a term called "material service density," defined as the volume of material satisfying a specific strength requirement. Migneault et al.[10] examined the effect of processing method on mechanical properties of three chemi-thermomechanical pulp (CTMP)/HDPE composites. They found that the physical and mechanical properties of the composites from injection molding process was better than those from extrusion process due to better fiber orientation and less fiber breakage were obtained from the injection molding process. Most recent work by Sombatsom-pop et al.[11,12] studied flexural, creep and fatigue properties of wood/PVC composite beams under a wide rage of die designs and testing conditions. Profile dies with low number of hollow cores with thick flanges and webs were recommended for the composites with higher mechanical properties.

The engineers and scientists have realized that, during processing the addition of wood particles or wood fibers into polymer materials causes a considerable increase in composite melt viscosity, especially when introducing secondary synthetic glass fiber and other property promoting agents. These will then make the processing become much more difficult as a result of high pressure drop built up during processing. This would eventually lead to a number of flow instabilities and finally physical distortions of WPC final products. Such behavior was supported by Maiti et al.[13] who investigated the melt rheological behavior of wood/isotactic polypropylene (i-PP/WF), and found that the apparent melt viscosity increased about 70% with increasing wood content. There have been a few attempts to ease the processabilities of metallic and nonmetallic materials in extrusion processes through the die design. Rawal and Davies[14] used a rotating square die to produce polyethylene net structure from an extrusion process, and found that the shape of the extruded PE filament using the rotating die deviated from its corresponding die at the die exit. Ma et al.[15,16] experimentally and theoretically investigated a forward extrusion of pure lead using rotating conical dies, and suggested that the extrusion load was reduced by die rotation. The molten lead exhibited a twisted flow at a finite distance from the punch, and the twisting level became larger and deeper by increas-ing the die rotating speed. Such works were further developed for the effects of steady and cyclic die rotations on the compression of aluminum.[17] A rotating die system was previously proposed by Intawong et al.[18] for studying the rheological properties, flow patterns, and extrudate swell of natural rubber (NR) compound in a capillary rheometer and found that the rotating die extrusion could reduce the extrusion load and finally resulted in decreases in NR extrudate swelling.

Recent literatures have indicated that methods to ease the process-abilities of wood/polymer composites are very rare and still open for wide discussion. This is because most studies have focused on mechanical, thermal, and morphological properties of the WPC composites whereas very few works have investigated the flow properties of wood/polymer composites, probably due to difficulties in viscosity control, limits of processing window, and incompatibilities of the wood and thermoplastic composites. Overcoming these processing problems, therefore, became our interests. In this work, a constant-rate capillary rheometer coupled with an in-house-developed rotating-die system, as similar to that proposed in our previous work,[18] was constructed and used to measure the viscous behavior in terms of applied forces, entrance pressure drop for highly viscous wood/polypropylene composite (WPP) melts. The study covered the effects of wood content, shear rate or volumetric flow rate, and die rotation speed. The extrusion processes used in this work were a constant-rate capillary rheometer and a single screw extruder, the differences in the experimental results obtained by these two extrusion processes being compared and discussed. The explanations for the differences in the flow behavior and changes in the extrusion load and die entrance pressure drop for molten PP and WPP composites due to die rotating effect were given in connection with flow visualization of molten PP developed in the rotating die, which was achieved through use of a color banding technique. It was hoped that die rotating technique proposed in this work could widen the processing window and reduce the composite viscosity for facilitating the processing of the WPC materials.

EXPERIMENTAL

Raw materials

1. Low molecular weight of polypropylene (PP Grade 1100NK) in granule form with a melt flow rate (MFR) of 9.8 was used and supplied by IRPC Public Co., Ltd (Bangkok Thailand).
2. Wood particles used in this work was obtained from carpentry and wood-working processes

and supplied by V.P. Wood Co., Ltd. (Bangkok Thailand) and had the average size of 250 μm. Wood particles must be dried to a constant weight. The maximum moisture content allowed was less than 5%, this being achieved using an oven at 80°C.[19] It should also be noted that it was not necessary to incorporate a coupling agent for wood treatment in this work since the chemical reaction between the coupling agent and the polymer dynamically changed during the extrusion (molten state). In addition, based on previous work by Sombatsompop and Chao-chanchaikul,[20] the changes in rheological properties due to the addition of silane coupling agents were relatively small (less than 10%) as compared with those in mechanical properties of wood/thermoplastic composites.

Preparation of WPP composites

The dried wood particles were then dry-blended with the PP using a high speed mixer before melt-blending in a twin-screw extruder (Haake Polylab-Rheomex CTW100P, Germany). The wood content used was varied from 0 to 30% weight (wt %) of the PP, depending on the type of extrusion process used. The blending temperature profiles on the twin-screw extruder were 160, 170, 180, and 190°C from hopper to die zones and a screw rotating speed used was 50 rpm. A three-strand die having a diameter of 3 mm for each strand coupled with a palletizing unit was used to produce the WPP composite pellets, and then held in an oven for 24 h at 80°C for redrying the WPP composites ready for further flow property measurements in a capillary rheometer and a single screw extruder. This experimental procedure was to ensure that the starting mixing qualities of the WPP in the rheometer and the single screw extruder were very similar.

Extrusion processes for PP and WPP composites

In this work, the molten neat PP and WPP composites were processed using two different extrusion processes which included a capillary rheometer and a single screw extruder, and their flow properties were evaluated during the extrusions. In the capillary rheometer the PP and WPP composite melt was left about 20 min in the barrel until the melt temperature across the barrel diameter (40 mm) was uniform before starting the flow. But, the PP and WPP composite melts in the single screw extruder were produced and extruded through the die continuously, the temperature of the melts being nonuniform at the starting point of extrusion and during the flow.
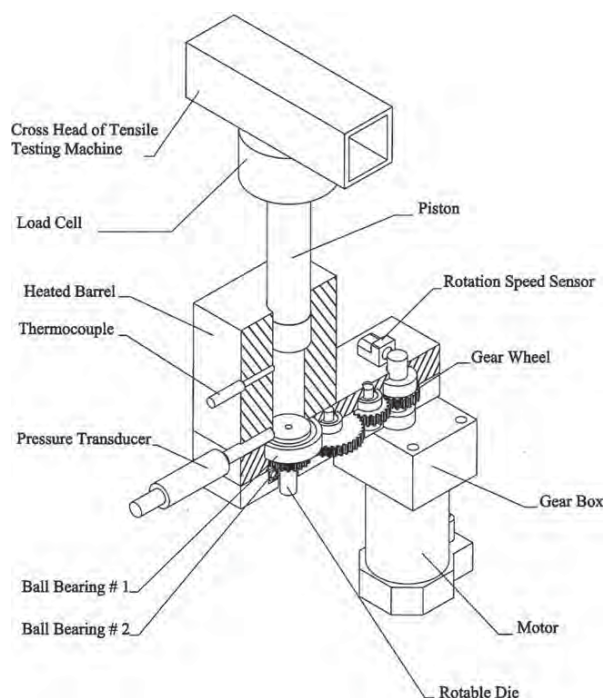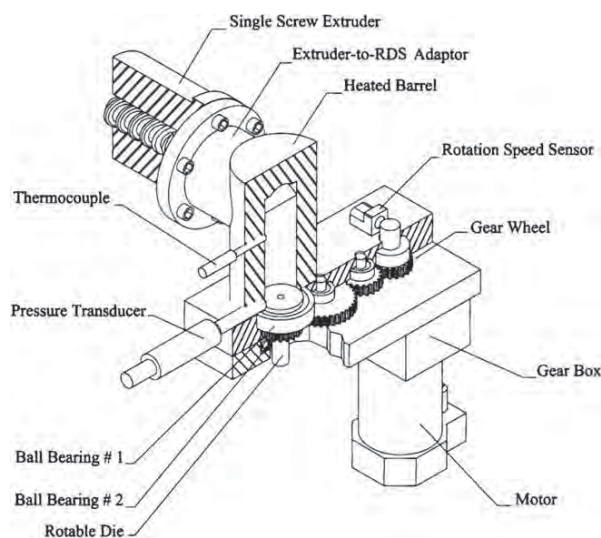
Figure 1 An experimental arrangement for flow property measurements of PP and WPP composite melts in a capillary rheometer.

Capillary rheometer

Figure 1 shows an experimental arrangement for flow property measurements of PP and WPP composite melts in an in-house-designed piston driven capillary rheometer coupled with a rotating die system. This experimental apparatus was a modification from that proposed in our previous work.[18] Thus, a brief description of the experimental rig was given. The barrel size of the rheometer used was 40 mm in diameter and 150 mm in length. A large circular die with 5 mm in diameter and 65 mm in length was located at the bottom of the barrel. The Ball Bearing#1 was to keep the alignment of the die during the rotation, and to lessen the friction of the die radius. Ball Bearing#2 at the bottom of the die base was used to lessen the friction on the axis which was in the same direction with piston movement. Four gear wheels were connected to the bottom part of the die base to transfer power from DC motor source to rotate the die system in the barrel. The rotation speed of the die can be adjusted in the range of 0–70 rpm which was measured using a speed sensor installed on the driving axis of the motor. This gear wheel set had a speed ration of 1/1; hence, the die rotation speed was the same as the speed of the motor axis. The barrel and die temperatures used in this work were 190°C. The piston speed was varied to obtain a wide range of shear rates. The apparent shear rates were calculated

Figure 2 An experimental arrangement for flow property measurements of PP and WPP composite melts in a single screw extruder.

based on the information of piston speed used and the known barrel diameter. The apparatus temperature was controlled using a DD6 temperature controller. The entrance pressure drop was measured using a pressure sensor (Dynisco, Model PT460E-2CB-6, Franklin, MA) which was situated at the base of the barrel just above the die face.

Single screw extruder

The rotating die equipment as described in the capillary rheometer was used and connected at the end of a single screw extruder using a specially-constructed adaptor (RMUTL SE001 MUSHIKING Poly-Lab supplied by RMUTL, Chiang Mai, Thailand) shown in Figure 2. The exact length-to-diameter (L/D) ratio of the barrel was 600/25 mm/mm, and the temperature profiles on the extruder were 170, 180, 190, and 190°C from hopper to die zones, and the screw rotating speed was varied to obtain a wide range of shear rates in the experiment. It should be noted that the temperature profiles along the barrel length for screw extrusion process are usually non-uniform, but tended to be given for melting and homogenizing the PP and WPP materials without degradation. The temperature reported in this work was "die temperature" which was carefully controlled by DD6 temperature controller, and the die temperatures in the capillary rheometer and the screw extruder are equal (190°C) for result comparison. The entrance pressure drop was measured using a pressure sensor (Dynisco, Model PT460E-2CB-6, Franklin, MA) which was situated at the base of the barrel just above the die face.

## Measurements of flow properties of PP and WPP composites

The flow properties of the PP and WPP composite melts were evaluated during extrusion from the barrel through the rotating die both in the capillary rheometer and the single screw extruder. In the capillary rheometer, the prepared PP and WPP were fed into the barrel and left about 20 min until the melt had a uniform temperature before the piston started to push the polymer down the barrel. The extrusion force exerted at the piston during the flow and the entrance pressure drop were then measured and recorded in real time (or piston displacement) using a high speed data-logging system having a scanning speed of 20 data/s. The piston speed and the barrel diameter were used for the apparent shear rate calculations, and the pressure drop at the die entrance was measured for the shear stress calculations.[18] In the screw extruder, the apparent shear rates were varied by varying screw rotation speeds and calculated based on the mass flow rate and melt density of the melt extruded from the die. Therefore, only entrance pressure drop as a function of extrusion time was of interest. It should be noted that Bagley's and Rabinowitsch corrections were not applied to the shear stress and shear rate data generated in this work due to two reasons. First, the shear stress and shear rate data were used solely for comparative reasons to illustrate the magnitude of the changes observed in the flow characteristics of the materials as a function of the die rotating speed and the wood content. Second, the die dimensions used were constant throughout this work which implies that the Bagley's corrections could be neglected in this case.

In both extrusion processes, the shear rates and the shear stress values were used to establish flow curves which were used to identify the flow behavior of the PP and WPP composites. Apart from the flow curves, the main experimental results reported in this work were the extrusion force and entrance pressure drop profiles during the real time extrusion by varying die rotating speeds from 0 to 70 rpm. It should also be noted that the PP and WPP composite melts extruded from the rotating die in this work did not experience any sharkskin, fractures or distortion, or oscillation at the die exit. This was because the large die size (low shear rate range) was used for appropriate range of die rotating speeds after a number of trial and error tests.

RESULTS AND DISCUSSION

Capillary rheometer

Figure 3 shows the extrusion force changes and Figure 4 shows the entrance pressure drop profiles as a function of extrusion time and die rotating speed for neat PP and WPP (WPP) composite melts at various
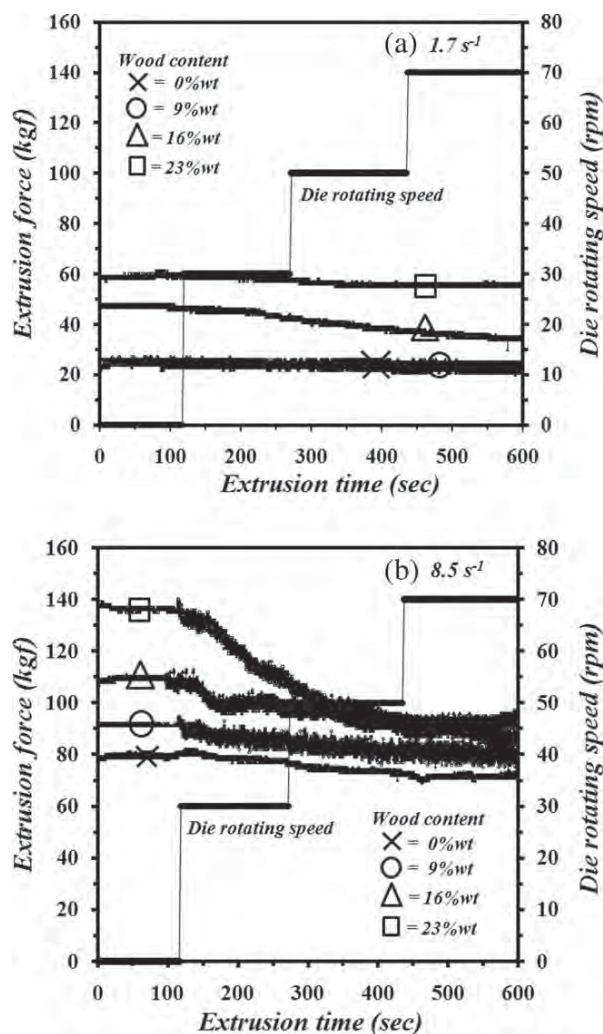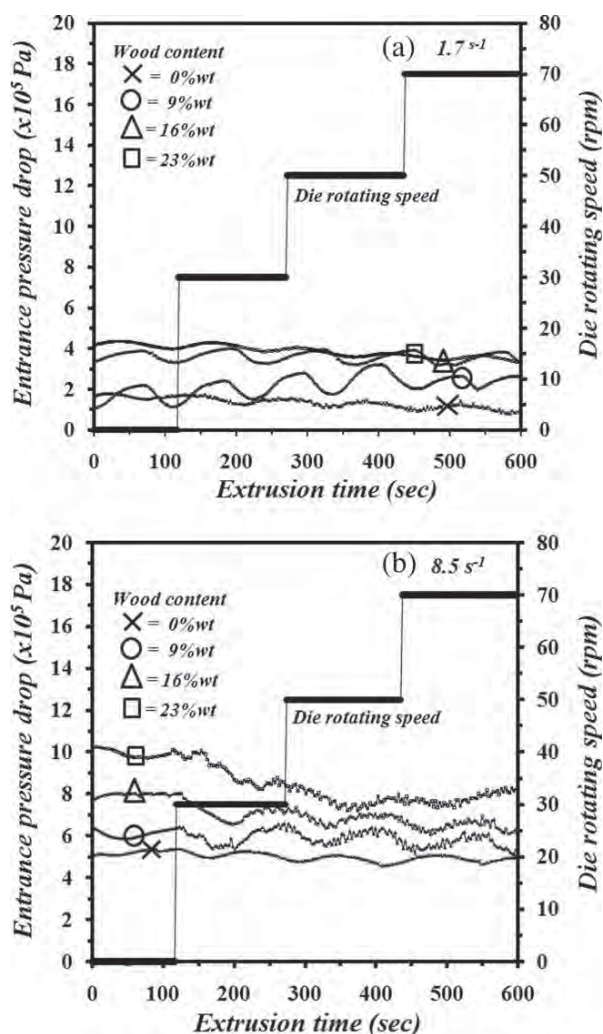
Figure 3 Extrusion force VS time for WPP composite melts for different wood contents. (a) 1.7 s^{-1} (b) 8.5 s^{-1}.

increasing die rotating speed from 0 to 70 rpm. This behavior was similar to the work by Ma et al.[15,16] who found the extrusion load reduction of pure lead by using rotating conical dies. The fluctuations in the entrance pressure drop during the measurements were probably caused by the flow of the composite melt which was continuously developing in the barrel as the piston moved down the barrel. The decreasing effects of the extrusion force and entrance pressure drop of the PP and its composites due to increasing die rotating speed were much more significant at the higher wood contents. This was because the addition of wood particles into PP would result in an increase in bulk viscosity of the composite melts, and this could generate more shearing stresses during the flow by the action of die rotation.

The viscosity changes due to the addition of wood particles could be substantiated by the results of

wood contents at apparent shear rates of 1.7 [Figs. 3(a) and 4(a)] and 8.5 s^{-1} [Figs. 3(b) and 4(b)]. All the data were recorded in real time using a high speed data logger. It should be noted that the shear rates used in this work were relative low due to the large diameter of the die used. Therefore, the recorded extrusion force and entrance pressure drop were relatively low. The extrusion force and entrance pressure drop were measured while the die rotation speed was increased in a stepladder manner. It was observed for low apparent shear rate (1.7 s^{-1}) that the extrusion force [Fig. 3(a)] and entrance pressure drop [Fig. 4(a)] did not change with increasing die rotating speed. However, at higher apparent shear rate (8.5 s^{-1}) the extrusion forces decreased from 140 to 90 kgf (by ∼ 60% reduction) for 23 wt % wood content used, and the entrance pressure dropped from 10 × 10^5 to 8 × 10^5 Pa (by 20% reduction) for 23 wt % wood content used by

Figure 4 Entrance pressure drop VS time for WPP composite melts for different wood contents. (a) 1.7 s^{-1} (b) 8.5 s^{-1}.
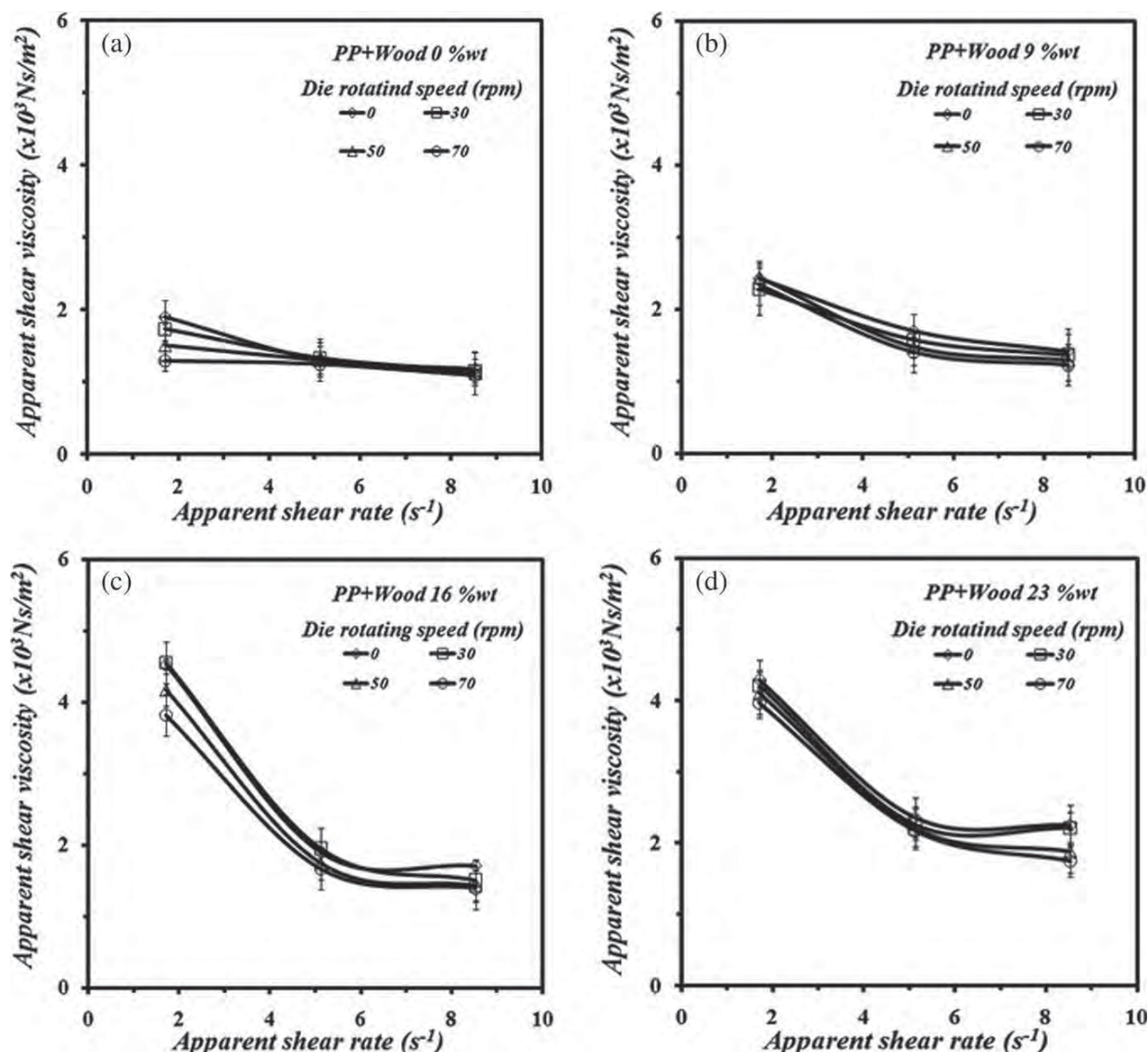
Figure 5 Flow curves for neat PP and WPP composites measured in the capillary rheometer at 190°C. (a) 0 wt % (b) 9 wt % (c) 16 wt %, and (d) 23 wt %.
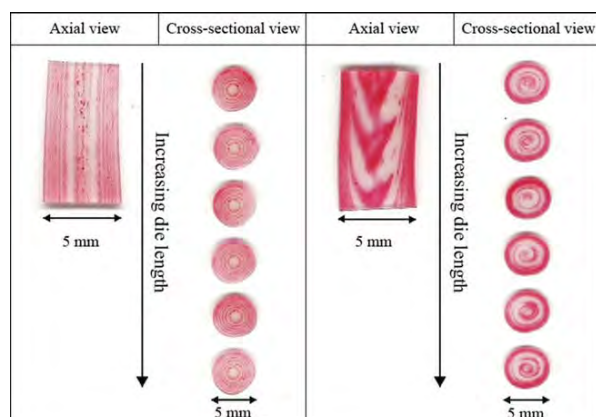
flow curves which were referred to as relationship between apparent shear viscosity and apparent shear rate for neat PP and WPP composites measured in the capillary rheometer given in Figure 5. It was found that the apparent shear viscosity decreased with increasing apparent shear rates, and this suggests a pseudoplastic non-Newtonian flow behavior. As expected, the viscosity of the PP melt increased with increasing wood content. This was supported by Maiti et al.[13] who found that the apparent melt viscosity of PP increased about 70% with increasing wood content. It was interesting to note that the decreasing magnitude of shear viscosity with increasing apparent shear rate was more obvious with the WPP composite melt with high wood contents (16 and 23wt %). It was observed that the die

rotating speed had no effect on the viscosity changes for PP and WPP composite melts although in some cases the viscosity slightly decreased with increasing the die rotating speed. However, the viscosity

TABLE I
Flow Properties for PP Melt with and without Red-24 Pigment Tested in a Capillary Rheometer

Apparent shear rate (s^{-1})	Apparent shear viscosity ($\times 10^3$ Ns/m^2)	
	Uncolored PP	Colored PP
6.22	1.56	1.73
12.44	1.00	1.02
18.66	0.74	0.75
31.10	0.50	0.50

Figure 6 Flow visulizations of PP melt in the capillary rheometer at axial and cross-sectional views at apparent shear rate of 8.5 s^{-1}. (a) Stationary die and (b) Rotating die. [Color figure can be viewed in the online issue, which is available at wileyonlinelibrary.com.]

changes were probably within the experimental errors (±5%). This implies that the reductions in extrusion load (Fig. 3) and entrance pressure drop (Fig. 4) were not caused only by the viscosity changes as a result of die rotation.

Changes in extrusion force and entrance pressure drop are usually in a direct relationship, i.e., the higher the extrusion force the greater the pressure drop developed at the die entrance. Therefore, the reductions in these two parameters found in this work practically indicate that higher extrusion outputs or productivities could be achieved either by increasing piston speed in piston-driven rheometers or by increasing screw rotation speed in single screw extruders. It was observed from the results in Figure 4 that the effect of entrance pressure reduction was higher at higher extrusion time or higher die-rotating speed when piston went closer to the capillary die entrance. In other words, when piston tip was far away from the capillary die entrance the effect of rotation on the pressure was negligible at low extrusion time or low die-rotating speed. This was probably due to contribution of capillary rotation. It was postulated that the decreases in extrusion force and entrance pressure drop were associated with flow development in the rotating die.

To support our reasons, flow visualizations for PP under the same testing conditions (PP material, die temperature, and apparent shear rates with and without die rotation) were performed. In this section, the same PP granules were used but made in two different colors for better resolutions by addition of 1.0 wt red-pigment (CI solvent Red-24 supplied by Orient Chemical Industries Co., Ltd, Osaka, Japan) for pigmentation of PP sample. The PP granules were dried in an oven at 75°C for 60 min to avoid any possible air traps and bubbles during sol-

idification. The flow property results in Table I shows that the addition of Red-24 pigment in the PP had no effect on the flow properties of the melt, indicating that the changes in the flow properties of PP did not result from the pigmentation process. The flow visualization experiment was carried out by preparing the uncolored and colored PP sample sheet with 3-mm-thick using a hydraulic press with a mold temperature of 210°C under a hydraulic pressure of 150 kg/cm^2 before cooling the molded sample to room temperature. The PP sheet was then cut into disks having 40 mm in diameter and 3 mm in thickness. The sample disks were then loaded into the heated barrel in color alternating sample disks. The piston was then mounted and slowly compressed the PP disks to ensure that there was no air trapped in the barrel. All the PP disks were left about 10 min under 190°C barrel and die temperatures until fully molten before being extruded for the required piston displacement (80 mm down the barrel in this case), this being achieved using a metal plate to block the die at the exit. After that the PP melt in the barrel was left to solidify using a rapid air cooling to avoid any voids and bubbles within the PP sample before unloading the PP sample rod, then sectioned in half, and the flow visualization was investigated. This experiment was then repeated for the maximum die rotating speed used in this work (referred to as 70 rpm), the die rotating during the extrusion of the PP melt for any required piston displacement.

Figure 6 shows the flow visualization of solidified PP at the axial (left) and cross-sectional (right) views of PP melt flowing along the die length using the stationary die and the rotating die in the capillary rheometer. It should be noted that different magnifications for axial and cross-sectional views were used to ease the resolution of the flow visualizations of PP melt. It can be seen that for the stationary die [Fig. 6(a)], the PP layers flowing in the stationary die were independent of one another indicating that each flow layer flowed along its flow path from the barrel into the die in a laminar form. In the case of die rotating system (Fig. 6b), each PP melt layer exhibited a continuous and twisting flow around and along the die length. The flow patterns of the PP melt observed in this work were very similar to those found for natural rubber compound in our previous work.[18] The twisting of the flow layers suggested a helical or spiral flow occurring in the rotating die and this was believed to produce torsional shear strain within the die. At higher shear rates or high composite viscosities, the torsional shear strain would be even higher, and this could lead to a circumferential slippage between the molten PP and the die wall during the flow in the rotating die and possibly additional shear heating to the PP and WPP
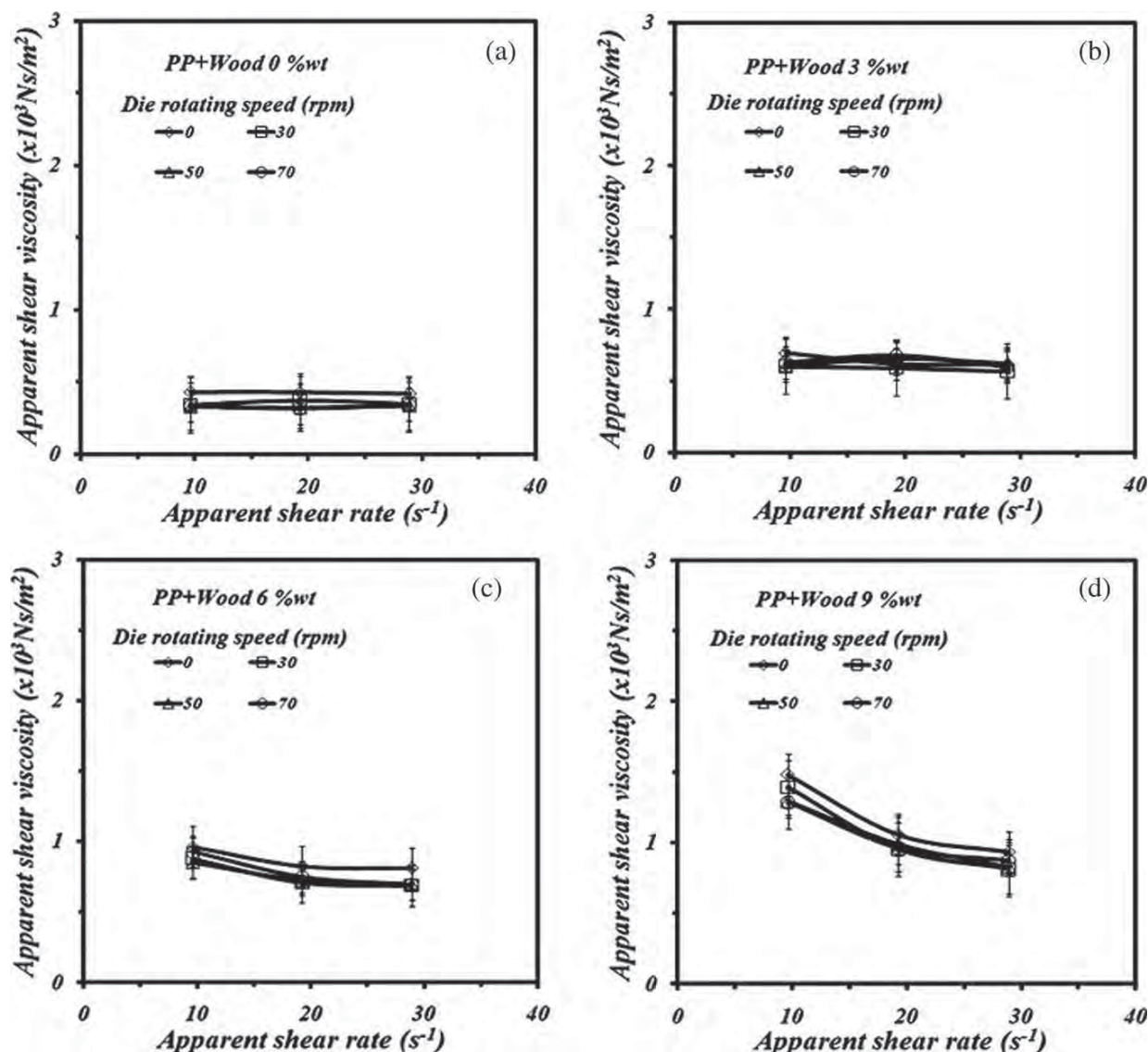
Figure 7 Flow curves for neat PP and WPP composites measured in the single screw extruder at a die temperature of 190°C. (a) 0 wt %, (b) 3 wt %, (c) 6 wt %, and (d) 9 wt %.

melts.[21] These effects caused the reductions of extrusion load and entrance pressure drop observed in Figures 3 and 4. The torsional shear strain effect was supported by the works of Ma et al.[15,16] extruded the molten lead using rotating conical dies, and found that the extrusion load was reduced by die rotation as a result of circumferential flows during extrusion equipped with a rotating die system.

Single screw extruder

It should be rementioned that it was not possible to obtain the extrusion force in a single screw extruder. This was because the neat PP and WPP composite materials were melted and pushed by the action of screw rotation simultaneously. It should be noted

that the motor amperage from in the screw extruder includes all the exerted forces (torques) to process the PP and WPP in various states (solid to fluid from feed to metering zones along the screw length) whereas the extrusion force for processing the polymer in the molten state was only required for direction comparison with those in the capillary rheometer (whose PP and WPP were was fully molten). Therefore, only pressure drop at the die entrance was recorded and examined. To prevent an overloading of the extruder, the wood content used for this case was reduced and varied from 2.9 to 9.0 wt %. Figure 7 shows the flow properties of neat PP and WPP composites in the single screw extruder in form of apparent shear viscosity VS apparent shear rate. It was interesting to note that the viscosities of
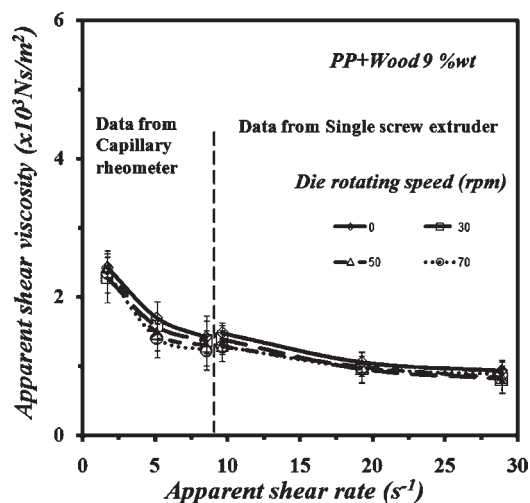
Figure 8 Viscosity data comparison for WPP composites containing 9 wt % wood from capillary rheometer and single screw extruder using a die temperature of 190°C.

neat PP and WPP with 3 wt % wood in the extruder did not change with shear rate. This may be due to low molecular weight of neat PP (as already mentioned by MFR value in Experimental section) and low shear rates used for screw extrusion process. However, the flow properties of WPP composites with higher wood contents (6 and 9 wt %) tended to follow shear-thinning non-Newtonian behavior. Similar to the results in the capillary rheometer, the viscosities for PP and WPP composite melts were unaffected by the die rotating speed, the variations in the viscosity data within the experimental errors (±5%).

It was interesting to compare the viscosity values of the molten PP and WPP composites in the capillary rheometer (Fig. 5) and the single-screw extruder (Fig. 7) although they were measured in different apparent shear rates. For general comparison, it was found that the changes in viscosity of PP and WPP in both extrusion machines obeyed pseudoplastic non-Newtonian behavior, especially when high wood contents were used. For more specific comparison, the viscosity data from the capillary rheometer and the screw extruder were merged and replotted in the same graph, allowing the flow properties of the melt in a wide range of apparent shear rates to be observed. An example of the merged viscosity data from the two extrusion machines was given only for the WPP composite with 9.0 wt % wood content and the result are shown in Figure 8. It was interesting to note that due to the differences in apparent wall shear rates used in the rheometer and the screw extruder, the viscosity of the WPP composite in the capillary rhemoter was higher than that in the screw extruder as one would expect since higher shear rates in the screw extruder would lower the melt viscosities. This observation clearly

confirmed the shear thinning behavior of the WPP composite melt as stated earlier. By combining the viscosity data of WPP composite from the capillary rheometer and the screw extruder in Figure 8, one could evidently say that the flow properties of the WPP composite was more dependent on the apparent shear rate than the extrusion design used.

Figure 9 shows the changes in entrance pressure drop against extrusion time at different apparent shear rates, wood contents, and die rotating speeds. It was found that the greater the apparent shear rates the higher the entrance pressure drops as one would expect. Increasing apparent shear rates from 9.6 to 28.9 s^{-1} resulted in the increase in entrance pressure drop about 6–7 × 10^5 Pa. For a given apparent shear rate, the entrance pressure drop increased about 6 × 10^5 Pa with increasing wood contents from 0 to 9 wt %. This was due to the increases in the bulk viscosity of the composite melt, similar to the case for the capillary rheometer. For the effect of die rotating speed, the experimental results suggested that the entrance pressure drop decreased with die rotating speed of 30 rpm, and then leveled off or slightly increased in some cases for higher die rotating speeds of 50 and 70 rpm. The most obvious change in the entrance pressure drop was the case where the wood content and the shear rate were high [Fig. 9(c,d)], the pressure drop reduction being up to 4 × 10^5 Pa (about 30% reduction). The changes in the entrance pressure drop occurring in the single screw extruder as a result of increasing die rotating speeds could also be explained in the same way as those in the capillary rheometer.

Comparative and supplemental comments

This section was intended to illustrate a comparison of flow properties for PP and WPP melts flowing in the capillary rheometer and the single screw extruder. First, the flow curves (apparent shear viscosity VS apparent shear rates) of the PP and WPP melts obtained were similar in the two extrusion processes, showing the shear-thinning now-Newtonian behavior. Second, the percentage reductions in the entrance pressure drop found in the capillary rheometer (20% reduction) in Figure 3(b) were slightly smaller than those occurring in the screw extruder (30% reduction) in Figure 9. This was probably due to differences in the initial shear rates and wood contents added into the PP. Finally, it was observed that the fluctuations or data scatterings in entrance pressure drop with increasing die rotating speed in the single screw extruder were more apparent than those in the capillary rheometer. This was associated with differences in the velocity profiles and the temperature profiles of the molten polymer composites across and along the flow channel occurring in these two extrusion processes. It has been
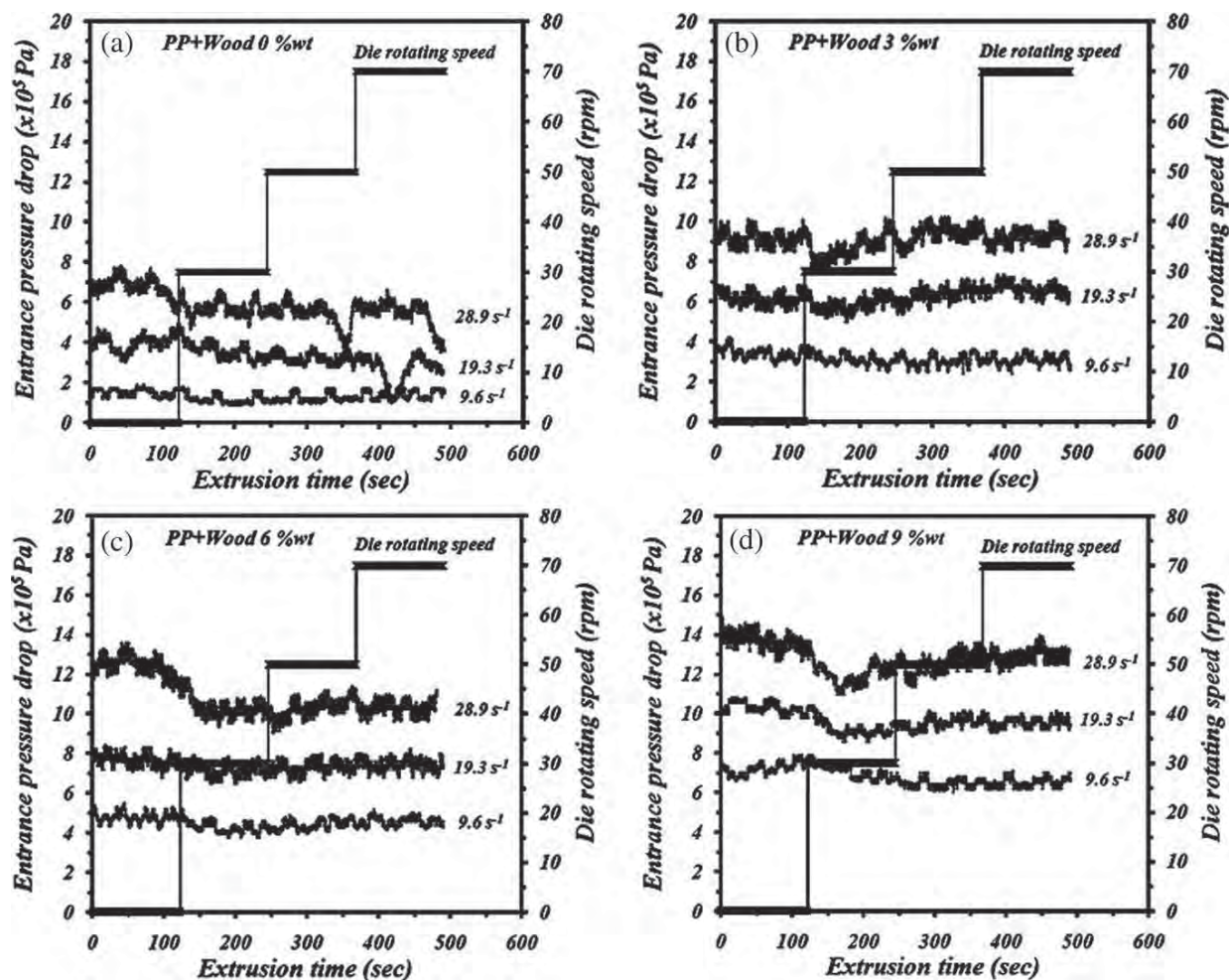
Figure 9 Entrance pressure drop for WPP composite melts for different wall shear rates and wood contents. (a) 0 wt %, (b) 3 wt %, (c) 6 wt %, and (d) 9 wt %.

known that the flows in the single- or twin-screw extruder combine between the drag flow and the pressure driven flow components whereas those in the piston-driven capillary rheometer is mainly the pressure flow. As a consequence, more melt temperature fluctuations with unstable velocity profiles of polymer melts were expected in the single screw extruder. This statement could be supported by previous studies on measurements of temperature gradients and velocity profiles of flowing thermoplastic melts in a capillary rheometer[22] and a screw extruder.[23]

In supplemental remark, it could be said that this was the first time that the die-rotating technique was applied for processing of wood/polymer composite (WPC) materials and their flow properties were discussed in association with the flow visualization. According to the experimental results, the die-rotating technique was relatively simple and suitable for reductions of extrusion loads and pressure built up in the extrusion processes, especially for the situations where

the shear rates and material viscosities (like WPC materials in this work) are high. It was also hoped that the die-rotating technique could be used to remedy some flow defects like sharkskin and melt distortions since it could reduce the pressure drop along the shaping die, probably with assistance of some lubricants. As stated earlier that the reductions of extrusion load and pressure build-up could practically increase extrusion outputs or productivities either by increasing piston speed in piston-driven rheometers or by increasing screw rotation speed in screw extruders. However, the use of die-rotating technique has one obvious limitation. That was, the technique can so far be used only for symmetry dies, such as circular or annular dies.

CONCLUSIONS

The results suggested that a proposed die-rotating system was possible and successful for moderating the

extrusion force and entrance pressure drop for PP and WPP composite melts in the capillary rheometer and the single screw extruder. The flow properties of the molten PP and WPP composites exhibited a shear-thinning character, the effect being obvious for the melt with high wood contents. The effect of die rotating speed was more pronounced for the WPP composite melts having high wood content and higher shear rate used in this work. The rotation of the die could reduce the extrusion load by 60% and entrance pressure drop by 20% in the capillary rheometer, and the entrance pressure drop by 30% in the single screw extruder for the WPP composites. The helical shearing flows and torsional shear strain developed as a result of die-rotation were responsible for the decreases in the extrusion force and the entrance pressure drop. The changes in the entrance pressure drop due to die rotation in the single screw extruder showed more fluctuation than those in the capillary rheometer. The flow properties of the WPP composite were more dependent on the apparent shear rates than the extrusion modes used.

References

1. De Albuquerque, A. C.; Joseph, K.; De Carvalho, L. H.; D'Almeida, J. R. M. Compos Sci Technol 2000, 60, 833.
2. Sombatsompop, N.; Yotinwattanakumtorn, C.; Thongpin, C. J Appl Polym Sci 2005, 97, 475.
3. Mendez, J. A.; Vilaseca, F.; Pelach, M. A.; Lopez, J. P.; Barbera, L.; Turon, X.; Girones, J.; Mutje, P. J Appl Polym Sci 2007, 105, 3588.
4. Tungjitpornkull, S.; Chaochanchaikul, K.; Sombatsompop, N. J Thermo Compos Mater 2007, 20, 535.
5. Rizvi, G. M.; Semeralul, H. J Vinyl Addit Technol 2008, 14, 39.
6. Faruk, O.; Matuana, L. M. Compos Sci Technol 2008, 68, 2073.
7. Liu, W.; Drzal, L. T.; Mohanty, A. K.; Misra, M. Composites B 2007, 38, 352.
8. Wolcott, M. P.; Englund, K. In Proceedings of 33rd International Particleboard/Composite Materials.Washington State University, WA, 1999.
9. Xu, X.; Jayaraman, K.; Morin, C.; Pecqueux, N. J Mater Process Technol 2008, 198, 168.
10. Migneault, S.; Koubaa, A.; Erchiqui, F.; Chaala, A.; Englund, K.; Wolcott, M. Compos A, 2009, 40, 80.
11. Sombatsompop, N.; Prapruit, W.; Chaochanchaikul, K.; Pulngern, T.; Rosarpitak, V. J Vinyl Addit Technol 2010, 16, 33.
12. Pulngern, T.; Choocheepsakul, S.; Padyenchean, C.; Rosarpitak, V.; Prapruit, W.; Chaochanchaikul, K.; Sombatsompop, N. J Vinyl Addit Technol 2010, 16, 42.
13. Maiti, S. N.; Subbarao, R.; Ibrahim, M. N. J Appl Polym Sci 2004, 91, 644.
14. Rawal, A.; Davies, P. J. Plast Rubber Compos 2005, 34, 47.
15. Ma, X.; Barnett, M. R.; Kim, Y. H. Intl J Mechan Sci 2004, 46, 449.
16. Ma, X.; Barnett, M. R.; Kim, Y. H. Intl J Mechan Sci 2004, 46, 465.
17. Ma, X.; Barnett, M. R. Mater Sci Eng A, 2008, 483–484, 444.
18. Intawong, N.-T.; Wongchaleo, C.; Sombatsompop, N. Polym Eng Sci 2008, 48, 1191.
19. Sombatsompop, N.; Chaochanchaikul, K. Polym Intl 2004, 53, 1210.
20. Sombatsompop, N.; Chaochanchaikul, K. J Appl Polym Sci 2005, 96, 213.
21. Wapperom, P.; Hassager, O. Polym Eng Sci 1999, 39, 2007.
22. Sombatsompop, N.; Patcharaphun, S. Polym J 2001, 33, 491.
23. Sombatsompop, N.; Chaiwattanapipat, W.; Panapoy, M. Mater Res Innovat 2000, 3, 271.